ABSTRACT

FEASILIBITY STUDY TO EXTRACT IRON AND CHROMIUM FROM CHROMIUM CONTAMINATED SOILS

by
Wiwat Kamolpornwijit

Chromium contaminated soils, besides being recognized for toxic and hazardous hexavalent chromium, contain high iron concentrations. At some sites, concentrations of iron oxide are higher than 30%. Both iron and chromium in soils have recyclable value provided they can be either concentrated in the oxide form or separated as metal. The concentrated oxide can be used as a substitute for the iron ore. The extracted metal can also be recycled in the steel industry. The objective of this study is to study the feasibility of extracting iron and chromium from soils.

Chromium contaminated soils, can be classified into two groups, one with high iron content having magnetic properties, and the other with low content of iron with no magnetic properties. The extraction of iron and chromium in their oxide forms was conducted using magnetic and gravitational separation techniques. The magnetic separation was found to be better than gravitational separation to concentrate iron and chromium from chromium contaminated soils for the experimental setup. However, the iron content in soil could not be concentrated to as high a level as high grade or processed iron ore, 60-70% iron content.

The reduction of iron oxide to metal can be accomplished at high temperature under the reducing environment. The reduction of iron oxide in soil was quite rapid at temperature higher than 1100°C. The solid carbon was used as a reducing agent for the

study of reduction in Thermo-Gravimetric Analyzer. The reduction process was found to be controlled by gasification with the activation energy of 45-55 kcal/mol based on the selected kinetic models. The complete reduction required at least 15% of carbon by weight.

The metal agglomeration and separation occurred when sand was added to soils. The substantial percentage of metal, 15-32 %, was separated from GAR and TPR soils mixed with 15-25% of sand and 15% carbon. The LSP soil mixtures yielded metal separation with sand addition above 20%. Phase and viscosity diagrams were used to explain the metal separation and behavior of the slag. Experimental results demonstrated that iron and chromium can be extracted from chromium contaminated soils found in Hudson County, NJ.

FEASIBILITY STUDY TO EXTRACT IRON AND CHROMIUM FROM CHROMIUM CONTAMINATED SOILS

by
Wiwat Kamolpornwijit

A Dissertation
Submitted to Faculty of
New Jersey Institute of Technology
in Partial Fulfillment of the Requirements for the Degree of
Doctor of Philosophy in Civil Engineering

Department of Civil and Environmental Engineering

August 2000

APPROVAL PAGE

FEASIBILITY STUDY TO EXTRACT IRON AND CHROMIUM FROM CHROMIUM CONTAMINATED SOILS

Wiwat Kamolpornwijit

Dr. Namunu J. Meegoda, Dissertation Advisor — Date
Professor of Civil and Environmental Engineering, NJIT

Dr. Methi Wecharatana, Committee Member — Date
Professor of Civil and Environmental Engineering, NJIT

Dr. Lisa Axe, Committee Member — Date
Associate Professor of Civil and Environmental Engineering, NJIT

Dr. Dana E. Knox, Committee Member — Date
Associate Professor of Chemical Engineering, NJIT

Dr. Hong Li, Committee Member — Date
Senior Researcher, Fiber Glass Science and Technology, PPG Industries, Inc.

BIOGRAPHICAL SKETCH

Author: Wiwat Kamolpornwijit

Degree: Doctor of Philosophy in Civil Engineering

Date: August 2000

Education:

- Master of Science in Environmental Engineering.
  New Jersey Institute of Technology, Newark, NJ, 1996

- Bachelor of Engineering in Environmental Engineering,
  Chulalongkorn University, Bangkok, Thailand, 1990

Major: Environmental Engineering

Presentations and Publications:

Kamolpornwijit, W., and J.N. Meegoda, 2000, "Feasibility Study to Extract Iron and Chromium from Chromium Contaminated Soils," Proceedings of the 32nd Mid-Atlantic Hazardous Waste, RPI, Troy, New York, pp. 777-787.

Meegoda, J. N., W. Kamolpornwijit, and G. Charleston, 2000, "Construction use of Vitrified Chromium Contaminated Soils," *ASCE Practice Periodical of Hazardous, Toxic, and Radioactive Waste Management,* Vol. 4, No.3, pp. 89-99.

Meegoda, J. N., Partymiller, K., Richards, M. K., Kamolpornwijit, W., Librizzi, W., Tate, T., Noval, B. A., Mueller, R. T., and Santora, S, 2000, "Remediation of Chromium Contaminated Soils -A Pilot Scale Investigation," *ASCE Practice Periodical of Hazardous, Toxic, and Radioactive Waste Management*, Vol. 4, No.1, pp. 1-11.

Meegoda, J. N., Kamolpornwijit, W., Vaccari, D. A., Ezeldin, A. S., Noval, B. A., Mueller, R. T., and Santora, S, 1999, "Remediation of Chromium Contaminated Soils - A Bench Scale Investigation," *ASCE Practice Periodical of Hazardous, Toxic, and Radioactive Waste Management,* Vol. 3, No.3, pp. 124-131.

This thesis is dedicated to my beloved parents.

ACKNOWLEDGMENT

The author wishes to express his sincere gratitude to his advisor, Dr. Namunu J. Meegoda, for his guidance and support throughout this research. Special thanks to Dr. Methi Wecharatana, Dr. Lisa Axe, Dr. Dana E. Knox, and Dr. Hong Li for serving as members of committee. The author appreciates the generosity of Dr. Henry Shaw and Dr. Trevor Tyson for allowing him to use the TGA and furnace. The author thanks Dr. Shin-Neng Hsieh and Mr. Patel who have been very helpful regarding the instruments in the geo-environmental laboratory. The author again thanks Dr Wecharatana for providing computer facilities.

The author thanks his beloved father and mother, his family, and friends who have long been very supportive and never lost faith in him. Special thanks go to Walairat Bumrongjaroen who has been very supportive. The author thanks all the Thai students who have willingly helped him in many matters.

And finally, a thank you to the people in Civil and Environmental Engineering Department for their help throughout these long years.

TABLE OF CONTENTS

TABLE OF CONTENTS
(Continued)

Chapter **Page**

TABLE OF CONTENTS
(Continued)

Chapter **Page**

TABLE OF CONTENTS
(Continued)

Chapter **Page**

TABLE OF CONTENTS
(Continued)

Chapter **Page**

TABLE OF CONTENTS
(Continued)

Chapter **Page**

LIST OF TABLES

LIST OF TABLES
(Continued)

Table **Page**

LIST OF TABLES
(Continued)

LIST OF FIGURES

Figure **Page**

LIST OF FIGURES
(Continued)

Figure **Page**

LIST OF FIGURES
(Continued)

Figure **Page**

LIST OF FIGURES
(Continued)

Figure **Page**

LIST OF FIGURES
(Continued)

Figure **Page**

LIST OF FIGURES
(Continued)

Figure **Page**

CHAPTER 1

INTRODUCTION

The idea of extracting iron out of chromium contaminated soils emerged during the feasibility study to treat chromium contaminated soils by cold top ex-situ vitrification. The vitrification process proves to be a very effective treatment technology for chromium contaminated soils and produces by-products with reusable values (Meegoda et al., 2000). As always, a satisfying or unsatisfying result leads to another innovative idea that provides a technically and economically better solution to environmental problem. This very research is no exception. The analysis of chromium contaminated soils shows high concentrations of iron. In some batches of vitrification, the separation of metal at the furnace bottom was reported. The separation of metallic iron prompted the need for a further investigation on the possibility of not only treating but also converting the hazardous waste into a reusable material with real and tangible value, the primary objective of the research. The reduction of chromium oxide to metallic chromium along with iron can potentially form an alloy of higher value provided it has similar composition to stainless steel. The by-products and slag will be no longer toxic due to the thermal treatment at high temperature. The slag will have similar properties to the vitrified product, which satisfies requirements as a construction aggregate set forth by American Society for Testing and Materials (ASTM) and New Jersey Department of Transportation (NJDOT) (Kamolpornwijit, 1994). The separation of iron and chromium can reduce the specific gravity of slag due to the lower metal content, beneficial to both preventing long term leaching and facilitating the use of slag as aggregates in the

construction work. The value of the recycled metal will subsidize the vitrification process, which is always cited as an energy intensive treatment.

The iron and steel industries though do not promise the tremendous growth as in the early 90's, they are industries that provide an essential infrastructure to the growing economy. The steel industry produces approximately 100 million tons of steel annually; an additional 25 million tons is imported. The value of the steel production is close to $50 billion annually (Kavanagh et al., 1998). Due to the depleting of the iron ore and environmental concerns, the industry is in search of a more efficient technology and better by-product recycling and management plans. Generally, the by-products from the process with high iron content are crushed, beneficiated, sintered or briquetted, and fed back to the process. The utilization of the slag depends on its properties; blast furnace slag contains very low concentration of iron and is used as aggregate and landfill material or in the cement industry, steelmaking slag has high iron content and is recycled to metal extraction process. The iron content in chromium contaminated soils is comparable to that of the steelmaking slag with less detrimental constituents namely zinc and phosphorus. Iron co-existed in natural chromite ore as a part of the spinel and was not extracted during the chromate extraction process. The chromium contaminated soils possess a potential as an iron source for the iron and steelmaking industry.

There are over two millions tons of chromium contaminated soils, accounted for more than 150 sites, in Hudson County, New Jersey. The contaminants were the consequence of the prosperous chromate extraction industry during the mid-nineteenth century. Chromium exists in soil mostly in two oxidation states, trivalent and hexavalent. Hexavalent chromium is well known as a group A human carcinogen with sufficient

evidence. Some chromate compounds are highly soluble and when released to surface and ground water threaten human health and environment. Many researchers take on the remediation of chromium contaminated soils by soil washing, stabilization, vitrification, etc. Most of the studies attempt to treat toxic chromium compounds either by reduction to less toxic trivalent form or containment in cement or glass matrix. The recovery of iron and chromium in contaminated soils is overshadow by its publicized toxicity, and gains less attention.

The recovery of iron and chromium from contaminated soils will preserve the natural resources, provide permanent treatment for contaminated soils, and produce some revenues.

1.1 Objective

The primary objective of this research is to determine the feasibility of the recovery or extraction of iron and chromium from chromium contaminated soils. Towards the goal of studying the feasibility, it also provides the basic understanding of the process, factors affecting the process, limitations, the optimum condition, and the applicability. The remediation of the chromium contaminated soil is also a concern. Because of the great efficiency of the thermal treatment process on treating chromium contaminated soils, the remediation of soil as another objective is readily satisfied. As the separated metal may create some revenues, it will subsidize the energy intensive yet effective thermal treatment technology.

1.2 Overview

The iron and chromium can possibly be recycled either in their oxides or metal forms. Both approaches will be studied beginning with the recycling as an oxide which is simpler and less energy intensive than the recycling in a form of metal. There are three major areas of study towards the research objective;

1) The characterization of chromium contaminated soils and their vitrified products and the study of iron concentrating techniques.
2) The reduction of iron oxide
3) The metal separation

The instruments used in the study include Thermo-Gravimetric Analyzer (TGA) for the reduction and separation study, High Temperature Furnace for the metal separation study, X-ray Diffraction Spectrometer (XRD) for phase identification, X-ray Fluorescence Spectrometer (XRF) for the chemical analysis, and Environmental Scanning Electron Microscope (ESEM) equipped with Energy Dispersive X-ray spectrometer (EDX) for the morphological and chemical analysis.

Before discussing the experiments and results, the basic understanding on the concentrating method, the iron and steelmaking processes, the reduction and metal separation process is provided in Chapters 2 and 3. Chapter 4 contains the framework of the experimental program. During the study there were some changes and adjustments which were given and discussed along with the presentation of the results.

The chromium contaminated soils obtained form nine sites are characterized and can be classified into two groups: high and low iron concentrations. For the high iron concentration group, the iron and chromium exist in a form of spinel and are magnetic. A

representative soil from each group is subjected to the concentrating by magnetic and gravitational separations. The result brings the conclusion on the possibility of recycling of iron and chromium in a form of oxide. Chapter 5 also provides characteristics of vitrified soils from both bench and pilot scales. The phases of vitrified products from different soils are surprisingly the same for each test scale. This implies the applicability of the process to a wide range of soils.

In Chapter 6, the results from the reduction of iron oxide in soils and some other pure oxides are presented. The factors effecting the reduction process including temperature, the amount of carbon, and time, are discussed. The reduction study used soil collected from Liberty State Park (LSP) as a representative of the high iron concentration soils. The reduction of soils collected from Colony Diner (CD), Garfield Avenue (GAR), and Turnpike Road (TPR), are also presented.

The reduction of iron oxide in soils was confirmed but there was no observable metal separation. The solid state of both metal and soil may account for the difficulty in metal separation. Sand was added to soil as an acidic oxide to balance with the basic calcium oxide in soil and to bring the melting temperature down. Four soils were studied: LSP, CD, GAR, and TPR. The metal separation was found for some tests with sand addition. The compositions of slag when metal separation occurred provided the suitable slag composition for the separation. Phase and viscosity diagrams are essential tools in the study of slag behavior. The simple application of them to predict the metal separation of soils was verified by the experimental results. These topics are studied and discussed in Chapter 7. The last chapter, Chapter 8, provides summary and conclusions and discussion on potential future work. Appendix A contains a brief discussion on

future research plan: the reduction study in more detail and the incorporation of different kinetic parameters to predict the reduction process.

This research covered a broad area of study and focused on the application approach. The use of real soil is preferred over the mixture of pure compounds to study the true feasibility of metal extraction.

CHAPTER 2

IRON AND STEELMAKING PROCESSES

The chapter covers some aspects of iron and steelmaking industries: the iron and steel market, the production of iron and steel, the recycling of iron and steel by-products, the slag chemistry, and the beneficiation of the mineral ores. It is worthwhile to explore iron and steelmaking processes due to theirs resemblance to parts of the research. The iron and steelmaking processes have long been a well-established technology, yet continuously developing toward better efficiency and environmentally sound processes.

Iron ore is a source of iron in the iron and steel production. They naturally exist as minerals rich in iron, i.e. hematite and magnetite. The ore of high concentration of iron could be used in the iron production directly without any modification. Iron ore has long been utilized and the depleting of high-grade ore came at no surprise. The consumption rate of low-grade ores increases continuously (Kuck, 1998). Low-grade ore contains possibly the same iron rich mineral but with a large amount of disseminated impurities, mostly oxides. It needs to be preprocessed to get rid of the impurities and to concentrate the iron concentration. The process, so called beneficiation, includes the grinding of ore to liberate iron-rich mineral grains. The liberated grains then are concentrated by magnetic separation, gravitational separation or floatation, the three major processes of beneficiation (Taggart, 1947). Fines always cause problem in any reactors, especially the counter current reactor (Lankford et al., 1985). The ground and concentrated ore needs to be agglomerated. The agglomeration processes include sintering, briquetting, and pelletizing.

Pig iron is the product from the reduction of iron ore, and steel is the refined iron. The blast furnace process is the main process for the iron production. The iron ore is reduced to metallic iron at high temperature. The quality and the cleanliness of the product depend on the separation of impurities, so called slag, during the iron production. The chemistry of slag is similar to acid-base chemistry in a sense that one compound reacts with the other and forms an intermediate compound. The acidic oxide reacts with basic oxide to form a stable intermediate oxide. Generally, the intermediate oxide has lower melting temperature than its basic and acidic reactants. Upon melting, it floats over the metal pool due to its lower density. The slag chemistry strongly influences the quality of both iron and steel. The refining process for the production of steel includes the oxidation of carbon remaining in pig iron to CO and CO_2, and the elimination of sulfur and phosphorus in iron by forming sulfides and phosphates with slag forming compounds. The oxidation of carbon is done by oxygen blowing. During this process, a fraction of metallic iron is also oxidized and imparts in the slag. The steel slag therefore contains a higher concentration of iron than that from iron production. The iron concentration sometimes is referred as iron unit value. The steel industry does not only produce steel, it also produces wastes. The recycling and reuse of wastes produced is critical for the environmental concern. Most wastes and by-products are reused or recycled. The slag is reprocessed provided it contains appreciable iron content or is used as fill material or aggregate depending upon its property. Steel is the most recycled metal far ahead of aluminum, paper, plastic, and glass combined (kavanagh et al., 1998). The market and price values of the product drive the production rate and the future of the industries.

The chapter contains many aspects of subjects mentioned earlier yet in brief. The recycling of iron and chromium oxide as a substitute for iron ore is equivalent to the very first step in iron and steel making, second only to the exploration and mining. Chromium contaminated soils contain mostly slag forming oxides with high iron contents which are similar to or even better than the steel slag. Unlike the steel slag, soils do not have high concentrations of zinc or phosphorus, which are deteriorative to the furnace refractory. The recycling of metal from soils and the reuse of vitrified products are therefore strongly viable.

2.1 Ores and Beneficiations

2.1.1 Iron Ore

The iron-rich minerals mostly found in iron ore are in many forms: oxide, carbonate, and sulfide (Table 2.1). The most important and commercialized form is oxide. Ores from different sources also have different iron contents. Table 2.2 provides compositions of ores from different sources. The usage of high-grade ore, ore of high iron content, is preferred provided that it is available. However, the utilizing of low-grade ore fits in some places economically, after considering the transportation of high-grade ore and the availability of the special low-grade-iron-production process. The examples are the usage of ore containing 25%Fe and 37%Fe in France and in Birmingham, Alabama (Lankford et al., 1985). These ores generally have no commercial values.

For low-grade ores, beneficiation is required to concentrate the iron content before being fed to blast furnaces. The iron content of processed ore can be as high as the iron content of high-grade ore. For example, the iron content of magnetite taconite, in

Minnesota, improves to 64-65% from 15-35% after being concentrated through magnetic separation. The silica content decreases from 40-50% to 4-7%.

Table 2.1 Iron-Rich Minerals Found in Iron Ore (Lankford et al., 1985)

Minerals	Names	S.G.	Iron Content (% wt.)	Color
Fe_3O_4	Magnetite	5.16-5.18	72.4	dark gray to black
Fe_2O_3	Hematite	5.26	70.0	steel gray to dull or bright red
$FeTiO_3$	Ilmenite		36.8 Fe 31.6 Ti	
$HFeO_2$, and FeO(OH)	Lepidocrocite Goethite	3.6-4.0	62.9	yellow to brown
$FeCO_3$	Siderite	3.83-3.88	48.2	white to gray and brown
FeS_2	Pyrite	4.95-5.10	46.6	pale brass yellow

S.G. - Specific Gravity

Table 2.2 Compositions of Iron Ore from Different Sources (Bogdandy and Engell, 1966)

Sources	Concentration (% wt.)								
	Water content	Fe	Mn	P	S	SiO_2	Al_2O_3	CaO	MgO
Brazil	1.0	68.2	0.06	0.02	0.01	0.53	0.83	0.35	0.1
Venezuela	7.8	59.6	0.04	0.11	0.03	0.81	1.55	0.28	0.1
Kiruna, Sweden	1.2	58.2	0.11	1.69	0.02	4.31	1.08	6.32	1.28
India	6.1	54.2	0.41	0.05	0.04	2.25	7.65	0.4	0.13
Northampton, UK	15.2	32.5	0.24	0.6	0.1	14.7	6.1	2.7	0.4
Frodingham, UK	10.7	22.7	0.96	0.31	0.16	8.1	5.1	18.2	1.0
Minette	9.9	23.5	0.18	0.51	0.05	10.4	4.47	19.8	0.81
Echte	6.4	23.6	0.12	0.49	0.1	11.9	8.33	17.7	1.97
Wabana, canada	1.52	49.3	0.17	0.92	0.04	13.1	5.88	3.35	0.71

2.1.2 Chromite Ore

The name "chromite" specifically refers to the mineral of composition $FeCr_2O_4$. However, the term chromite is generally used in a broader sense for the spinel containing chromium. In fact spinel is a mineral name of $MgAl_2O_4$. However, the term spinel has

also been used as a coumpound of formula $AO.B_2O_3$. The "A" represents cation of divalent charge, i.e. Fe^{2+} and Mg^{2+}. The "B" represents cation of trivalent charge, i.e. Fe^{3+}, Al^{3+}, and Cr^{3+}. Table 2.3 gives examples of spinels, generally found as a solid solution constituting chromite ore. These spinels have cubic structure at room temperature and normally crystallize as octagonal crystal (Ulmer, 1970). Small amounts of manganese, titanium, nickel, and vanadium are often found in the solid solution of chromite. The substitutions of other elements in the spinel, i.e. the substitution of Ca^{2+} and Si^{4+}, are also possible. With the Ca^{2+} substitution, $CaFe_2O_4$, the structure changes from cubic to orthorhombic.

Table 2.3 Physical Properties of Chromite Spinels (Udy, 1956)

Properties	Type of Spinel					
	$MgAl_2O_4$	$FeAl_2O_4$	$MgCr_2O_4$	$FeCr_2O_4$	$MgFe_2O_4$	$FeFe_2O_4$
Color	various	Bottle green	Pale green	Orange or deep red	Red brown, black	black
Hardness	7.5-8	7.5-8	NA	5.5	NA	5.5-6.5
S.G.	3.55	4.39	4.2	5.09	4.56-4.65	5.175
Unit cell (A)	8.086	8.119	8.308	8.344	8.366	8.374
Melting point (°C)	2135	1440	NA	1670	1750	1591
Magnetism	Non-magnetic	Non-magnetic	Non-Magnetic	Non-Magnetic	Strongly magnetic	Strongly magnetic

A - Angstrom
NA - not available

Chromium is utilized in various industries, mostly in metallurgical, refractory, and chemical manufacturing. The metallurgy grade ore has Cr_2O_3 content not less than 46% by weight. The refractory grade ore contains 44-45% of Cr_2O_3, and 34-35% for chemical grade. In the metallurgical industry, chromium is mostly supplied in a form of

ferrochrome, a solid solution of metallic iron and chromium from the reduction of chromite ore.

2.1.3 Beneficiation

The mineral ore consists of two major parts: minerals and gangues or rock-forming materials. As stated before, beneficiation is a process of separating the minerals, referred later as concentrate, from gangue materials, tail. The high-grade ore may not need further beneficiation unlike the low-grade ore. The treatment of ore generally constitutes of 2 steps. The first step includes grinding, crushing, floatation, magnetic separation, and gravitational separation. The second step is the primary metal production, including the reduction of metal oxide to metal, by chemical, pyrometallurgical or hydrometallurgical processes.

Three major processes of beneficiation are gravitational concentration, floatation and magnetic separation. Crushing of ore is often required to liberate the mineral grains from impurities before beneficiation. The degree of crushing depends on the nature of mineral agglomeration, high for the sparingly-dessiminated-mineral ore and low for ore containing large mineral grains.

The information provided may seem excessive if considering the beneficiation methods to be studied: dry and manual magnetic separation, and simple gravitational separation. Yet it gives good foundation in understanding and subsequently applying the beneficiation to any other materials not limited to chromium contaminated soils. In this section, there are brief descriptions on gravitational separation, floatation, magnetic

separation, other beneficiation techniques, technical difficulties with fines, and agglomerations of ground ores.

2.1.3.1 Gravitational Separation. The principle of gravity concentration lies on the fact that different grains of mineral with different specific gravity move through a medium with different speeds depending on the gravitational force, buoyancy force, and the resistant force against the medium. Particles of higher specific gravity, holding the other factors constant, fall faster than ones with lower specific gravity do. Particles having larger diameters gain larger velocity than that from smaller ones. And flat particles fall slower than the ones with equiaxial shape. The physical properties of the medium, viscosity and density, govern the resistant and buoyancy forces. The media can be liquid alone or liquid with dispersed solid so to increase the density of media. In cases where the media is a mixture of solid and liquid, the resistant force depends not only on those mentioned earlier but also on the size and interstitial spacing of dispersed solid particles, specific gravity, shape, and velocity of the interstitial fluid. The higher the difference in the specific gravity between mineral grains and impurities, the better the separation.

The concentration criteria, used to determine the applicability of the gravity separation, is determined by $(S_H - R)/(S_L-R)$, where S_H, S_L , and R are the specific gravity of the heavy mineral or iron ore, light mineral or gangue, and the medium, respectively. Generally, when the concentration criteria is greater than 2.5, separation is easy for all sizes down to finest sand. At 1.75 the separation by commercial separator is possible down to 65-100 mesh, and to 10 mesh at 1.5. At 1.25, the commercial separation is possible down to gravel size. Below 1.25 gravity separation without difference in weight

modification are not possible (Taggart, 1947). The example of processes using gravity separation technique are shaking table, sink float separation, spiral concentrator, and hydrocyclone.

In a shaking table, the shaken bed is formed by the movement of the support with adequate vigor to dilate the bed, but smooth enough to maintain all particle into substantial contact. Large particles then interlock and fine grains trickle down the interstitial space and then resist the further penetration by the larger particles, causing reverse classification. The heavier particles travel down to the lower level and form the reverse statra. The Multi-gravity separator, developed for fine and ultrafine particles is a rolling of a shaking table into a slightly inclined drum, rotating to create a centrifugal force. Belardi et al. (1995) found that the Cr_2O_3 concentration in chromite fine, with the liberation size of 100 μm, was improved from 23% to 50% with a recovery rate of 72% after passing through the multi-gravity separator for three cycles. Chan et al. (1991) demonstrated that the two-stage multi-gravity separator improved the Cr_2O_3 grade from 12% to 40% with 70% recovery rate and outperformed the existing high density magnetic separator at the Kemi Mine.

The sink float separation depends on the selection of media whose density supposedly lies between the ore and gangue materials. The heavier mineral falls down and the lighter particle floats up to the surface. Media can be either heavy liquid or mixture of fluid and fine solid particles, i.e. galena, sand, clay, magnetite, or ferrosilicon. The dense media separator is an instrument that utilizes the sink-float concept. It is a countercurrent reactor consisting of inclined cylindrical vessels having heavy media flows tangentially upward from the bottom, creating the open vortex. The mineral with

higher specific gravity than the media will be centrifugally forced to the surface, moves upwards and eventually removed as concentrate. Lighter particles remain suspended in the heavy media, and exit at the bottom. Kitsikopoulos et al. (1992) used a mixture of 70% atomized ferrosilicon and 30% milled magnetite to concentrate chromite ores. The Cr_2O_3 concentrations improve from 11-18% to 35-36% and 40-42% with the media density of 3.2 kg/l and 3.3 kg/l, respectively.

2.1.3.2 Floatation. The floatation process concentrates particles in a finely divided state, sufficiently fine to liberate the mineral grain. During the process, the specific gravity of certain mineral changes due to the selective bubble attachment and the mineral grain floats up to the surface. The floatation is applicable to the pulp with solid content between 15-35% and a maximum particle size of 48 mesh. The proper collecting agent selectively coats the surface of certain minerals with water-repellent film to which air bubbles attach. Certainly there are many kinds of minerals in the pulp and they at different degrees affect the separation. Floatation conditions can be adjusted by adding a conditioning agent to promote the selective coating of the collecting agent on the specific mineral surface. The frothing agent is also required to enhance the resistant of the bubble to external strain and maintain the frothing condition until the completion of the separation.

The function of the collector agent is to induce the ion exchange between the collector ions and mineral surface ions on one end and provide the hydrocarbon or hydrocarbon-like on the other end. The compound formed must be insoluble under the floatation condition. The gas bubbles, induced either by agitating, lowering pressure, or

aerating, form on the interface that has low surface tension or high vapor pressure. Comparing the vapor pressure of the mineral/water and hydrocarbon/water interface, the latter has lower surface tension and tends to be the gas forming sites. Collector agents are classified into cationic or anionic types. Cationic and anionic collectors are agents that when dissolved have cationic and anionic reactive groups, respectively.

The consumption of expensive collector agents decreases by proper conditioning. The conditioning agents work in two ways: either activation or depression. The activation process selectively promotes the reaction of desired mineral with the collector agent, and the depression works the other way. An example of conditioning agent is sulfuric acid, which depresses quartz and activates chromic oxide.

Raju et al. (1993) did a comparative study on the efficiency of inverse column floatation, by activating gangue instead of ore, against the existing combination of magnetic and gravitational separations at an existing iron ore plant. For the magnetic ore, the inverse column floatation was able to achieve 68.92% Fe, 1.32% SiO_2 with 88.08% recovery compared to 67.80% Fe, 2.37% SiO_2 with 90.12% recovery after secondary magnetic separation. For the non-magnetic portion, the inverse column floatation was able to achieve 66.11 % Fe, 2.4% SiO_2 with 73.34% recovery compared to 64% Fe, 6.5% SiO_2, 64% recovery from the two-step spiral concentrator. The cauticised starch was used as a conditioning agent, and tridecyletherdiamine acetate as a collecting agent for silica.

The cationic floatation improved the Cr_2O_3 content in the low grade chromite ore from 6.05% to 22.3%. Andrew (1990) used sulfuric acid as a pH modifier and a

conditioning agent and Armac C as a collector. The optimum condition for separation was at pH 2; the point of zero charge of chromite was in the pH range of 4.4-9.6.

2.1.3.3 Magnetic Separation. The magnetic separation utilizes magnetic force caused by the non-uniform magnetic gradient. The magnetic force imposed on the particle in a magnetic field depends on the relative permeability of the substance and its surrounding medium. The magnetic permeability is a measure of the ease with which magnetic properties can be induced in a mineral. Theoretically the magnetic separation is successful when the ratio of the magnetic permeability is larger than 5:1 to 10:1. The standard iron has the attractibility of 100, 40.18 for magnetite, 1.32 for hematite and chromite, 0.37 for quartz and 0.03 for calcite.

Parker (1993) classified modern magnetic separation techniques into two broad categories: particle entrapment and particle deflection. In particle entrapment, the feed material comes directly into contact with the magnetic surface, strong magnetic material is captured at the surface then weak magnetic material. Non magnetic or weakly magnetic is removed from the magnetic surface either by gravitational, inertia, or hydrodynamic drag force. The particle deflection lies on the fact that particles with different magnetic susceptibility, size, and specific gravity have different moving paths under non-uniform magnetic field. The commercial high density magnetic separators utilizing the particle entrapment concept include Jones Separator and Kolm-Marston separator. Jones separators can concentrate both coarse(<5mm) and fine-grain(<1mm) of weakly magnetic ores (Parker, 1993). The Kolm-Marston High Gradient Magnetic Separator (HGMS) produces magnetic flux density of two orders of magnitude higher

than that of the Jones Separator and is exclusively designed for fine particles (<100 μm) and paramagnetic substances.

The efficiency for the magnetic separation decreases when the particle size is smaller. The remedy for separation of fine relies mostly on using the carrier along with adjusting the zeta potential of the feeding pulp. Wang and Forresberg (1994) found that the separation efficiency increased when fines were agglomerated. The pH near the zero point of charge (zpc) promotes the homo-aggregation and minimizes the hetero-aggregation with gangue materials. The magnetic susceptibility of the paramagnetic substances increased as they flocculated with ferromagnetic substances. The factors governing the flocculation include pH, particle size distribution, pulp density, electrolytic coagulation, hydrophobic bonding, polymer bridging, and magnetic bonding. Svobado and Hencl (1985) proposed a theory for magnetic flocculation, which states that a suspension of magnetic particles can be flocculated within a sufficiently high external magnetic field. When the optimized magnetic field was applied, a uniform and high grade floc was formed. Increasing the magnetic field promoted numerous flocs of lower grade. Adding chemical additives enhanced the selectivity of floc formation. Pugh et al. (1994) studied the magnetic flocculation of hematite and chromite. They found that the best agglomeration was at pH near zpc, 5.3 for hematite and 6.0 for chromite.

2.1.3.4 Other Beneficiation. The alternatives to the three main beneficiation mentioned include but not limit to the direct leaching method and electrostatic precipitator. Amer (1992) concluded that the optimum condition for leaching chromite particles smaller than 64 μm as a sulfate compound was 50% sulfuric acid at 250°C for 30 min. Increasing

temperature, leaching time, acid concentration, and grinding enhanced the extraction of chromium.

Most of examples given are wet processes, which does not mean the dry processes do not exist. The electrostatic separation utilizes the electric field coping with other forces to develop a distinct trajectory for different particles. Under the electric field the conductive particles are polarized and exchange ions with the moving drum on which they are loaded. The gain or loss of electrons results in negative or positive charges. The uncharged particles remain falling in the same trajectory, while the conductive substances fall under the electric field on different trajectories. The factors effecting the electrostatic separation are conductivity, size, purity, and specific gravity.

2.1.3.5 Technical **Difficulty of Beneficiation with Fines.** Sivamohan (1990) described the difficulty in dealing with fines (100 μm) and ultrafines (20 μm) in the separation by floatation. The very fine particles have small mass but high surface area. Small mass leads to low particle momentum, particle entrapment, difficulty in overcoming the barrier between particles and particle, and particle and air bubble. High surface area causes high dissolution rate of surface ions, adsorption of a large quantity of chemicals, high viscosity, and particle and bubble coating. Fine particles have a high surface energy per unit area due to the crack, imperfection of crystals, and dislocation, which lead to non-specific adsorption of the reagent.

2.1.4 Agglomeration of Fines

Due to a century long of iron production, lump or bulk ore is depleting and the consumption of low grade ore is increasing. Low grade ore needs beneficiation including grinding and concentrating. The beneficiation unavoidably produces fines. The agglomeration of fines improves permeability of the charge into the furnace thus increasing gas-solid contact, reduced the dust blown out especially in the counter-current blast furnace, and reduced the burden on the off-gas treatment. The agglomerated particle should have its size between 6 to 25 mm and be sufficiently strong so to tolerate the transportation and storage. There are four major types of agglomeration including pelletizing, sintering, nodules, and briquettes. However, pelletizing and sintering are major agglomeration processes. The sintering process produces clinker-like particles from a mixture of fines and fuel. The sintering temperature is around 1300-1480°C. It is a simple process but needs a proper process control to get the optimum performance. Poor ignition causes spotted burning while too intense burning causes slag formation over the sintering bed. Sintering products degrade badly during the transportation and storage. The sintering plant normally is located close to the steelmaking plant. During pelletizing, fines are mixed with 9-12% of water and combining agent such as bentonite, clay, or hydrated lime and heated to form pellets or balls. Both of the agglomeration processes are found to improve the productivity of steel.

2.2 Production of Iron and Steel.

By definition, iron is an iron alloy that contains high concentration of carbon and is not formable by forging or rolling. Steel is an alloy of iron that is malleable within some

temperature ranges and contains manganese, carbon, and other alloying elements. In other words, steel is refined iron.

2.2.1 Ironmaking Process

There are three basic processes in the production of iron namely blast furnace, direct reduction, and iron smelting. The blast furnace produces most of pig iron in the US, 55 million tons comparing to the 0.44 million tons from the direct reduction process (Kavanagh et al., 1998). The feed materials for blast furnace mainly are iron ore, coke, and limestone or dolomite. The fed iron ore has iron content between 50 and 70%. The lower grade of iron ore needs grinding, beneficiation and finally pelletization or agglomeration. The pellet normally has iron content between 60 and 65%. The major minerals constitutes iron ore are hematite, magnetite, siderite, and goethite. Today, 97% of the usable iron ore is in a form of pellet of fine magnetite (Kuck, 1998). The addition of limestone is to react with the gangue materials, i.e. SiO_2, to produce slag with a composition that is suitable for the removal of sulfur and other impurities. The blast furnace operation is similar to the counter current reactor where the feed descends from the top and the heated air ascends to the top. The heated air enters the blast furnace through tyeers at 1600-2300°F. The heated oxygen in air then reacts with carbon in coke. The combustion releases energy bringing the temperature to between 3600 and 4200°F. With excessive carbon, CO_2 reacts with C and forms CO, the reducing gas. Equations 2.1 to 2.4 describe the reduction of iron oxide in the blast furnace, and the gasification of carbon by equations 2.5 and 2.6 (Ricketts, 1999).

$$3Fe_2O_3 + CO = CO_2 + 2Fe_3O_4 \quad \text{begin at } 850°F \quad (2.1)$$

$$Fe_3O_4 + CO = CO_2 + 3FeO \quad \text{begin at } 1100°F \quad (2.2)$$

$$FeO + CO = CO_2 + Fe \quad \text{begin at } 1300°F \quad (2.3)$$

or $$FeO + C = CO + Fe \quad (2.4)$$

$$C + O_2 = CO_2 + \text{heat} \quad (2.5)$$

$$C + CO_2 = 2CO \quad (2.6)$$

Approximately, the production of 55 million tons of pig iron requires 23 million tons of coke (Kavanagh et al., 1998). The excessive amount of carbon is required to allow the production of CO. It takes about 6-8 hrs for the feed to travel down to the bottom of the furnace. The resident time of heated gas is 6-8 seconds. The solid iron ore was reduced as it trickled through the furnace until completely reduced, melted, and formed liquid iron at the bottom of the furnace with separated lighter slag afloat on top. The liquid iron and liquid slag were tapped out of the furnace at preset intervals.

The pig iron contains 93.5-95.0% of Fe, 03-0.9% of Si, 0.025-0.05% of S, 0.55-0.75% of Mn, 0.03-0.09% of P, 0.02-0.06% of Ti, and 4.1-4.4% of C (Ricketts, 1998). The blast furnace requires the use of the good quality coke. The coke is a carbon concentrated coal, after being subjected to the carbonization process at 1100°C for 18-24 hrs under the oxygen deficit environment (Valia, 1999). The carbonization removes impurities such as hydrogen, oxygen, nitrogen, and sulfur from the coal.

The limitation of the coal of metallurgical grade promotes the search for new technology in iron making. The other technologies available in the market today are the direct reduction and iron smelting processes. However, the production of pig iron from blast furnace still dominates. The direct reduction produces less than 1 percent of the pig

iron production. The direct iron reduction technology allows the use of regular coal or natural gas as a source of reducing gas and thermal energy. The reduced iron is in a solid form. Many direct reduction technologies are under development, sharing the similarities in raw materials and reduction procedures. The commercially developed one in the industry is MIDREX process. The direct reduction process produces iron of a better quality, 90-94%Fe, which can substitute the steel scrap and can be charged directly into the steelmaking furnace. The direct reduction requires a high quality ore because there is no separation of impurities as slag. The operating temperature is high enough to allow the reduction but not to liquefy the ore.

The iron smelting process produces liquid iron from a mixture of coal and ore fines or concentrate. One such well-known iron smelting processes is COREX. The bath smelting process consists of the pre-reduction and smelting processes. During the smelting process the iron oxide is reduced and separated as liquid metal with slag covering on top. Oxygen is blown to the top of the slag. Heat is released from the burning of carbon or coal in a mixture to carbon monoxide. The slag acts as a separator between the oxidizing and reducing zones. Both direct reduction and iron smelting are under development and is believed to increase their production rates.

2.2.2 Steelmaking Process

There are two major steelmaking processes: the integrated blast furnace/basic oxygen furnace (BOF) and the electric arc furnace (EAF). The EAF production accounts for 40% of the liquid steel produced. Small scale or mini mills unlike the full scale BOF production operate the EAF. In the BOF, oxygen is blown to the hot metal to oxidize the

impurities such as C, Si, Ca, which are separated out as the liquid slag. Part of iron will also be oxidized to iron oxide, which subsequently incorporates into slag. The steelmaking slag, therefore, has higher iron concentration than that of blast furnace slag. The liquid pig iron, iron and steel scrap constitute the charge for the steelmaking furnace. Dolomite or lime can be fed initially or injected during the operation for the purpose of de-slagging. The quality of steel depends on properties of raw materials and the operating conditions during refining and tapping. The ladle then is sent to the secondary steel refining.

Most of minimills, EAF, use steel scrap instead of pig iron since they do not produce pig iron. The EAF is believed to continuously replace the BOF with its better energy efficiency and lower gas emissions. The liquid pig iron, accounting for 65 to 90% of raw materials, and the recycled scrap are raw materials for the BOF. The steel, after being tested and reaching the requirement, is cast into different forms: carbon steel, stainless steel, and other alloys. Table 2.4 gives examples on the constituents of carbon and stainless steel. The concentration ranges given are the broad concentration ranges covering series of steels of types specified.

The United States is a major producer of stainless steel. The important ingredient in stainless steel production is chromium. Chromium plays the important roles when it is present in the steel. It resists corrosion and helps preventing the oxidation at elevated temperatures. Higher chromium content gives higher corrosive resistance to the steel. The chromium concentration in metal alloy varies depending upon the application. The stainless steel contains higher than 12% chromium. The low chromium steel, structure

steels, and steel tools, contain chromium in the range of 0.5-3%. The chromium concentration in intermediate steels ranges from 4-10 %.

Table 2.4 Compositions of Carbon and Stainless Steels (Lankford et al., 1985)

Types of steel	Concentration (% wt.)						
	C	Mn	P	S	Si	Cr	Ni
Carbon steel							
-Carbon steel*	0.06-1.03	0.25-1.00	0.04	0.04-0.05			
-High-Manganese*	0.10-0.71	1.10-1.65	0.04	0.05			
Stainless steel							
-Wrought Cr-Ni austenitic	0.08-0.25	2.00-16.0	0.01-0.20	0.02-0.15	1.00-3.00	16.0-26.0	0.75-37.0
-Wrought martensitic Cr	0.10-1.20	1.00	0.04	0.03-0.04	0.50-1.00	4.0-18.0	
-Wrought ferritic Cr	0.08-0.20	1.00-1.50	0.04-0.06	0.03-0.15	1.00	10.5-27.0	

* - Applicable only to semifinished products for forging, to hot-rolled and cold-finished bars, to wire rods, and to seamless tube

The chromium is consumed mostly as ferrochromium in the steel industry. The ferrochromium is added during the production of steels or metal alloys in a proportion corresponding to the steel grades. The Ferrochromium is prepared from high-grade chromite ore. High-grade metallurgical ore should contian 48% of Cr_2O_3 and the Cr:Fe ratio should be higher than 3:1 (Udy, 1956). During the production of ferrochromium, chromite ore is ground in the electric furnace or open hearth furnace and mixed with a carbonaceous reductant such as carbon, or a non-carbonaceous such as silica or alumina. The impurities such as MgO, and $A1_2O_3$ are fluxed out as slag.

2.2.3 Slag Chemistry

The iron and steelmaking processes require the separation of impurities from the iron ore. Most of the impurities, as oxides, have very high melting temperatures; i.e. 1600°C for SiO_2. The separation of impurities at lower temperature requires the addition of compounds that have high affinity to the impurities and react with the impurities to form intermediate compounds having lower melting point. This process is so called fluxing.

The substances which are considered basic oxides are those which are compounds of the elements forming basic compounds in ordinary chemical reactions in water solution, i.e. CaO, MgO, and Na_2O. The SiO_2 is an only example of acidic flux. There are compounds of elements that act both as acid and base depending on the slag composition. For example, alumina behaves as a basic oxide in the slag rich in silica, but behaves as acidic oxide in the calcium rich slag. Different kinds of oxide serve different purposes. The CaO is preferred if the charge requires the sulfur removal. The slag rich in MgO is suitable for the construction application due to its high resistance to abrasion, but not suitable for the cement production.

The liquid slag shows wide diversity of properties at different chemical compositions and temperatures. The behavior of slag is mostly described through phase diagrams.

2.2.4 By-Products from Iron and Steelmaking Processes

By-products from both iron and steelmaking processes are slag, dust, and sludge. The sludge is produced after washing the flue duct with water. The compositions of slag of different kinds, from Japanese steel industry, are shown in Table 2.5.

Table 2.5 Compositions of Different Types of Slag (Okumura, 1993)

Types of slag	Concentration (% wt)						
	SiO_2	CaO	Al_2O_3	T.Fe	MgO	S	MnO
Blast furnace slag	33.7	41.5	13.9	0.2	6.5	0.99	0.5
Steel making slag							
-Hot metal pretreatment	13.8	44.3	1.5	17.5	6.4	0.07	5.3
-Electric furnace oxidation	19.0	38.0	7.0	15.2	6.0	0.38	6.0

T.Fe - Total Iron

The steel industry has increasingly reused and recycled by-products from iron and steel productions. Table 2.6 tabulates generation rates, uses, and limitations in application of those by-products. The steelmaking slag has a high concentration of iron, which can be recycled to the steelmaking process. The major sources of recycled iron are from by-products of steelmaking such as slag and the steel scrap.

The slag properties depend on chemical compositions and cooling rates. There are three different kinds of iron slag: air-cooled, expanded, and granulated slag. Air-cooled slag is produced from the molten slag cooling in an open pit. The air-cooled slag is porous due to the escaping gases. Upon crushing the slag forms a suitable aggregate for its rough surface, providing good friction to cement binder. It has a low coefficient of thermal expansion, good fire resistance, and high water absorption owing to its high porosity.

Under controlled cooling either by water or water with steam and compressed air, the expanded slag is formed. The steam and air give the vesicular nature and porosity to the slag. The expanded slag is lightweight and suitable for reuse as construction aggregate.

Table 2.6 Recycling Status of By-Products from Iron and Steel Industries. (Kavanagh et al., 1998)

	Production Per ton of iron/steel	Total production (Million Tons)	Iron Inclusion (%)	Recycling Values
Blast Furnace				
Slag	15-35%	12.4	<5%	Mainly used in land reclamation, landfill, and as an aggregate. No recycle of iron unit.
Flue Dust	1-4 %	0.4	10-35% Fe 30-75% C	Recycled to the sintering plant and fed back to the blast furnace. The fine size distribution limits the recycling.
Sludge	1-4 %	0.7	15-48% Fe 20-65% C	Mainly landfilled or stockpiled due to its high moisture content (25-45%), the fine size distribution, and its chemistry, high zinc adversely affect the refractory lining.
BOF				
Slag	100-440 lbs	6.0	20-25% Fe	Frequently crushed and fed back to the blast furnace to utilize the slag forming oxides and to recycle iron unit. Used as road construction aggregate, but not as worldwide as BF slag due to its potential hydration of free lime, and in cement industry. About 50% of iron are recovered. Less than 40% of slag is recycled.
Dust	8-62 lbs	0.3	60-67% Fe	Mainly used in the production of cement and as a coloring agent for concrete. The barriers to recycling back to BF are its fine size distribution, its high moisture content, it high zinc content. Less than 50% of dust is recycled.
Sludge	8-62 lbs	1.3	50-63% Fe	Similar to the reuse of the BOF dust.
EAF				
Slag	230 lbs	4.7	20-25% Fe	Similar to BOF slag. About 50% of iron are recovered.
Dust		0.6	20-40% Fe	Classified as RCRA-listed hazardous waste K061 due to its heavy metal contents from the steel scrap; i.e. lead and zinc from galvanized steel, chromium and nickel from stainless steel. Mostly is recycled for zinc recovery.

The molten slag, under high-pressure water jet, forms glass due to the very rapid cooling. This kind of slag, granulated slag, is particularly used in the cement production because of its pozzolanic characteristic.

Steel slag is dense and hard due to the iron impregnation. It is suitable for road base application. Steel slag contains free lime and normally requires stockpiled for at least 6 months to allow the complete hydration of free lime, and the expansion and disintegration of dicalcium silicate. In Japan, the reuse rate of slag both from iron and steel making industries is higher than 90%. The expansion of steelmaking slag is overcome by applying the steam aging process (Okumura, 1993).

2.3 Iron, Steel, and Chromium Market

2.3.1 Iron ore

The United States is the sixth biggest producer of iron ore and the third pig iron producer. From 1993 to 1998, the domestic production of iron ore satisfied only 75% of the domestic consumption, Table 2.7. The United States imported 25% iron ore for the domestic consumption, mainly from Canada. The value of the usable ore produced annually was approximately $1.9 billion.

Table 2.7 Iron Ore Production in the United States (Kirk, 1999)

Iron ore	Production rate(Million metric tons)		
	1996	1997	1998
Domestic production	62.1	63.0	62.0
Imports	18.4	18.6	18.5
Apparent consumption	72.0	73.0	74.3

Table 2.8 Quality of Iron Ore and its Supplied Forms (Kuck, 1998)

Year	Crude ore mined	Usable ore produced	Iron contained in usable ore	Recoverable iron content of crude ore (%)	Direct-shipping ores***	Concentrates	Agglomerates
1950	-	-	-	-	71.4	23.2	5.0
1955	-	-	-	-	67.8	29.2	7.6
1960	-	-	-	-	39.6	33.2	17.5
1965	180.8	88.0 (48.6%)*	50.2 (57.0%)**	27.8%	20.0	32.9	36.0
1970	215.9	90.4 (41.9%)*	53.7 (59.4%)**	24.9%	7.1	25.3	58.8
1975	218.0	79.6 (36.5%)*	48.8 (61.3%)**	22.4%	1.8	13.7	64.6
1980	215.5	70.7 (32.8%)*	44.6 (63.1%)**	20.7%	1.2	3.7	65.8
1985	151.6	49.5 (32.7%)*	31.8 (64.1%)**	21.0%	0.06	1.8	47.7
1988	183.2	57.5 (31.4%)*	36.5 (63.5%)**	19.9%	0.7	0.9	56.0
1989	187.8	59.0 (31.4%)*	37.4 (63.4%)**	19.9%	1.0	0.7	57.3
1990	181.4	56.4 (31.1%)*	35.7 (63.3%)**	19.7%	0.8	0.8	56.4

Weight - in million metric ton

* - Weight percentage of usable ore calculated from the production of crude ore

** - Iron content in usable ores

*** - Crude ore shipped as-is

From USGS Iron Ore Statistical Compendium, the grade of iron ore, or the iron content, has continuously decreased, Table 2.8. The lower grade ore required beneficiation; crushing to the liberation size and concentrating iron. Prior to charging, the concentrate needs to be agglomerated. The increasing of the usable ore supplied as agglomerates reflects the lower grade of iron ore. In 1990, the usable ore was only 31.3% by weight of the crude ore, the iron content of the usable ore was 63.3%, and the recoverable iron content in the usable ore was only 19.7% of the crude ore.

2.3.2 Steel

The steel demand in the United States is still strong though a large portion is imported due to the inexpensive price. The production of steel is approximately 100 million tons annually with additional 25 million tons imported. The value of the steel produced is close to $50 billion annually (Kavanagh et al., 1998). The United States is the third biggest producer of raw steel. Table 2.9 shows the production of raw steel and the product forms.

Table 2.9 Production of Iron and Steel (Fenton, 1998)

Iron and steel	Production rate(Million metric tons)		
	1996	1997	1998
Pig iron production	49.4	49.6	50.1
Raw steel production :	95.5	98.5	102
Carbon steel	84.9	97.0	88.0
Stainless steel	1.9	2.2	2.0
Other alloys	8.7	9.3	8.6
Still mill products:	91.5	96.0	97.8
Import	26.5	28.3	34.6
Export	4.6	5.5	4.7

Still mill products are end products of the raw steel, i.e. wires, pipes, sheets, and bars.

2.3.3 Chromium

The United States is not a major chromite ore production country, but a leader in the production of alloys and stainless steel. The United States consume 13% of the world chromite ore production. The metallurgical industry utilized most of the imported chromium. The stainless steel production accounts for 76% of chromium consumption in the metallurgical industry (Papp, 1999). The sources of chromium available in the market are chromite ore, ferrochromium, and chromium metal. Table 2.10 summarizes types of chromium imported by the United States.

Chromite ore is graded by its Cr_2O_3 content. Regular chromite ore has chromic oxide content ranging from 35-55%. Ferrochromium contain 50-65% of chromium while chromium steel contains high purity of chromium, over 99%. The United States presently imports chromium as ferrochromium instead of chromite ore as in the past.

Table 2.10 Statistics of Imported Chromium (Papp, 1999)

Chromium	Consumption rate (Thousand metric tons)		
	1996	1997	1998
Import			
-Chromite ore	79.2	96.6	118.0
-Chromic content (Cr_2O_3)	45.2%	45.1%	45.4%
-Chromium ferroalloy	267.0	237.0	245.0
-Chromium metal	8.7	9.8	9.5
Values (Imports)	$463	$450	$421
Values (Exports)	$111	$107	$102

Weight - in Thousand metric ton
Value - in Million dollars

2.3.4 Iron and Steel Slag

The iron slag from blast furnace accounts for 65% of the overall slag production. Table 2.11 summarizes the production of the slag and Table 2.12 contains the utilization of each kind of slag (Kalyoncu, 1998). The slag production in Table 2.11 was estimated from the crude iron and steel production: 25-30% of the crude pig iron production as iron slag, and 10-15% of the crude steel production as steel slag.

Table 2.11 Statistics of Slag Production (Kalyoncu, 1998)

Slag	Production rate (Million metric tons)		
	1995	1996	1997
Slag production	21	20.5	21.0
Import	0.28	0.35	0.35
Export	0.004	0.003	0.003
Consumption, apparent	21.3	20.8	21.4
Average Price ($/ton), f.o.b	6.9	6.9	7.0

The iron slag is more valuable than the steel slag because of its better characteristics. Table 2.13 shows the production of each type of slag and their prices. The expanded and granulated slags are much more valuable than air-cooled and steel slag. The granulated slag is included in the expanded slag to avoid disclosing company proprietary data.

Table 2.12 Application of Iron and Steel Slag (Kalyoncu, 1998)

Application	Iron slag (%)	Steel slag (%)
Road base	43	40
Fill	11	20
Asphalt concrete aggregates	40	16

The proportion of granulate slag to air cooled slag in Japan is 15.4 to 9.3 million tons (Okumura, 1993), which is unlike that of the United States. There appears to be a

growing demand in the US concrete industry for the granulated blast furnace slag as a pozzolan or cement extender. The production of granulated blast furnace slag declined due to the decommissioning of blast furnaces. It might be possible that the import of granulated slag will increase to compensate for the domestic decline (Kalyoncu, 1998).

Table 2.13 Production Rates and Unit Prices of Slag (Kalyoncu, 1998)

Slag types	Production (Million metric tons)		Unit price ($/metric ton)	
	1997	1998	1997	1998
Air-cooled slag	10.1	10.3	$5.73	$6.12
Expanded slag	1.8	1.9	$30.6	$33.6
Steel slag	7.0	6.2	$3.5	$3.7

2.3.5 Prices

The Pricing of iron and chromium ores are dictated by the steel market, since 98% of iron ore is consumed in the manufacture of iron and steel. Table 2.14 summarizes the pricing of components in iron and steelmaking industries (Papp, 1998; Fenton, 1998; Kulyoncu, 1998; Kuck, 1998). The decreasing price during 1998 is partly due to the economic crisis in Asia.

Table 2.14 Unit Prices

Components	1997	1998
Iron Ore, Fine	$28.9**	$29.7**
Iron Ore, Pellet	$52.1**	$53.6**
Hot-Rolled Steel Bar	$434.5*	$412.5*
Iron and Steel Scrap	$130.5*	$108.3*
Chromite Ore	$74*	$74*
Ferrochromium	$1212**	$1027**
Chromium Metal	$7419*	$7576*

* -- Per metric ton, gross weight

** -- Per metric ton of iron or chromium contained in ore or metal

The chemical compositions and structures of iron ore affect the blast furnace productivity in the ironmaking process. Fines refers to iron ore with majority of particles smaller than 4.75 mm. The production cost of iron from fines and pellets are the same. However, pellets are more expensive than fines due to its preprocessing cost. The selected form of feed ore also depends on the steel demand, if productivity is of no concern—low steel demand-- fines, as in Europe and Japan, will be used.

2.4 Summary

Chromium contaminated soils contain high iron concentrations and are a potential source of iron. Iron and chromium in soils can be concentrated as metal oxides or reduced and separated as metal. The concentrating, the reduction, and phase separation are similar in theory to the ore processing, reduction, and metal separation.

The ores of concern for the industry are iron and chromite ores. The high grade ore, both iron and chromite ores, require no furthur beneficiation unlike the low grade ore which contains larger amount of impurities. The concentrating process of mineral ore from gangue material begins with grinding to liberate the mineral grain. The concentrating techniquies then are applied to concentrate the ground ore. The differences in properties between minerals and impurities, either their magnetic properties, density, and the affinity to air bubble or certain chemicals, enable the separation. These separators are available in the commercial scale and very well researched. The concentrated ore need agglomeration before feeding to the furnace. The iron content of the agglomerate is normally as high as the high grade ore.

Under the reducing environment the metal oxide reduces to metal. The reduction occurs either in a solid state or liquid state. The iron and steel industry is one of the very well established industry, yet it continues developing and improving the processes to increase efficiency and reduce environmental impacts. The dominating iron production process is balst furnace process with the developing of the direct and smelting reduction. Iron is not directly used but further refined and cast as steel of different kinds. Steel is one of the most recylced materials and supplies almost half of the feed material for steel production besides pig iron. Chromium improves the quality of steel in term of the resistant to oxidation and corrosion. The stainless steel contains at least 12% chromium by weight.

The by-products from both iron and steel industry find their ways in the construction industries as road base material, construction aggregate, and in the production cement. The properties of slag dictate their destinies and values. The iron slag from blast furnace possesses better quality and is more valuable than steel slag. The slag satisfing the requirement of the cement industry has the highest monetary value.

Though the iron and steel industries do not raise much excitement in the market and the investment arena, their annual productions worth approximately $55 billions. The US imported iron ore, as much as 25% of its consumption, and chromium, almost 100% of its consumption. The iron ore costs $29/ton. The slag, depending on its properties, has values of $6 and $30/ton for construction and cement application. The processing of contmainated soil can create revenue which can at some degrees level off the operating cost.

The information regarding iron and steel industries available through publication still does not portrait the complete picture of the industry. To really get the recycling program to work, the corporation of the iron and steel industry is definitely required especially in terms of their needs, limitations, and specifications.

CHAPTER 3

REDUCTION PROCESS

The ironmaking process consists of two main steps: the reduction of iron oxide and the separation of metal. The reduction proceeds when the metal is more stable than its oxide state. Changing the environment parameters, i.e. temperature and oxygen partial pressure, affects their stability, represented by the free energy of the compound. The reduction of iron oxide occurs through either direct reduction or indirect reduction. Direct reduction refers to the reduction by solid carbon in direct contact with iron oxide. The reduction of iron oxide by carbon monoxide is called indirect reduction. Carbon monoxide reacts with iron oxide to form carbon dioxide, which further reacts with carbon and forms carbon monoxide, the gasification of carbon. There are several factors that affect the chemical reaction rate including but not limit to iron oxide species, iron oxide activity, and temperature. Not only the chemical reaction can govern the reduction rate but also the diffusion, the dissolution, and the transport of iron oxides.

For the direct reduction the governing factors are the gas flow rate, the diffusion of gas through boundary layer, the heat transfer, and so on. In bath smelting where the reduction occurs in the liquid state, the following factors contribute to the reduction rate: the viscosity, dissolution rate, mass transfer, the intensity of stirring, slag composition, and so on. Nonetheless these two processes are also subjected to the same influences, for example, the chemical reaction rate, the gasification rate, the reaction area, and temperature. Each factor subsequently influences the others, i.e. as the temperature

increases, the viscosity decreases, the mass transfer rate increases, and the reduction rate increases. The formation of products also affects the viscosity and the other factors.

The reduction of iron oxide is complicated not only because of the competing rate limiting processes but also the paths of reduction. The reduction occurs either in the solid state or liquid state or both. The reducing agent can be solid carbon or solute carbon or carbon monoxide or the combination. Not to mention that the iron or chromite ore can be mixed crystals, which is not as reducible as pure oxide. Even with the same crystal type, the different porosity could result in different reduction behavior. The other factor that aggravates the complexity is the instrument limitation. Regardless of all the complexity, the iron and steel industries established themselves more than half a century ago through extensive research. There is ongoing research, which brings a better understanding on the reduction process (Kavanagh et al., 1998).

In any research, there is always a theoretical background enabling ones to predict the outcome to which the experimental results will be compared. In this research the principle of reduction and metal separation is adopted from the iron and steelmaking research along with fundamental thermodynamics. Research and principles are gathered herein to provide a general background and basic understanding on the complicated reduction process.

It is far from possible to delineate the exact reduction path especially for a heterogeneous system such as soil. Most of the research performed tests on pure iron oxide or high grade or agglomerated ores. Many factors can be controlled when working with simple systems. Chapter 3 presents the reduction in the order of the stability, the

reducibility of different species of iron oxide, the gasification of carbon monoxide, the direct and indirect reduction, and factors affecting the reduction process.

3.1 Stability of Oxides Relative to Elements

3.1.1 Pure oxide

Equation 3.1 shows an example of the reduction of oxide to metal. The standard free energy of formation for a reaction, ΔG°, determines the stability of oxide and its element at different temperatures. At equilibrium the ΔG° is equal to –RTln(K), K is the equilibrium constant, Equation 3.2.

$$Fe_{(s)} + \frac{1}{2}O_{2(g)} = FeO_{(s)} \tag{3.1}$$

$$\Delta G^{\circ} = -RT\ln(K) = -RT\ln\left(\frac{a_{FeO}}{a_{Fe} * a_{O_2}^{1/2}}\right) \tag{3.2}$$

$$\Delta G^{\circ} = -RT\ln\left(\frac{1}{a_{O_2}^{1/2}}\right) \tag{3.3}$$

$$\Delta G^{\circ} = -RT\ln\left(\frac{1}{p_{O_2}^{1/2}}\right) \tag{3.4}$$

$$\ln\left(P_{O_2}^{1/2}\right)_{(eg,T)} = \frac{\Delta G^{\circ}_{(FeO_{(s)} = \frac{1}{2}O_{2(g)} + Fe_{(s)})}}{RT} \tag{3.5}$$

The solubilibity of oxide phase in metal phase and vice versa is negligible, therefore, composition of oxide and metal phase does not depart measurably from their pure phases (Dehoff, 1993; Gaskell, 1995; Mehl and Bever, 1953). Assuming the standard state of oxide and metal to be pure oxide and metal at the equilibrium temperature, the activity of both oxide and metal are equal to 1 (Dehoff, 1993; Lupis,

1983; Gaskell, 1995; Mehl and Bever, 1953). The equilibrium of metal and oxide then is govern by activity of oxygen, Equation 3.3. The operating pressure of the iron and steelmaking processes is at atmospheric pressure, 1 atm. At low pressure, up to several atm and at elevated temperature, the ideal gas behavior can be assumed (Smith et al., 1996; Lupis 1983; Dehoff, 1993). The activity of oxygen then is equal to its partial pressure (Equation 3.4). The required oxygen partial pressure for the equilibrium between oxide and metal phases is calculated from Equation 3.5.

The oxygen partial pressure can be controlled by applying a proper mixture of CO and CO_2. The equilibrium study of C-CO-CO_2-O_2 system allows the establishment of a relation between the oxygen partial pressure and the CO/CO_2 ratio. According to the first and second law of thermodynamics, after rearrangement, the change of entropy is the system is given in Equation 3.6. The definition of equilibrium system is an isolated system having a maximum of entropy (Dehoff, 1993). For an isolated system, dU and dV are equal to 0. Equation 3.7 subsequently defines the equilibrium condition. For the C-CO-CO_2-O_2 system, the equilibrium condition follows Equation 3.8. Equation 3.9 and 3.10 show the conservation of mass of the system. Equations 3.11 and 3.12 are derived from the differentiation of Equation 3.9 and 3.10. Substitute Equations 3.11 and 3.12 into Equation 3.8, Equation 3.13 is obtained.

$$dS = \frac{1}{T}dU + \frac{P}{T}dV - \frac{1}{T}\sum_{k=1}^{n}\mu_k dn_k \tag{3.6}$$

$$\sum_{k=1}^{n}\mu_k dn_k = 0 \tag{3.7}$$

$$\mu_{C_{(s)}} dn_{C_{(s)}} + \mu_{CO_{(g)}} dn_{CO_{(g)}} + \mu_{CO_{2(g)}} dn_{CO_{2(g)}} + \mu_{O_{2(g)}} dn_{O_{2(g)}} = 0 \tag{3.8}$$

$$n_{C_{(s)}} + n_{CO_{(g)}} + n_{CO_{2(g)}} = N_C \tag{3.9}$$

$$n_{CO_{(g)}} + 2\,n_{CO_{2(g)}} + 2n_{O_{2(g)}} = N_O \tag{3.10}$$

$$dn_{C_{(s)}} + dn_{CO_{(g)}} + dn_{CO_{2(g)}} = 0 \tag{3.11}$$

$$dn_{CO_{(g)}} + 2\,dn_{CO_{2(g)}} + 2\,dn_{O_{2(g)}} = 0 \tag{3.12}$$

$$\left[\mu_{CO_{(g)}} - \left(\mu_{C_{(s)}} + 1/2\,\mu_{O_{2(g)}}\right)\right] dn_{CO_{(g)}} + \left[\mu_{CO_{2(g)}} - \left(\mu_{C_{(s)}} + \mu_{O_{2(g)}}\right)\right] dn_{CO_{2(g)}} = 0 \tag{3.13}$$

$$\mu_{CO_{(g)}} - \left(\mu_{C_{(s)}} + 1/2\,\mu_{O_{2(g)}}\right) = 0 \tag{3.14}$$

$$\mu_{CO_{2(g)}} - \left(\mu_{C_{(s)}} + \mu_{O_{2(g)}}\right) = 0 \tag{3.15}$$

Equations 3.14 and 3.15 are the conditions of equilibrium of reactions 3.16 and 3.17. At equilibrium, the equilibrium constant (K) is related to the standard free energy of formation as given in Equation 3.2. Assuming the state for carbon is the standard state, pure carbon at the equilibrium temperature and pressure, its activity is equal to 1. The gas phase behavior follows the ideal gas mixture, activities of gas phase components are equal to their partial pressure. Equations 3.18 and 3.19 describe the equilibrium conditions of reactions given in Equation 3.16 and 3.17 (Gaskell, 1995). From Equations 3.18 and 3.19, the equilibrium relation among CO, CO_2, and O_2 is given in Equation 3.20.

$$C_{(s)} + 1/2\,O_{2(g)} = CO_{(g)} \qquad \Delta G^\circ = -111{,}700 - 87.7T \quad \textit{joules} \tag{3.16}$$

$$C_{(s)} + O_{2(g)} = CO_{2(g)} \qquad \Delta G^\circ = -394{,}100 - 0.84T \quad \textit{joules} \tag{3.17}$$

$$\Delta G^\circ{}_{Eq3.16} = -RT\ln(K) = -RT\ln\left(\frac{p_{CO}}{p_{O_2}^{1/2}}\right) \tag{3.18}$$

$$\Delta G^\circ{}_{Eq3.17} = -RT\ln(K) = -RT\ln\left(\frac{p_{CO_2}}{p_{O_2}}\right) \tag{3.19}$$

$$\ln\left(P_{O_2}^{1/2}\right) = \frac{\Delta G^\circ{}_{Eq3.17} - \Delta G^\circ{}_{Eq3.16}}{RT} + \ln\left(\frac{P_{CO_2}}{P_{CO}}\right) \tag{3.20}$$

Equation 3.5 and 3.20 show the partial pressure of oxygen at the equilibrium with iron oxide and carbon, respectively. For the reduction of iron oxide using carbon or CO/CO_2 as a reducing agent to proceed, the ratio of CO_2/CO has to be adjusted so that the oxygen partial pressure from Equation 3.20 is less than the one calculated from Equation 3.5. The $C\text{-}CO\text{-}CO_2\text{-}O_2$ system can also be view as a system of 4 unknowns, concentration of each component, with 2 equations, the mass conservation of O and C. It needs 2 more equations, bivariant system, to fully describe the behavior of the system. The two reactions, as given in Equation 3.16 and 3.17, are selected.

To facilitate the calculation of free enerygy change and partial pressure of oxygen, the free energy diagram, Figure 3.1, is prepared from the thermodynamic data: ΔH°, and ΔS°. The standard free energy change for any reaction can be expresses in terms of the standard enthalpy and entropy changes, Equation 3.21. The variation of enthalpy and entropy changes with temperature at constant pressure are given in Equations 3.22 and 3.23, where ΔC°_p is the heat capacity of products minus the heat capacity of reactants. The standard enthalpy and entropy changes of reactions are an order of magnitude larger than changes associated with altering the temperature of reaction. The second term from Equation 3.22 and 3.23 is therefore negligible. The standard free energy change of reaction, ΔG°, is expected to be linear with a slope equal to $-\Delta S^\circ$ and an intercept at T = 0K equal to ΔH°.

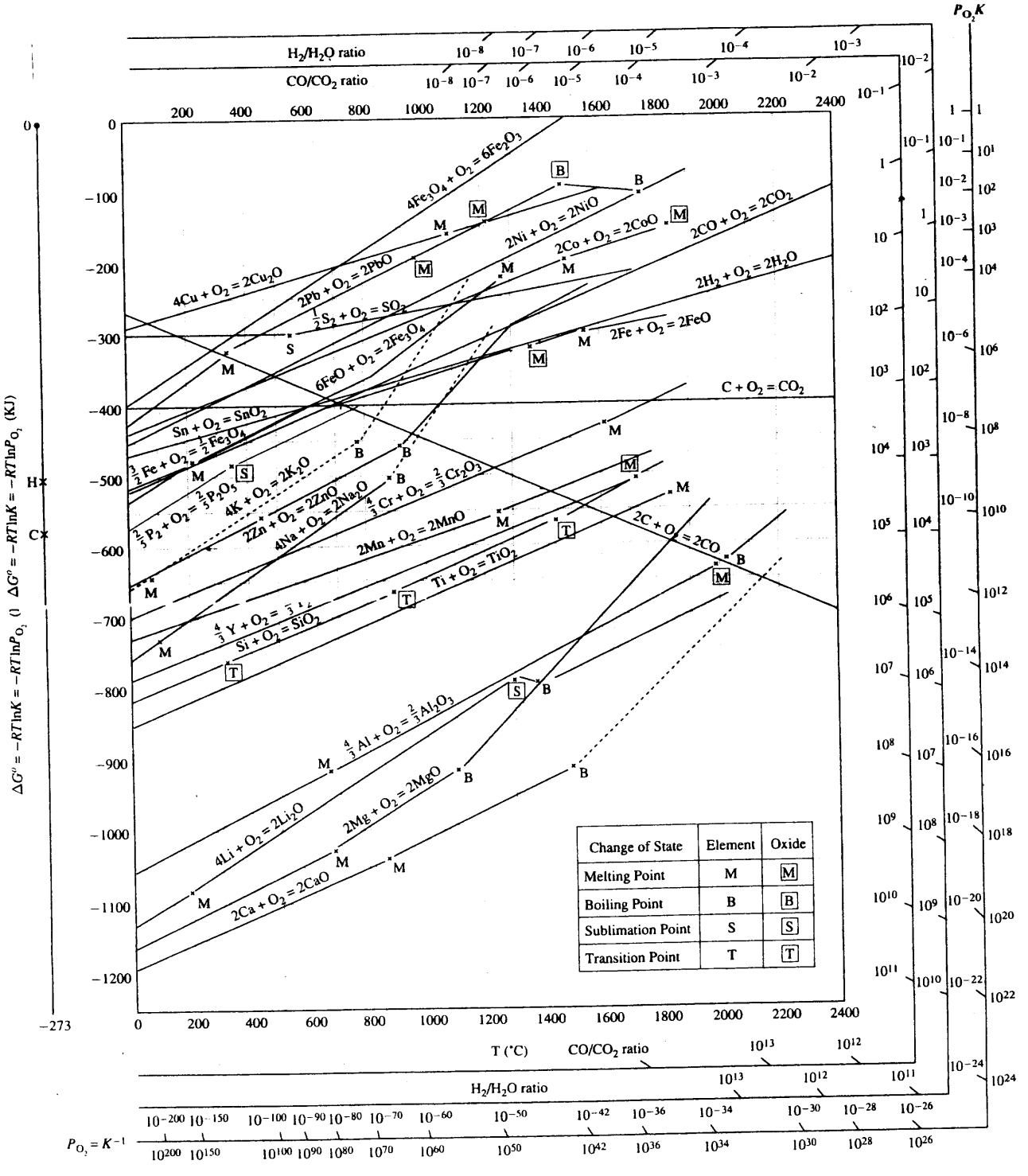

Figure 3.1 Free Energy Diagram (Dehoff, 1993)

$$\Delta G^\circ = \Delta H^\circ - T\Delta S^\circ \tag{3.21}$$

$$\Delta H^\circ = \Delta H^\circ(T_o) - \int_{T_O}^{T} \Delta C_p^o(T)dT \tag{3.22}$$

$$\Delta S^\circ = \Delta S^\circ(T_o) - \int_{T_O}^{T} \frac{\Delta C_p^o(T)}{T} dT \tag{3.23}$$

From the relation $\Delta G^\circ = 2.3RT\log(P_{O2})$, lines representing oxygen partial pressure can be drawn as shown in Figure 3.1. The figure serves as a guideline in determining the equilibrium condition for mixtures of oxides. The order of oxides in term of their stability at 1400°C is as following CaO> Al_2O_3> MgO> SiO_2> MnO> Cr_2O_3> FeO> Fe_3O_4> Fe_2O_3. The change in slope of the free energy lines at certain temperature is due to the latent heat from melting, boiling, transition, or sublimation as marked as [M], [B], and [S], respectively. The negative slope reflects the positive ΔS°, $d(\Delta G^\circ) / dT = -\Delta S^\circ$, due to the increasing volume after the reaction, for example $2C + O_2 = 2CO$. The diagram also provides the relation between the oxygen partial pressure and the CO/CO_2 ratio calculated from equation 3.20. Figure 3.2 illustrates the equilibrium of the C-CO-CO_2-O_2 system. The dash-cross line represents the equilibrium between gas phase and carbon. The dash area represents the condition where carbon deposition occurs.

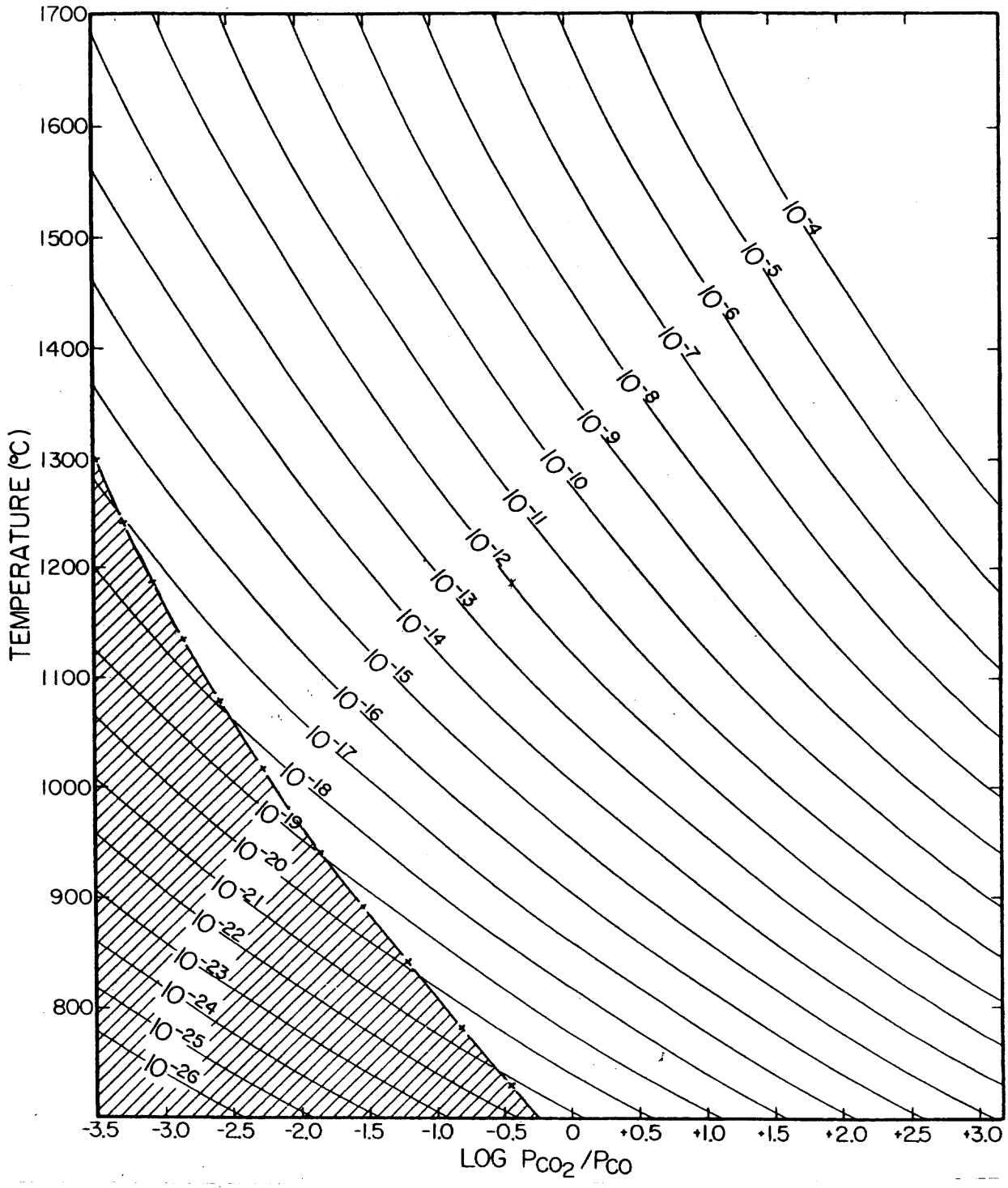

Line: oxygen partial pressures
Dash-cross line: the equilibrium conditions among CO, CO_2, O_2 and C
Shaded area: carbon deposition
Total pressure = 1 atm

Figure 3.2 Equilibrium of C-CO-CO_2-O_2 system (Muan and Osborn, 1965)

The stability of oxides relative to their carbonates and hydroxides are shown in Figure 3.3. It is obvious that the carbonate and hydroxide of calcium, magnesium, and manganese readily lose its CO_2 at temperature below 1000°C.

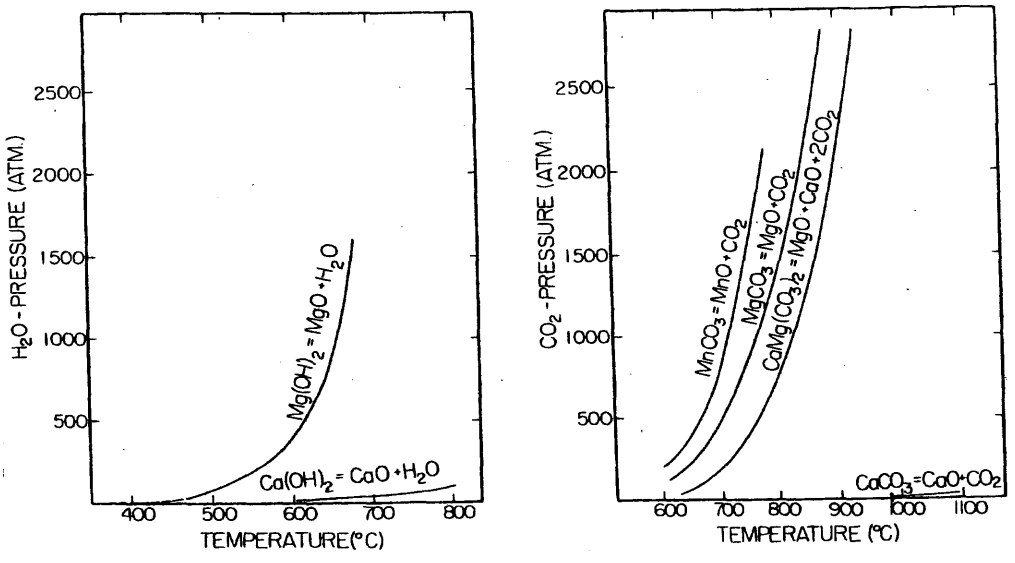

a) Oxide-Hydroxide b) Oxide-Carbonate

Figure 3.3 Equilibrium between a) Oxide-Hydroxide and b)Oxide-Carbonate (Muan and Osborn, 1965)

Figure 3.4 presents the relative stability of metals to their carbides. Figure 3.5 shows the stability of metal oxides relative to carbides and also the equilibrium of carbon and carbon monoxide.

$$2MeO + 2C = 2MeC + O_2 \quad (3.24)$$

$$2CO = 2C + O_2 \quad (3.25)$$

The equilibrium of oxide-carbide-carbon for iron and chromium is around 700°C and 1100°C. Above these temperature carbides are more stable than oxides. The oxide of metal is a stable phase compared to carbide at temperature where the solid line is above the dash line.

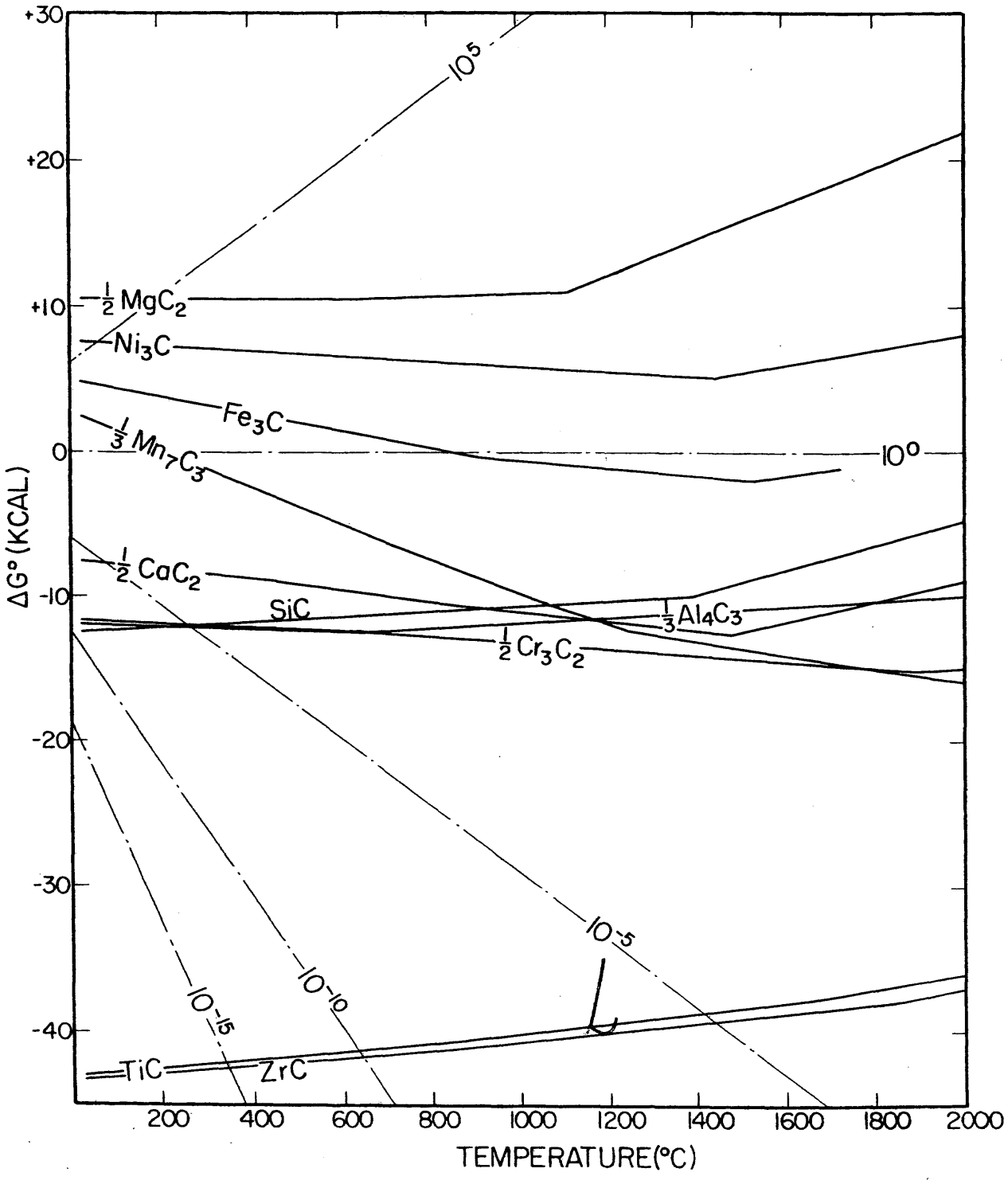

Figure 3.4 Free Energy of Formation of Carbides from their Elements (Muan and Osborn, 1965)

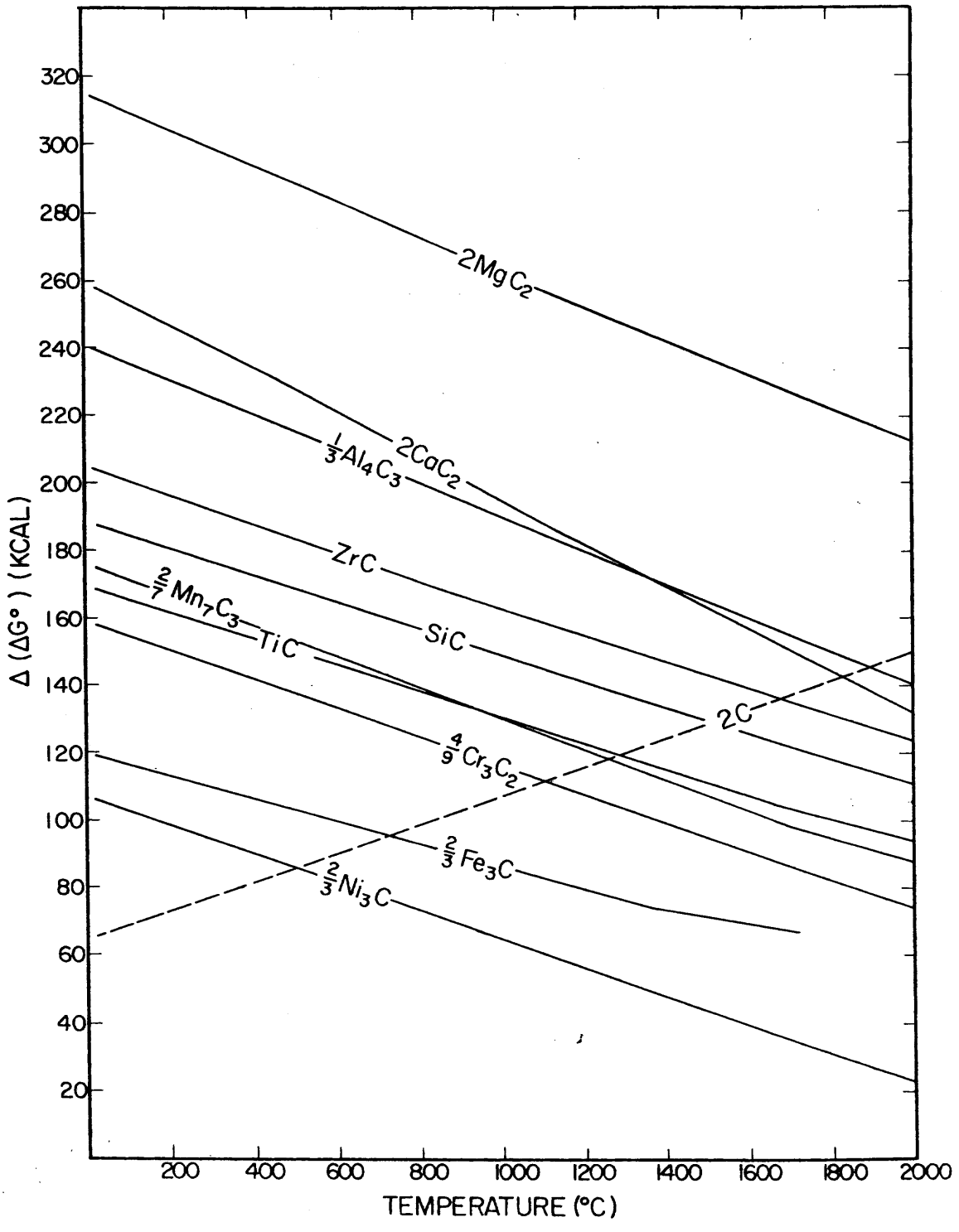

Figure 3.5 Relative Stability between Oxides and Carbides (Muan and Osborn, 1965)

The formation of nitride at the steelmaking temperature (~1500°C) takes place when p_{N_2} / p_{O_2} is larger than 10^{10} (Muan and Osborn, 1965). The condition hardly occurs during the experiment.

3.1.2 Stability of Solution of Oxides and Metal

The activity of oxide in solid solution of oxides may deviate from unity. Figure 3.6 shows the activity of FeO in the solid solution of FeO and MgO (Bogdandy and Engell, 1971). The activity of Fe in the metallic phase remains unity due to the presence of only Fe in the metal phase. The equilibrium condition is described in Equation 3.26. The oxygen partial pressure at equilibrium changes with a factor of $\ln(a_{FeO})$, Equation 3.27. The equilibrium ratio of CO/CO_2 also changes accordingly, Equation 3.20.

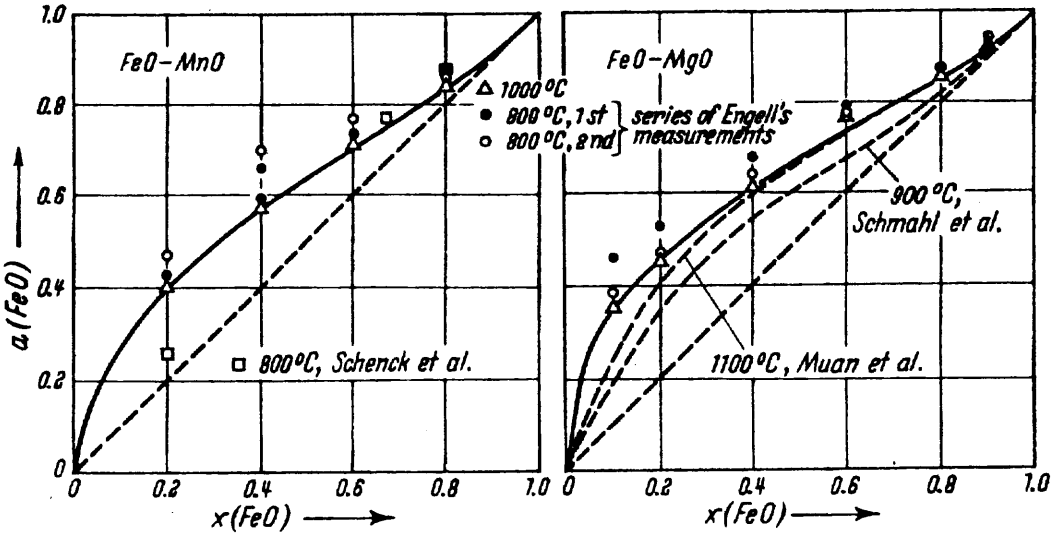

Figure 3.6 Activity of FeO and MgO in their Solid Solution (Bogdandy and Engell, 1971)

$$\Delta G^{\circ} = -RT\ln\left(\frac{a_{FeO}}{p_{O_2}^{1/2}}\right) \tag{3.26}$$

$$\ln\left(P_{O_2}^{1/2}\right)_{(eg,T)} = \ln(a_{FeO})\frac{\Delta G^{\circ}_{(FeO_{(s)} = \frac{1}{2}O_{2(g)} + Fe_{(s)})}}{RT} \tag{3.27}$$

The formation of solution of metal, for example the solution of Fe and Cr alloy, causes changes in the activity of both Fe and Cr. The reduction of the system containing iron and chromium oxide is studied by Gurevich et al. (1973). They studied the equilibrium among three oxide phases (Cr_2O_3, $FeCr_2O_4$, FeO), metallic phase (solid solution of Fe and Cr), and gas phase (mixture of H_2 and H_2O). They found that: 1) the dissolution of FeO in Cr_2O_3 was not measurable and the activity of each phase was equal to unity; 2) The reduction of chromite occurred only after the complete reduction of iron oxide; 3) at the equilibrium among all five phases, the dissolution of Cr in Fe was negligible and the activity of metal phase remained unity; and 4) The solubility of Cr in Fe increased substantially when there was only three phases (Cr_2O_3, metal, and gas).

3.2 Stability of Iron Oxide

The equilibrium among C, CO, CO_2, Fe_2O_3, Fe_3O_4, FeO, and Fe is shown in Figure 3.6. The carbon deposition occurs at temperature below 710 °C. The reduction of iron ore occurs mainly at temperature between 700 to 1000 °C. The sintering temperature is from 1100 to 1300 °C. The activity of wustite is generally reduced by its formation of a mixed crystal with other compounds especially silica.

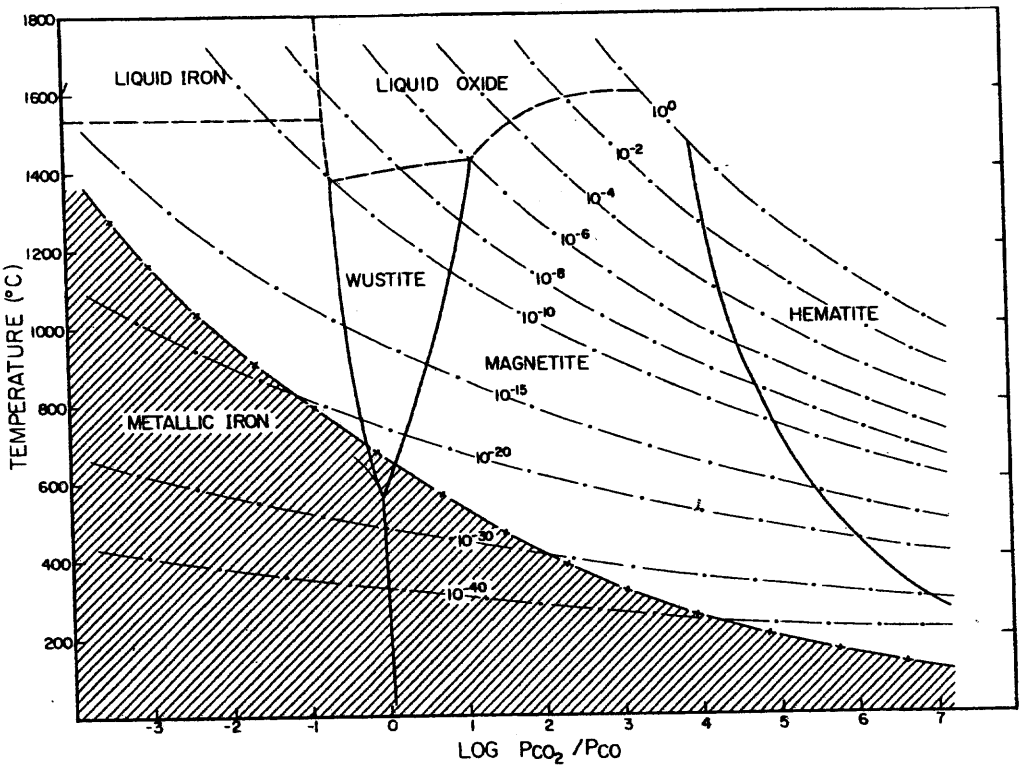

Dash-cross line: partial pressure of oxygen
Dash-cross line: Equilibrium between gas phase and solid carbon

Figure 3.6 Stability Relations among Metallic Iron and Iron Oxides as a Function of CO_2/CO Ratios and Temperature, at a Total Pressure of 1 atm (Muan and Osborn, 1965)

3.3 Reduction of Iron Oxide

The reduction can proceed either as a solid or liquid state reaction. Since the blast furnace has long been studied and still dominates the production of iron along with the developing of direct reduction, much research focused on the solid state reduction (Basamallick, 1995; El-Geassy, 1998; Kasai et al., 1995; Haque et al., 1992; Nasr et al., 1994; Ray and Prasad, 1992). That does not rule out the significance of the liquid state reduction which also occurs in the blast furnace and the smelting reduction (Paramguru et al., 1996; Balghi et al., 1993; Basu and Ray, 1995; Bafghi et al., 1992; Murthy et al.,

1994; Mroz, 1994). Under each state of reduction there are two possible paths: direct and indirect reduction. The measurement procedure and the determination of reduction kinetics will be presented first and is followed by direct and indirect reduction, the gasification of carbon, the reducibility of iron oxide, and the factors affecting reductions in both solid and liquid state.

3.3.1 Measurement of Reduction Rate and Reduction Kinetics

The observation on the reduction kinetics in iron and steelmaking process is not easy due to its high operating temperature. Unlike liquid, where the concentration of each specie is monitored, the removal rate of oxygen is mostly measured. The observation on the removal rate of oxygen in the solid state can be done by different ways: by monitoring the weight loss of the sample in Thermo-Gravimetric Analyzer (TGA) or similar reactors (Haque et al., 1992; Kasai et al., 1995; Nasr et al., 1994; Ray and Prasad, 1992; Paraguru et al., 1994; Pei and Wijk, 1993; Basu and Ray, 1995; Lekatou and Walker, 1997;), by analyzing the exhaust gas compositions using special gas analyzers (Tiwari et al., 1992; Mroz, 1994), and by analyzing the composition of molten slag, extracted during the melt through silica tube (Pei and Wijk 1993; Bafghi et al., 1993).

Table 3.1 Solid State Reduction Kinetics of Iron Oxide and Iron Ore, Gasification of Coal and Carbon, and their Activation Energy

No	Reactant	Reducing/ oxidizing agent	Reaction	Temp (°C)	Rate limiting process	Reduction kinetics	Activation energy (kcal/mol)
(1)	Ore	Coke	$FeO^* + CO = Fe + CO_2$ $C + CO_2 = 2CO$	950-1100	Gasification	$\frac{d(DOR)}{dt} = k(a\text{-}DOR)$ a-constant	29.7-55.2
(2)	Ore	CO	$FeO^* + CO = Fe + CO_2$	1000-1100	Phase boundary reaction	$\frac{d(DOR)}{dt} = k(1\text{-}DOR)$	7.8
	Coal	CO_2	$C + CO_2 = 2CO$	950-1050	Phase boundary reaction	$\frac{d(W_c)}{dt} = k(p_{CO2} - p^{eq}_{CO2})$	34.6
	Ore	Coal	$FeO^* + CO = Fe + CO_2$ $C + CO_2 = 2CO$	950-1050	Phase boundary reaction	$\frac{d(DOR)}{dt} = k(1\text{-}DOR)$	
(3)	Fe_2O_3	C	$3Fe_2O_3+CO = 2Fe_3O_4+CO_2$ $Fe_3O_4 + CO = 3FeO + CO_2$ $FeO + CO = Fe + CO_2$ $C + CO_2 = 2CO$	997-1097	Gasification (no grinding) Reduction/ gasification/ catalytic effect (after grinding)	$\frac{d(DOR)}{dt} = k(1\text{-}DOR)^n$ n - 0.853 to 0.307 (0 to 60 minutes of grinding)	54 - 4.5 (0 to 60 minutes of grinding)
(4)	Fe_2O_3 to FeO	CO/CO_2	Similar to (3)	900- 1200	Gaseous diffusion/ phase boundary reaction		10.2 and 14.4
	FeO to Fe	-CO		900- 1200	Solid state diffusion (CaO/MgO doped)		10.4 and 22.3
(5)	Coal	CO_2	$C + CO_2 = 2CO$	647-1177	Phase boundary reaction	$t \alpha (1-(1-W_c))^{1/3}$	53.8-43.0
		15%CO/ 17%H_2		647-1177	Phase boundary reaction	$t \alpha (1-(1-W_c))^{1/3}$ W_c – weight of coal	75.3-43.0

Table 3.1 Solid State Reduction Kinetics of Iron Oxide and Iron Ore, Gasification of Coal and Carbon, and their Activation Energy (Continued)

No	Reactant	Reducing/ oxidizing agent	Reaction	Temp (°C)	Rate limiting process	Reduction kinetics	Activation energy (kcal/mol)
(6)	C	Pure CO_2	$C + CO_2 = 2CO$	930-1100	Phase boundary reaction	$\frac{d(W_c)}{dt} = k_c n W_c$ k_c – chemical rate constant, n – effectiveness factor	48.9
(7)	C	Pure CO_2	$C + CO_2 = 2CO$	930-1100	Phase boundary reaction	$\frac{d(W_c)}{dt} = k_c n W_c$ k_c – chemical rate constant, n – effectiveness factor	31.7
(8)	Fe_3O_4	$C/CO/H_2$	Similar to (3)	1200	Heat transfer for the gasification	-	9.0-10.0
	C	$C/CO/H_2$		1200	gasification	$t \alpha (1-(1-W_c))^{1/3}$	25.0
(9)	Ore	40%CO/ 60%CO_2	$FeO^* + CO = Fe + CO_2$	850-1000	Phase boundary reaction	$t \alpha (1-(1-C))^{1/3}$	6.5
	C	Pure CO_2	$C + CO_2 = 2CO$	900- 1050	Phase boundary reaction	$d(W_c) = kt$	52.8

* - Reduction of iron oxide occurs in a stepwise manner similar to (3).

(1) - Nasr et al.(1994), (2) - Haque et al. (1992), (3) - Kasai et al. (1995), (4) - El-Geassy (1998), (5) - Weeda et al. (1990), (6) - Tiwari et al. (1992), (7) - Abraham and Ghosh (1979), (8) - Sun and Lu (1993), and (9) - Ray and Prasad (1992)

In this research the reduction study was conducted in the solid state using Thermo-Gravimetric Analyzer. The kinetic study based on the weight loss seems appropriate and was emphasized. Table 3.1 summarizs the reduction kinetic in the solid state reduction using different reducing agents. The table is given to provide examples for the study of reduction kinetics. More detail on each study is given in following sections. The reduction study can be separated into two broad groups, the reduction of iron oxide by CO and the gasification of carbon.

The reduction of iron oxide by CO mostly followed first order kinetics or shrinking core model, Equations 3.28 and 3.29. The gasification of carbon followed first order kinetics or shrinking core model. The Degree of Reduction (DOR) is defined by Equations 3.30 and 3.31.

$$\frac{d(DOR)}{dt} = k(1 - DOR) \tag{3.28}$$

$$\frac{d(DOR)}{dt} = k(1 - DOR)^{\frac{2}{3}} \tag{3.29}$$

$$\text{Degree of Reduction (DOR)} = \frac{\text{Weight of oxygen removed from iron oxide}}{\text{Total weight of oxygen in iron oxides}} \tag{3.30}$$

$$\text{or} = \frac{FeO_{(initial)} - FeO_{(at\ time\ T)}}{FeO_{(initial)}} \tag{3.31}$$

The rate constants for reduction at different temperatures are related by Arrhenius equation (Equation 3.32), where A is a constant, E_a is an activation energy, k is a reaction constant, R is a gas constant, and T is temperature. Plotting ln(k) and 1/T, the activation energy can be calculated according to Equation 3.33. The activation energy is the energy barrier that the process has to overcome before the reduction occurs. According to Table

3.1, the activation energy of carbon gasification ranges between 25-55 kcal/mol, and 7-22 kcal/mol for the reduction of iron oxide by gaseous CO.

$$k = A * \exp\left(\frac{-E_a}{RT}\right) \tag{3.32}$$

$$\ln(k) = \ln(A) - \frac{E_a}{RT} \tag{3.33}$$

3.3.2 Direct vs Indirect Reduction

The solid carbon acts as a reducing agent in the direct reduction like carbon monoxide does for indirect reduction. In indirect reduction the gasification of carbon through the endothermic Boudouard reaction plays a very important role on the reduction rate. Equation 3.34 simplifies the direct reduction, and 3.35 and 3.36 present the indirect reduction and gasification (Bogdandy and Engell, 1971).

$$Fe_nO_m + mC = nFe + mCO \tag{3.34}$$

$$Fe_nO_m + mCO = nFe + mCO_2 \tag{3.35}$$

$$mC + mCO_2 = 2mCO, \quad \text{Boudouard reaction} \tag{3.36}$$

The direct reduction occurs at the interface between iron oxide and solid carbon. Nonetheless, the contact between them is not continuous due to the product formation. This can cause a marked decrease in the reduction rate with the progress of reaction. The indirect reduction proceeds as a chain reaction between equations 3.35 and 3.36.

Bogdandy and Engell (1971) reviewed literature and concluded that direct reduction had no importance in the industrial reduction process. It rather took place as a part of chain reaction. The indirect reduction was widely accepted to account for the

reduction (Davies et al., 1973; Srinivasan and Lahiri, 1977; Otsuka and Kunni, 1969; Abraham and Ghosh, 1979; Baldwin, 1955; Szendrei and Van Berge, 1988).

However, there are some researchers who stressed the significance of the direct reduction. Sugata et al. (1974) studied the smelting reduction of FeO in molten slag by rotating solid carbon disk. The reduction of iron oxide at the interface of molten slag and solid carbon disk resulted in the CO gas formation. The CO bubbles acted as a barrier for the direct contact between iron oxide and carbon. They found that the reduction rate increased as they evacuated CO, allowing the direct contact between iron oxide and solid carbon. They concluded that the indirect reaction was less important than direct reduction. Bafghi et al. (1993) found that the rate of reduction of FeO by solid carbon increased with the evacuation of CO. The CO at low concentration of FeO, 2%, enhanced the agitation but acted as a barrier between the molten iron oxide and solid carbon at higher FeO concentration.

Kasai et al. (1995) studied the changing reduction rate due to the combinatorial grinding of hematite/iron ore and graphite/coal under TGA. The reduction temperature decreased as the grinding time increased. The reaction order and activation energy changed from 0.853 and 54 kcal/mol to 0.307 and 4.5 kcal/mol when grinding time changed from 0 to 60 min. They believed either the catalytic effect of metal on the gasification and/or the direct reduction improved the reduction.

It is hard to definitely conclude the reduction path. As a whole, for the industrial application where complicated process control, i.e. the removal of CO, is not achievable, the indirect reduction supposedly dominates due to the limited direct contact between the

iron oxide and solid carbon. However, the reaction by solid carbon, if possible, may proceed at a much faster rate than the reduction of iron oxide by CO.

3.3.3 Reaction Kinetics of Carbon Gasification

Bogdandy and Engell (1971) summarized that between 900 and 2000°C carbon and oxygen react and form mostly carbon monoxide. It is believed that above 1100 to 1200°C the reaction rate is independent of the temperature. The oxidation of solid graphite by air, in a hot bed of fluidized sand between 727-1127°C, yielded only carbon monoxide (Hayhurst and Parmar, 1998). The authors summarized, from literature, the ratio of CO/CO_2 at different temperatures and oxygen partial pressures, 1-21%. They suggested the major phase was CO at high temperature.

Literature (Davies et al., 1973; Srinivasan and Lahiri, 1977; Otsuka and Kunni, 1969; Abraham and Ghosh, 1979; Baldwin, 1955; Szendrei and Van Berge, 1988) suggested that the indirect reduction governed the reduction and the reduction rate was limited by the carbon gasification. The gasification is believed to follow first order kinetics or shrinking core model (Table 3.1). The activation energy of the gasification depended on the type of carbon and also on the gas composition. Weeda et al. (1990) studied the CO_2-gasification of different kinds of coal. They found the activation energy of the gasification under pure CO_2 was 53.8-62.1 kcal/mol; changed to 50.2-69.3 kcal/mol when the gas contained 15% of CO. The gasification was complete within an order of minutes up to 1177°C and expected to finish within seconds at higher temperatures.

3.3.4 Reducibility of Iron Oxides

Different species of iron oxide are reduced at different rates due to the differences in their structures, porosity, and degree of iron ion vacancy. Magnetite, Fe_3O_4, crystallizes in the cubic spinel lattice like γ-FeO and Fe_2O_3 but with different iron ion vacancy. Hematite, the α-Fe_2O_3, has rhombohedral structure. The magnetite formed by the reduction of hematite has greater porosity than magnetite formed by the reduction of γ-Fe_2O_3 due to the changing of the structure. The reduction rate of hematite therefore is greater than the reduction rate of magnetite and wustite.

The iron oxide and chromium oxides do not exist alone in nature. Instead they occur as spinel. They can form mixed crystals with many other oxides, i.e. MgO, FeO, and Al_2O_3, while maintain their cubic crystal structure. The reduction kinetics of mixed oxides differs from the pure oxide due to the changes in the activity of iron and chromium oxides, which subsequently change the reducing gas equilibrium. The new equilibrium of reducing gases can be calculated from the rate constants of reaction of pure and mixed oxides. There is no clarification on the fundamentals of reduction of mixed oxides since the porosity and the surface area have not been determined precisely. Table 3.2 contains the degree of reduction of different mixed oxides after reduction for 40 minutes in pure CO at 850°C.

Bogdandy and Engell (1971) showed that 2% addition of CaO to hematite increased the reducibility. It was shown experimentally that lime-bearing sinter has high porosity. However, the addition of CaO for more than 5 to 10% did not improve the reducibility of the mixture.

Table 3.2 Degree of Reduction of Sinter Minerals after 40 Minutes in Pure CO at 850°C (Mazanek and Jasiensaka, 1964)

Mixed Oxides	Degree of Reduction (%)
Fe_2O_3	49.4
$CaO.Fe_2O_3$	49.2
$2CaO.Fe_2O_3$	25.5
$CaO.2Fe_2O_3$	58.4
$3CaO.FeO.7Fe_2O_3$	59.6
$CaO.Al_2O_3.2Fe_2O_3$	57.3
$4CaO.Al_2O_3.Fe_2O_3$	23.4

3.3.5 Rate Limiting Process in Reduction

The reduction paths are slightly different for different processes. For the reduction by reducing gas occurring in the blast furnace, the reduction mechanism is as follows (Bogdandy and Engell, 1971). As the reducing gas flows through pores it forms the gas boundary layer. The reducing gas diffuses through this layer to the reaction site. The chemical reactions take place initially at the surface of the iron oxide particle. The chemical reaction includes the following mechanisms: the adsorption of the reducing gas (CO), the separation of oxygen from the oxide lattice, the desorption of gaseous product (CO_2) from the surface of oxides, and the formation and growth of the nuclei of metallic Fe as a product of reaction. As the layer of metallic iron grows inwards, for a non-porous layer of product, the diffusion in the solid state may render a strong effect on the reduction rate since there is no further direct contact between iron oxide and reducing gas. The reduction involves the following processes;

1) Heat and mass transfer across the gas-flow boundary layer.
2) Phase-boundary reaction. It was experimentally found (Bogdandy and Engell, 1971) that the removal rate of oxygen from iron oxide, rate of iron oxide reduction by CO,

followed first order kinetics on partial pressure of reducing agent (CO) as described in the relation, $dn_{(O)}/dt = -(k1p_{(CO)} - k2\ p_{(CO2)})$.

3) The diffusion of gas and iron ion through the layer of metallic iron forms at the surface of the iron oxide particle.
4) The interaction of diffusion and the phase-boundary reaction. The effect of diffusion of the reduction rate is stronger as the degree of reduction increases since the thicker layer of metallic iron is formed.

3.3.6 Factors Governing the Reduction in Solid State

In this section brief descriptions of rate limiting processes from literature will be provided, including the chemical reaction, gasification, diffusion, and effects from some other oxides. Cited references provide examples of each category. From the references it can be concluded that the chemical reaction of iron oxide is rapid and presumably does not control the reduction rate. The indirect reduction was cited by many researchers to be the main reduction path which also implied the gasification as a rate limiting process. The addition of MgO and CaO up to a certain concentration enhances the reduction rate. The interaction between these oxides and iron oxide could change the structure and increase the porosity. At some points they may interact with iron oxide and form a hardly reduced compound which retards the reduction rate. The interaction between these factors can furthur complicate the reduction process.

3.3.6.1 Chemical Reaction. The reduction of hematite to magnetite was fast as confirmed by Conejo and Martin (1997). They found that the reduction of hematite to

magnetite completed in 30 sec, for the mixture of H_2:CO, 6:1, at 590°C and 620°C. The time for complete reduction to metallic iron was 4 minutes. The slowest process was the reduction of FeO_x to Fe.

Ezz and Wild (1960) found that the ores of size 50 to 150 μm suspended in H_2, in the temperature range of 700 to 1100°C, reached 80% of degree of reduction between 20 and 30 seconds regardless of the grain sizes and origins of the ores. Ozturk and Fruehan (1992) summarized that hematite was readily reduced to magnetite at high temperature. When the oxygen partial pressure is 0.55 atm the required temperature for the reduction is 1400°C, 1450°C at 0.9 atm, and 1500°C at 2.08 atm.

The reduction of iron ore by 40%CO in the static bed followed the shrinking core phase boundary reaction model, $kt = 1-(1-DOR)^{1/3}$, Ray and Prasadd (1992). The activation energy was 27 kcal/mol. They suggested that sizes of ores did not have much effect on the reduction if they were porous.

In rotary kiln, a mixture of ore and solid carbon was fed into the furnace where carbon burnt with the oxidizing gas to supply heat for the Boudouard and direct reduction. The flame separates the oxidizing environment above and the reducing environment below. From the experimental result (Bogdandy and Engell, 1966) the chemical reaction was the rate limiting subprocess at 1000-1100°C, the porous diffusion governed at higher temperature, and diffusion in the gas boundary layer at even higher temperature.

3.3.6.2 Gasification. Nasr et al. (1994) concluded that the first order gasification was a rate limiting subprocess in the solid-state reduction of compact high grade iron ore fines

(<75μm). The activation energy, 950-1100°C, decreased from 55 to 29 kcal/mol when the coke content increased from 5 to 20%. The reduction occurred in a stepwise manner. The temperature and coke content affected the reduction rate.

Ray and Prasadd (1992) suggested the gasification of coal char bed followed the first order reduction kinetics. The activation energy was 52.8 kcal/mol at 900-1050°C.

The activity of FeO had effect on the reduction rate though the gasification is a rate limiting step (Ghosh, 1994). The reduction rate was proportional to the difference between the equilibrium partial pressure of CO with C and FeO, which changed with the activity of FeO.

3.3.6.3 Diffusion. When the reduction of iron oxide occurred, iron formed at the surface of the iron oxide. If the product is not porous, the reduction must proceed through either the diffusion of reducing agent (CO), iron (Fe), or oxygen (O). Due to the smaller atomic size (Bogdandy and Engell, 1971), the Fe atom (radius = 0.67°A) is more likely to diffuse than the O atom does (radius = 1.4°A). Yun (1961) studied the reduction of finely powdered hematite and solid carbon under vacuum. He found that the reduction rate was controlled by the diffusion of iron. The reduced iron at the surface diffused inward and reacted with iron oxide to form lower iron oxide as shown in Equations 3.37-3.39. These oxides have the similar cubic structure but are differentiated by the iron ion vacancy. The reduction did not occur below 900°C. At higher temperature, there was substantial transformation to metallic iron.

$$FeO + C = Fe + CO \quad \text{or} \quad FeO + CO = Fe + CO_2 \tag{3.37}$$

$$Fe_3O_4 + Fe = 4FeO \tag{3.38}$$

$$4Fe_2O_3 + Fe = 3Fe_3O_4 \quad (3.39)$$

However, Baldwin (1955) conducted a test on the reduction of iron oxide by carbon under the flowing nitrogen. The reduction rate decreased as the flow rate of nitrogen increased. Increasing flow rate of nitrogen through the mixture of carbon and iron oxide during the reduction increased the removal rate of CO and CO_2 from the sample mass and effected the reduction rate. His result implied the significance of the effect on reduction by gas or the gasification.

3.3.6.4 Other Oxides. El-Geassy (1998) found that doping the compact iron oxide with 1% of CaO/MgO, under the controlled CO/CO_2 ratio at 900-1100°C, enhanced the reduction at the early stage due to the increasing porosity. At the later stage MgO retarded the reduction by forming the hardly reduced magnesioferrite. On the other hand, CaO formed calcium ferrite or calcium magnesium ferrite which were easily reduced. They concluded that mixed mechanism controlled the reduction rate at the early stage and the interfacial chemical reaction at the later.

On the other hand, Basumallick (1995) found that CaO did not enhance the reduction by solid carbon at 900-1000°C, instead increased the porosity of the hematite-lignite pellet by forming the needle-like calcium ferrite, which was beneficial for gaseous reduction.

Sugiyama (1974) concluded that the addition of MgO enhanced the reduction at 1300°C but retarded the reduction at lower temperature. The MgO content of 6-14% in blast furnace provided the optimum slag composition in terms of the fluidity and sulfur removal.

El-Geassy (1996) studied the gaseous reduction of Fe_2O_3 compacts doped with MgO, 0.5-5%, by CO at 1173-1473K. The doped MgO did both improve and retard the reduction, observable at the intermediate stage. The addition of MgO caused the disorder in the iron oxide lattice and increased the porosity. However, the formation of magnesioferrite retarded the reduction. The addition of MgO larger than 1% retarded the promotion effect. The combined effects of interfacial reaction and gaseous diffusion govern the reduction rate during the initial stage and changed to solid state diffusion at the later stage.

3.3.7 Factors Governing the Reduction in Liquid State

The liquid state reduction is as complicated as the solid state reduction with additional factors, i.e. the dissolution of iron oxide, and the slag viscosity. These factors are not independent from the others, i.e. viscosity changes with the slag composition and also the temperature. Literature is cited as examples of each effect on the reduction rate.

Though it is not conclusive, the dissolution rate of oxide seems to have less impact on the reduction rate unlike the chemical reaction and diffusion. Both factors are temperature-dependent and their rate constants are related by Arrhenius equation. The dependence of mass transfer rate on temperature is not as strong as that of the chemical reaction rate. In other word, the activation energy of the mass transfer rate is normally less than that of chemical reaction rate.

3.3.7.1 Dissolution of Oxides. The dissolution of the oxide with high melting temperature, i.e. chromite, allows the reduction at lower temperature. The dissolution rate

of chromite ore into a slag, having a CaO/SiO_2 ratio (basicity) of 1.5 at 1630°C in graphite crucible, was faster than the chemical reaction rate and therefore do not limit the reduction (Pei and Wijk, 1993). The dissolution rates were the same regardless of the particle sizes. The viscosity of slag affected the dissolution rate strongly, since the slag of high fluidity can penetrate better into the oxide grain. The addition of MgO up to 10% into slag keeping the same basicity reduced the dissolution of chromium oxide tremendously due to the increasing in the slag viscosity (Pei and Wijk, 1993).

The iron oxide, both hematite and wustite, pellets dissolved within 10 seconds in the slag with a composition of $40\%CaO\text{-}40\%SiO_2\text{-}20\%Al_2O_3$, at 1450°C (Ozturk and Fruehan, 1992). Heat and mass transfer controlled the dissolution rate. The slag foaming enhanced the dissolution rate by increasing the heat and mass transfer.

3.3.7.2 Chemical Reaction Vs Diffusion. In the smelting reduction of Cr_2O_3 in $CaO\text{-}SiO_2\text{-}MgO\text{-}Al_2O_3$ slag in graphite crucible, the Cr_2O_3 reduced first to CrO, and then formed Cr_3C_2 (chromium carbide) layer at the interface of graphite and slag (Wenguo and Olle, 1993). At temperatures lower than 1525°C the chemical reaction controlled the reduction, up until 1550°C the diffusion of carbon through the liquefied carbide layer took control, and at temperature higher than 1575°C the mass transfer of the CrO to the graphite interface governed.

Morales et al. (1987) found that the slag does not wet the graphite particles injected with gas into the slag but there was a nucleation of CO around the graphite particles. They assumed the mass transfer of iron oxide to the slag-gas interface governed the reduction rate. They suggested the retarding effect of silica by its competing for the

reaction sites between iron oxide and CO at the bubble surface. Their model also predicted the higher reduction rate in the basic slag than the acidic slag at high graphite injection rate.

Mroz (1994) found that between 1350°C and 1400°C, diffusion controlled the reduction rate for a $CaO-SiO_2-FeO$ slag with a basicity of 1.2. At 1450°C, the chemical reaction controlled the reduction rate. This may be due to the decreasing of viscosity at higher temperatures.

Koch et al. (1988) concluded that the reduction rate of iron oxide by top blowing of CO in the smelting reduction corresponded to the diffusion model. Pei and Wjik (1994) found that the smelting reduction of $(Fe.Mg)(Cr.Al)_2O_4$ in silicate slag followed first order kinetics. The $FeCr_2O_4$ was reduced during the early stage of reduction and $MgCr_2O_4$ was reduced in the later stage. They concluded that the chemical reaction governed the reaction when slag had low melting point. The chemical reaction and dissolution shared their influences when the slag had high melting temperatures. The activation energy was approximately 59.7 kcal/mol.

The reduction of magnetite to wustite depended on many factors including the activity of FeO which depended on slag compositions, oxygen partial pressures, and temperatures, i.e. when activity of FeO = 1, at 1450°C, the reduction proceeded when the partial pressure of oxygen is lower than 0.216 atm.

3.3.7.3 Solid and Solute Carbon. The reduction rate of iron oxide in the $CaO-SiO_2$ slag by solid carbon is slow than 10 times of that by solute carbon and tended to follow Johnson-Mehl relation instead of first order kinetics as in the reduction by solute carbon (Paramguru et al., 1996). The Johnson-Mehl equation, $-\ln(1-DOR) = (kt)^n$, is used to

describe the nucleation and growth model, where DOR is degree of reduction, t is time, k and n are constants. The activation energy of the reaction was 21.5 kcal/mol. The optimum basicity for the reduction is 1.5.

Basu and Ray (1995) analyzed the smelting reduction of iron oxide by solute and solid carbon. The reduction by solute carbon, carbon saturated iron bath, follow first order kinetics with the activation energy of 20-26 kcal/mol. The CaO/SiO_2 of 1.5 gave the best reduction rate at 1400°C. The solid carbon reduction did not follow first order kinetics but more likely the Johnson-Mehl equation, which typically described the nucleation and growth model with the activation energy of 25.8 kcal/mol.

3.3.7.4 Slag Composition, Activity, and Viscosity. The ideal slag should provide a high dissolution rate, a rapid reduction rate, a low viscosity melt, a high mass transfer rate, a high yield of metal, and the least attack to the refractory lining. Mroz (1994) studied the effect of CaO/SiO2 or basicity, viscosity, and temperature on the reduction rate. Rate of reaction was found to be first order with time and second order with basicity (for basicity less than 1.54). The FeO activity increased with increasing basicity. As the viscosity decreased the reaction rate and transport increased. The maximum rate reaction occurred at basicity of 1.05, with CO removal, because at this basicity the slag had the lowest viscosity. Mroz (1994) hypothesized that for the melt viscosity of less than 1 poise, the chemical reaction controlled the overall reaction rate.

The basicity of 1.5 was found to be the best ratio for the reduction of chromic oxide in terms of the solubility, reduction rate, and chromium partition ratio (%Cr in slag / %Cr in metal) (Pei and Wijk, 1993). The addition of calcium fluoride lowered the

liquidus temperature of the calcium-silicate slag, and increased the solubility, the mass transfer, and consequently the reduction rate. However, CaF_2 attacked the refractory lining severely. After the complete dissolution of chromite ore, the reduction rate followed first order kinetics. The temperature and slag basicity strongly affected the reduction rate.

Morales et al. (1987) suggested the effect of silica activity on the chemical reaction by covering the bubble surface, the reaction sites of iron oxide and CO. The addition of SiO_2 for the reduction of chromite ore by solid carbon generally improved the reduction rate up to the critical values where the dilution effect reduced the contact area of chromite grain and the solid carbon (Lekatou and Walker, 1997). The addition of SiO_2 enhanced the reduction by combining with MgO leaving alone the Fe_2O_3 and Cr_2O_3 to be reduced, and forming the molten slag to which the chromium and iron oxide dissolved and subsequently reduced at the slag/carbon and slag/metal carbide interface at 1400°C. The following free energy and equilibrium temperatures (Equation 3.40-3.43), where P_{CO} is equal to 1 atm, shows the benefit of SiO_2 addition; the equilibrium temperature is lowered after the addition of SiO_2.

$$2(MgO.Cr_2O_3) + 6C = 2MgO + 4Cr + 6CO; \quad (3.40)$$

$$\Delta G°_T = -RT \ln(p^6_{(CO)}) = 1735.83 - 0.987T, \quad T = 1487°C$$

$$2(MgO.Cr_2O_3) + SiO_2 + 6C = 2MgO.SiO_2 + 4Cr + 6CO; \quad (3.41)$$

$$\Delta G°_T = 1672.57 - 0.986T, \quad T = 1423°C$$

$$2(MgO.Fe_2O_3) + 6C = 2MgO + 4Fe + 6CO; \quad (3.42)$$

$$\Delta G°_T = 1040.85 - 1.044T, \quad T = 695°C$$

$$2(MgO.Fe_2O_3) + SiO_2 + 6C = 2\,MgO.SiO_2 + 4Fe + 6CO; \quad (3.43)$$

$$\Delta G°_T = 947.55 - 1.044T, \quad T = 634°C$$

3.3.7.5 Slag Foaming. The formation of CO caused foaming in slag. The foaming increased the interfacial area between iron oxide and CO, and CO and C. It also increased the stirring intensity, and heat and mass transfer. Katayama et al. (1992) found that the reduction rate increased with slag volume, stirring intensity and the quantity of carbon in slag.

3.3.7.6 Gasification. Sasaki and Soma (1977) found that during the reduction of FeO by solid carbon, the gas composition was close to the equilibrium condition of FeO-Fe and concluded the gasification is a rate limiting step. Increasing the graphite surface area shifted the gasification forward and the chemical reaction of FeO and CO controlled the reduction rate. The reduction rate was proportional to FeO^n, where $1<n<2.5$. It is suggested that n is larger than 1 due to the vigorous gas evolution at higher FeO.

3.3.7.7 Thick Layer of Slag. The slag in bath smelting reduction also played a role as a seperator of the oxidizing and the reducing zones and as a medium for heat transfer. Katayama et al. (1992) conducted a study on the reduction and heat transfer of iron oxide in smelting reduction with thick layer of slag. They found that the stability of the slag was better with the addition of carbonaceous material, which suppressed the slag foaming. Large amount of slag acted as a better barrier between two zones and increased the reduction rate provided the heat transfer was improved by the addition of sufficient

carbonaceous material. The reduction rate also increased with the rate of buttom CO_2 gas bubbling. Gas bubbling increased the degree of stirring, heat transfer, and mass transfer, therefore increasing the reduction rate. The carbon consumption was around 10-40 %. The amount of slag required was about 6-50%.

3.4 Volatilization

At high temperature, there is a chance for both elements and compounds to vaporize. Figure 3.8 presents the pressure of vapor phases of elements and oxides at equilibrium. The pressures are the total pressures resulting when the substances volatilize into a vacuum.

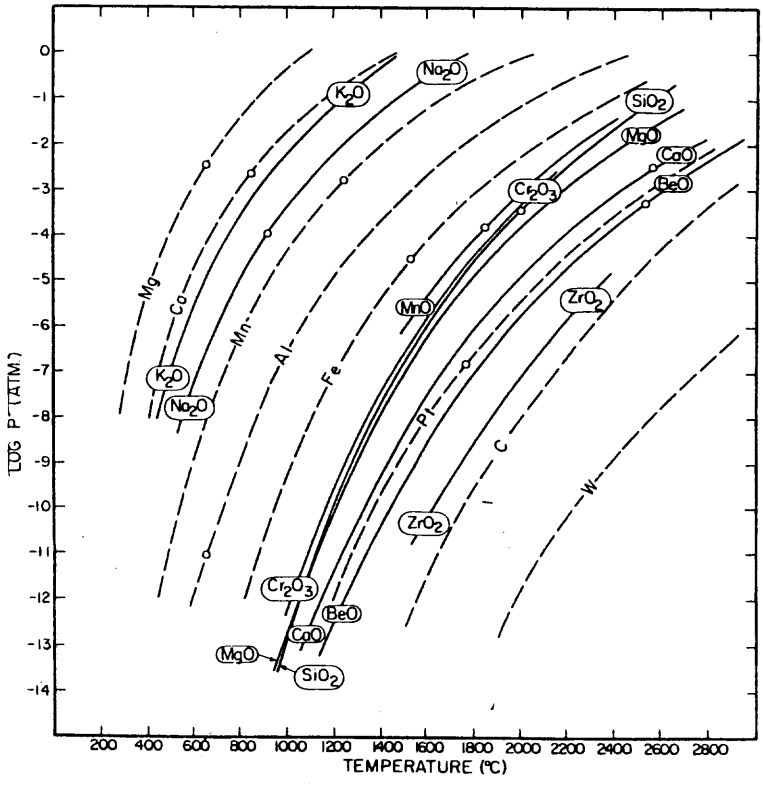

Figure 3.8 Vapor Pressures of Different Elements and Oxides, under Vacuum (Muan and Osborn, 1965)

CHAPTER 4

EXPERIMENTAL PROGRAM

The separation of iron and chromium is possible by two approaches: the separation as iron and chromium oxides, and the separation as metallic iron with chromium. The separation in a form of oxide is not complicated or energy-intensive and will be recommended provided there is satisfactory yield. However, in terms of the environmental concern, the separation of iron and chromium oxide does not remediate chromium contaminated soils though it might reduce the concentration of chromium oxide. The vitrification process can effectively treat chromium contaminated soil. The vitrified product passes the TCLP for metals and the standard for aggregate (Kamolpornwijit, 1996) set forth by both New Jersey department of Transportation (NJDOT, 1989) and American Society for Testing and Materials (ASTM, 1998). Under reducing environments, the reduction of iron and chromium oxide to metal can be accomplished. The separation of iron and chromium in a metallic form would satisfy not only the purpose of metal recycling but also the remediation of contaminated soil.

The experimental program constitutes of three parts: the characterization of chromium contaminated soils and the concentrating of iron and chromium oxides, the study of the reduction of iron oxide in soils, and the metal separation. In fact the reduction and metal separation occur at the same time. However, the term "metal separation" in this research means the observable metal agglomeration. The limitation of the instrument prevented the simultaneous study of reduction and metal separation.

As for any experiments, the result from one test can change the whole experimental strategy or the setup for the next experiment. These changes and details will be mentioned in the result and discussion chapters rather than in this chapter. This chapter provides the framework of the experimental program, the standard setup, instrumentation, and sample descriptions and properties.

The first section of the chapter provides a description of samples: chromium contaminated soil, vitrified soil both bench scale and pilot scale. The instrumentation section explains the instrument used in the research, its application, limitation, and calibration. The last section is about the experimental design where the three areas of study will be explained in detail.

4.1 Samples

The chromium contaminated soil collection, and their physical and chemical properties were described earlier by Kamolpornwijit (1996). There are total of nine different soil samples with their IDs and locations in Table 4.1. The TCLP for chromium and some important properties are also provided in the table. Table 4.2 contains some parameters of vitrified soils, bench scale.

The vitrification process is effective in treating chromium contaminated soils. The leachate from vitrified soil passed TCLP tests for eight metals. There were both bench scale and pilot scale demonstrations. In bench scale, 5-10 lbs. of soils from nine contaminated sits were mixed with 25% sand, 5 % moisture content, and 2-4 gm of carbon. The mixed soils then were placed in silica crucible and heated to 1590°C for 3 hrs, then slowly cooled to room temperature.

Table 4.1 Characteristics of Chromium Contaminated Soils

ID	Location	TCLP Cr^{6+} (ppm)	Total Cr HF (mg/kg)	Cr^{6+} (ppm)	Percentage of Cr^{6+} in Total Cr	S.G
LSP	Liberty State Park	32.41	16125	1240	7.7	3.21
CD	Colony Diner	68.58	25573	4800	18.8	2.72
GAR	Garfield Avenue	8.67	11729	246	2.1	2.98
TPR	TurnpikeBayview	2.09	12228	29	0.2	2.76
RDI	Roosevelt Drive-in	46.74	20275	4440	21.9	2.76
RR	River Road	3.83	2853	20	0.7	3.02
CPR	Green Acres	5.81	17738	29	0.2	3.12
DS	Diamond Shamrock	1.65	8086	62	0.8	2.78
RM	Reed Mineral	4.62	455	0	0	2.90

HF – Hydrofluoric digestion
S.G – Specific gravity

Table 4.2 Characteristics of Vitrified Soils, Bench Scale

ID	TCLP Cr^{6+} (ppm)	Cr^{6+} (mg/kg)	S.G. Fine	Total Cr Soft Digestion (mg/kg)
LSP	0.093	<5.2*	3.33	111.2
CD	0.025	<5.2*	3.21	15.2
GAR	0.542	<5.2*	3.12	15.5
TPR	0.213	<5.4*	3.13	153
RDI	0.015	<5.2*	3.18	0.061
RR	0.233	<5.2*	2.89	47.5
CPR	2.239	<5.1*	3.40	423.4
DS	1.649	<5.3*	2.63	46

* - Below the detection limit

The New Jersey Department of Environmental Protection set up the cleanup criteria for trivalent chromium to be 500 ppm, 10 ppm for hexavalent chromium, in 1993. In September 1998, the NJDEP has amended the criteria for trivalent chromium, in insoluble forms, to be 78,000 ppm for residential area and 120,000 ppm for non-residential area (NJDEP, 1998). All vitrified soils satisfied the new criteria.

The pilot scale demonstrated the effectiveness of the vitrification process on six tons of mixtures of soils from CD and LSP. The vitrification furnace, in Buffalo, New York, is a water cooled, double-walled, and steel vessel with a feed from the top and a tap at the bottom to maintain the cold top condition. It can operate at a rate of 50-ton-per-day of contaminated soil. It contains three molybdenum resistant heating submerged electrodes. Prior to the feeding of soil, the furnace went through the shakedown period until the stable operating condition was reached. The material used for the shakedown was mulcoa, the oxide of alumina and silicate. The reported temperature was as high as 5000°F while the operating temperature was 3142°F. After the four-hour-holding period, the molten soil was tapped and drained into the graphite molds. The filled molds were left to slowly cool down. A baghouse was used to capture particulates. The flue gas emission and power consumption were monitored thoughout the demonstration.

Table 4.3 Chromium Content of Processed Soils and Vitrified Soils, Pilot Scale

ID	Soil		Vitrified soil		
	Total Cr (mg/kg)	Cr^{6+} (mg/kg)	Total Cr (mg/kg)	Cr^{6+} (mg/kg)	TCLP ppm
LSP	3527	774	272	9.5	1.34
CD	18700	2860	138	4.8	0.31

The analysis of flue gas emission after the baghouse showed that the mass emission rates of most dioxins and furans were either not detected or close to the detection limit and were below the New York State Department of Environmental Conservation (NYSDEC) Annual Guideline Concentration (AGC) (NYSAG, 1991). The trace metals: antimony, arsenic, barium, beryllium, cadmium, chromium, cobalt, copper, lead, manganese, mercury, nickel, selenium, thallium, vanadium, and zinc, were either

below or close to the detection limits. The oxygen and carbon monoxide concentrations were close to their atmospheric concentrations with a rather high carbon monoxide concentration.

The power consumption from the pilot scale test was 776 KWH per ton of blended soil. The operation of vitrification, therefore, costs $22.8 to $45.6 per ton of soil, based on $0.03 to $0.06 per KWH. The overall cost including pretreatment, vitrification, and operation was estimated to be from $80 to $204 per ton depending on the application/disposal of the vitrified soils. The treatment cost was $80 when vitrified product was used as aggregate, $89 when used as backfill material, and $204 for disposing in a landfill. Both vitrified soils from bench and pilot scales satisfied requirements for the construction aggregate set forth by NJDOT and ASTM (NJDOT, 1989; ASTM, 1998).

4.2 Instrumentation

The instruments used in this research are Environmental Scanning Electron Microscope (ESEM) with Energy Dispersive X-Ray spectrometer (EDX), X-Ray Diffraction spectrometer (XRD), and X-Ray Fluorescence spectrometer (XRF), Thermo-Gravimetic Analyzer (TGA), and the high temperature furnace.

4.2.1 Environmental Scanning Electron Microscope (ESEM)

The ESEM is made by ElectroScan, model 2020. The electron beam bombards the sample causing different phenomena. One of them is the emission of secondary electron, which is captured by the secondary electron detector for the study of the morphology of

samples. Equipped with the EDX, the ESEM also allows the study of the sample composition. The instrument requires no extensive sample treatment as SEM does. The electron beam does not only excite secondary electrons from the surface but also excites different elements constituting the sample. The excited atoms emit their own characteristic x-rays, x-ray fluorescence. The EDX is in fact the x-ray detector capturing all characteristic x-rays and separating them by their energies, so-called Energy Dispersive X-ray fluorescence spectrometer. The EDX software, called micro-mapping, allows the quantitative study, if calibrated, of the elemental distribution.

The EDX, in this research, gives semi-quantitative results since it is calibrated against the instrument software not a prepared set of standards. Another factor effecting the accuracy of the quantitative result is the topology of the sample surface. The result would be of good quality if all characteristic x-rays reach the detector with intensities correctly proportional to their concentrations. For the non-smooth surface, the x-rays could be absorbed by other elements obstructing its path to the detector. The x-ray energy absorbed can further excite the secondary fluorescence x-ray of itself or other elements. The intensity reaching the detector, therefore, deviates from the actual intensity. The sample height also affects the accuracy, since different x-rays were adsorbed differently by the same media.

4.2.2 X-Ray Fluorescence Spectrometer (XRF)

The XRF is made by Philips, model PW2400. Elements in the sample are excited by high-energy incident x-ray beam, Rhodium tube with tungsten anode. Upon the excitation, they emit their own characteristic x-rays, called fluorescence. The

characteristic x-rays, of different energy and wavelengths, were separated by wavelength as they diffracted through the crystal of known d-spacing. The diffracted angles relate to the wavelength by Brag's Law, $n\lambda = 2d\sin(\theta)$, where n – integer (the full wavelength path difference between successive plane), λ - wavelength, d – d-spacing of the crystal plane perpendicular to the surface, θ - the incident angle between the x-ray and the surface plane of the crystal. The Philips, PW2400, is a simultaneous spectrometer, analyzing for all specified elements in one measurement. This is possible by the mobile detector mounted on the rotating goniometer, allowing the detection of x-rays diffracted at different angles. The instrument allows two working environment; under vacuum or helium. The vacuum environment is better than the helium since there is less gas particles in the chamber and consequently less absorption of characteristic x-ray. The vacuum is suitable for solid sample, pressed powder, and fused glass. Helium allows the analysis on loose powder with no sample preparation. For the analysis by helium, a mylar film of 5 micron thickness, is used to support the sample.

The software package provides both full quantitative and semi-quantitative analysis. The full quantitative analysis required a calibration against the standards. The theoretical calculation, based on the fundamental parameter, for correction on the sample matrix absorption is also available. The Fundamental Parameter corrects for the secondary excitement of one element by the others in the sample matrix. The x-ray of one element excites or is absorbed by the other element or the same element as it penetrates through the sample. The degree of absorption and excitement depend mainly on the absorption edge and mass absorption coefficient of both the exciting and excited elements, the so-called fundamental parameter. The relationship between the intensity

and concentration is not linear but for a short range of concentration a linear relation can be assumed. The accuracy in analyzing the sample against the calibrated standard depends on many factors including but not limited to the accuracy of the instrument, the sample preparation, the sample and standard matrix including particle sizes and the homogeneity of the sample, and human error. The accuracy of the instrument is excellent and in most case the error comes from the other sources. The characteristic x-ray of element is hardly affected by its oxidation state and this allows XRF to analyze any sample against the standard of different phases. However, the phases effect the summation of the concentration. For example, Ca exists in standards as CaO, but the sample indeed contains $CaCO_3$. If the sample is analyzed as CaO, the summation of the sample weight percentage will certainly be less than 100% due to the unaccounted mass of CO_2 in calcium carbonate. Human error mostly occurs during the sample preparation. The nature of the sample also accounted for the error in sample preparation.

The semi-quantitative is a semi-empirical calculation. It theoretically calculates the sample composition based on the Fundamental Parameter. There is a set of standards calibrated to account for the instrument error from the optical system, since the theoretical calculation has no way to compensate for this discrepancy. The software performs the trial and error computation until it reaches the best match of intensity. The semi-quantitative analysis is a very useful tool for a sample of small quantity or when the standards are not available. The semi-quantitative standards are in a form of fused glass, which provides the best condition in term of the homogeneity of soil and the particle sizes. The advantage of x-ray for its independent from the oxidation state of the element allows the use of fused glass as standards to which samples of different matrix are

calibrated. Nonetheless, the weakness of the semi-quantitative program also evolves from the exercising of its advantage. There is no correction factor for the differences in sample and standard matrix: particle size, void, and homogeneity, which effect the intensity of characteristic x-rays.

The XRF has limitation on analyzing light elements, lighter than oxygen. The characteristic x-rays from light elements are very low in energy and can be absorbed by air and helium as it travels towards the detector, or by the diffracting crystal, or the detector window.

The characteristic x-ray fluorescence has energy less than the incident x-ray, and therefore does not penetrate the sample as deep as the incident x-ray. The incident beam may excite the whole sample mass, but not all excited x-rays can penetrate out of the sample and reach the detector. The largest thickness of the sample that characteristic x-rays can penetrate is called penetration depth, the analyzed layer. The penetration depth is calculated based on the energy level of the characteristic x-rays, not the incident x-ray, and the sample matrix. Due to the limited penetration depth, the particle size has a very strong influence on the analysis when the matrix is heterogeneous. A system with non-uniform distribution of elements gives different results at different orientations. The effect is aggravated if the particle size is larger than the penetration depth. The reduction of particle size helps alleviate both the particle size effect and the heterogeneity of soils. Preparing samples into a pressed disk also improves the accuracy of the analysis. The surface of the pressed sample is smoother and it provides less void space than the loose sample.

4.2.3 X-Ray Diffraction Spectrometer (XRD)

The XRD is a Philips, X'Pert. The XRD is accompanied by a software package, Philips's reduced database-PDF1, containing diffraction patterns of over 80,000 compounds prepared by the International Centers for Diffraction Data (ICDD). The incident x-ray, Cu$k\alpha$, is diffracted by the sample of different phases, or same phase but different orientations, at different angles. The diffracted angles relate to the d-spacings, the crystal lattice parameters of a unit structure according to Bragg's law. The series of diffracted angles from the sample then is identified against standard patterns in the database. Though the searching for the matching pattern is automatically done, the identification is manual by comparing the match in terms of the position and relative intensity.

The particle size is also critical for the diffraction analysis. It has to be sufficiently fine so that all d-spacings have the same chance to orient perpendicular to the sample surface. The preferred orientation occurs when certain orientations appear too frequent. The sample is placed in the sample holder in such a way to minimize the preferred orientation. However, when the sample size is too small to fit in the standard sample holder, the sample is spread over the top of a plastic plate. The sample would unavoidably be subjected to certain degrees of preferred orientation.

4.2.4 Thermo-Gravimetric Analyzer (TGA)

The Thermo-Gravimetric Analyzer is made by Perkin-Elmer, model TGA7. The TGA is a combination of the furnace and microbalance where the weight loss of sample under the controlled temperature and environment can be monitored. The high temperature furnace can heat the sample up to 1500°C. The microbalance is able to hold a weight of 1.3 gm.

Excluding the weight of sample pan, and limited by the capacity of the pan, the sample weight is limited to at most 100 mg. The microbalance mounts over the furnace dropping the hangdown wire to which the sample is attached. The furnace, located under the microbalance, moves up upon testing along the axis of the hangdown wire and seals its chamber against the atmospheric environment. The nitrogen flushing passes through the concealed microbalance chamber down into the furnace and to the exhaust tube at the bottom of the furnace. The oxygen free environment requires extensive nitrogen flushing. The furnace control allows the operating in heating mode, cooling mode, isothermal, and the combination.

4.2.5 High Temperature Furnace

High temperature furnace is made by Thermolene. It is capable of heating up to 1600°C and allows for gas flushing. The furnace environmental is not as controllable as the TGA but it allows a large of number of samples to be tested at one time. The heating rate of high temperature furnace is much slower than that of TGA. It takes approximately 2.5 hr to heat the chamber to 1480°C. The furnace is not designed for the removal or insertion of sample at high temperature thus ruling out the phase study at high temperature. To prolong the life of the furnace components, the samples were taken out after the test at room temperature.

4.3 Experimental Design

4.3.1 Characterization of Soils and Vitrified Soils

The characteristics of concern are chemical compositions, phases, and morphology of chromium contaminated soils, vitrified soils both bench and pilot scale, vitrified by-products. The preparation of the XRF standard for full-quantitative analysis is described in the following section.

4.3.1.1 Standards for XRF. There are two sets of standards to satisfy the short-range linear relationship. One has high content of iron and the other with high content of silica. The standard set with high iron concentration was used to prepare calibration curves for the iron concentrated soils. The XRF standards are prepared from certified standards of known compositions mixed with other pure compounds. The analysis of soil by both semi-qualitative XRF and the acid digestion and Atomic Absorption Spectrometer (AA), were used as guidelines for the standard preparation. Table 4.4 contains compositions of standards and pure compounds. The GXR-2 and GXR-3 are standards purchased from United States Geological Survey (USGS). The NOD-A, NOD-P, and San Jouquin are standards from National Institute of Standards and Technology (NIST).

The mixing proportions and final compositions of standards of low and high iron sets are presented in Tables 4.5-4.7. There are six standards for each set of calibration: low and high iron calibrations. At least six standards are statistically required for the linear relationship, three standards per an unknown.

Table 4.4 Compositions of Certified Standards

Std	SiO_2	Fe_2O_3	Al_2O_3	MgO	MnO	CaO	K_2O	Na_2O	P_2O_5	F	W	LOI	Total
GXR3[(1)]	13.36	27.18	12.10	1.34	2.88	19.00	0.88	1.13	0.25	8.62	1.07	23.41	111.2
GXR2[(2)]	47.54	2.66	31.10	1.41	0.13	1.30	1.65	0.75	0.24	-	-	14.15	101.9
NOD-A[(3)]	3.81	15.60	3.87	4.76	23.90	15.40	0.60	1.00	1.40	-	-	-	70.9
NOD-P[(4)]	13.90	8.30	4.80	3.30	37.60	3.10	1.20	2.20	0.46	-	-	-	75.4
San Jouquin[(5)]	63.45	5.00	14.17	2.50	0.01	2.64	2.45	1.56	0.14	-	-	-	91.9

Sources
(1) - From a hot spring deposit in Humboldt county, Nevada
(2) - From Park City mining district, Summit county, Utah
(3) - From Atlantic Ocean along the Blake Plateau at a depth of 788 meters
(4) - From Pacific Ocean at a depth of 4300 meters
(5) - From a plowed field in Central California, San Joaquin valley

Table 4.5 XRF Standard Sets

Standard	Weight Percentage Proportion(%)							
	GXR-3	GXR-2	NOD-A	NOD-P	San Jouquin	Fe_2O_3	Cr_2O_3	MgO
Low Iron Set								
Std1	94.9	-	-	-	-	-	5.12	-
Std2	77.7	9.7	9.7	-	-	-	2.92	-
Std3	77.9	-	-	-	19.5	-	2.63	-
Std4	78.6	9.8	-	9.8	-	-	1.75	-
Std5	69.4	9.9	-	-	19.8	-	0.88	-
High Iron Set								
Std1	40	-	-	-	-	42	10	8
Std2	52	-	-	-	-	32	9	7
Std3	59	-	-	-	-	27	8	6
Std4	66	-	-	-	-	22	7	5
Std5	73	-	-	-	-	17	6.3	3.7
Std6	80	-	-	-	-	12	5	3

Table 4.6 Compositions of Standards having Low Iron Concentrations.

Std	Concentration (% wt)													
	SiO_2	Cr_2O_3	Fe_2O_3	Al_2O_3	MgO	MnO	CaO	K_2O	Na_2O	P_2O_5	F	W	LOI	Total
Std1	12.67	5.12	25.79	11.48	1.27	2.73	18.03	0.83	1.07	0.24	8.18	1.02	7.22	95.64
Std2	15.36	2.92	22.88	12.79	1.64	4.57	16.38	0.90	1.05	0.35	6.69	0.83	6.46	92.87
Std3	22.76	2.63	22.15	12.18	1.53	2.24	15.32	1.16	1.18	0.22	6.71	0.83	5.93	94.85
Std4	16.53	1.75	22.44	13.03	1.52	5.97	15.37	0.97	1.78	0.27	6.77	0.84	6.54	93.23
Std5	26.56	0.88	20.44	14.28	1.57	2.01	13.84	1.26	1.17	0.23	5.98	0.74	5.84	94.47
Std6	32.76	0.15	18.21	12.11	1.37	2.25	12.08	1.54	1.29	0.25	5.16	0.64	4.56	92.36

Table 4.7 Compositions of Standards having High Iron Concentrations

Std	Concentration (% wt)												
	SiO_2	Cr_2O_3	Fe_2O_3	Al_2O_3	MgO	MnO	CaO	K_2O	Na_2O	P_2O_5	W	LOI	Total
Std1	5.34	10.00	52.87	4.84	8.54	1.15	7.60	0.35	0.45	0.1	0.43	6.32	101.4
Std2	6.94	9.00	46.13	6.29	7.70	1.50	9.88	0.46	0.59	0.13	0.56	8.22	101.9
Std3	7.88	8.00	43.04	7.14	6.79	1.70	11.21	0.52	0.67	0.15	0.63	9.32	102.1
Std4	8.81	7.00	39.94	7.98	5.88	1.90	12.54	0.58	0.75	0.17	0.71	10.43	102.4
Std5	9.75	6.33	36.84	8.83	4.64	2.10	13.87	0.64	0.82	0.18	0.78	11.53	102.6
Std6	10.68	5.00	33.74	9.68	4.07	2.30	15.2	0.70	0.90	0.2	0.86	12.64	102.9

There are limitations to every measurement, and XRF is of no exception. It is worthwhile to address constraints that limit the accuracy of the results from the XRF. The accuracy depends on the similarities of particle sizes and phases between standards and samples. Though XRF is well known for its capability to quantitatively analyze elements in samples regardless of their chemical states, phase identification helps completing the full quantification. Soils are heterogeneous in terms of their particle size distributions and phases. It is nearly impossible to replicate a soil sample, and therefore the standards prepared are intrinsically different from soils. There are several measures taken to alleviate the effect of dissimilarities. Grinding sample reduces the particle size effect and the heterogeneity of soil. Pressing sample smoothes the analyzing surface and reduces the effect of both particle size and particle shadowing. There are also two sets of calibration standards, one with high concentration of iron oxide and the other with high silica, to allow the valid assumption of the short-range linear relationship between the x-ray intensity and concentration. With all corrective measures taken the results are reasonably reliable.

To minimize the particle size effect and level the surface, the standards then are thoroughly mixed with additive and pressed to a pressure of 27,000 psi backing by aluminum cup (Figure 4.1). Each pressed disk is prepared from 4.8 gm of standard and 1.5 gm of boric acid. The standards are calibrated under the vacuum environment. The samples were ground to smaller than 80 microns and prepared in exactly the same way.

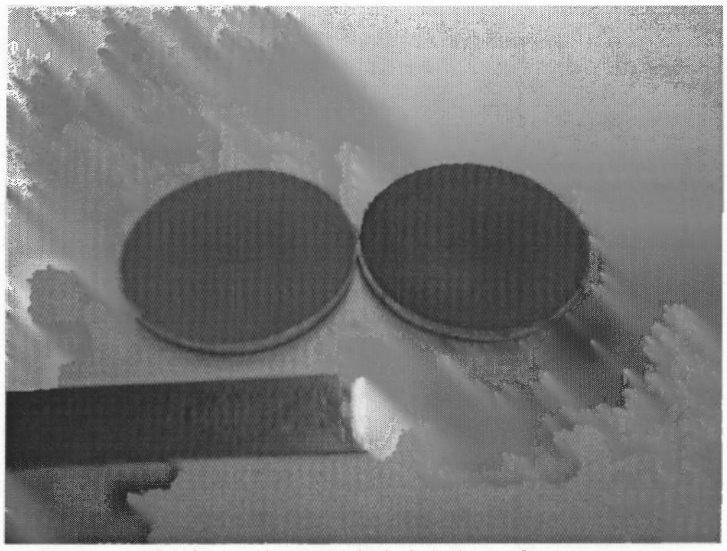

Figure 4.1 Standards: Low (Left) and High (Right) Iron Content

4.3.2 Magnetic and Gravitational Separation

The study on the concentrating of iron and chromium oxide deems mainly to look at the possibility of the concentrating not testing the separation techniques. All processes and experiment setups were simple and straightforward.

4.3.2.1 Magnetic Separation. The magnetic separation is done manually using a magnet under dry conditions. The magnet used is a low field permanent magnet with a magnetic field of 82 milliTesla measured by a Gaussmeter made by Lakeshore. It has a round shape with a diameter of 2 cm and 2.5 mm in thickness. The soils, CD and LSP, were sieved to different sizes: #200, #70, #40, #10, #4, ½", ¼", and ¾". They were then separated by dry magnetic separation with their weight percentages recorded. The separated magnetic and non-magnetic portions were ground to size smaller than 80 microns using a grinding machine.

For the analysis of chemical compositions, samples were prepared the same way as standards were. There was a difference in the media selection for the non-magnetic

analysis. Since the non-magnetic samples could not be well pressed, possibly due to the high SiO_2 content. They were readily broken after the pressing, unlike the magnetic portion, which formed a very solid pressed sample. To prevent the contamination and loss of the sample under the vacuum environment, the helium environment was used with a mylar film to prevent spilling.

The phase identification by XRD and morphological study by ESEM were also performed on both magnetic and non-magnetic portions.

4.3.2.2 Gravitational Separation. The samples, CD and LSP, were preliminarily separated manually by differences in their specific gravity. The soil samples were mixed with cold and hot water in crucibles. Hot water, 80°C, was used to check if there was a change in the separation efficiency above room temperature. A squeeze bottle was used to add water and agitate the sample at the same time. The water overflowed from the crucible with carry-over light particles. The experiment finished when the separation was clean. Records of weight percentages were kept. The concentrate and tail were then analyzed for their compositions and phases, using semi-quantitative XRF. The specific gravity of the concentrate and tail were determined according to the procedure given in ASTM D 854.

For any separation techniques, there is always difficulty when dealing with fines. Soils with larger particle sizes were tested with the laboratory setup (Figure 4.2). The cross section area of the column was 45.62 cm^2. The water flow rate was 1.52 l/min. There were two media tested: water and a mixture of water and bentonite. The mixture of water and bentonite had a specific gravity of 1.15. It was used to verify if the

separation improved with the increasing of the media density. The concentrate and tail were ground and subjected to XRF for semi-quantitative analysis.

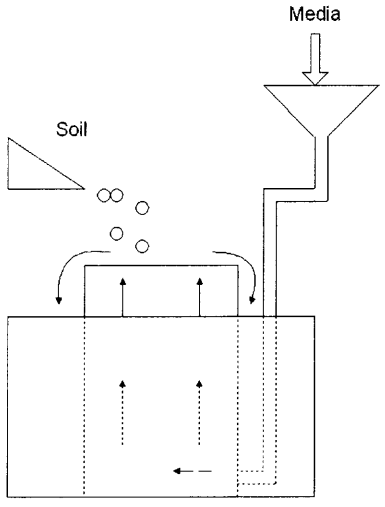

Figure 4.2 Setup for the Gravitational Separation

4.3.3 Reduction of Iron Oxide

The reduction study was done using TGA. There were many aspects studied including but not limit to the reduction of Fe_2O_3, $MgOFe_2O_3$, $CaCO_3$, LSP, CD, GAR, and TPR soils. The effect of temperature, time and reducing agent on the reduction, and preliminary metal separation were also studied. The purpose of the reduction study was to find the optimum condition for the reduction, the reducibility of soils compared to pure Fe_2O_3 and $MgOFe_2O_3$ and to soil from different sites. The reducing agent used throughout was powdered carbon.

The weight loss pattern was recorded and was plotted to identify the reduction temperature and the reduction pattern. The use of solid carbon does not allow for optional study on the reduction at the required temperature. As the furnace heats up, the

carbon starts to react with sample or CO_2 after a certain temperature and the reduction uncontrollably proceeds. The rate constants and the approximated activation energy were also calculated.

The phase identification by XRD was done intensively to identify reduction products. There was no attempt for the quantitative analysis on phases in products since sample sizes were very small, less than 50 mg. The standard sample holder required much larger quantity. A plastic plate was used as a sample holder. The plastic plate causes a background below 20° in 2θ, Figure 4.3. The manually ground sample was spread on top of the plate. By the sample preparation practice, there would have some degrees of preferred orientation. The morphology and composition of samples were also studied using ESEM and EDX.

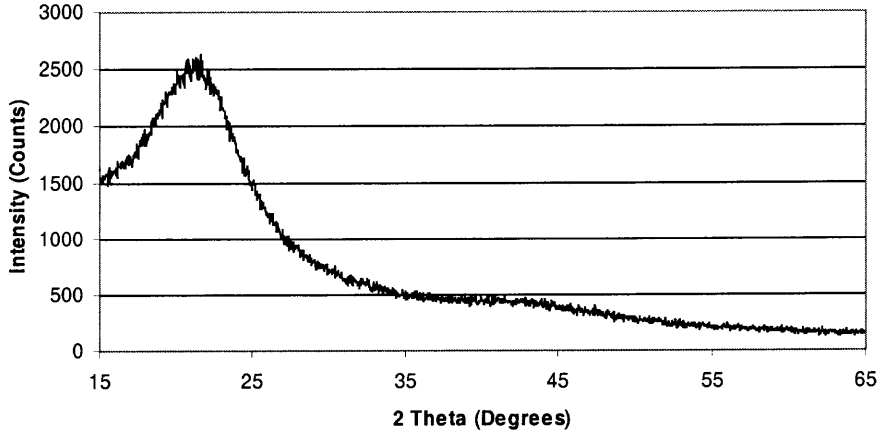

Figure 4.3 Background from Plastic Plate

Two kinds of crucibles used in this research were alumina and graphite crucibles (Figure 4.4). The alumina crucible was used throughout except for a few experiments on the metal separation where the graphite crucible was used. The graphite crucible seemed

to attack the thermocouple, though theoretically it should not. For safety reasons, the graphite crucible was reserved for the metal separation with the high temperature furnace. The TGA comes with its standard platinum pan, which is known to be very inert. However, the samples attacked the platinum pan badly. For metallurgical tests, an alumina crucible is the solution. The presence of alunina, which is also a major element for slag can affect the property of the melt: i.e. the viscosity if ever melted, the slag basicity and the activity of other compounds. An experiment showed that soil melt at or below 1400°C when silica was added. The test with sand addition is not possible for the high price of alumina crucibles. The melted soil also adhered strongly to the crucible and the crucible could not be reused. The test with TGA was therefore limited to the solid state reduction. The metal separation was studied under the high temperature furnace.

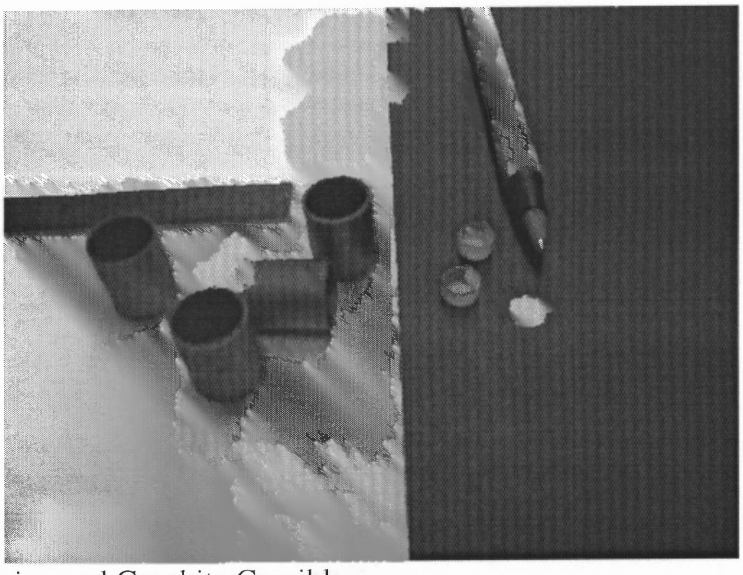

Figure 4.4 Alumina and Graphite Crucibles

4.3.4 Metal Separation

Mixtures of soils with 15% of carbon and different concentrations of sand were heated and cooled down in the high temperature furnace under nitrogen flow. It took 2-3 hrs for the furnace to reach 1500°C. The heating rate is fast at low temperature and very slow at high temperature. The samples were analyzed for their phases using XRD.

Soils studied in this section included, LSP, CD, GAR, and TPR. The samples weighted from 0.5-0.7 gm and were put in graphite crucibles, which were put on alumina boats. The furnace chamber was flushed with nitrogen at a rate of 200 CC/min. The graphite crucible was very sensitive to oxidation by oxygen at high temperature. The flushing of nitrogen was not capable of providing the oxygen-free environment. During the preliminary test, the graphite crucibles were completely oxidized under the nitrogen flow. The furnace is not completely sealed; there is a chance for oxygen to leak into the furnace through the gas inlet and outlet. To preserve the graphite crucible, graphite powder was used to fill the space between the graphite crucibles within the alumina boat to prevent the oxidization of graphite crucibles.

CHAPTER 5

DISCUSSION OF RESULTS: CHARACTERIZATION AND METAL OXIDE SEPARATION OF CHROMIUM CONTAMINATED SOILS

The chapter contains thorough investigation on the characteristics of chromium contaminated soils, bench scale vitrified soils, pilot scale vitrified soils from CD and LSP and their by-products, and the iron and chromium separation techniques including magnetic and gravitational separation. A chapter summary is provided at the end. The basic understanding of the properties of chromium contaminated soils in terms of their chemical compositions and phases will benefit in rationalizing their behavior during the concentrating, reduction and phase separation. The analysis on the bench and pilot scale vitrified products bring about the understanding of the product formation and the significance of the process control on the formation of products of different characteristics.

Chromium contaminated soils with high iron and chromium concentrations may substitute the raw iron and chromium ores supply for the iron and steelmaking industry, if their iron and chromium content can be concentrated to a level of iron or chromium ores. The magnetic and gravitational separations are concentrating processes employed in this research. Their efficiencies and the analysis of the heavy/light and magnetic/non-magnetic fractions are presented.

5.1 Chromium Contaminated Soils

The sample collection, physical properties, and TCLP for eight metals of chromium contaminated soils used in this research were given earlier by Kamolpornwijit (1996).

Chromium contaminated soils are rich in calcium, iron, silica, alumina, magnesium, and chromium as analyzed by XRF (Table 5.1). The average weight percentage of iron oxide is 23%, 24% calcium carbonate, 23% silica, 13%alumina, 6% magnesium oxide, and 5.6% chromium oxide. The results are different from what reported earlier especially on silica content (Kamolpornwijit, 1996). The XRF allows larger quantity of sample and is more effective in analyzing silica than the acid digestion method, which at times does not attain the complete dissolution of silica. Ignoring the sites with highest silica and calcium contents, RDI and RR, all other sites have iron oxide concentrations larger than 20% by weight. Soils with high chromium concentrations also have high iron content.

Some of chromium contaminated soils have iron content comparable to that of low grade ore, 30-40%, and certainly requires further beneficiation, while some are not qualified as a source of iron. Though not qualifying for iron extraction, the high concentration of calcium in CD, DS, and RDI, raises the possibility of utilizing it in cement production. The composition of cement is approximately 62-68% CaO, 21-24% SiO_2, 4-8% Al_2O_3, and 2-5% Fe_2O_3 (Ahmad and Asgarani, 1999). The CaO content of 21-24% is equivalent to the $CaCO_3$ content of 37-43%. Calcium was reported as calcium carbonate since it was the major phase for calcium identified by XRD. The summations of oxides, assuming the existence of calcium as calcium carbonate, were approximately 100%. Selecting calcium carbonate does not rule out the existence of other calcium phases or the absence of other elements from Table 5.1 implied their non-existences. The semi-quantitative analysis showed trace quantities of titanium and vanadium, which were not calibrated for the XRF standards used for results in Table 5.1. The elements selected

for calibration and analysis were major and minor elements. Trace elements were analyzed if they were readily present in the standard.

Table 5.1 Compositions of Chromium Contaminated Soils

Site	Concentration (% wt)										
	Na_2O	MgO	Al_2O_3	SiO_2	P_2O_5	K	$CaCO_3$*	Cr_2O_3	MnO_2	Fe_2O_3	Total
LSP	0.7	6.5	13.3	7.4	-	-	25.9	7.7	0.16	33.1	94.6
TPR	0.7	8.8	12.0	14.9	-	0.09	24.8	8.0	0.12	27.7	96.9
CPR	1.1	5.3	10.6	45.2	0.04	0.08	11.6	6.6	0.07	20.8	101.0
GAR	0.6	8.2	10.8	10.0	-	-	26.7	10.7	0.12	30.4	97.3
RM	1.0	3.1	15.9	31.4	0.3	1.1	12.8	1.8	0.04	22.9	90.4
CD	-	6.3	14.1	10.4	0.2	-	44.8	4.7	0.31	15.7	96.4
DS	0.7	10.5	10.4	10.6	0.1	-	44.3	5.3	-	15.4	97.1
RR	1.6	4.4	14.5	48.9	0.1	2.0	11.6	1.5	0.05	10.7	95.3
RDI	0.7	5.1	14.1	7.9	-	0.02	58.2	2.7	0.04	14.4	103.0

*: Adjusted from the analyzed CaO content

Figure 5.1 shows diffractograms of soils from nine chromium contaminated sites from Hudson County, NJ. There were two groups of soils categorized by the presence and the absence of spinel peaks. Soils from LSP, CPR, TPR, GAR, and RM had intense spinel peaks, the others had distinct peaks of silica and/or calcium carbonate. The types of ores and extraction processes could be accounted for differences. There are two main processes reported for the chromate extraction: formerly high lime extraction and latter low lime extraction. Spinel can be a solid solution of a wide range of elements. Though different kinds of spinel have different lattice parameters, they are very similar. The XRD along with the prone-to-human-error sample preparation does not allow the precise identification of spinel types not to mention the highly possible existence of mixed crystal spinel. However, certain kinds of spinels, i.e. MgO.Fe2O3 and FeO.Fe2O3, posses magnetic properties, which may help narrowing down the type presumption.

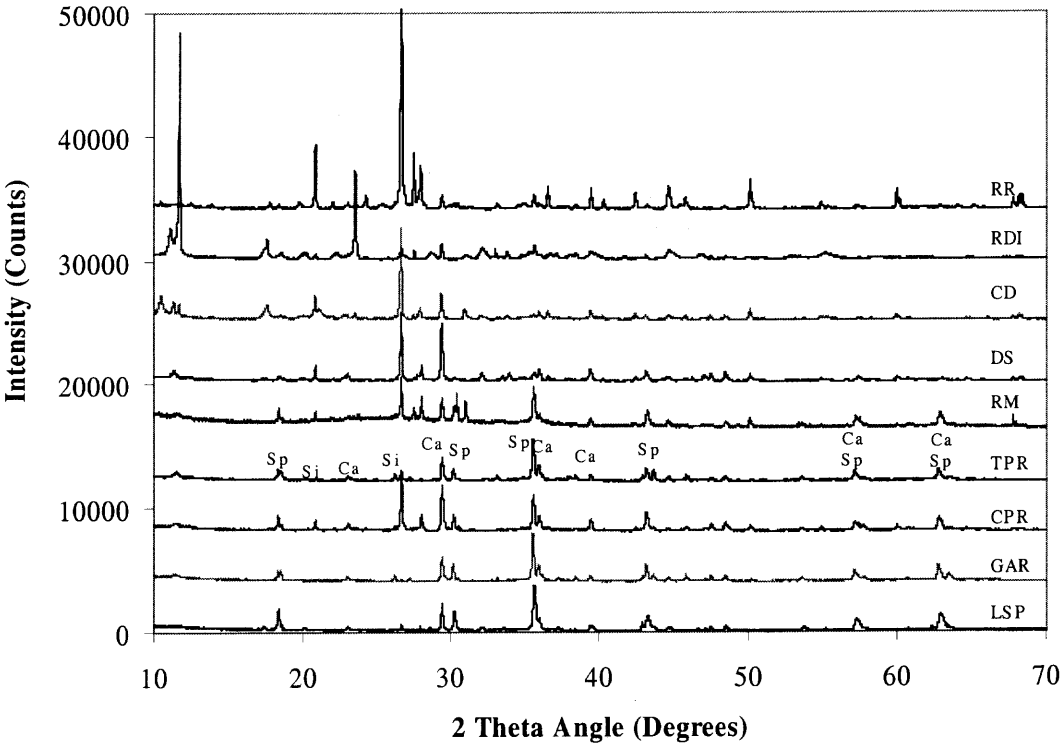

Sp: Spinel
Ca: $CaCO_3$
Si: SiO_2
Scanning Program: step size – 0.01°in 2θ, time/step – 2 seconds

Figure 5.1 Diffractograms of Chromium Contaminated Soils

Most of soils were magnetic, with very high weight percentages for soils from LSP, CPR, GAR, and TPR, for which spinel peaks were identified. The RM and RR soils were fairly attracted to magnet. The XRD/XRF results and the magnetic property of soil lead to the assumption that spinel in soils was of magnetic type and rendered soils the magnetic property. The magnetic property of soils induced the proposed magnetic separation as a concentrating process. The spinels of iron oxide have high specific

gravity, which may allow the separation by gravitational method as well. Both separation techniques are discussed in this chapter.

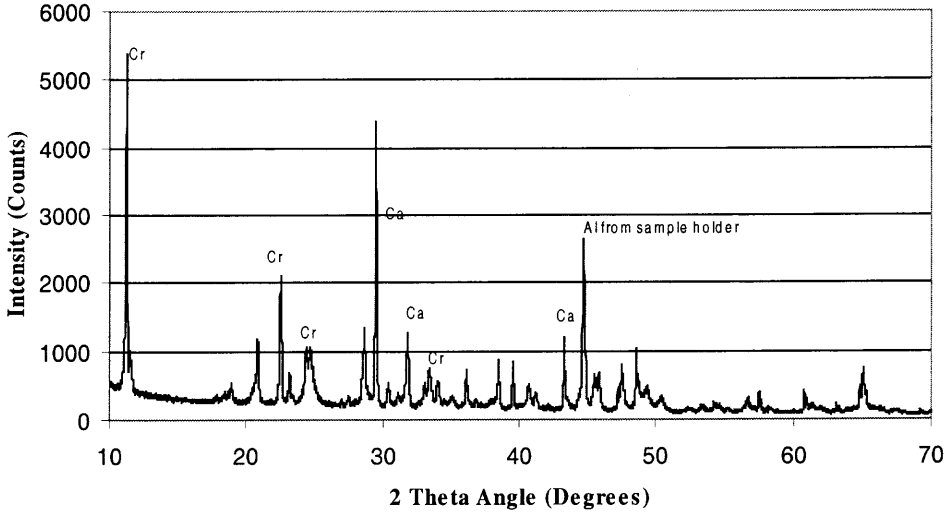

Ca : $CaCO_3$
Cr : $CaCrO_4.2H_2O$
Scanning Program: step size – 0.01°in 2θ, time/step – 2 seconds

Figure 5.2 Diffractogram of Filtrate from CD Soil

The phase identification in soil is not trivial and very often not conclusive due to the heterogeneity of soils. It is not possible to identify all phases present in soils. The identification of major phases, spinel, silica, and calcium carbonate, were of very high confidence. The spinel as a solid solution can be taken as a source of Fe, Mn, Cr, Mg, and Al, which cover most of elements in Table 5.1. The existing of hexavalent chromium in soil is a concern but its presence cannot be identified. Hot water extraction and filtration was utilized to extract chromate from CD soil. The filtrate was yellowish and was allowed to dry in an oven at 100°C. The precipitate, Figure 5.2, was identified as calcium carbonate and $CaCrO_4.2H_2O$, chromatite hydrate. The hexavalent chromium concentration in soils and its percentage out of the total chromium are given in Table 4.1.

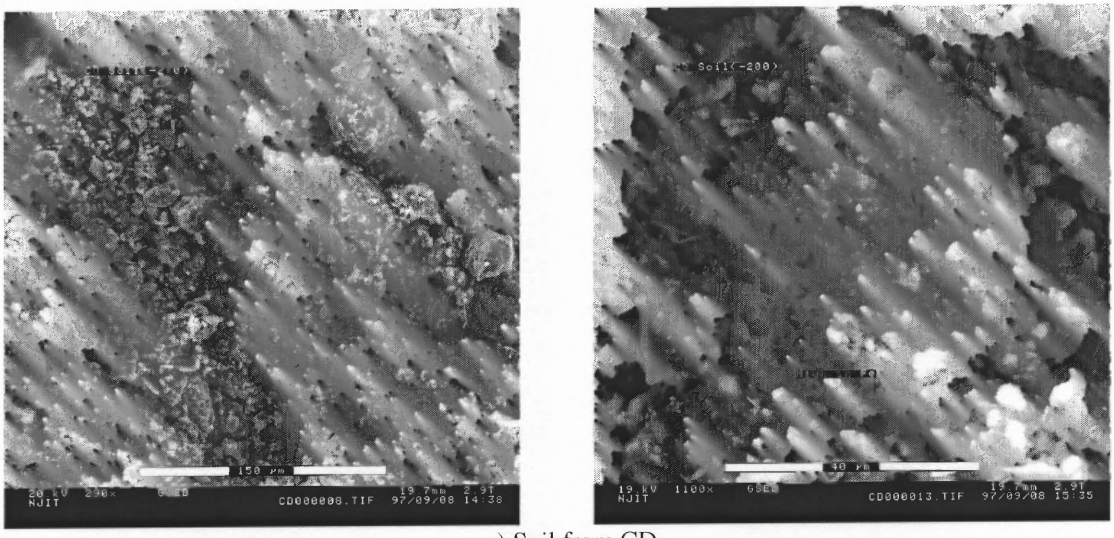

a) Soil from CD

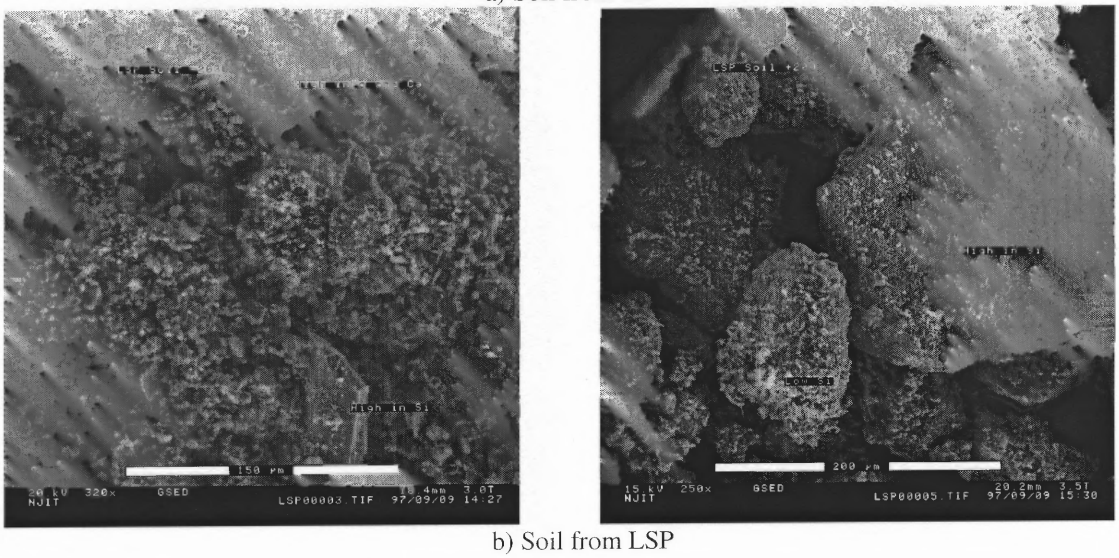

b) Soil from LSP

Size – 256*256, Dwelling time – 10 seconds

Figure 5.3 Morphology of CD and LSP Soils

Figure 5.3 shows the morphology of soils from CD and LSP. The element distribution of soil from LSP by micro-mapping is in Figure 5.4, and shows a pattern of grouping. Silica closely aligned with alumina, while the other metals, iron, chromium, calcium, magnesium, and manganese, grouped together. The elements distributing with the most density were iron and calcium. The coexisting of calcium and iron implied the possible existence of calcium ferrite, $CaO.Fe_2O_3$, and dicalcium ferrite, $2CaO.Fe_2O_3$, which have the reducibility comparable or slightly better than hematite and magnetite.

However, they were not magnetic and their diffractograms from XRD did not match those from soils.

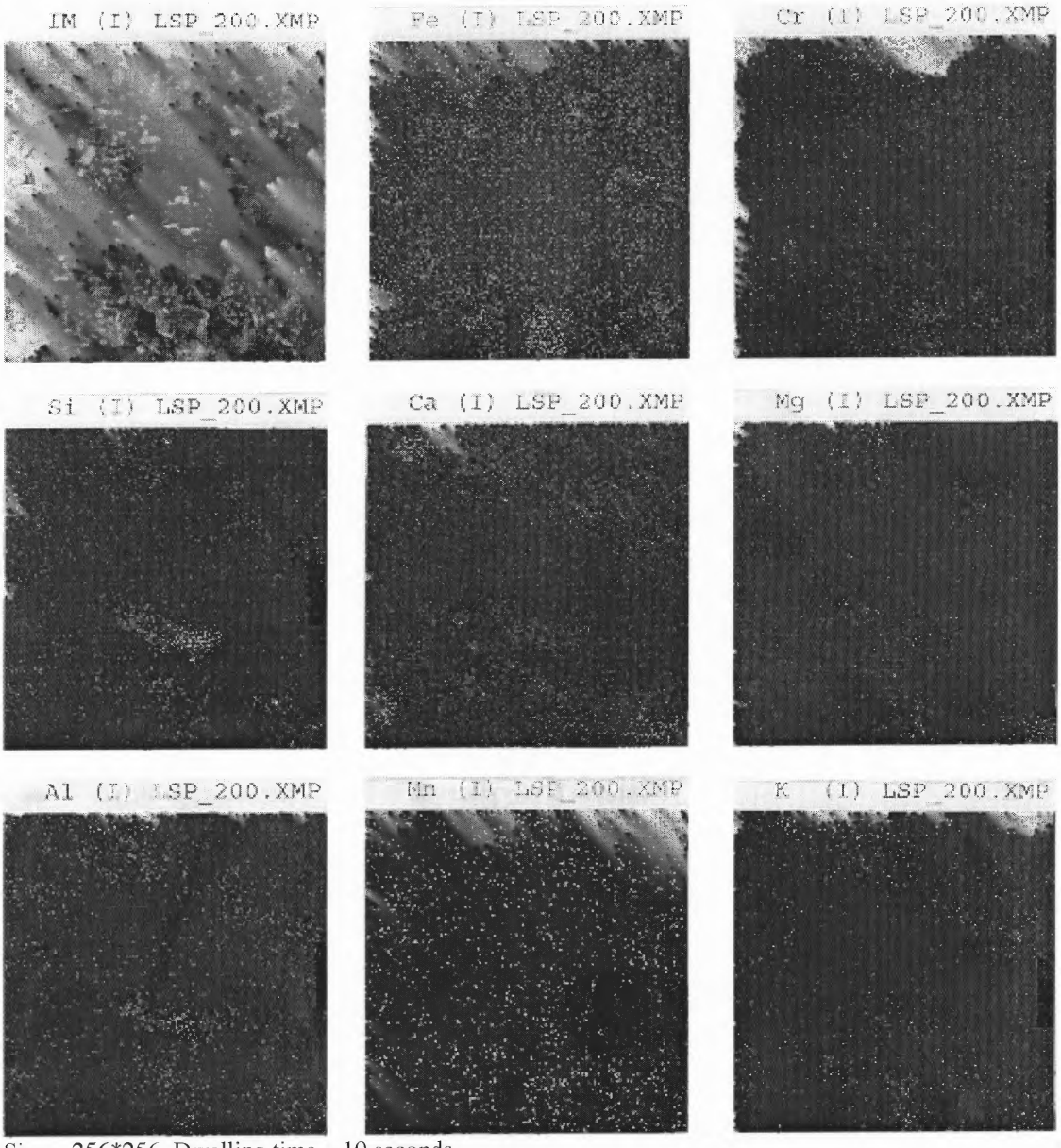

Size – 256*256, Dwelling time – 10 seconds

Figure 5.4 Distribution of Elements in LSP Soil

5.2 Bench Scale Vitrified Soils

The diffractograms of bench scale vitrified soils from nine different sites surprisingly shows similar patterns, Figure 5.5. They were identified as silica, spinel, augite (Ca(Fe, Mg)Si_2 O_2), and diopside ($Ca(Mg,Al)(Si,Al)_2O_6$), though the original soils contained different phases. Augite, diopside, and spinel are sources of Ca, Mg, Fe, and Al in vitrified soils. The result signifies the applicability of the vitrification process to soils with various phases and compositions. The bench scale soils were mixed with 25% sand. The sufficiently high silica content can govern the phase changes, and/or elements behave ideally in a liquid state regardless of their initial species. The trace elements did not have a strong effect on the phase formation and could be either encapsulated within the matrix or can form mixed crystals. The hexavalent chromium was reduced to trivalent chromium as confirmed by TCLP tests.

The properties of vitrified soils satisfied both ASTM and NJDOT requirements for construction aggregate. They also satisfied TCLP tests for eight metals. During the bench scale test, soils from DS and GAR yielded small quantities of metal droplets.

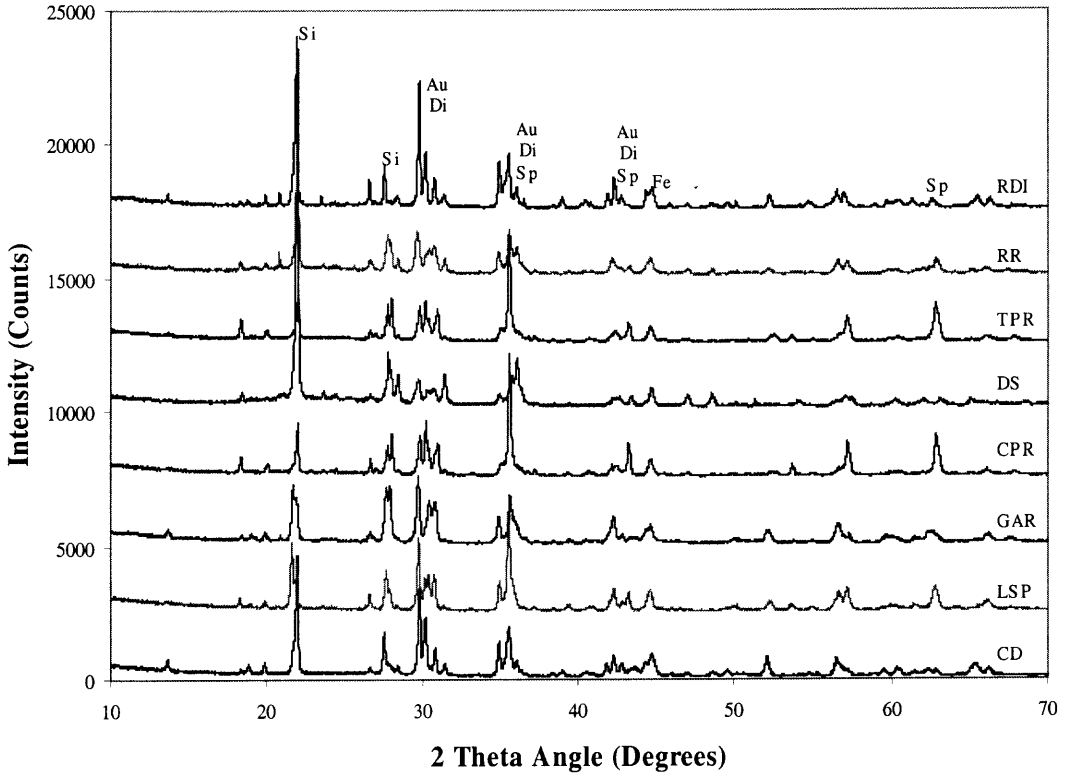

Si : SiO_2
Di : $Ca(Mg, Al)(Si, Al)_2O_6$ (Diopside)
Au : $Ca(Fe, Mg)Si_2O_6$ (Augite)
Sp : Spinel
Scanning Program: step size – 0.01°in 2θ, time/step – 2 seconds
Figure 5.5 Diffractograms of Bench Scale Vitrified Soils

5.3 Pilot Scale Vitrified Soils

Soils from CD and LSP were selected for the process demonstration. The process used electric arc furnace with molybdenum electrode to create high heat induced from the electrical resistance. Figure 5.6 contains diffractograms of vitrified soils from CD and LSP. The vitrified soil from LSP has two phases, crystalline and glass, Figure 5.7. The glass phase was analyzed twice, as powder and bulk forms. The powder pattern indicated the cross-contamination of metal, peak at 43° in 2θ, from the grinding machine.

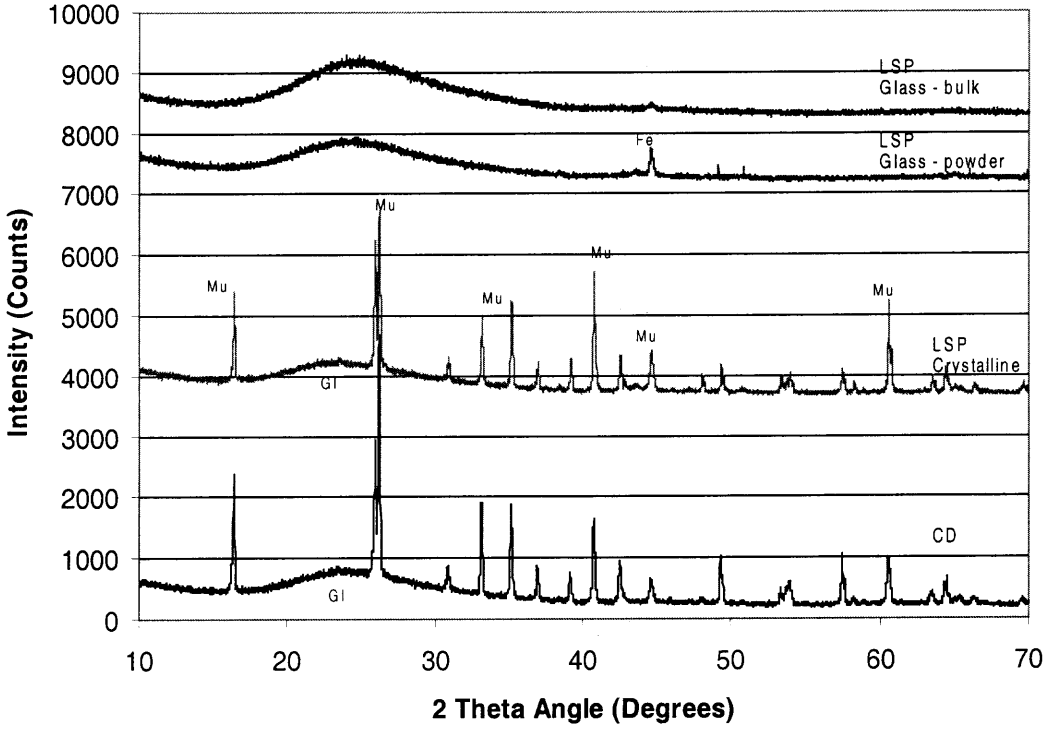

Mu: $Al_6Si_2O_{13}$ (Mullite)
Gl: Glass
Scanning Program: step size – 0.01°in 2θ, time/step – 2 seconds

Figure 5.6 Diffractograms of Vitrified Soils from CD and LSP

Though appearing as crystalline phase, the encapsulation of glass phase was identified as strong background between 15-30° in 2θ in both CD and LSP diffractograms. The only major phase of vitrified soil was mullite, $Al_6Si_2O_{13}$, the oxide of silica and alumina. The addition of sand and the dissolution of mulcoa possibly saturated the molten mass with alumina and silica. As the melt cooled down, silica and alumina stoichiometrically crystallized as mullite. The remaining liquid was viscous and formed glass. Glass and crystalline phases were analyzed semi-quantitatively for their chemical compositions, Table 5.2. The glass phase has high concentrations of iron and

all others element, while crystalline phase has very high concentration of alumina and silica.

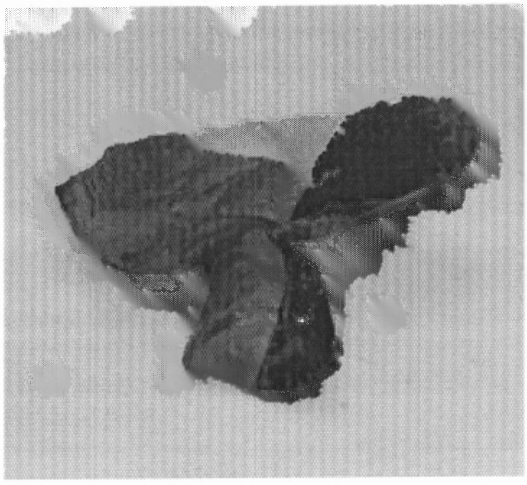

Figure 5.7 Picture showing Glass and Crystalline Phases

Table 5.2 Compositions of Vitrified Soil from LSP

Phases	Concentration (% wt)						
	Si	Ca	Mg	Fe	Cr	Al	Ti
Crystalline	40.8	4.4	3.2	5.9	1.4	27.1	1.6
Glass	23.3	10.2	2.0	29.8	6.1	18.4	4.0

Table 5.3 Compositions of Ferrofurnace Bottom

Ferrofurnace Bottom	Concentration (% wt)						
	Fe	Cr	Si	Al	Mo	Mg	As
Area 1	85.7	5.2	4.6	1.1	0.7	0.4	0.3
Area 2	85.5	5.7	4.6	1.0	0.7	0.4	0.3

During the vitrification of LSP soil, there was a formation of metal, which separated and settled at the bottom of the furnace, ferrofurnace bottom. Table 5.3 has the compositions of two areas of ferrofurnace bottom cut by water jet. They were very high

in iron 85.6%, with 4.6% of silica, and 5.5% of chromium. The bench scale test on the LSP soil did not yield ferrofurnace bottom.

Table 5.4 Material Balance (Fe) of Soil and Vitrified Soil from LSP

LSP soil	Weight (kg)	Fe content (% wt)	Fe (kg)
Vitrified soil	3320[1]		
- Glass	1330	29	385
- Crystalline	1990	6	120
- Ferrofurnace	100	86	86
Total			590[3]
Initial soil	2490[2]	23	570[3]

(1) - Weight after sand addition
(2) - Dry weight
(3) - Error ± 20 kg

Figure 5.8 Morphology of Vitrified Soil from CD

Approximately 100 kg of ferrofurnace bottom was collected during the pilot scale vitrification of 3 metric tons of LSP soil, 3.3% by weight of the initial soil. The vitrified product filled 10 graphite molds from which three molds were sent to NJIT for analysis. The glass portion approximately accounted for 40% by weight of the total mass. The material balance of iron in initial and vitrified soils is given in Table 5.4.

During the sample preparation for vitrification, 4.4 gm of carbon was added to each kilogram of soil, 0.44% by weight. The reduction of iron oxide to metallic iron was not complete; the glass portion still contains high concentration of iron.

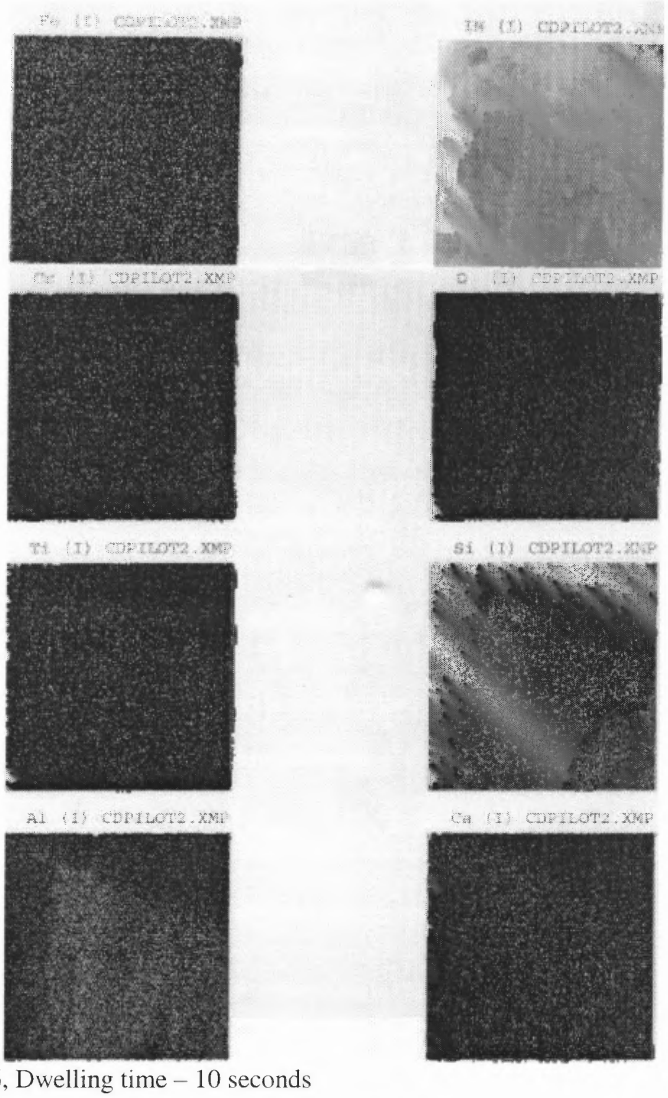

Size – 256*256, Dwelling time – 10 seconds

Figure 5.9 Elemental Distribution of Vitrified Soil from CD

The images of vitrified soils from CD and its elemental distribution are illustrated in Figure 5.8 and 5.9. The uniform distribution of elements implied the complete dissolution and high fluidity of molten soils during the vitrification process.

5.4 Magnetic Separation of Soils

The possibility to recycle iron concentrate as a substitute source of iron ore needs verification. The magnetic separation was selected for its simplicity, the magnetic property of soil, and the least possibility of cross-contamination. Dry soils were sieved and separated manually by magnet. The weight percentages of magnetic mass compared to non-magnetic mass at different particle sizes are given in Table 5.5. Soil from LSP is highly magnetic unlike soil from CD. Table 5.6 has the chemical composition of magnetic (M), initial (I), and non-magnetic (NM) soils for different particle sizes using full quantitative XRF analysis.

The magnetic separation is able to concentrate iron and chromium oxides from 25.5-37.9% and 4.5-7.8% to 34.9-40.9% and 6.3-8.6% (Table 5.6). The recovery rate of iron and chromium oxides, weight percentages of iron and chromium oxides concentrated in magnetic portion, are 84.9-99.2% and 86.6-99.8% (Table 5.7). The recovery rate is very high since most LSP soil is magnetic. Silica content decreases from 9.5-29.6% to 5.2-9.9% in magnetic portion and increases to 47.1-74.6% in non-magnetic portion. The magnetic portion also has higher concentration of calcium carbonate and magnesium oxide. There was no significant difference in the distribution of alumina between both portions. The results suggest the agglomeration of iron, chromium, magnesium, and calcium.

Diffractograms of magnetic and non-magnetic soils from CD and LSP are given in Figures 5.10 and 5.11. The first number in the sample ID represent the particle size while the second number signifies the magnetic property, "1" for magnetic and "2" for non-magnetic. The magnetic portion had distinct peaks of spinel, while the non-magnetic

portion had an intense peak of silica. The CD soil did not show much difference between the magnetic and non-magnetic fractions except for larger intensity of spinel peak at 43° in 2θ. The diffractograms of both magnetic and non-magnetic fractions at different particle sizes did not show any differences in phases, and likewise for the chemical compositions. From the results, the magnetic portion of LSP soil contains mostly spinel phase, which comprises of iron, chromium, magnesium, and calcium as its major elements.

Table 5.5 Distribution of Magnetic/Non-Magnetic Soils at Different Particle Sizes

Size	ID	LSP			CD		
		Distribution %	Magnetic %	Non-mag %	Distribution %	Magnetic %	Non-mag %
Pan	LSP8	11.9	100.0	0.0	6.0	0.0	100.0
200	LSP7	8.7	75.9	24.1	13.2	1.9	98.1
70	LSP6	7.5	60.8	39.2	21.0	1.8	98.2
40	LSP5	18.9	75.9	24.1	40.9	1.5	98.5
10	LSP4	14.7	81.4	18.6	8.9	3.0	97.0
4	LSP3	21.4	86.3	13.7	8.4	0.0	100.0
1/2	LSP2	12.5	90.4	9.6	1.5	0.0	100.0
3/4	LSP1	4.5	100.0	0.0	0.0	0.0	100.0
Sum		100.00			100.00		

Table 5.6 Composition Using XRF of Different Particle Size Fraction with respect to Magnetic Composition(M), Initial Composition(I), and Non-Magnetic Composition(NM)

Compound	LSP7			LSP6			LSP5			LSP4			LSP3			LSP2		
	M	**I**	NM	M	**I**	NM	M	**I**	NM	M	**I**	NM	M	**I**	NM	M	**I**	NM
Na2O	0.56	**0.66**	0.96	0.56	**0.67**	0.85	0.52	**0.64**	1.01	0.49	**0.63**	1.23	0.50	**0.59**	1.17	0.57	**0.58**	0.68
MgO	12.93	**10.26**	1.87	13.83	**9.00**	1.50	14.24	**11.13**	1.33	13.50	**11.28**	1.55	14.48	**12.74**	1.80	14.29	**13.03**	1.14
Al2O3	13.37	**13.09**	12.20	12.86	**11.92**	10.46	12.99	**13.16**	13.70	10.69	**12.26**	19.12	11.13	**11.42**	13.23	11.00	**11.88**	20.19
SiO2	9.88	**18.84**	47.06	8.97	**29.61**	61.62	8.85	**24.70**	74.61	6.32	**13.96**	47.38	5.87	**12.53**	54.48	5.23	**9.45**	49.19
P2O5	0.08	**0.07**	0.04	0.08	**0.08**	0.09	0.07	**0.08**	0.12	0.06	**0.07**	0.13	0.05	**0.06**	0.10	0.05	**0.07**	0.29
K	0.22	**0.40**	0.98	0.18	**0.43**	0.83	0.18	**0.14**	0.00	0.13	**0.11**	0.00	0.09	**0.08**	0.00	0.07	**0.20**	1.46
CaCO3	24.55	**21.32**	11.16	26.93	**19.60**	8.23	26.29	**22.70**	11.41	22.09	**20.82**	15.26	24.79	**23.22**	13.36	23.65	**21.99**	6.40
Cr2O3	7.66	**6.40**	2.44	6.27	**4.49**	1.72	6.57	**5.30**	1.30	8.47	**7.19**	1.59	7.98	**7.03**	1.03	8.59	**7.83**	0.66
MnO2	1.15	**0.88**	0.02	1.15	**0.71**	0.02	1.15	**0.87**	0.00	1.15	**0.94**	0.00	1.15	**0.99**	0.00	1.15	**1.04**	0.00
Fe2O3	34.94	**28.84**	9.62	36.32	**25.49**	8.70	38.12	**28.99**	0.22	40.90	**33.49**	1.04	39.72	**34.32**	0.31	39.97	**37.92**	18.66
Total	105.3	**100.8**	86.4	107.2	**102.0**	94.0	109.0	**107.7**	103.7	103.8	**100.7**	87.3	105.8	**103.0**	85.5	104.6	**104.0**	98.7

Table 5.7 Iron and Chromium Recovery Percentage

	LSP7	LSP6	LSP5	LSP4	LSP3	LSP2
Recovery rate (%)						
- Fe_2O_3	90.84 %	84.90 %	94.09 %	95.89 %	97.96 %	99.17 %
- Cr_2O_3	91.95 %	86.63 %	99.80 %	99.41 %	99.88 %	95.29 %
Concentration ratio of compound - Magnetic/Non-magnetic						
- Fe_2O_3	3.63	4.17	171.51	39.46	126.62	2.14
- Cr_2O_3	3.14	3.65	5.07	5.34	7.72	13.02
- MgO	6.91	9.22	10.68	8.72	8.04	12.54
- $CaCO_3$	2.20	3.27	2.30	1.45	1.86	3.70
- SiO_2	0.21	0.15	0.12	0.13	0.11	0.11

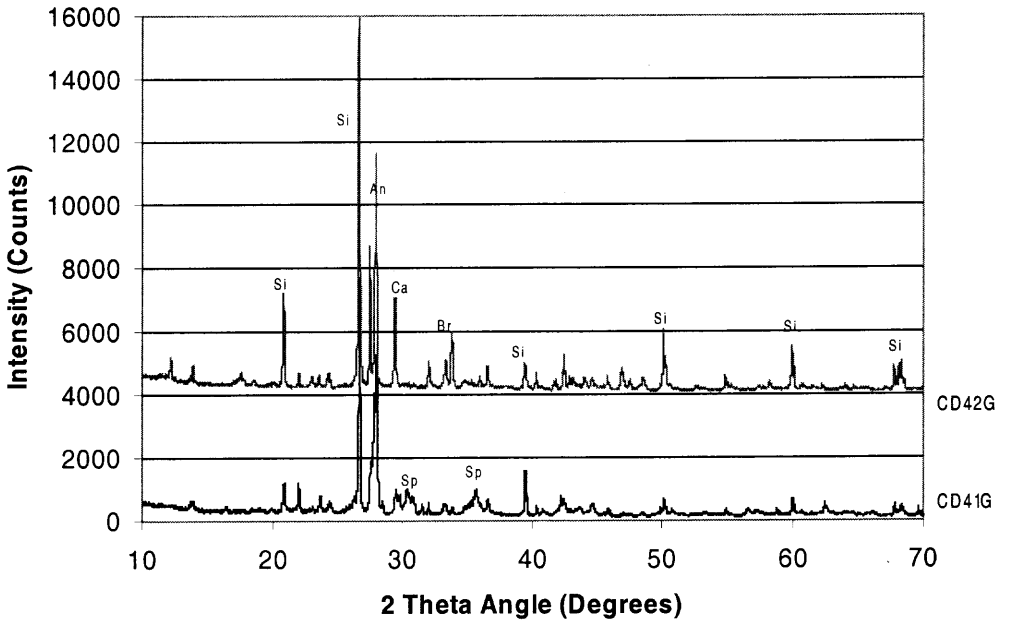

Sp : Spinel, Ca : $CaCO_3$
Scanning Program: step size – 0.01°in 2θ, time/step – 2 seconds
Figure 5.10 Diffractograms of Magnetic/Non-Magnetic soils from CD

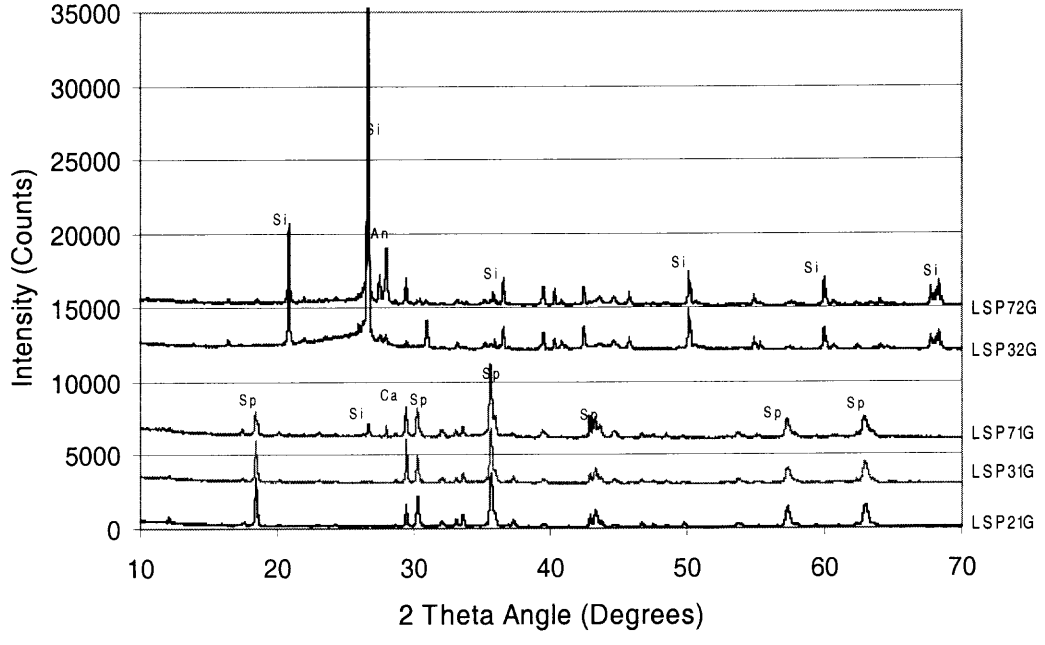

Sp: Spinel, Ca: $CaCO_3$
Scanning Program: step size – 0.01°in 2θ, time/step – 2 seconds
Figure 5.11 Diffractograms of Magnetic/Non-Magnetic Soils from LSP

Figure 5.12 has images of the magnetic soil from LSP and octagonal crystals, which are distributed throughout the soil. The chemical analysis of the octagonal crystal indicated high concentration of Fe - 36.2%, Cr – 13.9%, and Mg - 7.8%, Al – 4.4%, Ca – 6.2%, and Si – 3.0%. It is believed to be the spinel crystal. More morphology studies are presented along with the gravitational separation results.

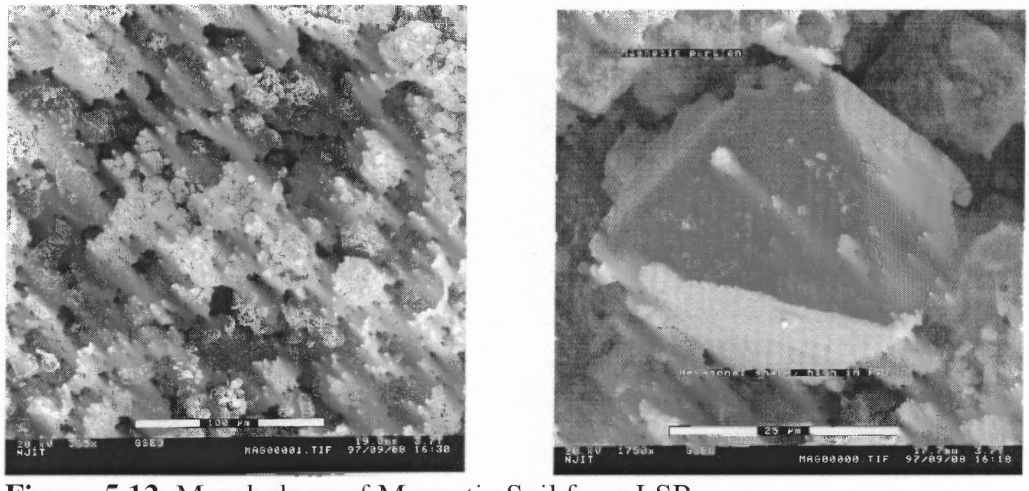

Figure 5.12 Morphology of Magnetic Soil from LSP

The magnetic separation was able to concentrate the iron and chromium contents due to the magnetic properties of the spinel, a source of iron and chromium. However, the spinel crystal did not contain only iron and oxygen, it also had rather high concentration of Mg. In other words, the spinel was not solely magnetite but a mixture of $(Mg, Fe)O.(Fe, Al, Cr)_2O_3$.

During the natural ore processing, the low grade ore is ground to liberate the mineral grain and subjected to further concentrating processes. The liberation size is the crushed size that the mineral grain is liberated. The liberation size relates to the energy consumption, the smaller the liberation size the higher the degree of grinding. The

physical appearance of the magnetic particles of LSP soil looked more like the agglomeration of fines than solid particles. Upon grinding, they were readily broken unlike the hard-to-grind sandy grains. The contents of iron and chromium were quite the same regardless of the particle sizes. Therefore, it can be concluded that there is no liberation size for the LSP soil since iron and chromium already exist as fines or agglomeration of fines and readily liberated. The LSP soil requires no further grinding for the liberation of iron and chromium but the magnetic separation to concentrate iron and chromium.

5.5 Gravitational Separation of Soils

The difference in specific gravity between the iron and chromium ore and impurities prompted the possibility of applying the gravitational separation technique. During the separation, the sample, < 75 micron, was fed with water, agitated, and drained repeatedly till the separation was clean. The tail appeared as brown and fine particles, finer than the concentrate. The concentrate was brown and dark gray. Table 5.8 contains the weight percentages of each portion.

Table 5.9 contains chemical compositions of LSP and CD, both concentrates and tails. The results show slight concentrating of iron and chromium. The tail still has high concentrations of iron and chromium compared to the results from magnetic separation. Diffractograms of both concentrates and tails showed similar phases (Figures 5.13 and 5.14). From the physical appearances, compositions, and phase analysis, the gravitational separation separated the particles of different sizes rather than of different phases for this experimental setup.

Table 5.10 contains the specific gravity of concentrates and tails from LSP and CD soils. The specific gravity of the concentrate and tail did not differ as much as expected. The closer the specific gravity between them, the harder the separation is. The efficiency and the recovery rate of the gravitational separation were not as good as those from the magnetic separation, for this experimental setup.

Table 5.8 Weight Percentages of Concentrates and Tails

Soil	Cold Water		Hot Water	
	Concentrate	Tail	Concentrate	Tail
LSP	52%	48%	56%	44%
CD	38%	62%	38%	62%

Table 5.9 Compositions of Concentrates and Tails from LSP and CD Soils, semi-quantitative XRF

Soils	Concentration (% wt)					
	MgO	Al_2O_3	SiO_2	$CaCO_3$	Cr_2O_3	Fe_2O_3
LSP						
LSP_C_CW	11.1	11.5	4.3	16.2	10.5	45.7
LSP_C_HW	11.3	9.8	4.0	15.8	10.6	47.5
LSP_T_CW	9.3	14.4	7.6	27.7	6.1	31.8
LSP_T_HW	9.7	14.7	7.9	28.7	5.6	31.1
CD						
CD_C_CW	9.9	14.5	16.4	38.8	1.9	17.1
CD_C_HW	10.6	14.5	14.3	38.9	1.9	17.2
CD_T_CW	8.4	18.2	18.2	39.3	1.4	12.4
CD_T_HW	8.2	17.7	18.1	38.7	1.4	12.5

T : tail
C : concentrate
CW : cold water
HW : hot water

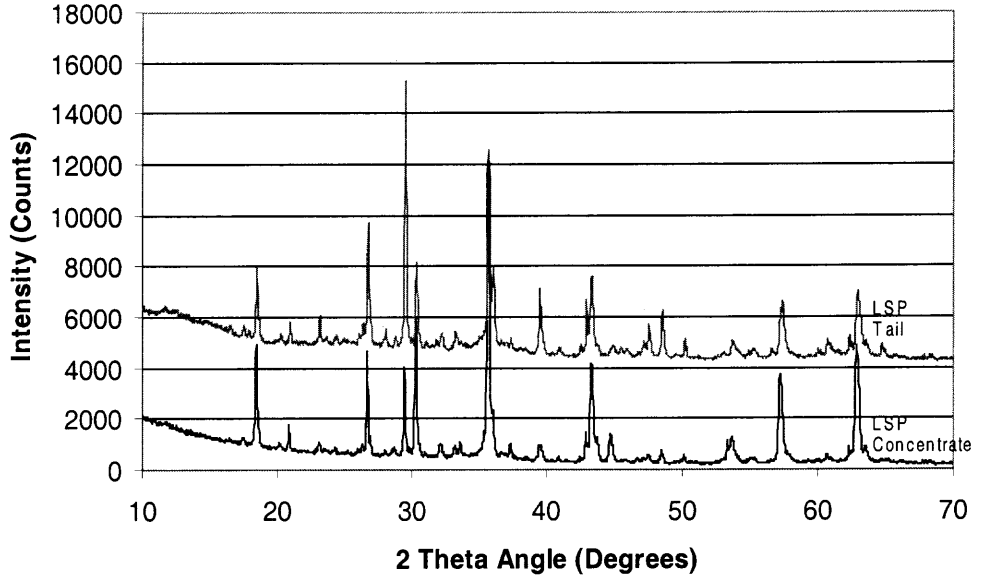

Scanning Program: step size – 0.01°in 2θ, time/step – 2 seconds

Figure 5.13 Diffractograms of Concentarte and Tail from LSP Soil

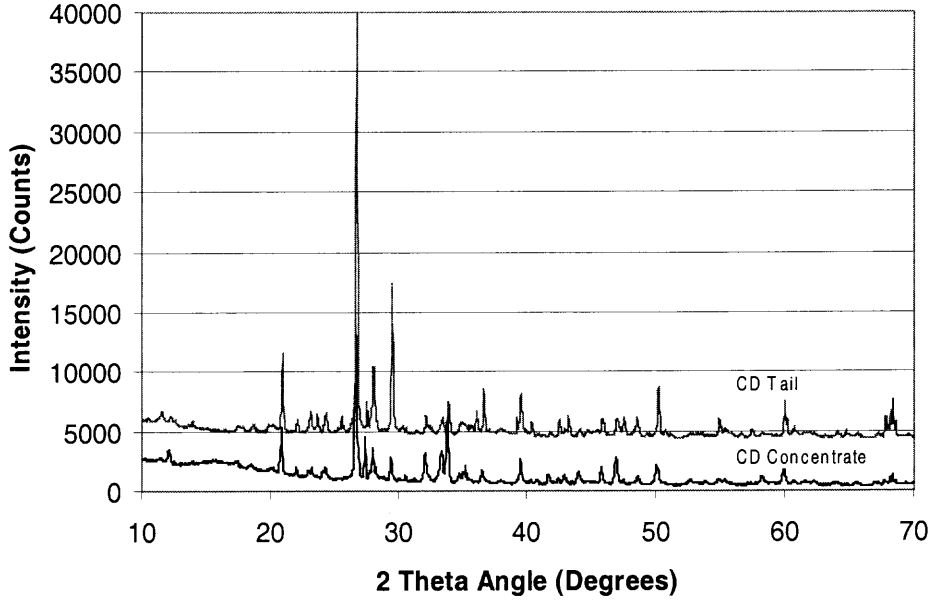

Scanning Program: step size – 0.01°in 2θ, time/step – 2 seconds

Figure 5.14 Diffractograms of Concentrate and Tail from CD Soil

Table 5.10 Specific Gravity of Concentrates and Tails

Soils	Specific Gravity			Ratio (Concentrate/Tail)
	First value	Second value	Average	
LSP_C_CW	3.39	3.50	3.45	1.19
LSP_C_HW	3.26	3.35	3.31	1.19
LSP_T_CW	2.99	2.82	2.91	-
LSP_T_HW	2.78	2.80	2.79	-
CD_C_CW	2.74	2.96	2.85	1.08
CD_C_HW	2.76	3.00	2.88	1.08
CD_T_CW	2.63	2.66	2.65	-
CD_T_HW	2.60	2.74	2.67	-

T : tail
C : concentrate
CW : cold water
HW: hot water

The gravitational separation did not give an applauding result, which can be due to the separating difficulties caused by the fineness of particles. Table 5.11 presents the weight percentages of concentrates and tails of LSP soil of larger particle sizes separated by using two different media, water and a mixture of water and bentonite. The experimental setup is given in Chapter 4. Table 5.12 contains compositions of concentrates and tails using XRF, semi-quantitative program.

Table 5.11 Weight Percentages of Concentrates and Tails using Different Media

Soil	Particle Size	Water		Bentonite+Water	
		Concentrate	Tail	Concentrate	Tail
LSP7	75μm<size<212μm	52.7%	47.3%	28.2%	71.8%
LSP6	212μm<size<425μm	97.6%	2.4%	67.9%	32.1%
LSP5	425 μm<size<2mm	99.8%	0.2%	95.0%	5.0%

Table 5.12 Compositions of Concentrates and Tail

Soils	Concentration (% wt)					
	MgO	Al_2O_3	SiO_2	$CaCO_3$	Cr_2O_3	Fe_2O_3
Water						
LSP5-C	11.2	12.2	10.3	23.2	6.1	36.2
LSP6-C	10.4	11.4	16.9	22.8	5.4	32.1
LSP7-C	10.7	13.9	7.1	23.4	7.7	35.7
LSP5-T	4.8	26.4	19.8	16.4	2.4	23.2
LSP6-T	6.4	25.5	18.7	21.8	3.0	15.7
LSP7-T	8.0	13.8	8.0	30.0	4.6	23.2
Bentonite + Water						
LSP5-C	11.2	12.2	9.2	23.7	6.2	36.6
LSP6-C	10.1	11.7	17.5	23.0	5.2	31.2
LSP7-C	10.0	14.1	9.9	22.2	7.6	34.6
LSP5-T	6.7	20.6	15.7	20.3	4.1	27.2
LSP6-T	7.3	17.6	10.4	23.1	5.7	29.3
LSP7-T	10.2	15.2	8.8	23.8	6.8	33.4

Table 5.13 Comparison between Magnetic and Gravitational Separations

Separation Techniques	Concentrate (% wt)	Ratio of Concentrate/Tail				
		Fe_2O_3	Cr_2O_3	MgO	SiO_2	$CaCO_3$
LSP7						
Magnetic	75.9	3.5	3.1	6.9	0.2	2.2
Gravity: water	52.7	1.5	1.7	1.3	0.9	0.8
Gravity: water+bentonite	28.2	1.0	1.1	1.0	1.1	0.9
LSP6						
Magnetic	60.8	4.2	3.6	9.2	0.1	3.3
Gravity: water	97.6	2.0	1.8	1.6	0.9	1.0
Gravity: water+bentonite	67.9	1.1	0.9	1.4	1.7	1.0

The results were similar to that from the separation of particle of size smaller than 75 μm. A mixture of bentonite increased weight percentages of tail, but it did not improve the quality of concentrates. Table 5.13 compares results from the magnetic and gravitational separation. Except for $CaCO_3$, the magnetic separation attained better concentrating results than the gravitational separation did. It might be the solubility of $CaCO_3$ that increased contents of $CaCO_3$ in tails.

The morphology study of the concentrates and tails from both LSP and CD soils brought interesting observations, which were presented in the following section.

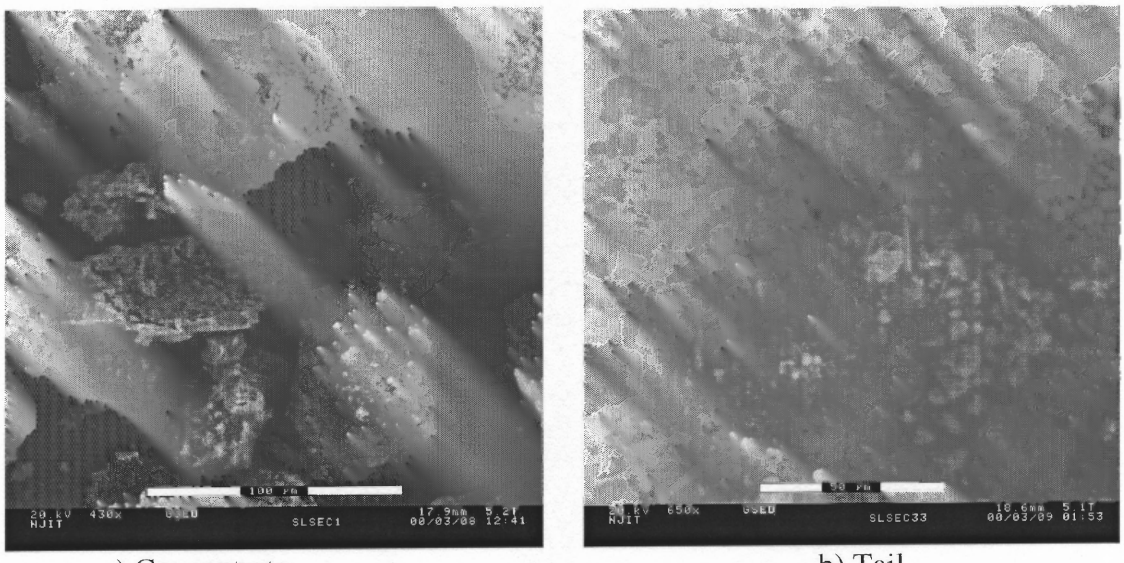

a) Concentrate b) Tail

Figure 5.15 Morphology of Concentrate and Tail from LSP Soil

The concentrate and tail had different physical appearances in terms of their colors and sizes. The concentrate from LSP soil, of size smaller than 75 µm, was dark gray and discrete while the tail was brown and very fine. The images, Figure 5.15, show that tails had particle sizes smaller than 50 µm while concentrate particles were larger than 50 µm. The concentrate particles can be grouped into three difference morphologies based on their physical appearances: particles having rough surface (Shape A, Figure 5.16), flat surface resembling spinel crystals with high iron contents (Shape B, Figure 5.17), and flat surface with high contents of rock forming minerals (Shape C, Figure 5.18). The concentrate contains mostly of particles of shape A and B. Their chemical compositions are given in Table 5.14.

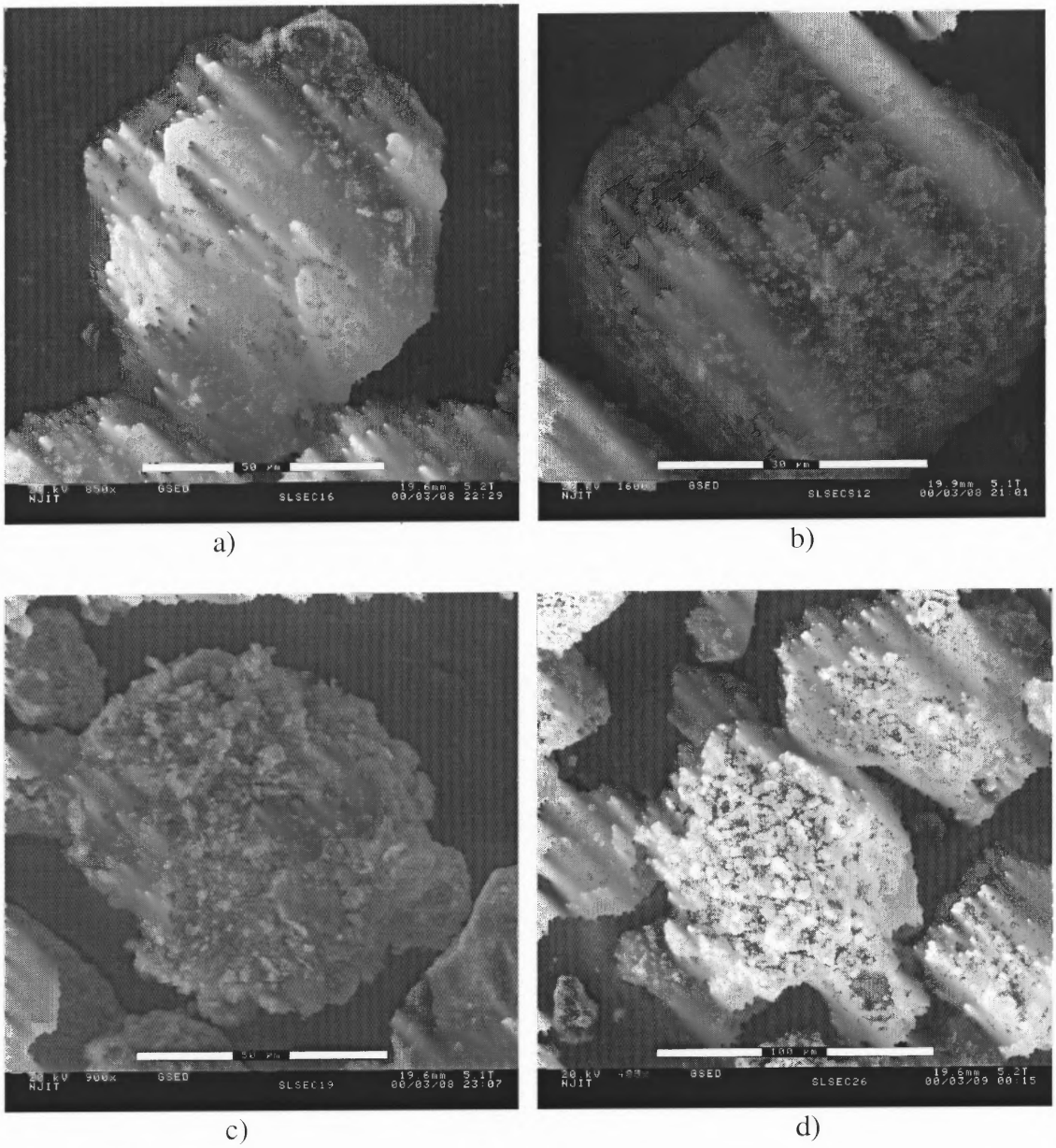

a) b)

c) d)

Figure 5.16 Morphology of Shape A Particles

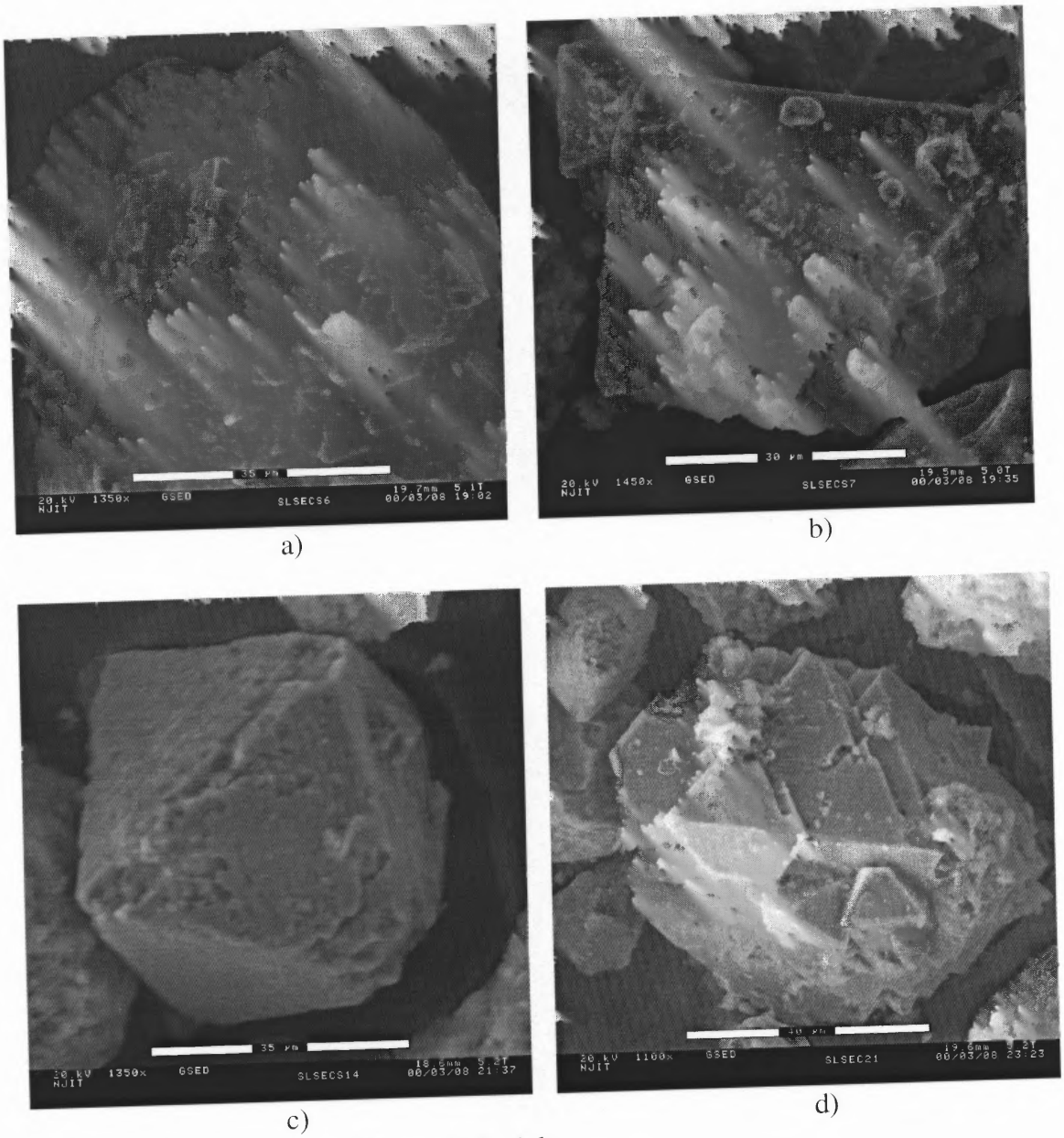

a) b)

c) d)

Figure 5.17 Morphology of Shape B Particles

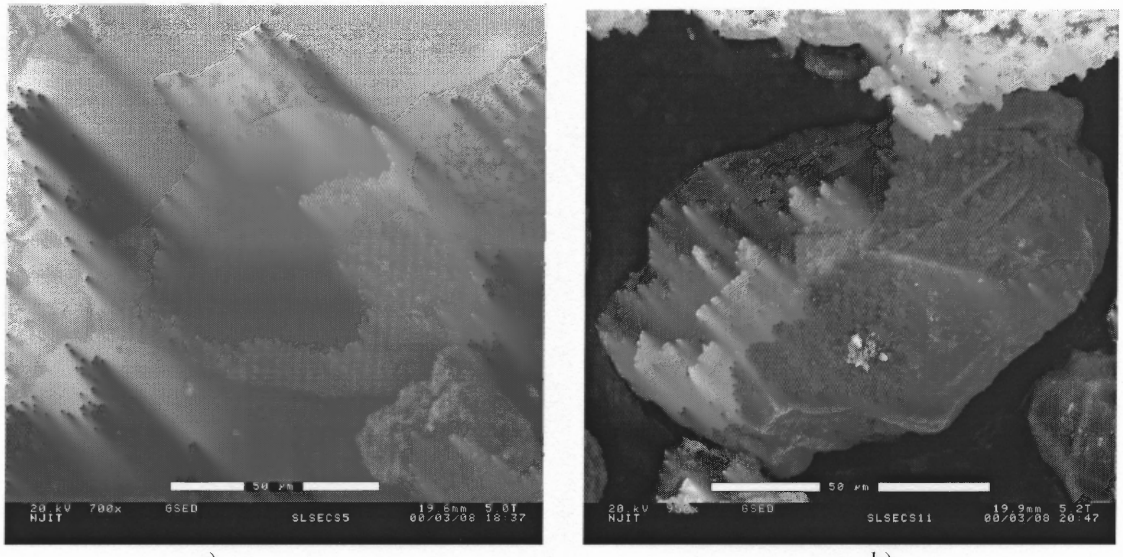

a) b)

Figure 5.18 Morphology of Shape C Particles

From the results, high chromium content accompanies high content of iron. The concentrations of both elements decreased in the order of Shape B> Shape A> Shape C particles. As chromium content decreased from particle B, A, and C, calcium concentration increased. During the chromate extraction process, calcium oxide reacted with chromite ore and subsequently formed calcium carbonate, which either separated from or deposited on the ore surface. The reaction proceeded inward and so did the formation of products. The observation on the morphology and the composition brought the assumption that Shape B particles represented the unoxidized ore, and the partially or fully oxidized and leached ores were Shape A particles. Figure 5.19 shows the timely perspective of ores at different stages along the extraction process: intact crystals, partially desurfaced crystals, and totally desurfaced crystals. The changing in chemical compositions, Table 5.14, reflects the degree of reaction of ores with calcium, decreasing in iron and increasing in calcium content.

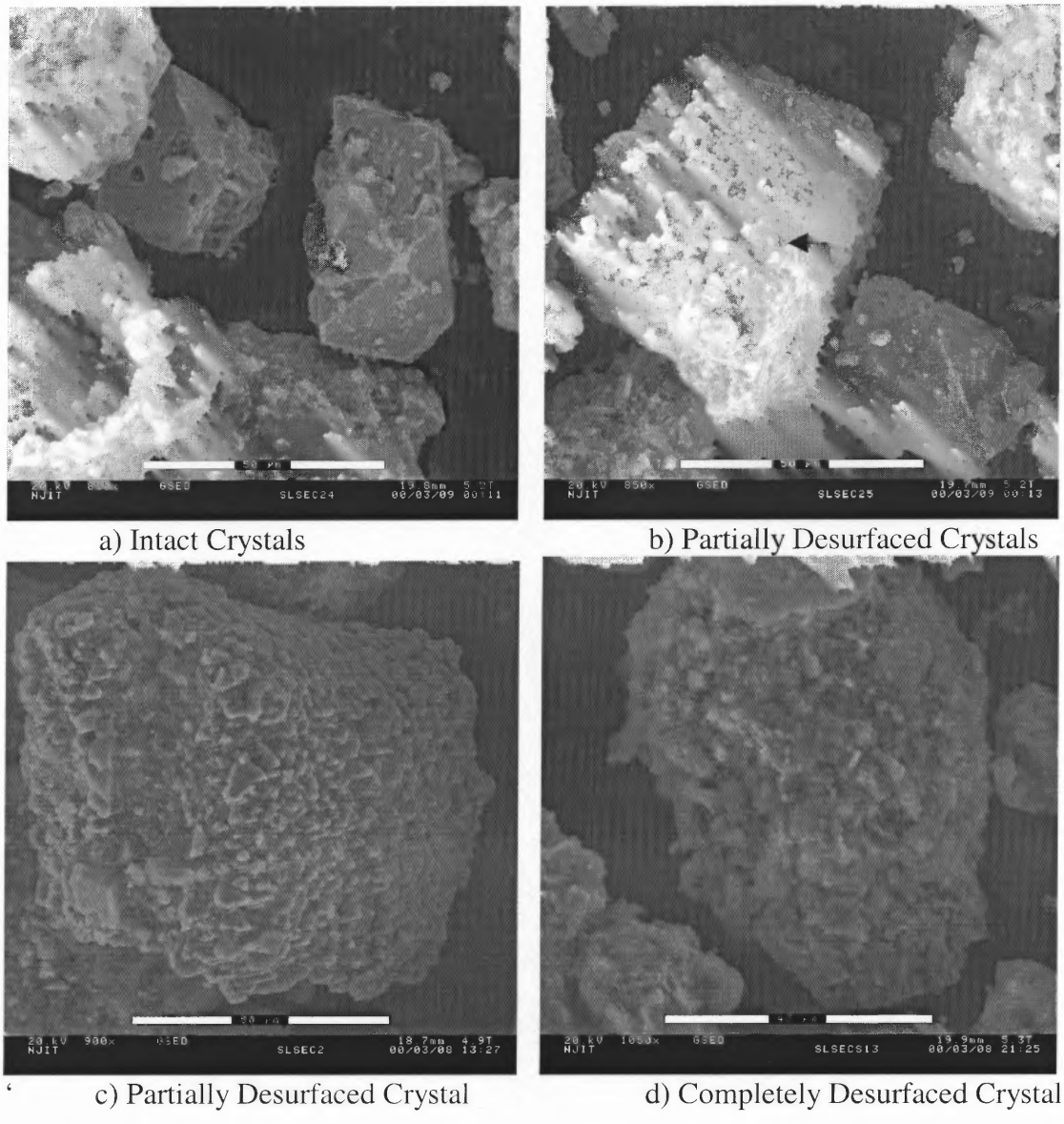

Figure 5.19 Assumed Deteriorating Process of Ores

The assumption that the calcium reacted and deposited on the ore surface allows a possibility that soils may contain higher iron contents. The XRF and XRD analysis are surface sensitive due to the x-ray penetration depth and the absorption. The impurities concentrating on the particle surface could absorb iron characteristic x-ray and emit their own characteristic x-rays. The result may have a lower concentration of iron oxide and higher concentration of impurities. For example, the photon energy of Fe$K\alpha$ is 6.39 keV.

The energy required to excite Ca $K\alpha$ is 4.038 keV. The mass absorption coefficient of Ca at the Fe$K\alpha$ wavelength is 312.71 cm^2/gm (Bertin, 1984). The density of Ca is 1.55 gm/cm^3 (Krause, 1979). According to the Lambert Law, $I = I_0 \exp(-(\mu/\rho)\rho t)$, where I-attenuated intensity, I_O – initial intensity, μ/ρ - mass absorption coefficient in cm^2/gm, ρ - density in gm/cm^3, t – thickness in cm, five percents of Fe$K\alpha$ intensity is absorbed by a Ca layer of 1 micron. Bertin (1984) intensively discusses the principle of x-ray. However, it is not possible to quantify this absorption effect due to the heterogeneity of soils.

The analysis of the composition of soils by acid digestion reported very different compositions (Kamolpornwijit, 1996). It reported high concentrations of Na and low concentration of Si, and was less reliable than results from XRF. The XRF still seems to give the best compositional analysis.

The tail with slightly lower specific gravity was initially believed to be different from the concentrate morphologically and chemically. However the XRF and XRD results suggest similarities. The observation on the morphology of the tail, Figure 5.20, leads to a few conclusions. First, tail particles are smaller than concentrate particles, the separation was mainly due to the difference in particle sizes. The tail has similar chemical concentration to the Shape A particle from the concentrate with slightly higher calcium content, see Table 5.12. The richer in Si, Al, and Ca causes the lower specific gravity of the tail. The tail also contains small octagonal crystals. Generally the tail still contains rather high content of iron.

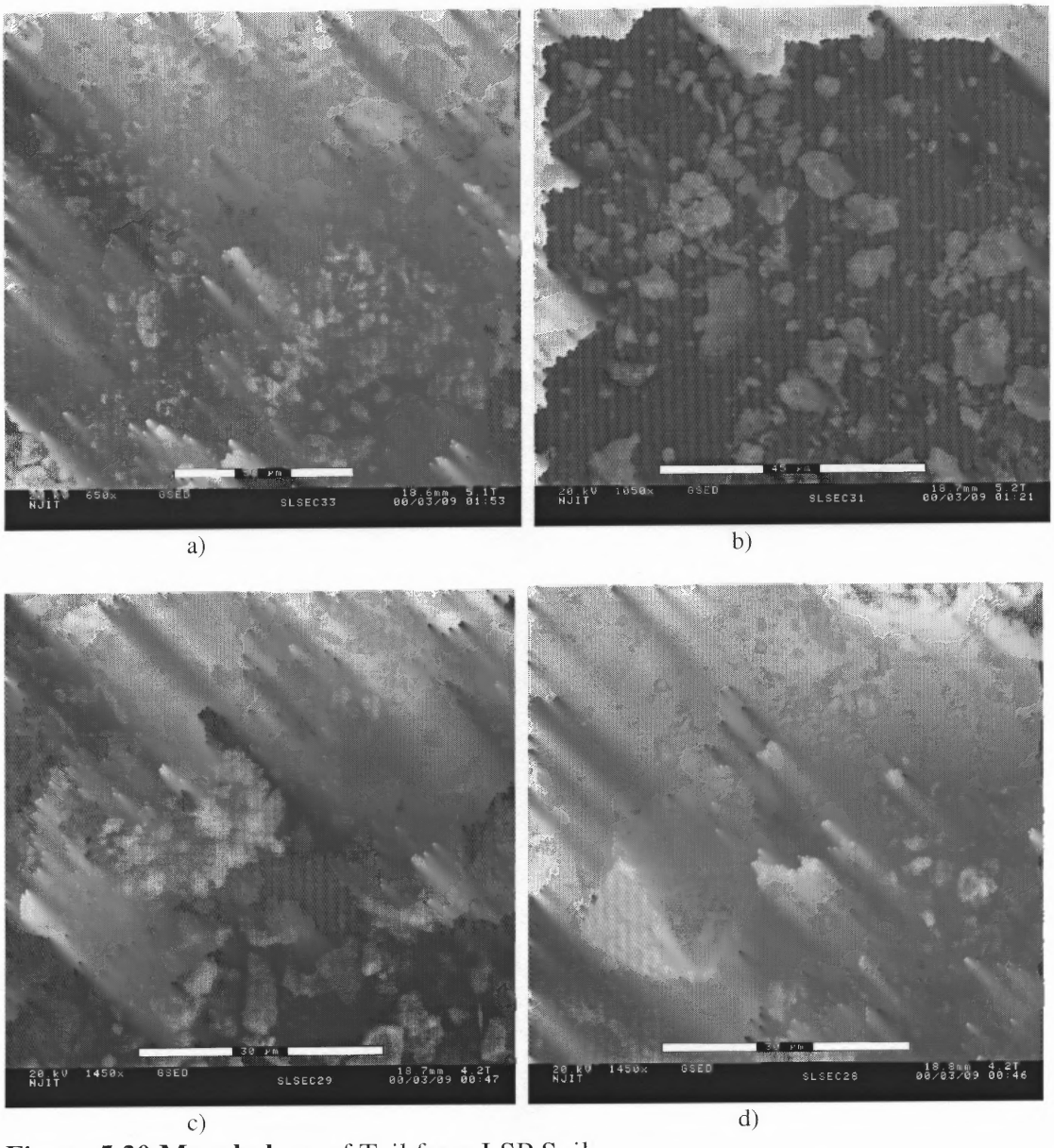

a) b)

c) d)

Figure 5.20 Morphology of Tail from LSP Soil

From the morphology and the microstructure analysis, the maximum iron and chromium contents in the concentrate are affected by the impurities, i.e., Mg, Al, and Ca, imparting in the spinel matrix, and calcium deposited on the particle surface. The iron and chromium contents of Shape B particles reflect the maximum iron and chromium contents, approximately 45% combining both iron and chromium concentrations. It is still lower than the high grade or processed ore, 60-70%. Therefore, the possibility of

reusing the concentrate as a substitute of iron ore in the currently operating process is rather slim.

Table 5.14 Compositions of Particles/Areas from LSP Soil

Particles/Area	Concentrations (% wt)							
	Fe	Ca	Si	Al	Mg	Cr	Others	O
Figure 5.16								
b) Shape A	28.6	10.6	4.0	8.4	8.2	4.8	-	35.4
c) Shape A	23.8	16.4	6.8	6.6	5.1	2.0	-	39.4
d) Shape A	21.8	16.5	4.0	7.8	6.4	2.4	-	41.1
Figure 5.17								
a) Shape B	40.1	4.5	2.3	8.3	11.5	5.0	-	28.4
b) Shape B	40.9	7.6	5.3	5.2	6.4	7.6	-	27.0
d) Shape B	36.2	6.2	3.0	4.4	7.8	13.9	-	28.5
Figure 5.18								
a) Shape C	6.6	3.2	21.5	18.7	1.3	-	K-9.5	38.6
b) Shape C	8.1	9.1	25.0	11.4	1.6	-	Na-5.6	39.2
Figure 5.19								
a)	52.0	5.7	2.5	5.4	5.6	8.1	-	20.8
b)	34.6	10.6	2.3	6.5	6.7	9.4	-	30.0
c)	31.9	10.7	4.2	11.0	8.0	14.6	-	15.8
Figure 5.20								
a)	21.8	13.4	8.8	9.4	6.1	3.8	-	36.7
b)	14.1	15.0	7.7	10.8	5.1	-	Cl-1.8	45.6
c)	28.0	18.1	3.9	5.7	2.8	4.7	Cl-1.7	35.0

The morphology of CD concentrate and particles of different shapes are given in Figure 5.21, and 5.22 and 5.23. Table 5.15 contains their compositions, using EDX. Particles in Figure 5.22 are sand or gravel, they have high concentration of Si. Particles in Figure 5.23 are similar to Shape A particles of LSP soil. They represented the processed ores.

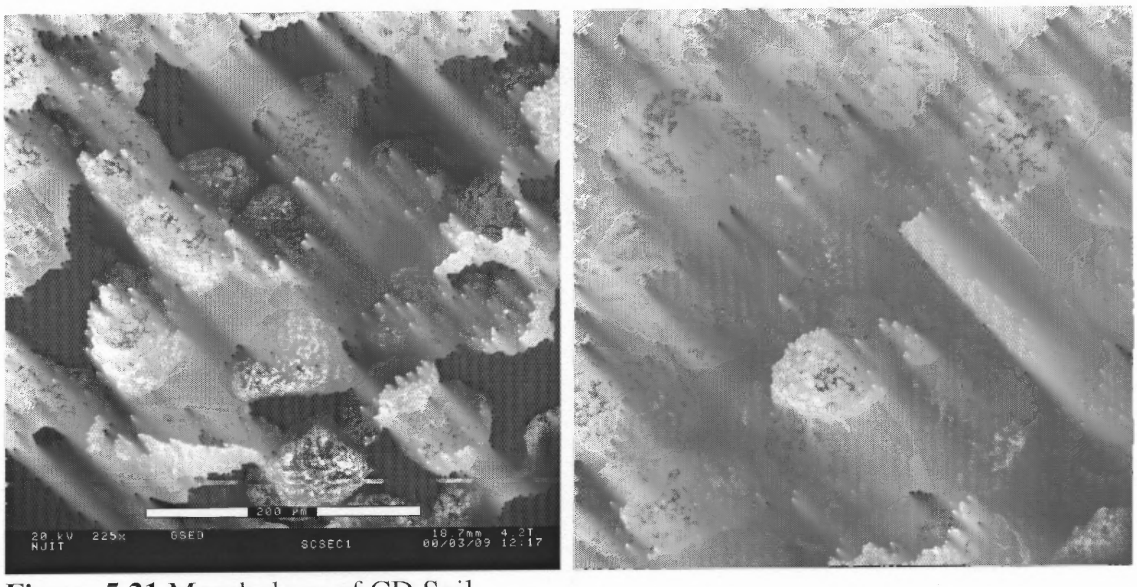

Figure 5.21 Morphology of CD Soil

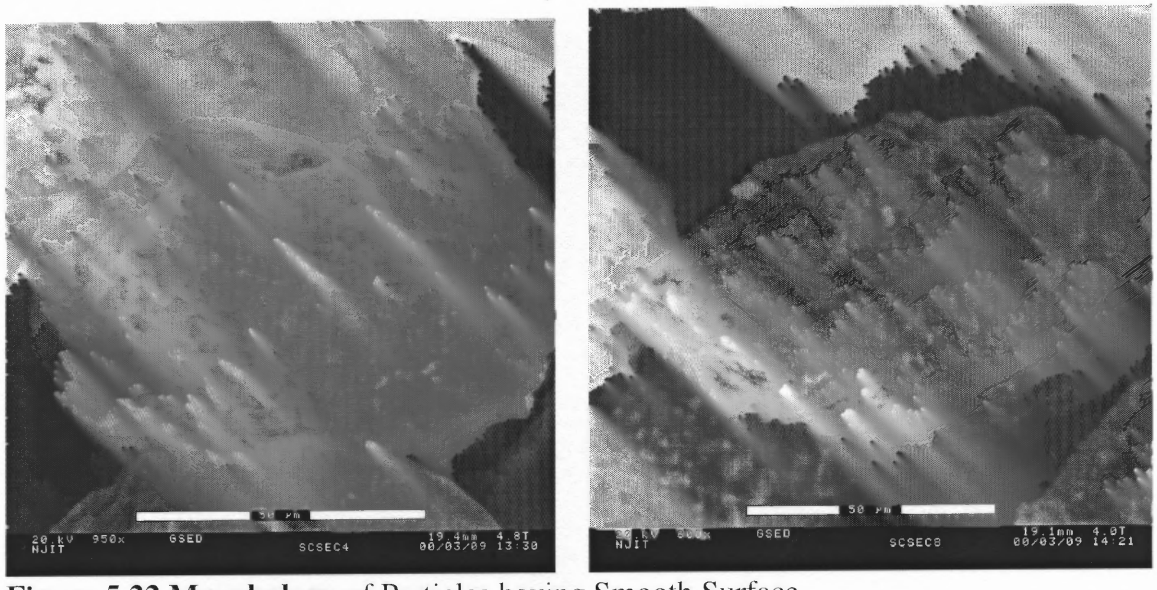

Figure 5.22 Morphology of Particles having Smooth Surface

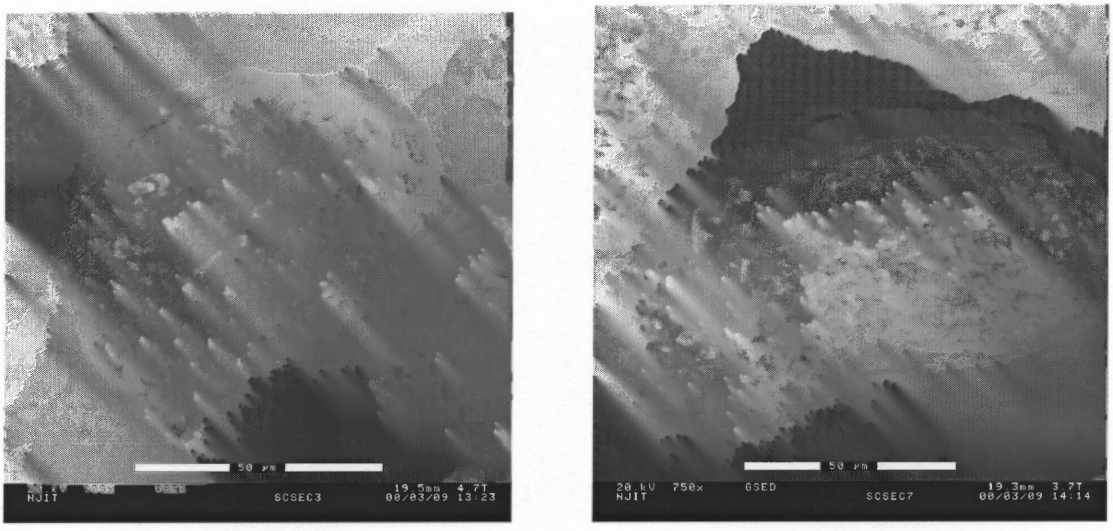

Figure 5.23 Morphology of Particles having Rough Surface

Table 5.15 Compositions of Particles/Areas from CD Soil

Particles/Areas	Concentration (% wt)							
	Fe	Ca	Si	Al	Mg	Cr	Others	O
Figure 5.22								
a)	3.6	3.5	42.6	2.8	2.3	-	-	45.3
b)	10.2	6.7	22.6	8.5	2.6	-	Na - 4.1	45.3
Figure 5.23								
a)	13.2	20.0	5.6	6.1	7.6	2.2	-	45.3
c)	21.0	21.6	4.1	5.4	4.6	2.4	-	41.0

5.6 Summary

There are two major studies in this chapter: the characterization of chromium contaminated soils and vitrified products, and the possibility to concentrate iron in soils to the same concentration of iron in iron ore using magnetic and gravitational separation techniques. The vitrification process plays a part in this research since it is an effective thermal treatment for chromium contaminated soils with similar operating temperatures to the iron and steelmaking process. In the next two chapters, the possibility of iron oxide reduction and metal separation of soils at high temperature will be presented.

Most of chromium contaminated soils contain high concentrations of iron, 23 % by weight on average, and have a potential of being a substitute of iron source for the iron and steel industry if the iron can be concentrated or extracted. Chromium normally coexists with iron as soils with high chromium content always have high iron content. There are two different groups of chromium contaminated soils, one with high iron concentrations (>20%) as magnetic spinel and the other having low iron but high silica or calcium contents. The iron is believed to exist in soil along with chromium, magnesium, and possible alumina as a solid solution of spinel, mostly magnetic for the first group of soils. The other major phases include calcium carbonate and silica. The spinel containing iron has higher specific gravity than the SiO_2 or $CaCO_3$. From the differences in magnetic property and the density the separation of iron and chromium might be possible through the magnetic and gravitational separation. The LSP soil was selected as a representative for soils with high iron content in a form of spinel. The CD soil represented the other group.

The magnetic separation yields a better efficiency and recovery rate for both iron and chromium than the gravitational separation. The iron concentration from the magnetic soil therefore serves as the highest iron content possibly concentrated. Both techniques are more efficient toward soils with high iron content, a group of soils represented by LSP, than soils with low iron content, represented by CD. Soils from LSP, CPR, GAR, and TPR, has iron concentration higher than 20% by weight and possesses magnetic properties. The gravitational separation, in this research, does not really separate particles with different specific gravity but rather with different sizes. The specific gravity of the concentrate and tail do not differ much causing the difficulty in the

gravity separation. The LSP soil is mostly magnetic unlike CD soil. The magnetic separation is able to concentrate iron and chromium oxides from 25.5-37.9% and 4.5-7.8% to 34.9-40.9% and 6.3-8.6% (LSP soil). The recovery rates of iron and chromium oxides are 84.9-99.2% and 86.6-99.8%. The morphology of LSP soil showed that soil is mostly in fact the mixture of unreacted, partially reacted, and fully reacted ores. The concentrate particles represent the products of different degree of extraction: intact crystal, partially reacted especially on the surface, and fully reacted. Based upon the given order, they have decreasing iron and increasing calcium contents. Unlike LSP soil, CD soil does not contain crystals resembling spinel but mostly rock-forming minerals.

Though the magnetic separation can concentrate iron and chromium, the iron and chromium concentration are not as high as high grade or processed ore. The usable iron ore in the Unites States for the past 35 years has iron content (Fe) not less than 57 %, concentrated from crude ore containing only 9-25% of iron (Kuck, 1998). The limitation in concentrating chromium contaminated soils is the species of iron oxide. The iron oxide is believed to exist as a mixed crystal spinel $(Mg, Fe).(Fe, Cr, Al)_2O_3$, which does not give as high iron content as Fe_3O_4 or the like. The pure magnesioferrite, $MgO.Fe_2O_3$, contains 55.8% of iron, less than the 72% of iron in magnetite. The chemical composition of magnetic soils from LSP do not change much as the particle size increases and the iron spinel is already liberated. The large magnetic and high iron content particles from LSP are in fact the agglomeration of fines.

The observation on the phases of the vitrified product from both bench and pilot scale ensures the application of the thermal treatment technology to soils of different chemical compositions and phases. The bench scale vitrified products yielded exactly

same phases but at different concentrations. The pilot scale showed the consistency of the products but with different phases from bench scale due to the contamination of the shakedown material. The phases of the product are controllable by adding sufficient major elements to govern the phase changes. The pilot scale test of LSP soil yielded the separation of ferrofurnace containing 86% by weight of iron. The production of ferrofurnace accounted for 3.3% by weight of the initial soil. During the pilot scale vitrification, the major concern was the treating of chromium contaminated soil not the recycling of metal. The percentage of carbon addition, 0.44% by weight, was not sufficient for the complete iron oxide reduction, which resulted in high iron concentrations in vitrified products. Nonetheless, the separation of ferrofurnace supports this research study.

The magnetic separation is able to concentrate iron and chromium contents in soils. Their concentrated contents are not as high as those of high grade or processed ores. The ironmaking process normally takes high grade or processed iron ore with 60-70% iron content. Nonetheless, the iron and chromium can possibly be extracted during the thermal treatment process, i.e. vitrification process, and be recycled in a metallic form instead of an oxide form.

CHAPTER 6

DISCUSSION OF RESULTS: THE REDUCTION OF IRON AND CHROMIUM OXIDE FROM CHROMIUM CONTAMINATED SOILS

The iron concentration results unveiled that the iron oxide content in soils is not as high as usable iron ores, which hinders the recycling of the iron and chromium concentrate as a substitute for an iron ore directly. The study of the reduction and metal separation then becomes necessary in this research. Though it is energy intensive due to its high operating temperature, it can be accommodated in existing treatment plants with minimal modification. The vitrification process is known for its efficiency in treating soils contaminated with heavy metal. At the vitrifying temperature, hexavalent will readily loose its oxygen and be reduced to trivalent chromium (Clark et al., 1975). Subsequently trivalent chromium is capture in the vitrified matrix by encapsulation, replacing with Si due to their similar atomic sizes, and bonding with non-bridging oxygen (EPA, 1992). By adding sufficient amount of carbon to soils and controlling the environment of the furnace, the metal oxide in soils should be reduced and separated during the vitrification. The modified vitrification process provides both remediation of chromium contaminated soils and production of metal, which possibly can be recycled to the iron and steel industries. The recycle metal would create some revenues thus bringing the operating cost down. The other crucial aspect of metal extraction comes from the regulatory point of view. To fully recycle the treated product, it has to satisfy specifications for metal. The metal separation would provide the ultimate solution with respect to long-term impacts. The application of vitrified product as construction aggregate also gains benefit

from the metal separation. The separation of metal decreases the specific gravity of the vitrified product, which facilitates the construction work.

The reduction study was performed in a Thermo-Gravimetric Analyzer (TGA) where the samples, placed in the alumina crucible, was flushed with nitrogen to create an oxygen-free environment. The reducing agent used throughout this research was solid carbon. Initially, TGA was planned to be used only as a furnace that supplies high heat under a controlled environment. Progressively understanding the process and the equipment has broadened the area of interest. The TGA later was used to study reductions under different conditions, the comparisons in reduction behaviors of different oxides, and the course of reaction.

The usage of solid carbon as a reducing agent has both advantages and disadvantages. The solid carbon, mixed with the sample, uncontrollably starts reacting with iron oxide in soils at high temperature unlike carbon monoxide which can be supplied at any time during the test. The use of carbon monoxide would provide a better observation of kinetic parameters. However, the solid carbon was selected over the carbon monoxide due to its potential use in a full scale or real applications. The study with reduction by carbon monoxide certainly is beneficial and can proceed provided time and funding are available.

In this chapter the reduction of iron oxide in chromium contaminated soils is discussed along with the reduction of hematite, magnisioferrite, calcium carbonate, and the oxidation of carbon. Most of results are described qualitatively. The approximated activation energy for the reduction of iron oxide in soils is also presented. Hematite represents the pure iron oxide and is tested for comparison. The magnesioferrite was

suggested in Chapter 5 as one of major phases of spinel. Soils also contain high concentrations of calcium carbonate. The results and discussion are presented in the following order: the reduction of soils including LSP soil and its approximated activation energy, CD, TPR, and GAR soils, hematite, magnesioferrite, chromate, calcium carbonate, and the oxidation of carbon.

6.1 Reduction of Iron Oxide in Soils

The reduction study was conducted using LSP soil as a representative of chromium contaminated soils containing high iron concentrations. The results and discussion from the reduction of LSP soil provided a framework to which test results of other soils were compared. The particle size of soils used was smaller than 75 μm. Parameters studied were time, temperature, and carbon contents. Unless otherwise stated, the standard test condition was 2 hours flushing with nitrogen at a rate of 40 cc/min at atmospheric pressure and room temperature, ramping at a rate of 40°C/min to a set temperature, maintaining in isothermal state for 1 hr, and cooling at a rate of 30°C/min down to 300°C. Soil is always heterogeneous and chromium contaminated soil is no exception. It was difficult to delineate all trivial behaviors during the course of reaction but focused on the main reactions.

6.1.1 Reduction of Iron Oxide in LSP Soil

The pure LSP soil, with no carbon addition and no nitrogen flushing, was tested and the result was illustrated in Figure 6.1. The total weight reduction of pure LSP soil was 12%. After 900°C the weight change was insignificant. Calcium carbonate starts losing it CO_2 around 650°C, as presented later in this chapter. There was 5% weight loss between

650°C and 850°C, which was mainly due to the transformation of calcium carbonate; accounted for approximately 10% calcium carbonate which was one half the concentration from the chemical analysis. The result suggested that not all Ca existed as $CaCO_3$. The calcium could be part of the spinel but not a major part due to its non-magnetic property when $CaO.Fe_2O_3$ was formed. There was a slight weight loss between 1200°C – 1400°C, which could be due to the transformation of oxide. The diffractogram did not show the presence of metal but the disappearance of calcium carbonate. The reduction to metal did not occur for a mixture of LSP soil and carbon without nitrogen flushing prior to heating. The oxidation of carbon with the remaining oxygen in the furnace was the cause.

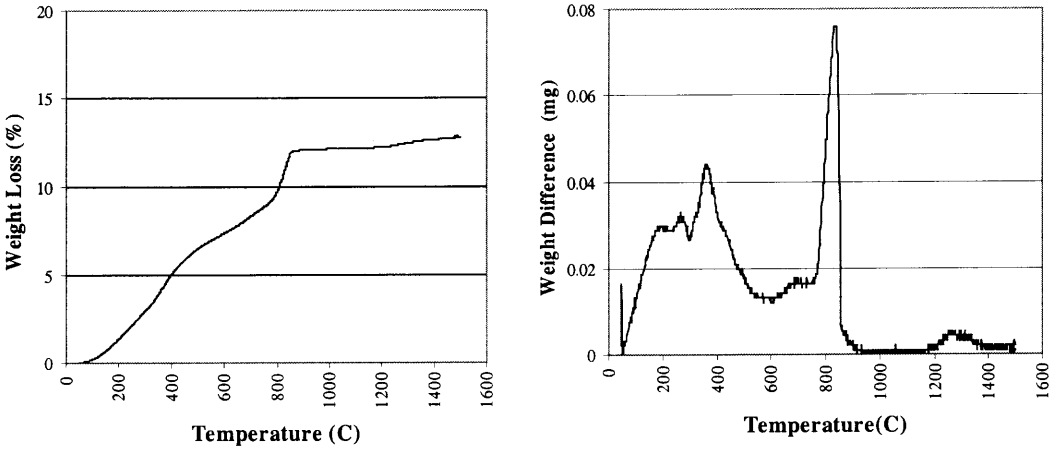

Figure 6.1 Weight Loss and Weight Difference Patterns of LSP Soil

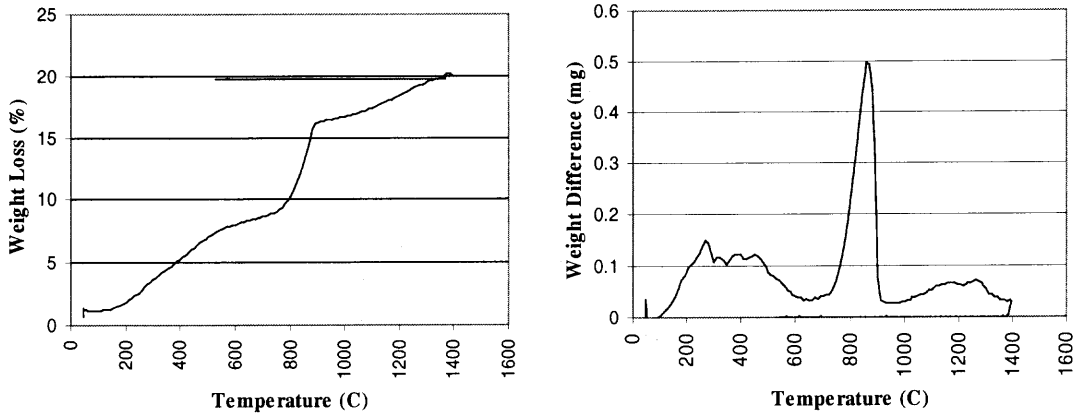

Figure 6.2 Weight Loss and Weight Difference Patterns of LSP Soil Purged with Nitrogen for 2 hrs Prior to Heating

The flushing of nitrogen for 2 hrs before subjecting sample to heating yielded weight loss of 4%, between 900°C and 1400°C, possibly due to the transformation of oxide in soils. The flushing of nitrogen reduced the oxygen partial pressure and may allow some reduction to take place, i.e. the reduction of Fe_2O_3 to Fe_3O_4. At such high temperature, the sintering can occur through diffusion and there might have some rearrangement of crystals. Figure 6.2 shows the weight loss and weight difference patterns of LSP soil.

6.1.1.1 Temperature. The following series of test results explained the reduction at different temperatures of LSP soils mixed with 20% carbon and flushed with nitrogen for 2 hours prior to heating. The percent weight losses at different temperatures were tabulated in Table 6.1, and graphically represented in Figure 6.3. Figure 6.4 shows the weight differences, the weight loss at each time step, at different temperatures.

Table 6.1 Percent Weight Loss at Different Temperatures

Tests	%Weight loss (during ramping period)	%Weight loss (Total)	Remark
L20_1400	30	40	2hr F, 20%C, 1400°C 1 hr
L20_1300	28	34	2hr F, 20%C, 1300°C 1 hr
L20_1200	22	28	2hr F, 20%C, 1200°C 1 hr
L20_1100	12	19	2hr F, 20%C, 1100°C 1 hr
L20_1000	11	13	2hr F, 20%C, 1000°C 1 hr
L20_900	10	11	2hr F, 20%C, 900°C 1 hr
L20-800	9	11	2hr F, 20%C, 800°C 1 hr
L20_700	7	10.5	2hr F, 20%C, 700°C 1 hr
L20_600	4.5	5	2hr F, 20%C, 600°C 1 hr
LSPG	12% upto 900°C	0.8% from 900 –1500°C	0 hr F, 0%C, 1500°C 0hr
LSPGC	15% up to 900°C	4% from 900-1400°C	2hr F, 0%C, 1400°C 1 hr

2 hrs F – 2 hrs flushing with nitrogen prior to heating

There were three main peaks in the plot of weight differences and temperatures, Figure 6.4 shows the weight loss from the moisture in sample and the oxidation of carbon with absorbed and remaining oxygen at 400°C, from $CaCO_3$ at 800°C, and from iron oxide at 1200°C. Between 600°C and 900°C, there was a weight loss of 4.5% from the formation of CaO which was similar to the weight loss from pure LSP soil. The weight loss increased drastically after 1000°C, unlike the result for pure LSP soil. It was clear that carbon facilitated the reduction of iron oxide in LSP soil. The reduction proceeded very fast and readily finished before the isothermal period for the 1400°C test, implied by the declining of weight differences, at 1200°C. The formation of metal phase was confirmed at 1100°C and above, Figure 6.5. There was also a formation of white fluffs when there was a reduction to metal. The LSP soil contained approximately 41% of iron and chromium oxides, which was diluted to 32.8% after the addition of carbon 20% by weight. The weight losses of 17.4% or 13.7% are expected for the product formation of CO or CO_2: $Fe_2O_3 + 3C = 2Fe + 3CO$ and $Fe_2O_3 + 1.5C = 2Fe + 1.5\ CO_2$. The percent

weight loss from the 1400°C test, from 1000 – 1400°C, was 19%. The result suggested the product formation of CO over CO_2.

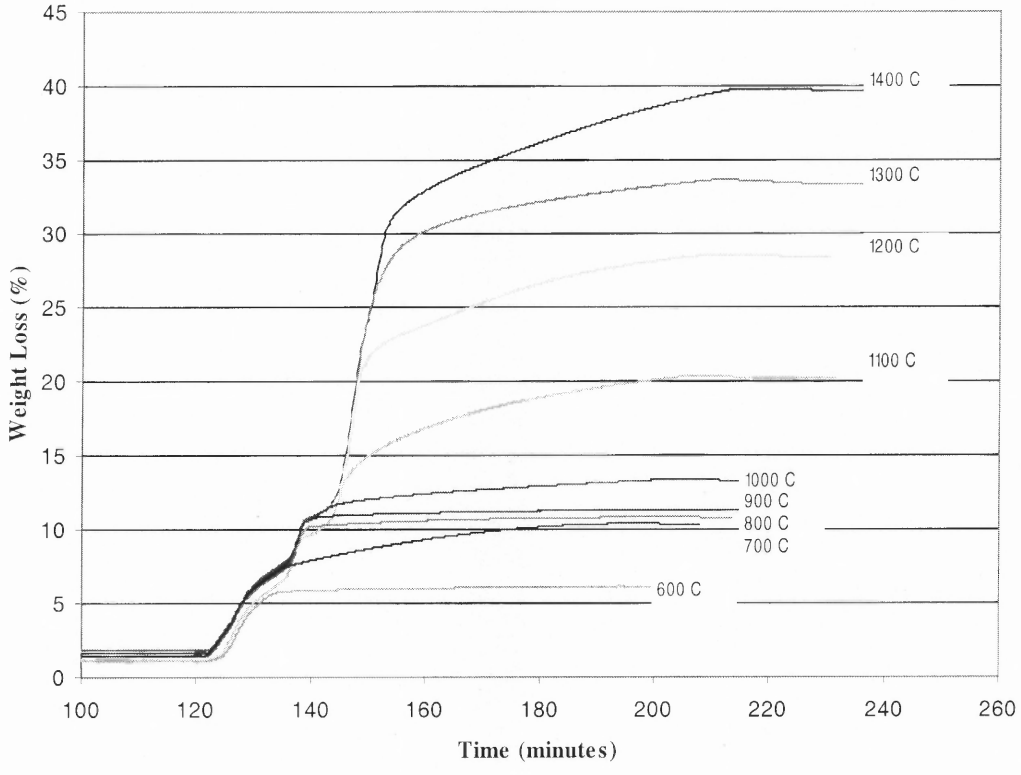

Figure 6.3 Percent Weight Losses of LSP Soils Mixed with 20% Carbon at Different Testing Temperatures

Figure 6.5 shows phases of tested samples at different temperatures. The detailed identifications of phase changes are shown in Figure 6.6. Unlike the reduction of iron oxide, where the complete reduction can be identified by the constant weight or by the formation of iron droplets, the reduction in soil is more complex and the complete reduction to metal has to be confirmed by XRD.

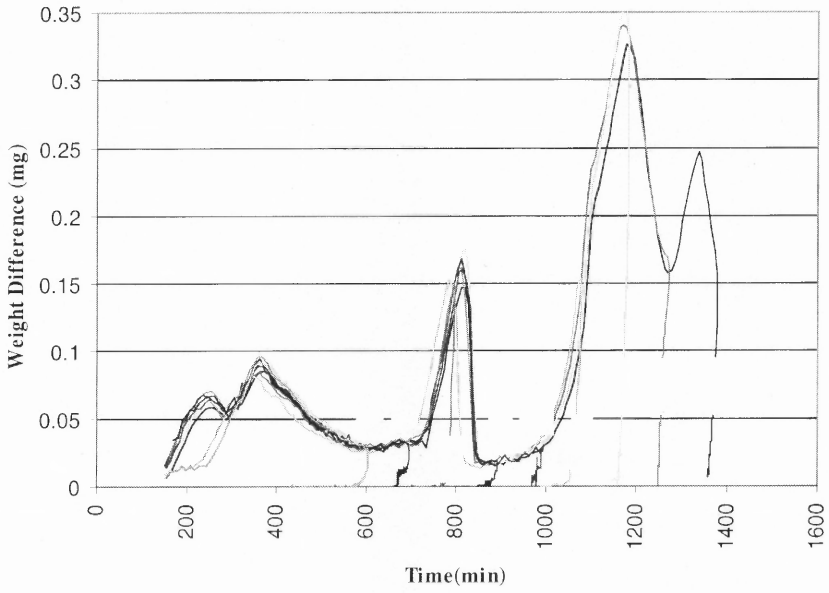

Figure 6.4 Plots of Weight Difference and Temperature of LSP Soils Mixed with 20% Carbon at Different Temperatures

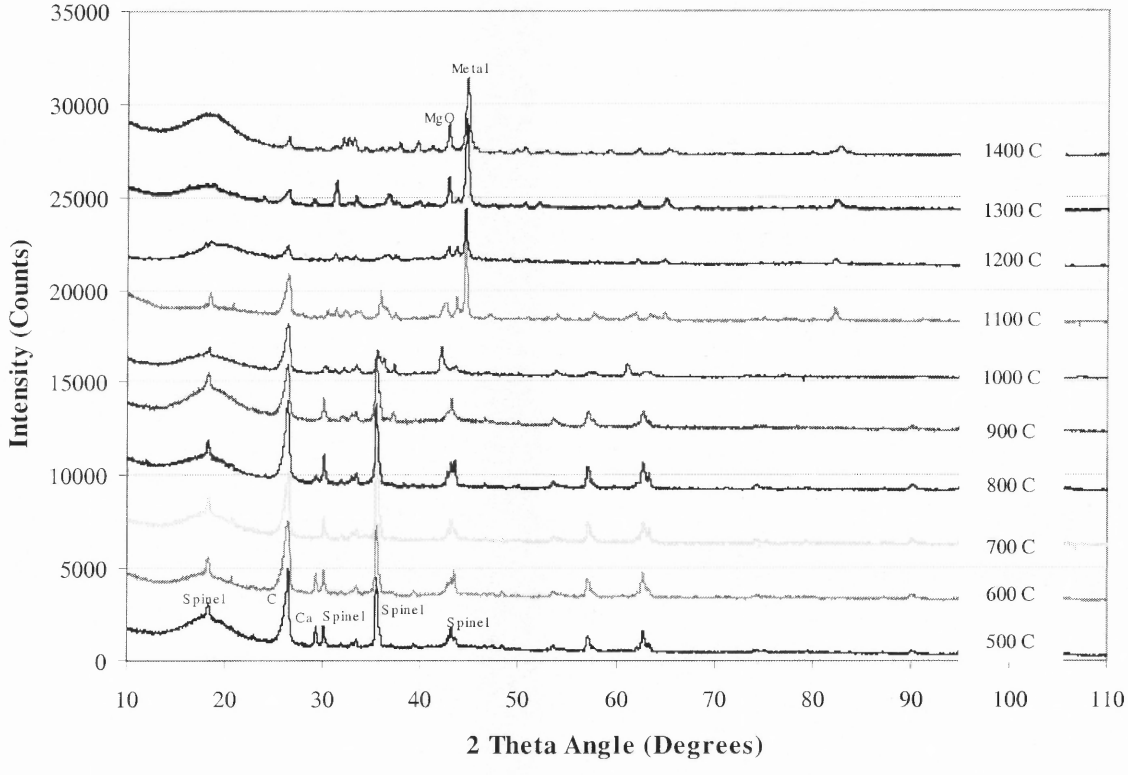

Ca : $CaCO_3$, C : Carbon

Figure 6.5 Diffractograms of LSP Soils at Different Temperatures, 20%C

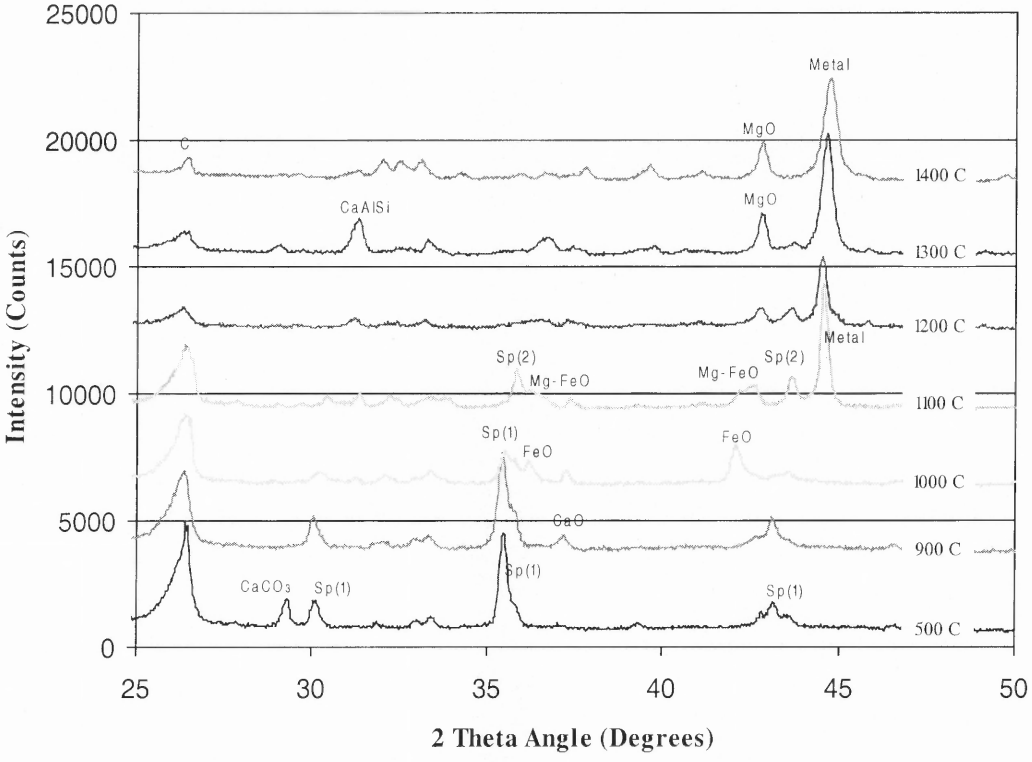

Sp(1) : (Fe, Mg)(Cr, Fe)$_2O_4$, $MgFeAlO_4$, $MgCr_2O_4$
Sp(2) : (Mg, Fe)(Cr, Al)$_2O_4$, $MgCr_2O_4$, Fe(Cr, Al)$_2O_4$
Mg-FeO : $Mg_{1-x}Fe_xO$
CaAlSi : $2CaO.Al_2O_3.SiO_2$
Scanning program: step size – 0.03° 2θ, time/step – 5 seconds

Figure 6.6 Diffractograms of LSP Soils, 25-50° in 2θ

There are definite changes observed from Figures 6.5 and 6.6, the disappearance of spinel and $CaCO_3$, and the formation of MgO and metal at high temperature. The metal peaks formed at an expense of the spinel. The $CaCO_3$ is not stable beyond 700°C and the formation of CaO was first observed for 700°C test. For the 1000°C test, the spinel peak at 43° in 2θ almost disappeared and the FeO peak gained its intensity. There was still no metal peak. The reduction of iron oxide in soils started at this temperature resulting in the formation of FeO. At this temperature, the spinel was more likely to be of the following types; Fe(Cr, Al)$_2O_4$, $MgFe_2O_4$, and $MgFeAlO_4$. The reduction to metal

occurred and showed in the 1100°C test. There was still the remaining of spinel. The spinel were identified in the order of the likeliness as (Mg, Fe)(Cr, Al)$_2O_4$, $MgCr_2O_4$, and Fe(Cr, Al)$_2O_4$. There was also the formation of Mg_{1-x}-Fe_xO, the mixed crystal of MgO and FeO. The spinel peak disappeared at 1200°C, and there was a separation of MgO. The reduction was complete for the 1300°C and 1400°C tests with intense MgO peaks. The intensity of carbon peak reduced as the temperature increased, and was hardly seen in the 1400°C test.

From the results, the existence of mixed crystal spinel with different degrees of reducibility was concluded. The position of spinel peaks moved for half a degree at 1100°C. The identification of spinel types was still not as clear and there were quite a few candidates as given in Figure 6.6. Ignoring other factors, the stability of oxides is in the order of Al_2O_3> Cr_2O_3> FeO> Fe_3O_4> Fe_2O_3. The highly reducible type, possibly Fe_3O_4 and Fe_2O_3, was reduced to FeO at 1000°C. At 1100°C, FeO was reduced to metal. There was also the separation of MgO possibly from $MgO.Fe_2O_3$. The MgO further reacted and formed mixed crystal with FeO. Or in another word, the $MgO.Fe_2O_3$, magnesioferrite, was reduced to MgO.FeO, magnisiowustite. After this point only the hardly reduced spinel was left, i.e. $MgAl_2O_4$ and $MgCr_2O_4$. At higher temperatures, 1300C° and 1400°C, the spinel peaks totally disappeared which can be either through the reduction or the formation of a new phase. The formation of $2CaO.Al_2O_3.SiO_2$ was also frequently reported as a reduction product.

The white fluffs observed on top of the sample or on the hangdown wire were identified as MgO. The formation was very pronounced at 1400°C. It suggested the existence of spinel of type $MgO.Fe_2O_3$, which are strongly magnetic, the property of soil

from LSP. The deposition of MgO on the hangdown wire must be via the gas phase since there is no direct contact between the wire and the sample. Literatures (Lekatou and Walker, 1997) suggested the separation of MgO and Fe_2O_3 prior to the reduction. The separation is an inverse process of the spinel formation. The sintering of MgO and Fe_2O_3 can yield $MgO.Fe_2O_3$ spinel through the solid state diffusion. There are at least five proposed mechanisms for the spinel formation, for example, the counter cation diffusion, or oxide diffusion, or cation diffusion and gaseous oxygen diffusion (Holt, 1967). The evaporation of oxide during the spinel formation was also reported (Hauffe, 1967). For the disintegration of spinel, the opposite mechanism may apply. The Mg may evaporate into gas phase while it diffused through the ion lattice. Referring to the evaporation chart, Figure 3.8, the elemental Mg and Ca have higher vapor pressures than those of MgO and CaO, under vacuum. The boiling point of Mg is 1100°C compared to the 3600°C for the MgO. The MgO has less chance to evaporate than the elemental Mg. After the evaporation, Mg vapor reacted with CO to form MgO and C, a chemical reaction that occurred at temperature below 1900°C (Emley, 1966), and deposited on top of the sample and the hangdown wire.

Table 6.2 Concentrations and Mass of Ca and Mg Lost during the Experiment

ID	Volume (ml)	Ca			Mg		
		A[1]	ppb[3]	µg	A[1]	ppb[3]	µg
Blank	3.5	0.043	473	1.65	0.109	76	0.266
Sample	3.2	0.047	517[2]	0[2]	0.964	599[2]	1.65[2]

(1) - Average values from three readings
(2) - Values after the subtraction of concentration/mass of blank
(3) - Concentration is calculated based on an extrapolation of the linear calibration curve: 70 ppb to 400 ppb for Mg, and 1.1 ppm to 3 ppm for Ca.

The evaporation of Mg can cause a weight loss at high temperatures which may be misinterpreted as a weight loss from the reduction of iron oxide. A water trap was employed to capture the Mg and Ca volatilizing from the furnace through exhaust tube during the 1400°C test of LSP soil. The Atomic Absorption Spectrometer showed the increased absorption of only Mg (Table 6.2). Though the sampling water had an adsorption value 9 times higher than blank, it accounted for only 1.65 microgram of MgO in soil sample. The weight loss through the evaporation of Mg is therefore trivial.

6.1.1.2 Reducing Agent. The reduction to metal did not occur without the addition of reducing agent. The required amount of solid carbon for complete reduction was investigated. Different amounts of carbon, 5%, 10%, 15%, and 20%, were added to LSP soil and tested at 1400°C. Figure 6.7 and 6.8 show weight loss patterns and diffractograms for the above tests. The 5% test yielded FeO or $Mg_{1-x}Fe_xO$, not metal. The metal peak and the FeO or $Mg_{1-x}Fe_xO$ formed at the 10% test. The minimum of 15% carbon addition was required for a complete reduction to metal. The diffractogram of a test with 20% carbon addition showed a peak of remaining carbon. The larger percentage of carbon means a larger number of contact sites for the solid state reduction or the gasification and should result in a higher reduction rate. The result agrees with the assumption, the reduction rate was faster for the 15% and 20%, Figure 6.7. The effect was more pronounced at higher temperature. Below 1000°C, increasing of the carbon addition did not have much effect. It is possibly due to the very slow rate of direct reduction at low temperature. The reduction rate of the 25% test was slower than the 20% test confirmed by another set of experiments.

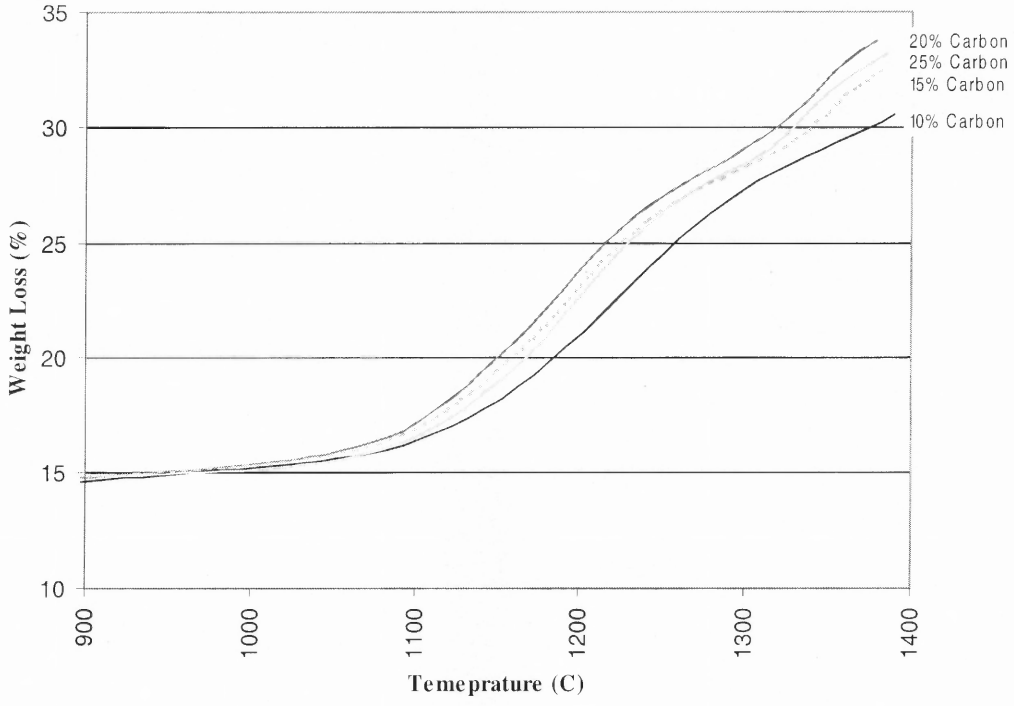

Figure 6.7 Weight Loss Patterns of LSP Soils with Different Amounts of Carbon

With larger numbers of contact sites, the reduction produced larger quantity of product, CO. Larger partial pressure of CO could enable the reduction to take place at a lower temperature. Observing the weight loss pattern, there was a slightly decrease in the temperature where the sample started losing weight at the 15% and 20% carbon contents. The 10-20% tests also showed the dependency of the reduction process on the quantity of carbon. As carbon content increased, at the expense of iron oxide content, the reduction rate increased. The results suggested the dependency of the reduction on carbon rather than iron oxide. The 25% test, where the reduction rate was slower than the 20% test, reflected the dilution effect by adding too large quantity of carbon, too small quantity of iron oxide

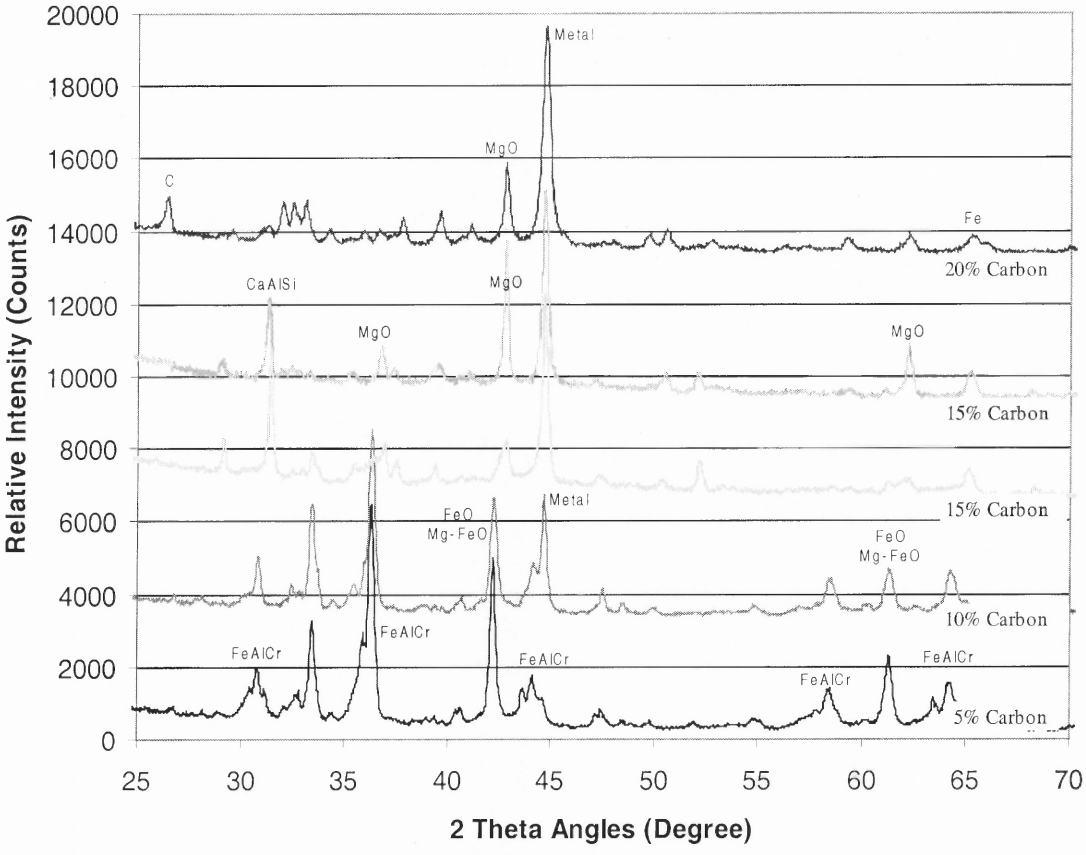

FeAlCr : $Fe(Al, Cr)_2O_4$
Mg-FeO : $Mg_{1-x}Fe_xO$
CaAlSi : $2CaO.Al_2O_3.SiO_2$
Scanning program: step size – 0.03° 2θ, time/step – 5 seconds

Figure 6.8 Diffractograms of LSP Soils with Different Carbon Additions

For the reduction of Fe_3O_4 and $MgOFe_2O_3$, approximately 17.3% and 6.5% of carbon are stoichiometrically needed for the CO formation. The spinel presumably containing iron constitutes slightly less than half of the soils mass, the amount of carbon needed was then half of those given numbers. The test result showed that approximately 15% was needed for the complete reduction. The possibility for the excessive carbon consumption were the oxygen remaining in the furnace, the larger content of iron oxide, and the reduction of other oxide. From the test with pure carbon, it lost 2.0 and 2.9 mg during the ramping period for tests with 2 and 3 hours of nitrogen flushing prior to

heating. The mass of carbon for the 2-hr test and 3-hr test were 26.6 and 32.2 mg. The 15% carbon addition to a 40 mg of sample is 6 mg. Subtracting 2.5 mg of carbon consumed with no contribution to the reduction, the adjusted weight percent carbon is 9%.

Hematite needs respectively 18.5% and 10.5% carbon to form CO and CO_2. The test results showed that the addition of 15% carbon allowed partial reduction of Fe_2O_3 to Fe with some remaining FeO. The reduction to metal droplet was complete for the test with 25% carbon with physically observable amount of carbon. Following the same calculation of 40 mg of sample, 25% is 10 mg. Subtracting 2.5 mg, the adjusted carbon percentage was 19%.

After taking the loss of carbon into account, the percentage carbon required is closer to the stoichiometric percentage. The excess carbon consumption was more likely due to the absorbed oxygen on the sample, which increased with the sample mass. The result suggested that the carbon consumption was subjected to the experimental setup.

6.1.1.3 Time. The results suggested the possibility of a complete reduction during the ramping period. A series of tests with varied isothermal periods were investigated. The samples were flushed and heated at the standard ramping rate, 40°C/min, to 1400°C and then kept at different isothermal period. The percent carbon addition was 15%. The diffractograms of tested samples kept isothermally at 0, 5, 30, and 45 minutes did not show many differences except for the presence of a very small spinel peak at 44° in 2θ for the 0-minute test, Figure 6.9. The result confirmed the complete reduction within the

first 5 minutes of the isothermal period. Therefore time is not critical for the reduction at temperature as high as 1400°C.

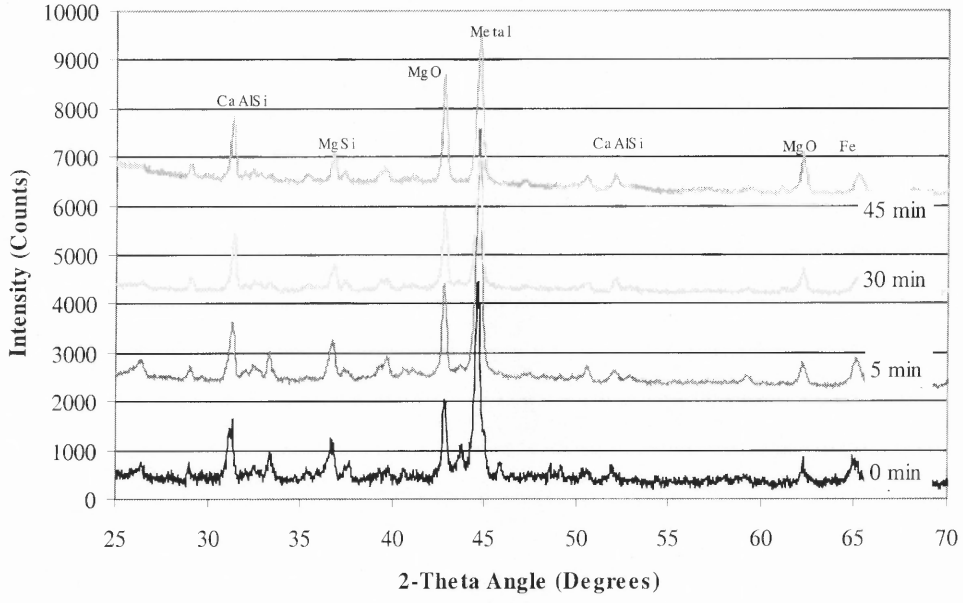

MgSi : $2MgOSiO_2$
CaAlSi : $2CaO.Al_2O_3.SiO_2$
Scanning program: step size – 0.03° 2θ, time/step – 6 seconds

Figure 6.9 Diffractograms of LSP Samples at Different Isothermal Periods

The weight loss patterns, Figure 6.10, show the constant weight after 15 minutes. There was no difference among the 15, 45, and 120 minute tests. The result suggested the complete reduction within the first 5 minutes. The oxidation results of pure carbon showed that carbon lost weight duirng isothermal period at 1400°C. The weight losses were 2.2 and 2 mg for tests with 2 and 3 hr nitrogen flushing prior to heating. The complete depletion of carbon resulted in the constant weight at the end of the reduction. However, at such high temperature, chances of reductions of other oxides or other chemical reactions might occur as well.

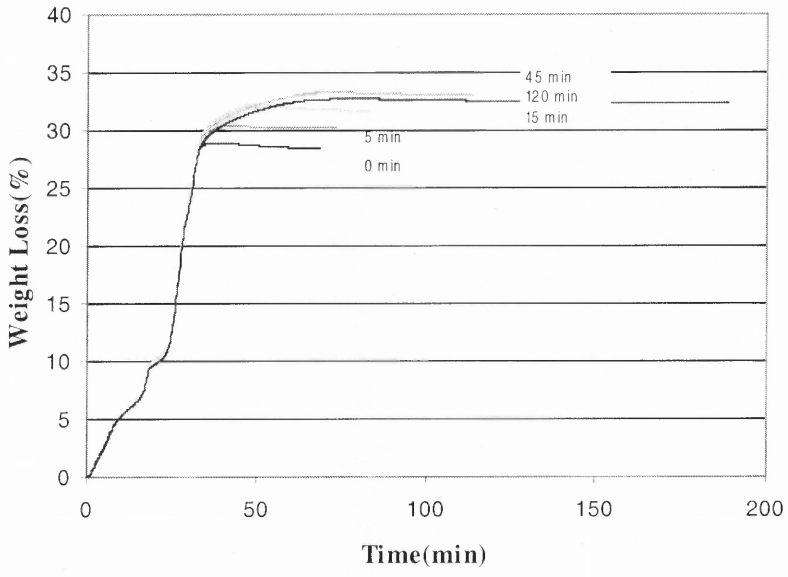

Figure 6.10 Weight Loss Patterns of Soils at Different Isothermal Periods

6.1.1.4 Rate Limiting Processes

Literature (Section 3.3.1) suggests the Boudouard reaction was the rate limiting process and the chain reaction of direct and indirect reduction, mostly through indirect reduction, was accounted for reduction of iron oxide in the solid state. Even though the indirect reduction is a main path for the reduction that does not mean that the product has to be rich in CO_2. Provided that the reduction proceeds at a certain CO/CO_2 ratio at a design temperature, the reduction and gasification propagate toward this equilibrium ratio. For example, at 1400°C the reduction of FeO to Fe requires a ratio of CO/CO_2 to be 5, which render approximately $5*10^{-11}$ atm partial pressure of oxygen. The majority of the product is still CO. Therefore, the weight loss of LSP soil, which was similar to weight loss from the formation of CO, is not necessarily caused by direct reduction.

If direct reduction, which produces CO, governs the rate the building up of CO partial pressure would retard the reduction process, and the increasing of purge gas flow rate should increase the reduction rate. Two sets of tests were conducted: one using a lid with a pinhole to cover the crucible allowing the building up of CO at the beginning of the reduction, the other applying different purging rates of nitrogen. For the first set of experiment, the samples were slowly heated, at a rate of 5°C/min from 825°C to 1350°C, for a better observation of weight changes. The weight loss pattern for tests with and without lid showed not much difference at high temperature, Figure 6.11. At lower temperature where the gasification and solid reduction rates were slow, confining the sample helped increasing the reduction rate by increasing the CO partial pressure. The lid has a pinhole and does not provide a completely sealed crucible. However, the presence of a lid retarded the diffusion of CO from the crucible at the beginning of the reaction. At high temperatures where the CO/CO_2 ratio between the equilibrium among $C\text{-}CO\text{-}CO_2\text{-}O_2$ and $FeO\text{-}CO\text{-}CO_2$ is very different and the gasification rate was fast, the partial confinement has little effect. The above results suggested that the indirect reduction played an important role in the reduction of iron oxide by solid carbon.

Figure 6.12 shows weight loss patterns of LSP soil mixed with 25% carbon at different nitrogen flow rate: 40 and 50 cc/min. The reduction proceeds faster at the lower nitrogen flow rate, which agrees with the results given by Baldwin (1955). In creasing the removal rate of CO should have positive effect on the direct reduction: $FeO_{(s)} + C_{(s)} = Fe_{(s)} + CO_{(g)}$. The results suggest the opposite and imply the effect of the gas phase on the reduction rate, the indirect reduction.

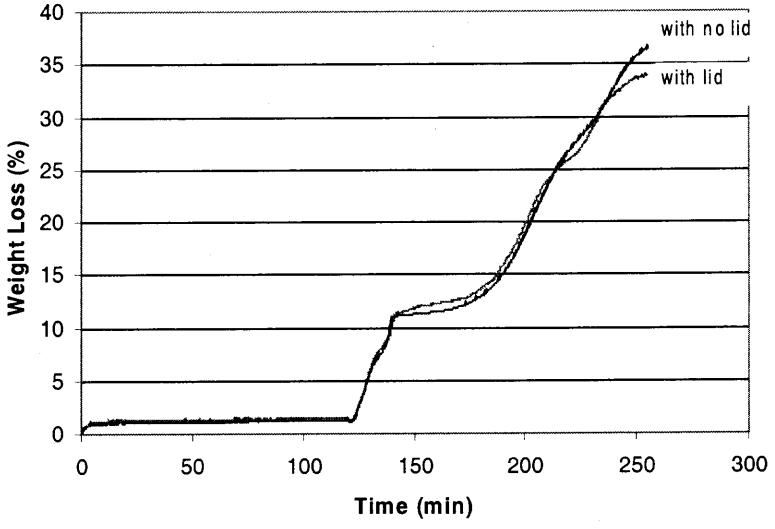

Figure 6.11 Weight Loss Patterns of LSP Soil with and without a Lid

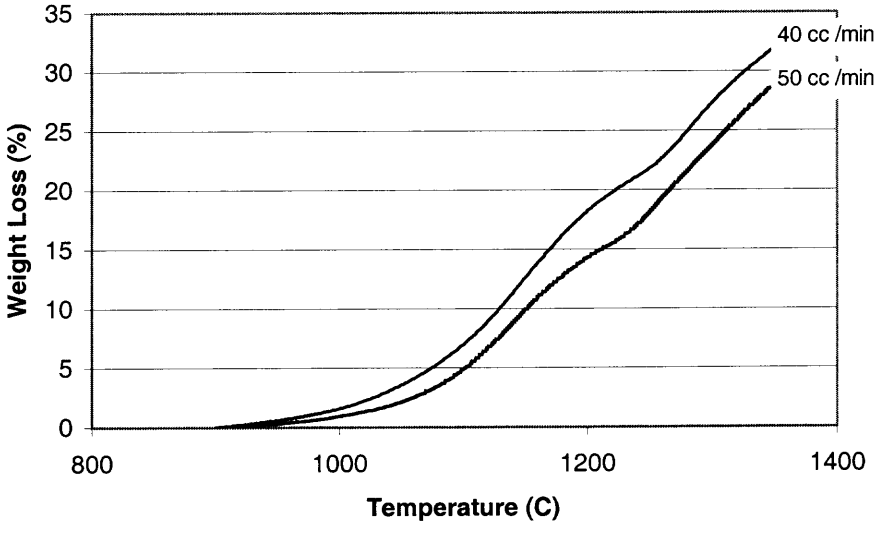

Figure 6.12 Weight Loss Patterns of LSP Soil at Different Purging Rates

The weight loss pattern of the LSP soil did show a transition around 1200°C, Figure 6.12. The formation of iron oxide mixed crystal changes the activity of iron oxide and the equilibrium ratio of CO/CO_2. According to the literature, the separation of

iron oxide and other oxides should proceed before the reduction (Lekatou and Walker, 1997). The transition might reflect the diffusion of the mixed crystals, which was the rate limiting process at that moment. After the transition stage, the reduction of remaining iron oxide occurred. The transition may as well be the stage where the reduction was almost complete. From Figure 6.11, A test with a lid faced an early transition, showing the enhancing effect of the increasing CO partial pressure.

Regardless of the reduction path, the reduction chain was initiated by the direct reduction for the formation of CO. Unlike the reduction by controlling CO/CO_2 ratio that can proceed at low temperature, the reduction by solid carbon start above 900°C as reported by Yun (1961) and in agreement with research results reported in this study. After the initial direct reduction the CO reacted with iron oxide yielding CO_2 which reacted, as part of the chain reaction, with carbon to form CO.

The results suggested the indirect reduction governed the process. However, in this research, the reduction of iron oxide in soil to metal does not occur at temperature below 1100°C. Considering the equilibrium between O_2, CO and CO_2, Figure 3.2, the CO/CO_2 ratio at 700, 800, 900, 1000, 1100°C are 1.8, 7, 39.8, 158.5, and 501 respectively. For the reduction of FeO to Fe at 700, 800, 900, 1000, 1100°C, Figure 3.1, the CO/CO_2 ratio must be between 5 and 4. During most of the tests crucible was not capped and they never reached the equilibrium condition. The closer the equilibrium ratio of CO/CO_2 between $CO\text{-}CO_2\text{-}O_2$ and $FeO\text{-}CO\text{-}CO_2$ systems, the lesser the chance the reduction will proceed. The difference grows larger at higher temperature. At 1000°C, the ratio are 39.8 to 5. It was this temperature where the reduction of iron oxide

to FeO occurred. Above this temperature, there was a reduction of iron oxide to metal. The process was complicated by the intertwining not only of the direct and indirect reduction but also temperatures. The direct reduction initiated the reduction, followed by the chain reduction of direct and indirect reduction which built up the CO partial pressure. Below a certain temperature, the reduction could not proceed due to the lack of proper CO/CO_2 ratio possibly due to the slow gasification rate. The increasing of the amount of reducing agent and the partial pressure of CO enhanced the reduction.

The results from Section 6.1.1.2 (Figure 6.7) suggested that the reduction rate was dependent on the amount of added carbon. The reduction rate increased from 10 to 20% carbon additions. The iron oxide concentrations decreased at the expense of the increasing carbon additions and did not have observable retarding effect on the reduction rate. The reduction rate was, therefore, influenced by carbon not iron oxide concentration.

There are three main kinetics models describing the reduction of iron oxide by CO: the first order phase boundary reaction, the shrinking core phase boundary model, and the solid state diffusion model (Bogdandy and Engell, 1971; Haque et al., 1992; Ray and Prasad, 1992). The gasification of carbon followed first order kinetics or shrinking core model (Table 3.1) Equations 6.1-6.6 describe the relationship of each model to the degree of reduction (DOR).

First order $$\frac{d(DOR)}{dt} \quad \alpha \quad (1 - DOR) \tag{6.1}$$

or $$\ln(1 - DOR) \quad = \quad kt \tag{6.2}$$

Shrinking core $$\frac{d(DOR)}{dt} \alpha (1-DOR)^{\frac{2}{3}} \quad (6.3)$$

or $$1-(1-DOR)^{\frac{1}{3}} = kt \quad (6.4)$$

Diffusion $$\frac{d(DOR)}{dt} \alpha \frac{(1-DOR)}{1-(1-DOR)^{\frac{1}{3}}} \quad (6.5)$$

or $$1-\frac{2}{3}(DOR)-(1-DOR)^{\frac{2}{3}} = kt \quad (6.6)$$

Figure 6.13 shows plots of DOR and d(DOR)/dt between three different models and a test results at 1200°C, 20% carbon addition. The pattern of the 1200°C test is more likely to follow the phase boundary reaction model especially the shrinking core model.

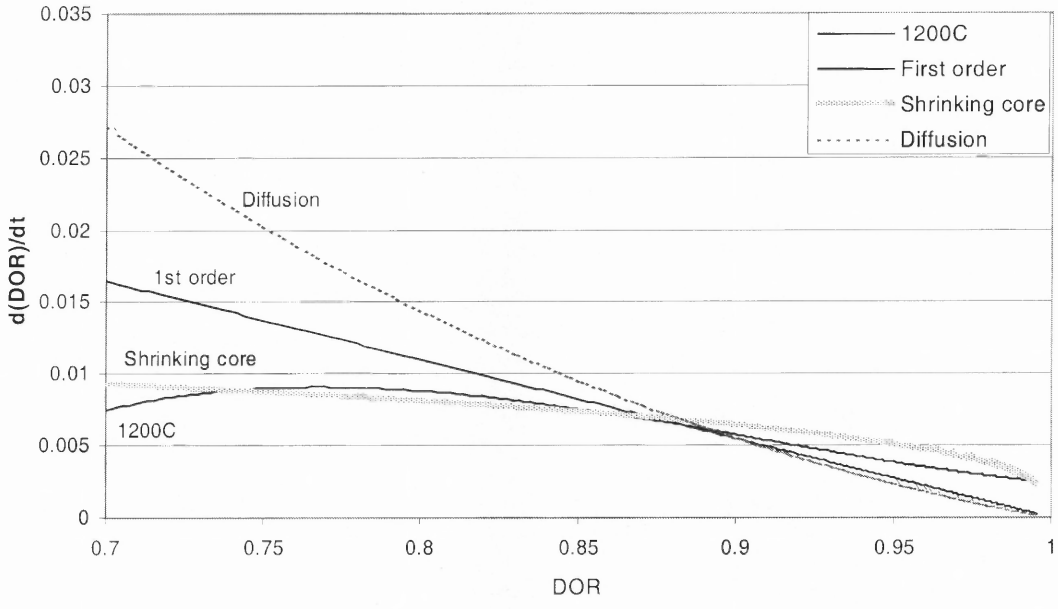

Figure 6.13 Plots between Isothermal Data from the 1200°C Test and Three Different Kinetic Models

The chemical reduction rates change with iron species. The chemical reduction of iron oxide to metal is limited by the reduction of FeO to Fe. The reduction to FeO occurred during the 1000°C test, however, there was no significant change in patterns of weight losses at this temperature, Figure 6.7. The activity of FeO deviates from unity when forming solid solution with other oxide, in this case MgO. The formation of FeO_xMgO_{1-x} at 1100°C should have changed the reduction rate if the phase boundary reaction between iron oxide and CO was the limiting process. The reduction experiment was conducted on the sample of size smaller than 75 microns. The retarding effect on the reduction from diffusion should be at minimum. Iron also diffuses at different rate in different oxides. The diffusion coefficient of Fe in FeO and MgO were $4.6*10^{-7}$ and $5.7*10^{-11}$ cm^2/sec, calculated from the relation $D = D_o exp(-E/RT)$, given by O'Keeffe (1967). The effect of the different diffusion coefficient should reflect in the weight loss pattern, provided that it is the limiting process. It seemed that these two subprocesses did not govern the reduction in this experiment.

The conclusive determination of the rate controlling subprocess is not an easy task, since at different stages along the reduction path one or the others may alternatively play an important role. Nonetheless, test results described in this section suggested that the indirect reduction governed the reduction of iron oxide and the gasification of carbon was a rate limiting process for the following conclusions: 1) the gas phase had strong effect on the reduction, 2) the reduction is dependent on the concentration of carbon instead of iron oxide, 3) the good fit of the isothermal data with the phase boundary reaction.

6.1.1.5 Reduction Kinetics. Generally the reduction study provides insight into kinetic parameters including the rate constant and the activation energy. As mentioned earlier, the use of solid carbon as reducing agent does not allow the reduction study at designed temperature. Because of the use of solid carbon, it was not possible to start the reduction at each set temperature at zero degree of reduction. By knowing that the reduction starts at or above 900°C, the weights at 900°C from each test was used as the initial weight and the weight loss for the complete reduction was calculated based on the stoichiometric 17.5% of the Fe_2O_3 weight: $Fe_2O_3 + 3C = 2Fe + 3CO$. The degree of reduction (DOR) was calculated from,

$$\frac{\text{weight at time t} - \text{weight at 900°C}}{\text{total weight loss calculated from 17.5\% of weight at 900°C}}$$

The previous section suggested the phase boundary reaction of carbon as a rate limiting step. The plots of isothermal data at 1200°C followed, though not precisely, the shrinking core model. Both shrinking core modal and first order kinetics will be used to approximate the kinetic parameters of the isothermal data.

Figure 6.14 shows the plot of ln(1-DOR) or $\ln(C/C_o)$ and t, DOR - degree of reduction, t – isothermal time, first order kinetics. The rate constants were calculated from the slopes. The graphical illustration of rate constants is given in Figure 6.15: a) all temperatures, b) 600-900°C for the transformation of $CaCO_3$, c) 1000-1200°C for the reduction of iron oxide, and d) 1300-1400°C. It is interesting to note that the slope for the 1300°C test is small than those for the 1200°C and 1100°C tests. The diffractogram showed an incomplete reduction for the 1100°C and 1200°C tests, thus the reduction of

iron oxide extended into the isothermal period. The 1300°C test yielded a rather complete reduction and the rate constant at 1300°C might reflect different reduction processes, i.e. the reduction of other oxides or the oxidation of the remaining carbon. The transformation of $CaCO_3$ also raised the slope of the 700°C test over the slope for the 1000°C test. Even though Figure 6.14 and Figure 6.6 shows different reduction rates and final products, the calculated rates may not represent the formation rate of those phases. The reduction rates at each temperature, instead, represent the reduction rate of the limiting process, the carbon gasification from 1000-1200°C. Since the rate constants described the same reaction, they can be related through Arrhenius equation: $k = k_o exp(-E_a/RT)$, k – rate constant, k_o – constant, E_a – activation energy, R – gas constant, and T – temperature in kelvin.

The slope of a plot between -ln(k) and 1/T was equal to the term Ea/R. Figure 6.16 shows the plot of –ln(k) and 1/T for the 1000°C, 1100°C, and 1200°C tests. The activation energy was 55.6 kcal/mol, similar to the value from the gasification controlled reduction (Table 3.1). Figures 6.17 and 6.18 show the similar plots but following the shrinking core model. The activation energy was 43.7 kcal/mol which is within the range of the activation energy of carbon gasification (Table 3.1).

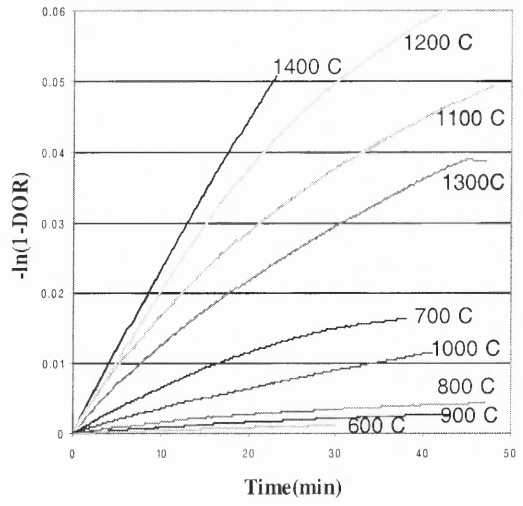

a)All temperatures

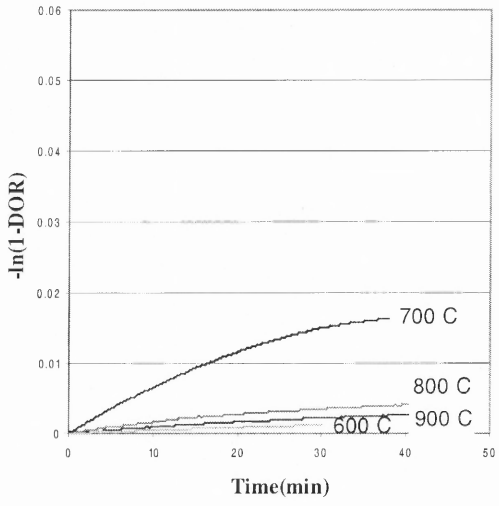

b) 600-900°C

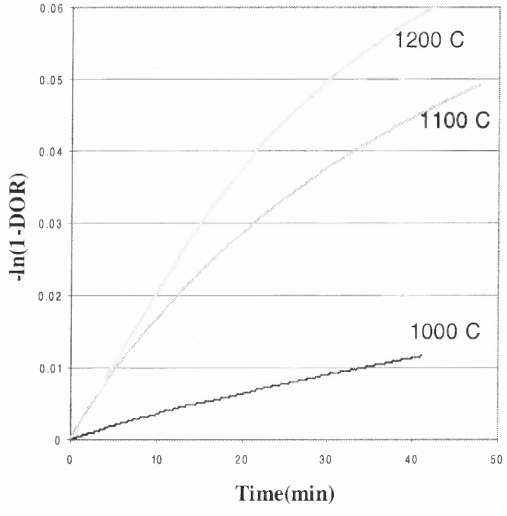

c) 1000-1200°C

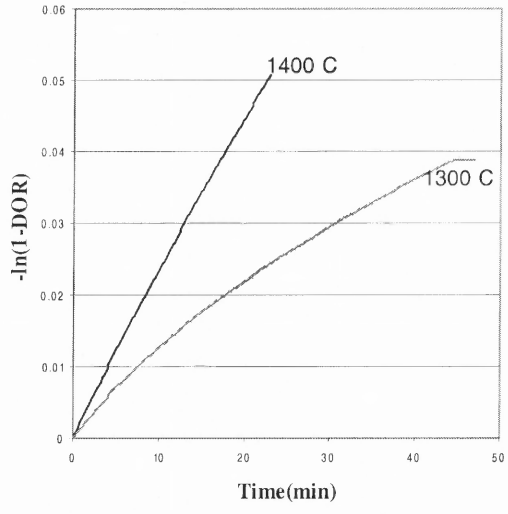

d) 1300-1400°C

a) At all temperatures
b) Temperature range, 600-900°C, where $CaCO_3$ transforms to CaO; sample loses moisture; or absorbed oxygen oxidizes carbon.
c) Temperature range, 1000-1200°C, where the reduction of iron oxide in soils occurs.
d) Temperature range, 1300-1400°C, where the reduction is almost complete and other reaction at high temperature might occur.

Figure 6.14 Plots of -ln(1-DOR) and Time.

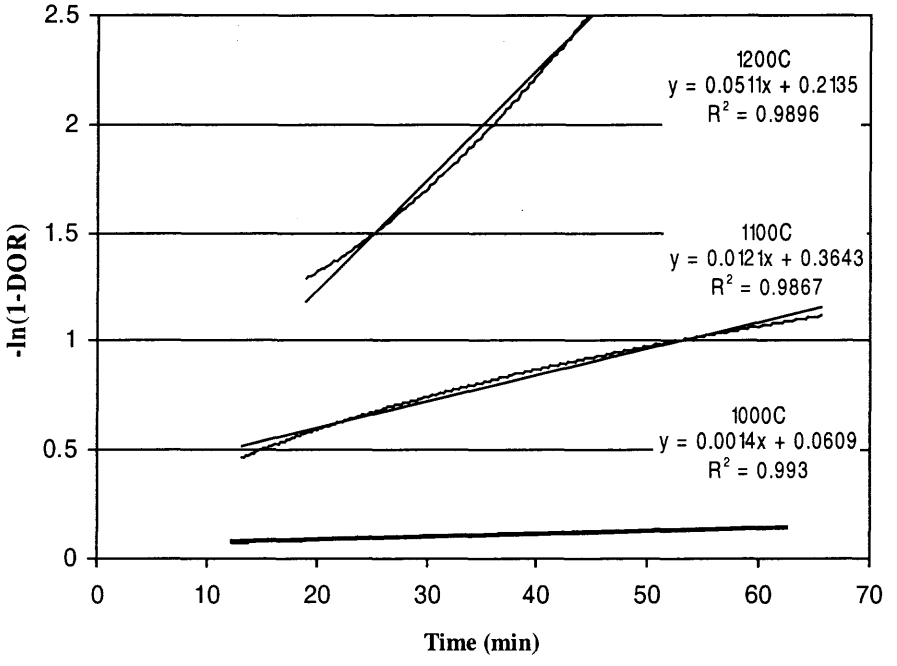

Dash line – Trendline

Figure 6.15 Plots of -ln(1-DOR) and Time with Trendlines and Rate Constants (First Order Kinetics)

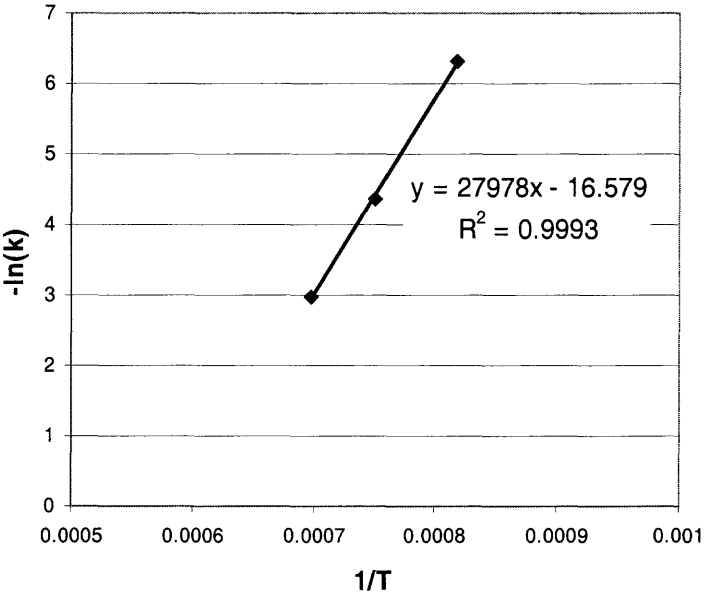

Figure 6.16 Plot of –ln(k) and 1/T (First Order Kinetics)

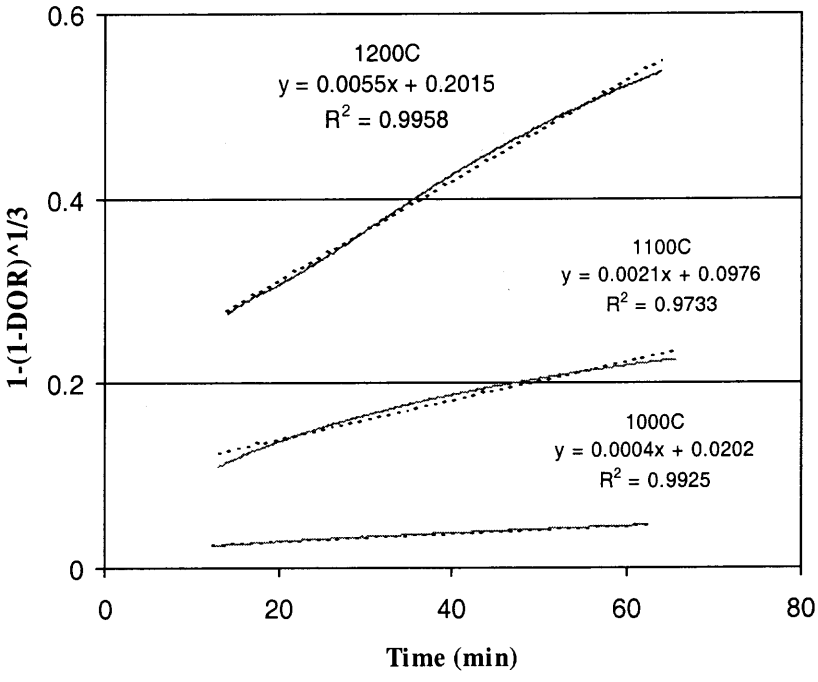

Dash line – Trendline

Figure 6.17 Plots of -ln(1-DOR) and Time with Trendlines and Rate Constants (Shrinking Core Model)

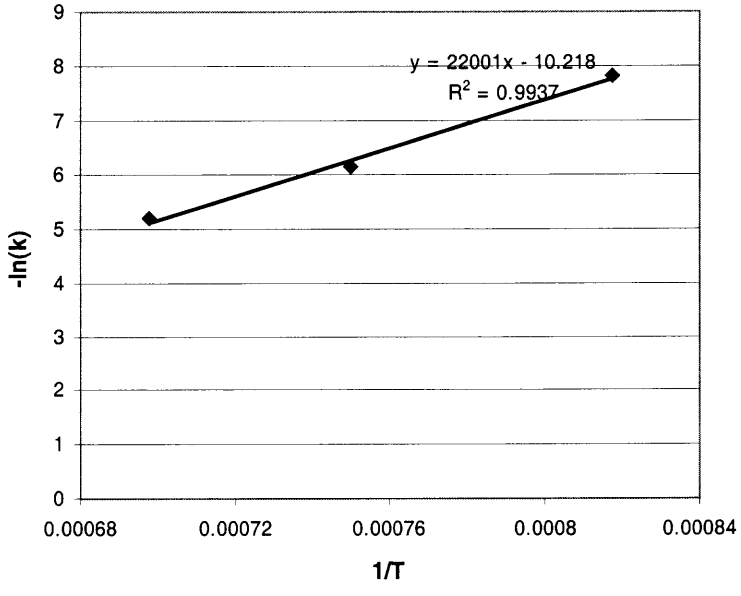

Figure 6.18 Plot of –ln(k) and 1/T (Shrinking Core Model)

6.1.2 Reductions of GAR, TPR, and CD soils

The weight loss and weight differences of soils from GAR, LSP, TPR, and CD are plotted in Figure 6.19. Figure 6.20 shows the degree of reduction at different temperatures. The degree of reduction was defined as the ratio of weight different between 900°C and each temperature and weight difference between 900°C and 1400°C. From the plot of degree of reduction, the reducibility ordering from high to low is LSP> CD> TPR> GAR. The CD soil contained low percentage of iron so its weight loss was less than corresponding values from the others. The diffractograms of the tested soils from GAR, TPR and CD, are presented in Figures 6.21, 6.22, and 6.23.

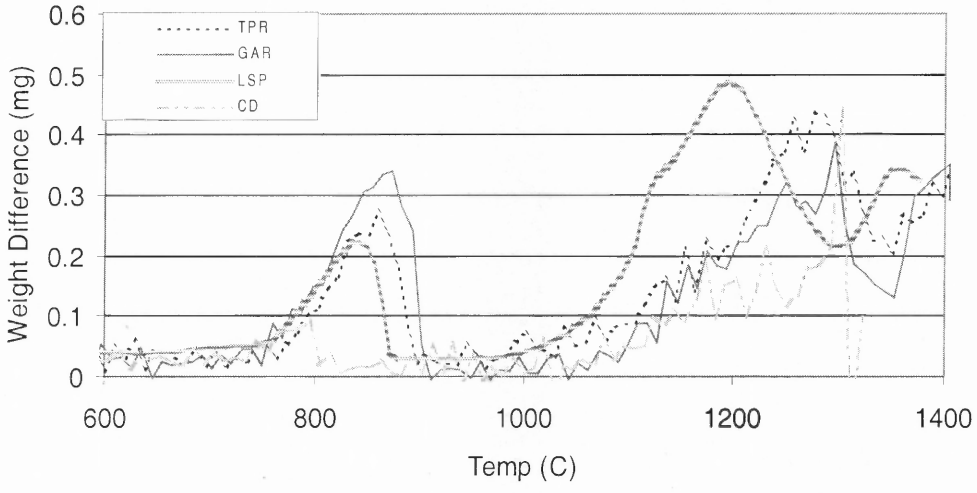

Figure 6.19 Plots of Weight Differences of LSP, TPR, GAR, and CD Soils

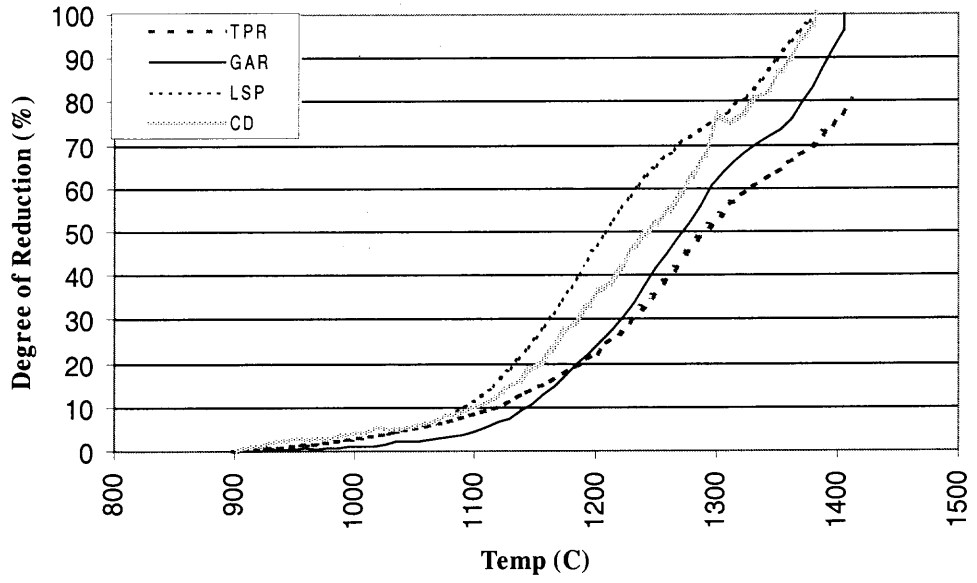

Figure 6.20 Plots of Degree of Reductions of LSP, TPR, GAR, and CD

The XRD results showed that the spinel in GAR soil was readily reduced to metal with a very intense MgO peak, Figure 6.21. The formation of $2CaO.Al_2O_3.SiO_2$ as one of products was observed as in the test of LSP soil with 15% carbon. The formation of large quantity of MgO implied the existence of the spinel containing MgO. The GAR soil started losing weight at temperature higher than the others, which could be due to the diffusion and separation of MgO from the spinel. Later in the chapter the comparison between soils and pure oxides will be presented.

The TPR soil yielded incomplete reduction at the experimental condition where other soils were completely reduced. The diffractogram of TPR allowed a better identification of spinel types. The intensity ratio of Sp(3)/Sp(2) decreased in the tested sample, showing the spinel of easily reduced type, Sp(3). The incomplete reduction might be due to the insufficient amount of carbon.

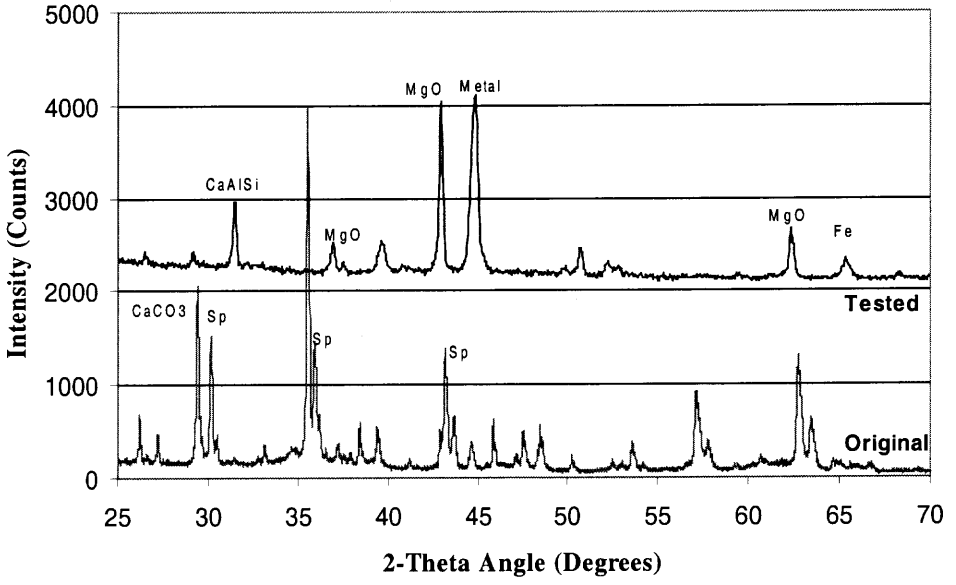

Sp : spinel
CaAlSi : $2CaO.Al_2O_3.SiO_2$
Scanning program: step size – 0.04° 2θ, time/step – 2.5 seconds

Figure 6.21 Comparison between Phases of Tested and Original GAR Soil

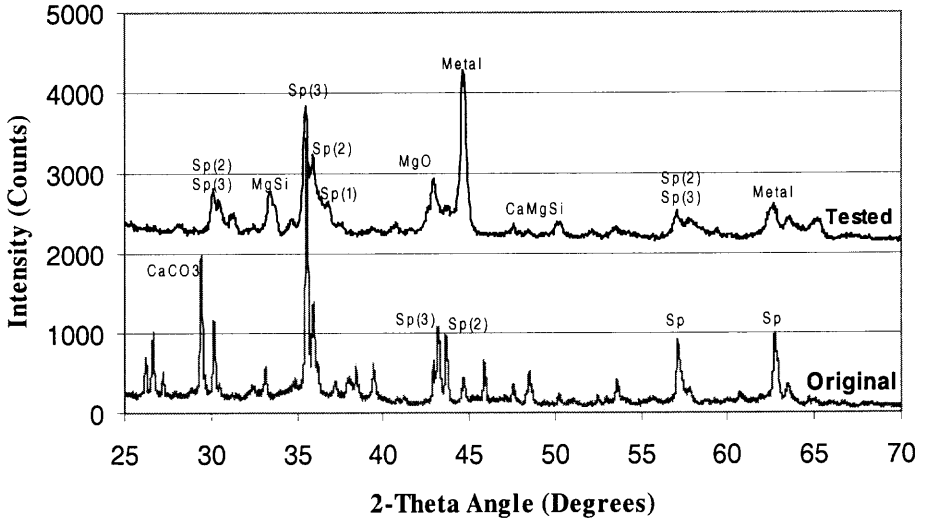

Sp(1) : $MgAl_2O_4$
Sp(2) : $(Mg, Fe)(Cr, Al)_2O_4$
Sp(3) : $MgFe_2O_4$, $FeCr_2O_4$, Fe_3O_4
MgSi : $2MgO.SiO_2$
Scanning program: step size – 0.04° 2θ, time/step – 2.5 seconds

Figure 6.22 Comparison between Phases of Tested and Original TPR Soil

The metal formation in CD soil was not as distinct as in the others. However, the diffratogram showed a significant change in phases. From phase identification, SiO_2 and $CaCO_3$ were identified as major phases in CD soil. After the test $2CaO.MgO.2SiO_2$ was found to be the major phase. The solid state diffusion was possible at or below the test temperature, 1400°C. The background between 15-25° in 2θ was from the plastic plate.

Though there was a presence of metallic phase there was no observable metal separation. The soil from CD had magnetic properties after heating possibly due to the existence of metallic phase. The magnetic portion was possibly imparted in the non-magnetic portion and rule out the possibility of the magnetic separation for CD soil.

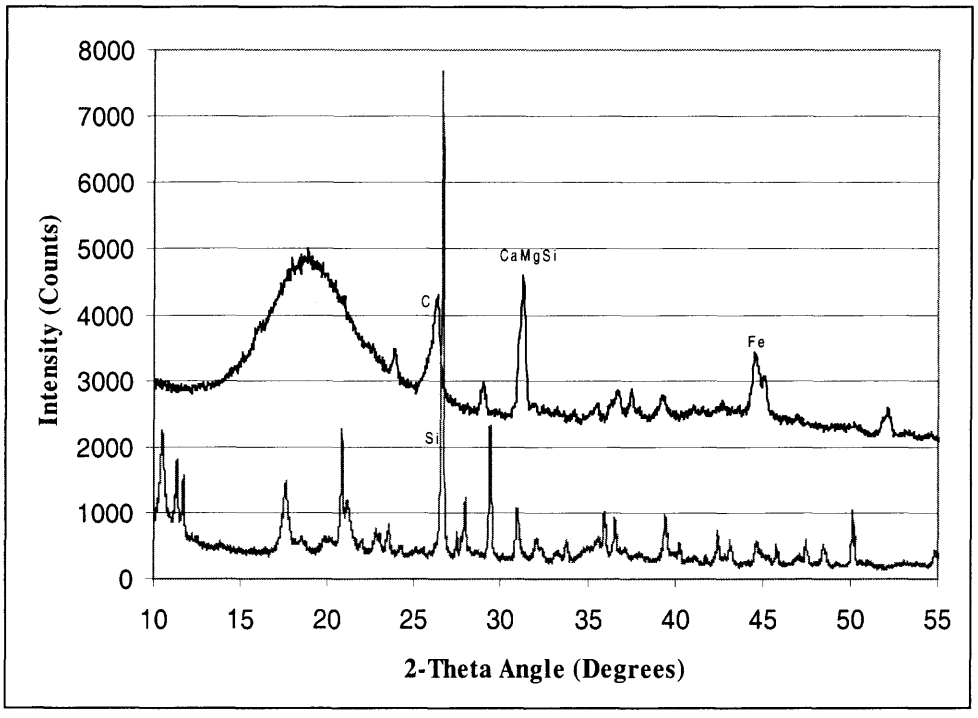

CaMgSi : $2CaO.MgO.2SiO_2$
Si : SiO_2
Scanning program: step size – 0.04° 2θ, time/step – 2.5 seconds

Figure 6.23 Comparison between Phases of Tested and Original CD Soil

6.2 Reduction of Fe_2O_3

The study on the reduction of hematite, Fe_2O_3, represents the reduction of a pure iron oxide. The pure hematite started losing its weight at 1400°C (Figure 6.24), the test condition was heating the sample at a rate of 40°C/min under nitrogen purging at 40 cc/min, at atmospheric pressure. There was no purging period prior to heating. The total weight loss was approximately 3%, which was similar to stoichiometric weight loss for the transformation of Fe_2O_3 to Fe_3O_4, 3.4%, according to the reaction: $2Fe_3O_{4\,(s)} + 1/2O_{2\,(g)} = 3Fe_2O_{3\,(s)}$. The diffractogram identified the major phases as a mixture of Fe_2O_3 and Fe_3O_4.

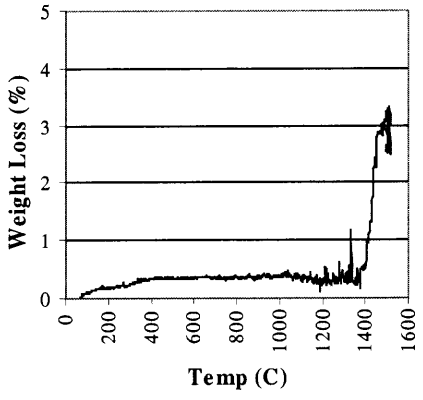

Figure 6.24 Weight Loss Pattern of Hematite with no Carbon or Nitrogen Flushing Prior to Heating

The test of a mixture of Fe_2O_3 and 25% carbon without nitrogen flushing yielded the same phases. According to the test with pure carbon, the remaining oxygen in the furnace oxidized 12 mg of carbon during the ramping period. The added carbon could be completely oxidized during the ramping period. According to the stability diagram, the lower oxygen partial pressure decreased the equilibrium temperature between the oxide and its reduced form. The test with five hours long of flushing period prior to heating

resulted in a complete reduction to Fe_3O_4, but not FeO or Fe. The reduction started at 1200°C. According to the free energy diagram, the equilibrium oxygen partial pressure with Fe_2O_3 and Fe_3O_4 at 1200°C is 0.001 atm and 0.8 atm at 1400°C. The nitrogen flushing for 5 hrs prior to heating was able to bring the oxygen partial pressure down to 0.001 atm which is still to high for the reduction of FeO to Fe: $5*10^{-11}$ atm at 1400°C and $1*10^{-13}$ atm at 1200°C. Certainly, carbon addition is required for the reduction of iron oxide to metal.

With 3-hrs nitrogen flushing and 1 hr isothermal at 1400°C, the iron oxide with 25% carbon addition was readily reduced to metallic iron in a form of tiny metal balls. Figure 6.25 shows the weight loss and weight difference patterns. Their morphology is presented in Figure 6.26. The total weight loss at 1250°C was 37.5% compared to 41.5%, calculated based on the formation of CO as a product of the reduction of Fe_2O_3 to metallic iron. The result suggested the formation of both CO and CO_2, the indirect reduction. The plot of weight difference and time postulated two distinct peaks at 900 and 1200°C, of which were believed to be the reduction of Fe_2O_3 to Fe_3O_4 and Fe_3O_4 to Fe. From 900 to 1000°C, there was 3% weight reduction, similar to the weight reduction when forming Fe_3O_4.

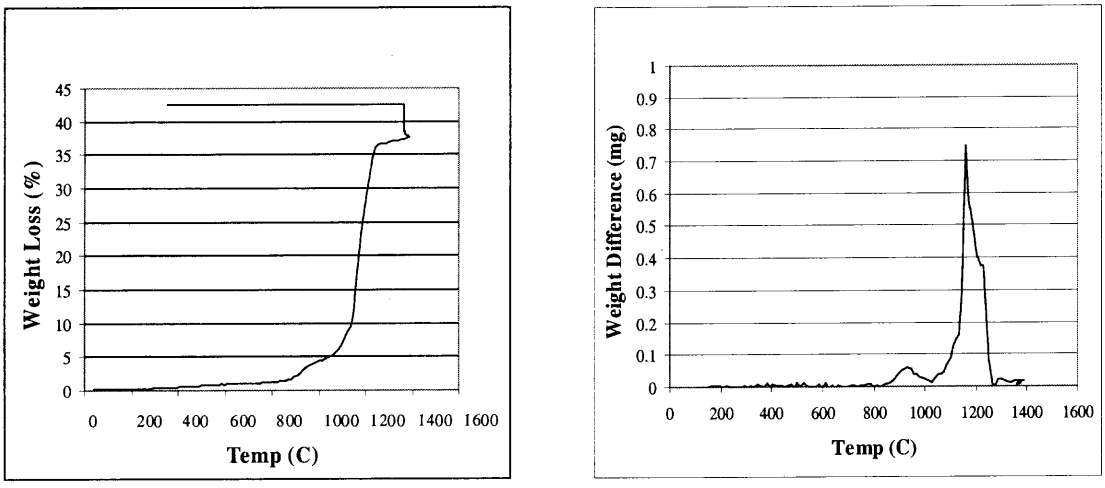

Figure 6.25 Plots of Weight Loss and Weight Difference of Hematite

From the weight loss pattern the reduction to metal was rapid and finished at 1250°C which was confirmed by another test with no isothermal period. The final products after the reduction were tiny metal droplets with carbon powder. The reduction of magnetite, Fe_3O_4, to metal droplets showed the pattern of weight loss with no weight change at 900°C unlike that for hematite, Figure 6.27. The weight changed at 900°C then represented the weight loss for the formation of Fe_3O_4.

The influence of the amount of carbon on the reduction was clear from Figure 6.27. Increasing carbon content lowered the temperature where sample started losing weight. The reduction from both Fe_2O_3 and Fe_3O_4 were rapid and finished between 1250 and 1300°C.

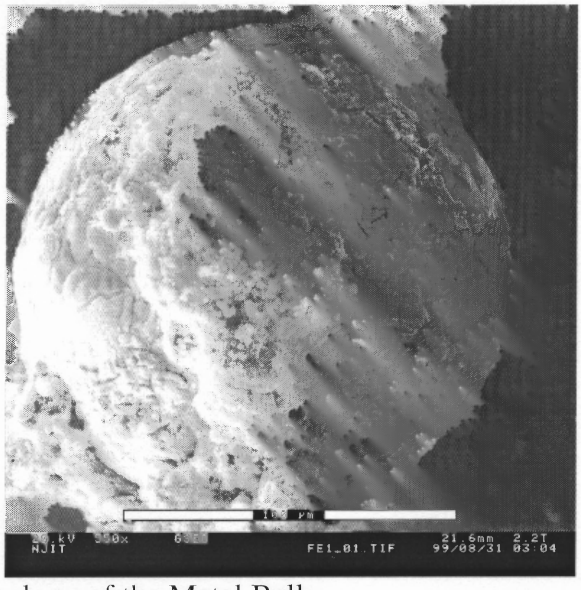

Figure 6.26 Morphology of the Metal Ball

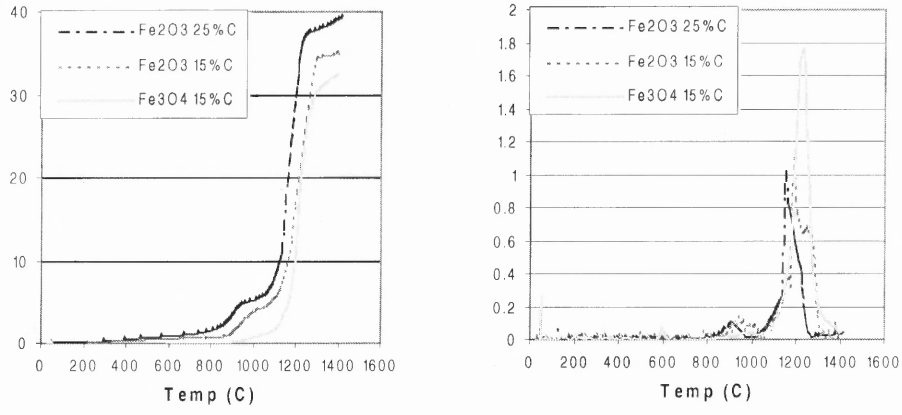

Figure 6.27 Plots of weight loss and weight differences of Fe_2O_3 and Fe_3O_4

The addition of 15% carbon was found to be inadequate during the study on the phase change of iron oxide at different temperatures. The samples were flushed with nitrogen for 2 hr, heated to set temperatures and cooled down to 300°C with no isothermal period. Figure 6.28 shows the final phases at different temperatures. The carbon peak started disappearing at 1200°C. The reduction was not complete at 1400°C

due to the depletion of carbon. At the end of 1000°C test, Fe_2O_3 remained as the major phase, not as assumed earlier. The Fe_3O_4 and metal formed at 1100°C and 1200°C, respectively. The test with 25% carbon showed a complete reduction to metal balls. The Fe_3O_4 mixed with 15%C also showed a complete reduction to metal balls for the same test condition. The hematite required 18.5% and 13.5% for the formation of CO and CO_2. The results are not quite conclusive with respect to the percentage carbon required for the complete reduction and the species of iron oxide at different temperatures. However the amount of carbon required should be over 15% but less than 25%.

It can be noted that at 1150°C, the weigh loss increased sharply, Figure 6.27. Formation of metal occurred at this temperature. Literature suggests a catalytic effect of metal on the gasification and might be responsible for the sharp increase of degree of reduction (Kasai et al., 1995; Baldwin, 1955).

The approximate activation energy was calculated from step heating. During the ramping periods, the sample was kept isothermally for 20 minutes at 950, 1000, 1050, 1100, 1050, and 1100, 1200, and 1250°C. At 1200°C the reduction was almost complete and the rate constant decreased. Therefore, The 1200°C and 1250°C data were excluded from the calculation of activation energy. The activation energy of 58Kcal/mol was obtained, which is similar to the activation energy value obtained from the reduction of soil. This supported the conclusion on the gasification as a rate limiting process.

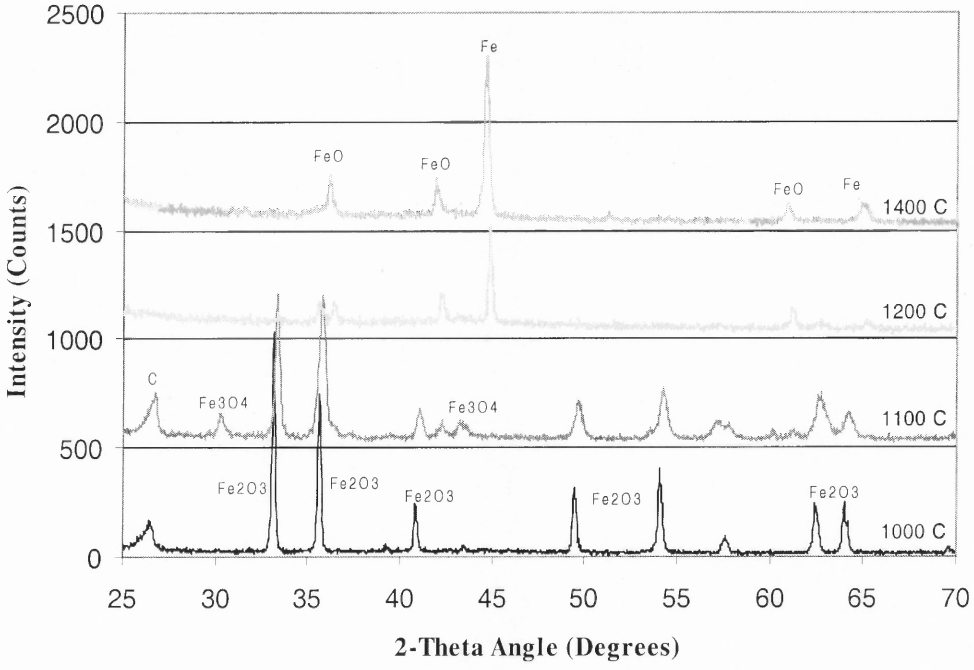

Scanning program: step size – 0.03° 2θ, time/step – 4 seconds

Figure 6.28 Phase Changes of Iron Oxide at Different Temperatures

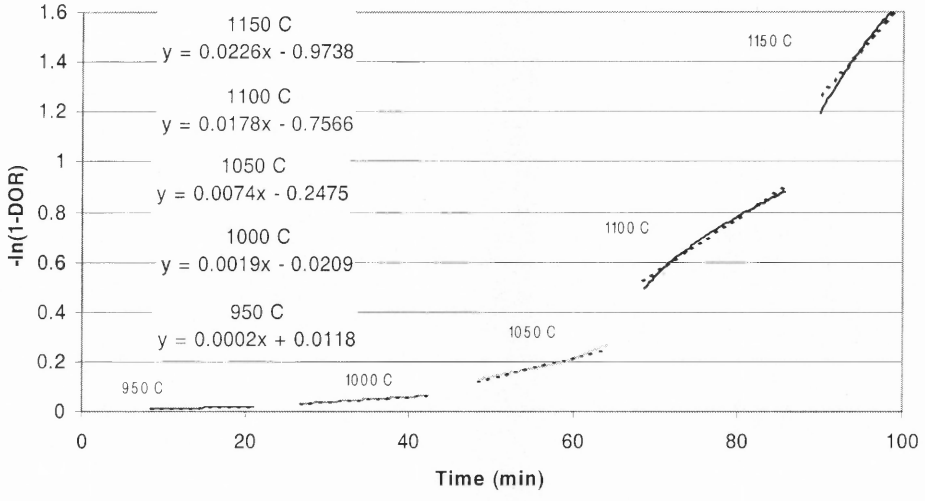

Dash line - Trendline

Figure 6.29 Plots of –ln(1-DOR) and Time

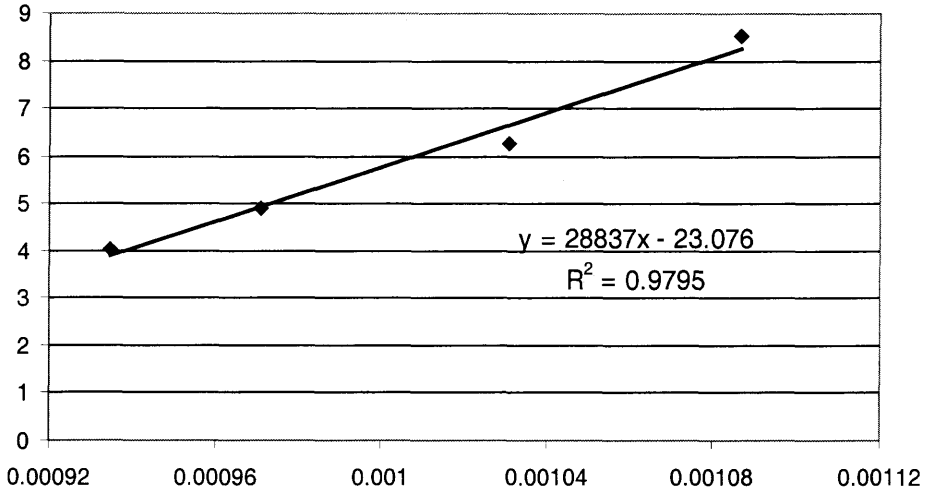

Figure 6.30 Plots of –ln(k) and 1/T

6.3 Reduction of $MgO.Fe_2O_3$

The $MgFe_2O_4$ was prepared by mixing Fe_2O_3 with MgO and heating to 1500°C. The heating rate was set at 40°C/min and it took less than half an hour to reach 1500°C. The furnace remained rich with oxygen, which enhanced the formation of magnisioferrite (MgFe2O4). The presence of magnisioferrite was confirmed by XRD and by its magnetic property (Figure 6.31). The magnisioferrite was mixed with more than sufficient amount of carbon and tested at 1400°C for 45 minutes after flushing with nitrogen for 2 hrs. The white crystal, MgO, appeared on top of the sample and the XRD confirmed the presence of metallic iron, MgO, and carbon.

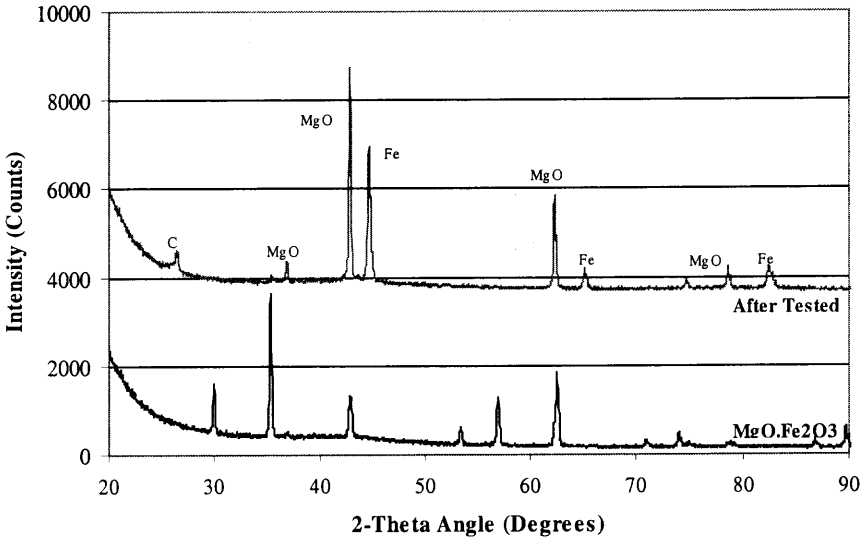

Figure 6.31 Phases of Original and Tested $MgO.Fe_2O_3$

Figure 6.32 shows the percent weight loss and weight differences of magnesioferrite as a function of temperatures. The reduction complete at temperature between 1300°C and 1400°C. For the 15% carbon addition, the higher temperature was required. The magnesioferrite required higher temperature, which reflected the change in the activity of iron oxide when mixed with MgO. Though the reduction to metal phase was confirmed, there was no formation of metal droplet unlike the outcome from the reduction of iron oxide.

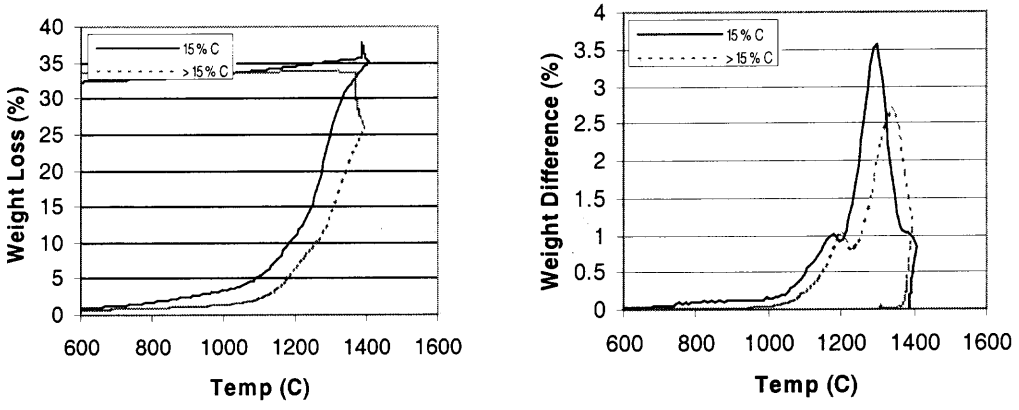

Figure 6.32 Plots of Weight Loss and Weight Differences of $MgO.Fe_2O_3$

6.4 Comparison of LSP, TPR, GAR, Fe_2O_3, Fe_3O_4, and $MgO.Fe_2O_3$ Results

The reduction pattern of LSP did not follow either Fe_2O_3 or $MgO.Fe_2O_3$, but rather a combination of both (Figure 6.35). The reduction pattern of GAR and TPR were similar to the reduction of $MgO.Fe_2O_3$ (Figure 6.36).

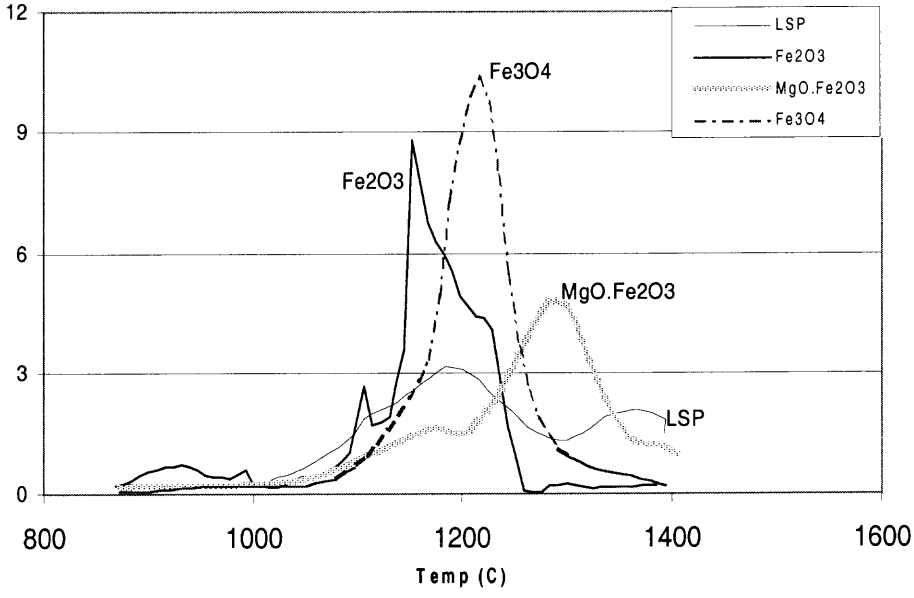

Figure 6.33 Plots of Weight Difference of LSP Soil and Other Pure Oxides

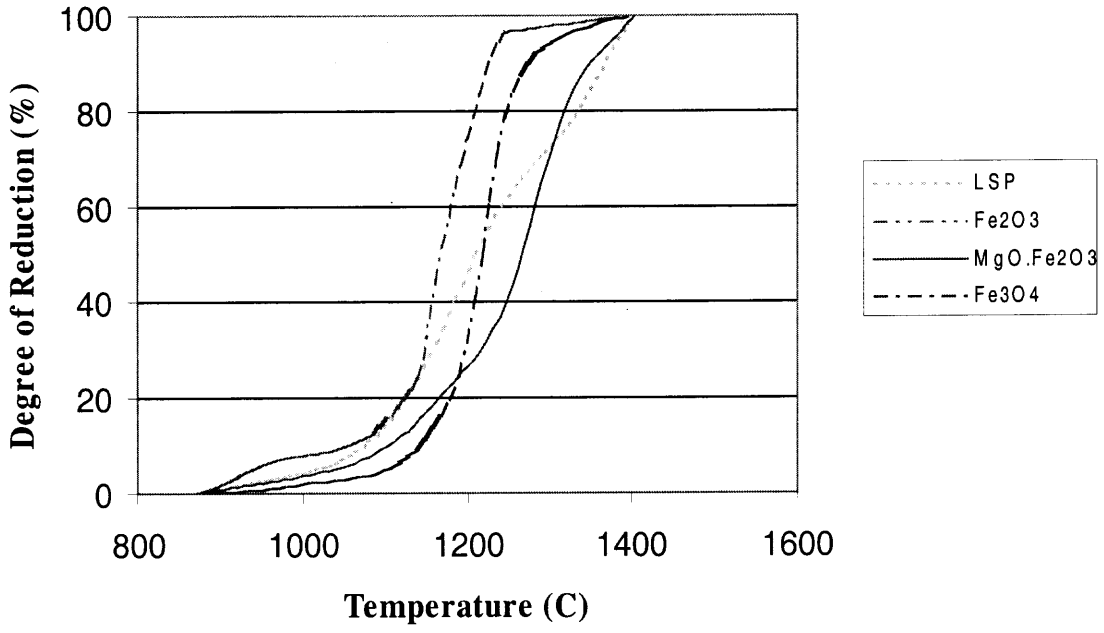

Figure 6.34 Plots of Degree of Reduction of LSP Soil and Other Pure Oxides

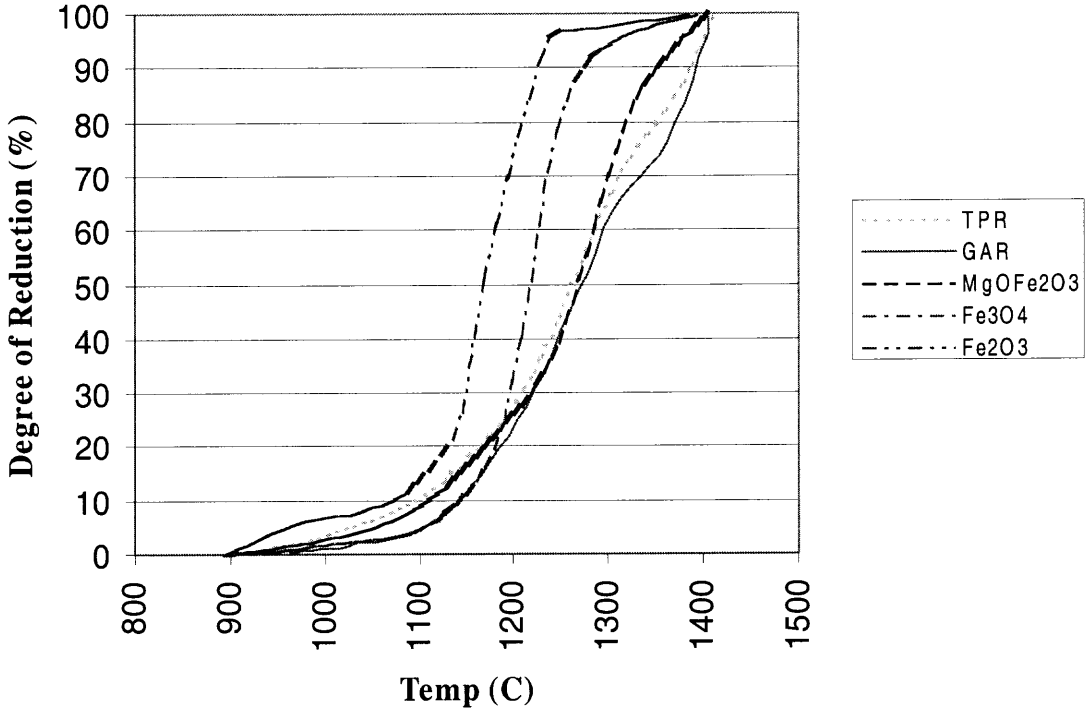

Figure 6.35 Plots of Degree of Reduction of TPR and GAR Soils and Other Pure Oxides

6.5 Reduction of Chromate

Chromate was found to lose its oxygen and reduce to trivalent chromium at high temperature (Clark et al., 1975). To confirm the changing in the oxidation state of chromate at high temperature, the extracted $CaCrO_4.2H_2O$ and $CaCO_3$ from CD soil without carbon addition were subjected to the test at 1400°C. The hexavalent chromium was reduced to trivalent chromium, $Ca_6Al_2Cr_2O_{15}$ ($6CaO.2Al_2O_3.Cr_2O_3$), Figure 6.36.

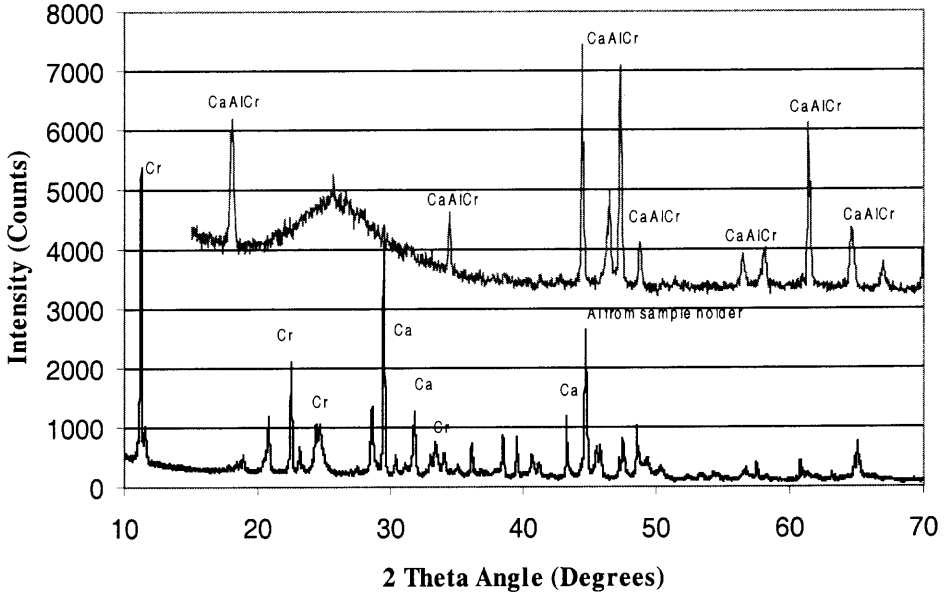

Ca : $CaCO_3$
Cr : $CaCrO_4.H_2O$
CaAlCr : $Ca_6Al_4Cr_2O_{15}$
Figure 6.36 Phase Changes of Chromate

6.6 Reduction of $CaCO_3$

Calcium carbonate is abundant in all chromium contaminated soils. It started losing its CO_2 around 700°C; the reduction was complete at 950°C, Figure 6.37. The weight loss occurred regardless of the nitrogen flushing or the carbon addition. The stoichiometric weight loss from the transformation of $CaCO_3$ to CaO was 44%, which agreed fairly well

with the experimental result of 41%. This would give a predictable of weight loss pattern for the soil sample and can also indirectly be proportional to the concentration of calcium in soil. At temperature higher than 950°C there was no observable weight loss confirmed the stability of CaO at 1400°C.

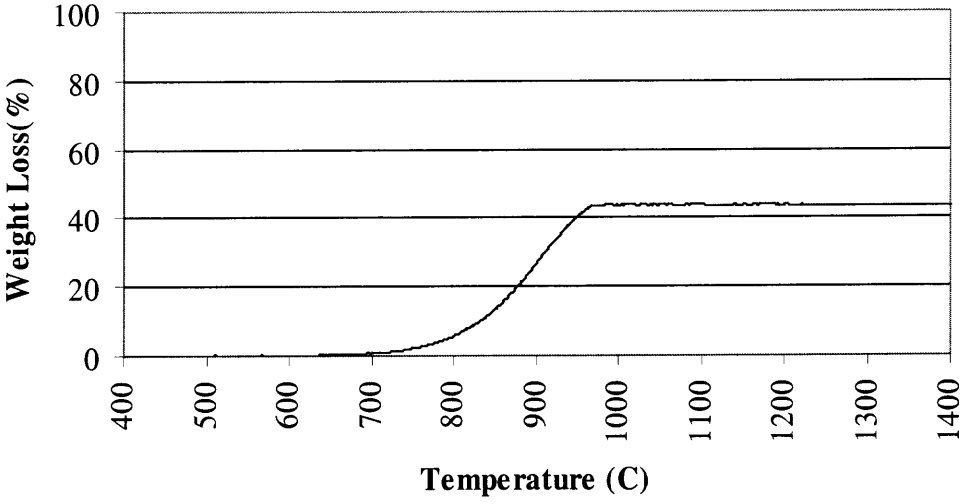

Figure 6.37 Weight Loss Pattern of $CaCO_3$

6.7 Oxidation of Carbon

Both oxygen in the furnace and the oxygen as an oxide consumed carbon. Carbon is long known as an excellent adsorbent widely used in many applications. The conduction of carbon experiment was mainly to establish the reasonable flushing period that would allow the reduction to occur. To be able to determine the consumption of carbon by remaining oxygen or absorbed oxygen on carbon, a series of experiments with different duration of nitrogen flushing prior to heating were conducted. Table 6.3 contains weight losses and the rate constants from the tests.

Table 6.3 Percentages of Carbon Weight Loss at Different Flushing Periods

Sample	K	Wt loss (Ramping period)	Wt loss (Total)	Remark
0_C_C	0.0341	45% (10mg)	90% (12 mg)	Carbon, no flush, 1400°C 1hr
1-C_C	0.0045	15% (3.7 mg)	35% (5.2 mg)	Carbon 1 hr flush, 1400°C 1 hr
2_C_C	0.0014	7% (2.0 mg)	17% (2.2 mg)	Carbon, 2hr flush.1400°C 1 hr
3_C_C	0.0001	7% (2.9 mg)	16% (2.0 mg)	Carbon, 3 hr flush, 1400°C 1hr

The percent weight loss of carbon with no flushing period was very high, 90%. In fact, there was no powder carbon left in the crucible but a black solid sticking to the crucible. Carbon could be completely oxidized when there was no nitrogen flushing prior to heating. The percentages of weight loss were almost the same for the 2 and 3 hrs tests. Therefore practicing of 2-hr flushing was used throughout the experimental program unless otherwise stated.

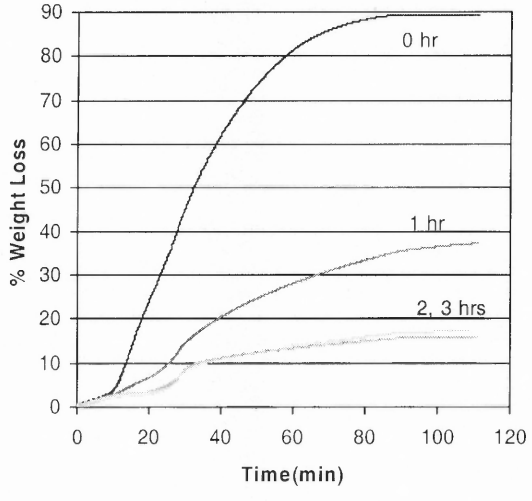

Figure 3.38 Plots of Weight Loss at Different Flushing Periods

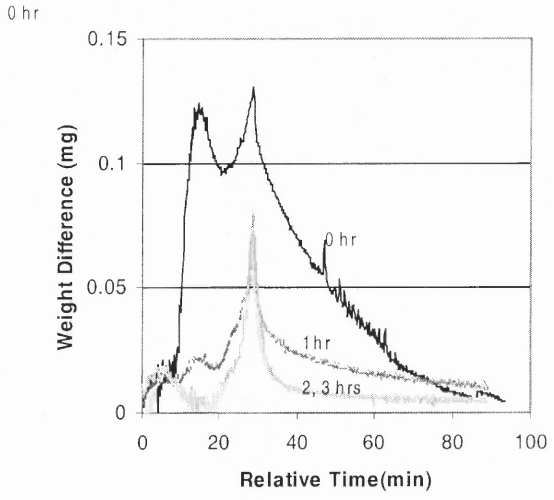

Figure 6.39 Plot of Weight Differences of Carbon at Different Flushing Periods

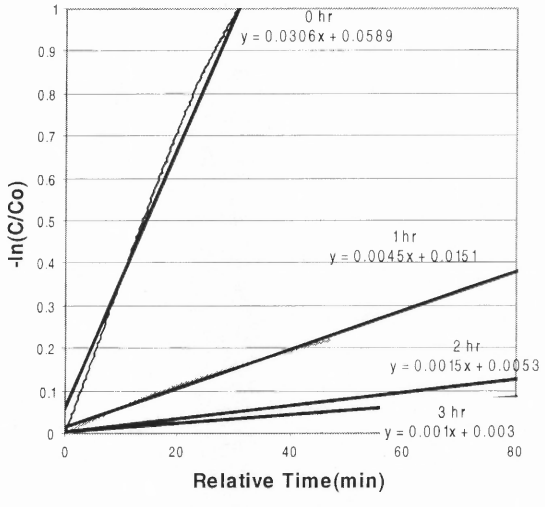

Figure 6.40 Plots of Rate Constants of Carbon Oxidation at Different Flushing Periods

The plots of weight loss with temperature, Figure 6.38, showed a change in weight loss pattern at 700°C. The change was easier to notice in the plot of weight differences. According to the free energy diagram, CO is stable at temperature above 700°C, otherwise CO_2 is stable. The weight difference decreased at temperature around 700°C, a point where the stability of CO and CO_2 were comparable, this may explain the

slowing down of the oxidation. The 700°C was also the highest temperature that carbon deposit can occur. After 700°C the oxidation was faster due to the temperature dependent of the reaction and the formation of CO, which consumed one mole of oxygen per one mole of carbon.

6.8 Summary

The reduction of iron oxide in chromium contaminated soil to metal was achievable under the oxygen free environment with sufficient amount of reducing agent. The reaction occurred very rapid at high temperatures and completed during the heating period from 1000°C to 1400°C, in less than 10 minutes. There were at least two different kinds of spinel in the LSP soil: one was easily reduced at or below 1100°C and the other above 1100°C. The spinel reduced above 1100°C was beleievd to be of type containing MgO, Cr_2O_3, Al_2O_3. The reduction of iron oxide in soil started at 1000°C through the direct reduction. The indirect reduction and gasification occurred afterward and were the main path for the reduction. Though it is not easy to identify the rate controlling subprocess, the results suggested the gasification. The activation energy of LSP soil, calculated from first order kinetics and shrinking core model, and hematite were approximately 55, 43, and 58 kcal/mol. These values were similar to the activation enregy for the gasification.

The LSP soil required at least 15% addition of carbon to complete the reduction, at the above testing condition. Time was not critical for the reduction at high temperature. The reduction at low temperature, as in the direct reduction process, was not

important for the study. Since the concentration result did not satisfy the high quality ore, thus the direct reduction process would not be appliable. The separation of metal has to be done in a liquid state at high temperature. The reduction patterns of LSP were similar to the combination of Fe_2O_3 and $MgO.Fe_2O_3$. Both forms of oxides were completely reduced at 1250°C and 1400°C.

The carbon content had a strong influence on the reduction, a larger percentage can lower the reduction temperature and increase the degree of reduction. It increases contact sites for both direct reduction and the gasification thus creating larger partial pressure of CO.

Soils from other sites, under the same reduction conditions, followed the same reduction pattern but at a slower rate. The TPR and GAR soils followed a reduction pattern similar to that of $MgO.Fe_2O_3$. The phase identification showed the reduction to metal in all soils. The reduction in GAR was complete with intense MgO peaks, unlike TPR soil where some non-reduced spinel remained.

The toxicity of chromate is also of great concern. The chromium changed its oxidation state from hexavalent to trivalent when heated to1400C°. The reduced chromium was of the form $6CaO.2Al_2O_3.Cr_2O_3$.

There was no observable metal separation from any soil, yet the iron oxide reduction yielded metal droplets. The main objective of this research therefore was not satisfied. The extensive study on the reduction process may not be worthwhile, if the metal separation never occurs. In the next chapter the result and discussion on the metal separation will be explored.

CHAPTER 7

DISCUSSION OF RESULTS: METAL SEPARATION

Based on test results presented in previous chapter, it can be stated that the complete reduction of iron oxide to metallic iron occurred but no separation of metal was observed. The reduction of iron oxide is very rapid, therefore the limiting step for the iron droplet formation would depend on the grain growth and metal separation. It is presumably the slow solid state diffusion that impedes the process. The metal separation is easier in the liquid state. Most soil components have high melting temperatures. However, the solid state diffusion of acidic and basic oxides at high temperature may yield intermediate compounds having lower melting temperatures and subsequently melt and form a liquid pool to which the high melting temperature compounds can be further dissolved.

The metal separation occurs just after the reduction. However, the instrument limitations on operating temperature, sample weight, and crucible material disallow the simultaneous study of reduction and metal separation. The samples attached to the alumina crucible as they melt and the graphite crucible attacked the TGA thermocouple. Therefore, a high temperature furnace was used to study the metal separation. Different percentages of sand were added to adjust the basicity, which in turn changed the melting temperature and the viscosity of the melt. However the high temperature furnace does not allow the sample extraction at operating temperature hence prohibits the process monitoring in terms of phase change and reduction process. Its environment is less controllable than that of TGA including the temperature ramping rate and the inert environment.

The composition of soil dictates the melting temperature and the viscosity. By adjusting soil composition so that it melts at low temperature and has low viscosity, metal separation could be achieved. The phase diagram graphically described the otherwise complicated behavior of slag at different temperatures. The phase and viscosity diagrams can be used to estimate the melting temperature of the melt and the possibility of metal separation at the selected composition.

This chapter provides the discussion of the metal separation from the preliminary test using TGA for LSP soil, the final test using high temperature furnace for LSP, TPR, GAR, and CD soils, and the simple use of phase diagram to determine the possibility of metal separation and phase formation.

7.1 Preliminary Tests from TGA

Before the availability of the high temperature furnace, the TGA was also used to study the metal separation. By increasing temperature and isothermal period, and adding sand, the metal separation might occur. The results will be presented chronologically along with the discussion.

7.1.1 Metal Separation in TGA, no Sand Addition

The test program reported in Chapter 6 did not induce metal separation. Therefore, a new test program was developed where LSP soil mixed with 20% carbon was kept at 1400°C for 1 hr, at 1450°C for 2 hrs, and at 1500°C for 1 hr. The instrument limitation forced to use the step heating. The presence of tiny shinny specks were observable throughout the sample after the test. There were tiny metal balls embedded wihtin the sample mass.

There were also white crystals of MgO deposited on top of the sample. The sample melted and struck to the alumina crucible. The observation by ESEM and EDX confirmed the separation of iron from the oxide mass. The image, Figure 7.1, shows two distinct phases, metallic and oxide. The EDX results confirmed that the hemi-spherical phase contained mostly iron and chromium, the other area contained primarily oxides of aluminum, calcium, and silicon, see Table 7.1. Figure 7.2 shows the morphology of two separated metal balls, their chemical analysis are presented in Table 7.1. The oxide phase had several morphology, i.e. needle-like and aggregate-like (Figure 7.3). Their compositions are also tabulated in Table 7.1.

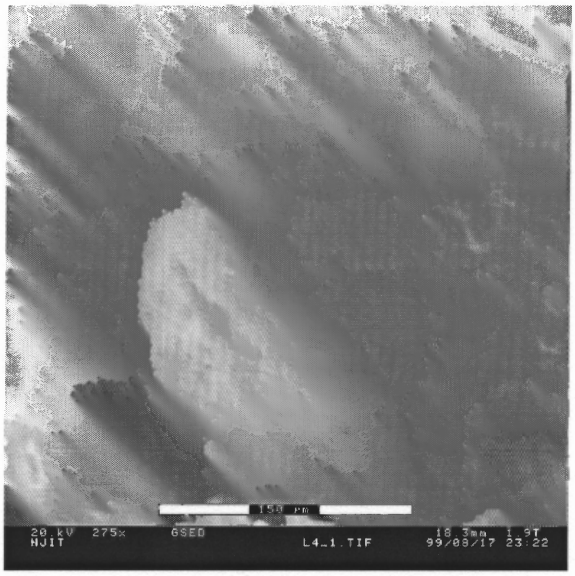

Figure 7.1 Morphology of Metallic Phase Embedded within Oxide Phase

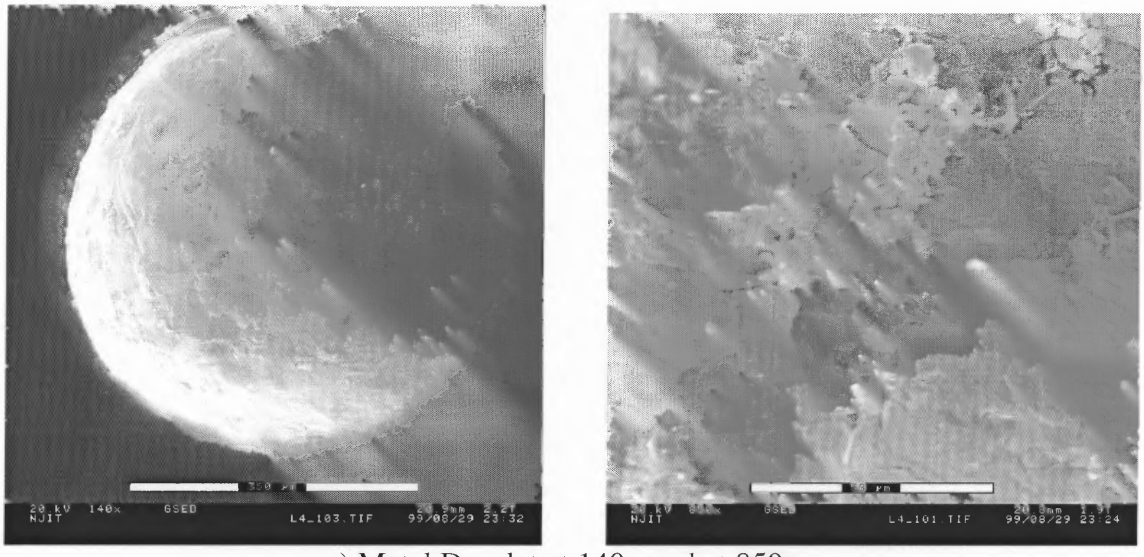

a) Metal Droplet at 140x and at 850x

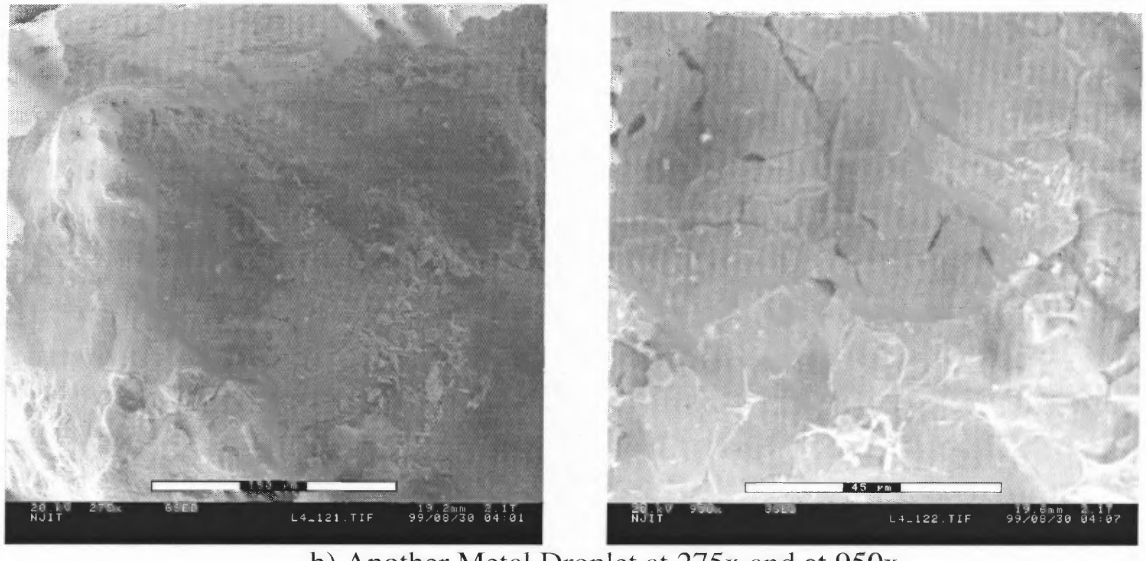

b) Another Metal Droplet at 275x and at 950x

Figure 7.2 Morphology of Two Metal Droplets

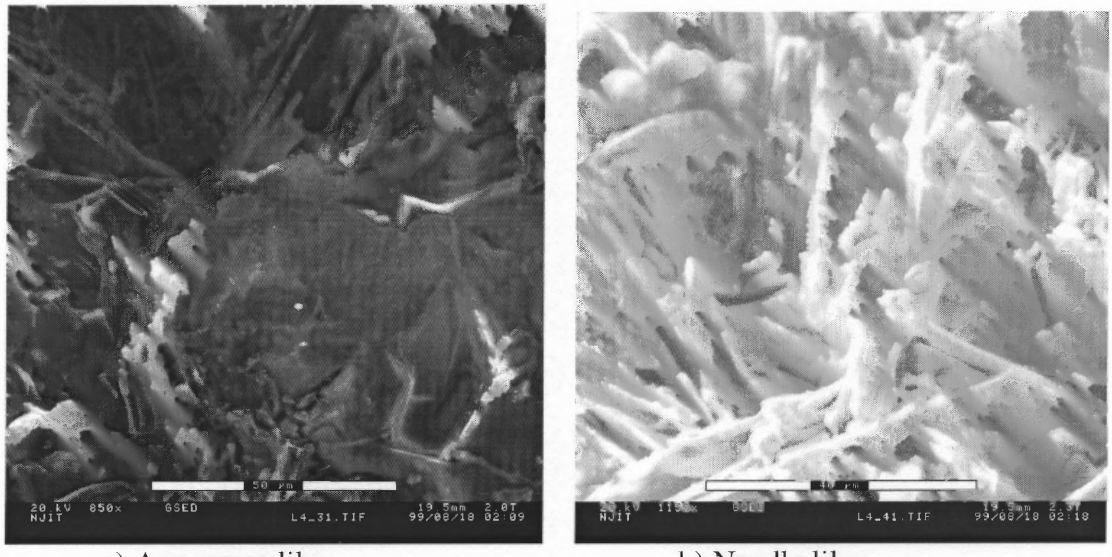

a) Aggregare like b) Needle like

Figure 7.3 Morphology of Oxide Phase Surrounding Hemi-Spherical Droplets

Table 7.1 Compositions of Particles/Areas

Fig.	Particles/Areas	Concentration (% wt)								
		Fe	Cr	Al	Ti	V	Si	Ca	S	O
7.1	Hemi-sphere	39.0	34.1	4.4	-	1.2	7.4	3.1	10.9	-
	Surrounding area	7.6	1.3	13.9	-	-	5.4	17.9	-	53.9
7.2	a) Metal droplet	68.7	6.4	7.1	4.3	1.0	12.6	-	-	-
	b) Metal droplet	61.6	6.0	15.3	1.8	0.3	12.9	2.2	-	-
7.3	a) Aggregate like	2.0	-	15.4	-	-	10.8	25.1	-	46.8
	b) Needle like	10.0	-	14.6	-	-	4.5	26.6	-	44.3
7.4	Area a	52.5	22.7	13.5	-	-	4.1	-	-	7.2
	Area b	68.1	6.2	9.6	1.9	-	12.6	1.6	-	-
	Area c	74.2	3.9	9.5	7.4	1.0	2.6	1.5	-	-
	Area d	21.8	6.7	22.8	10.1	-	7.4	8.8	1.0	21.5
7.5	a) High iron	18.5	2.8	21.6	2.4	0.4	8.3	12.0	-	34
	b) Low iron	3.1	1.4	25.7	2.3	0.8	6.3	13.1	-	47.4
7.6	b)	9.6	3.9	31.3	1.1	-	8.9	15.1	-	30.2

Not all shiny particles were truly metallic. One of shiny particles turned out to be a mixture of metallic and oxide phases. Figure 7.4, with a corresponding compositional analysis in Table 7.1, shows the image and analyzed areas.

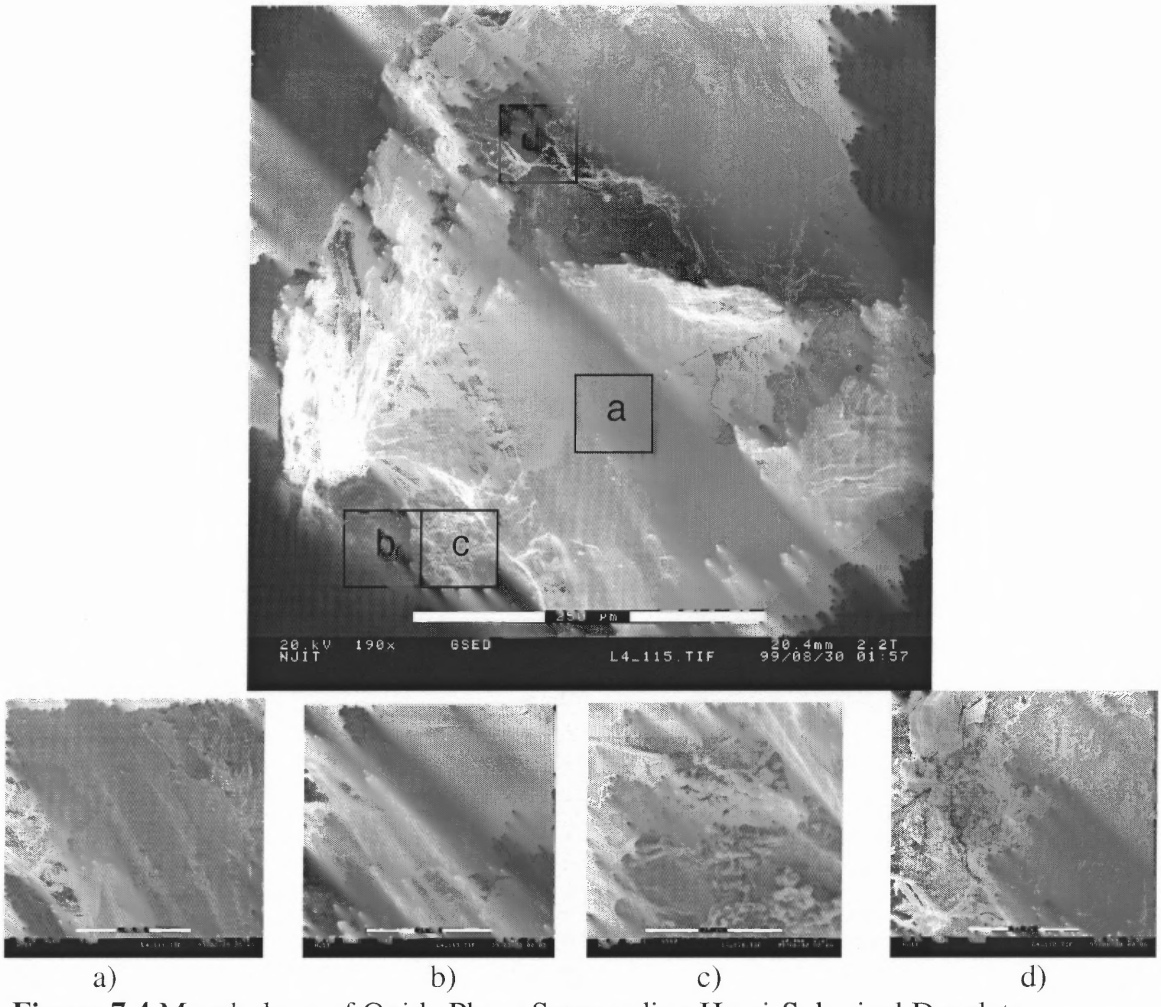

Figure 7.4 Morphology of Oxide Phase Surrounding Hemi-Spherical Droplets

The observation of particls showed local variation of chemical compositions. Figure 7.5 shows two different morphologies, one with high and the other with low concentrations of iron and chromium. The area having high concentrations of iron and chromium had a noticeable smooth surface while the low iron fraction was porous. Large diameter holes were not unusual and occurred possibly due to the separation of tiny metal droplets and the reduction of oxides. From the compositional analysis, area with high chromium content always had high iron content. Metal droplet had rather high concentration of Si.

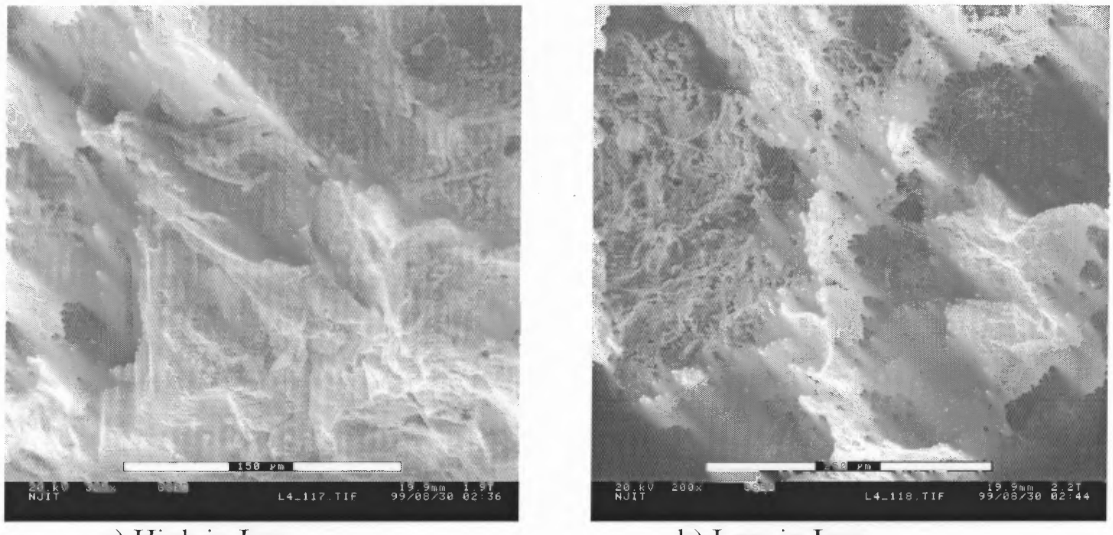

a) High in Iron b) Low in Iron

Figure 7.5 Morphology of Areas containing Oxides

The sample was strongly attacted to the alumina crucible used in this experiment. The interface of sample and alumina crucible was magnified and shown in Figure 7.6. The composition of the sample at the interface is given in Table 7.1 and shows high alumina content. The diffusion of alumina into the sample could influence the separation. This promted to change the crucible material from alumina to graphite.

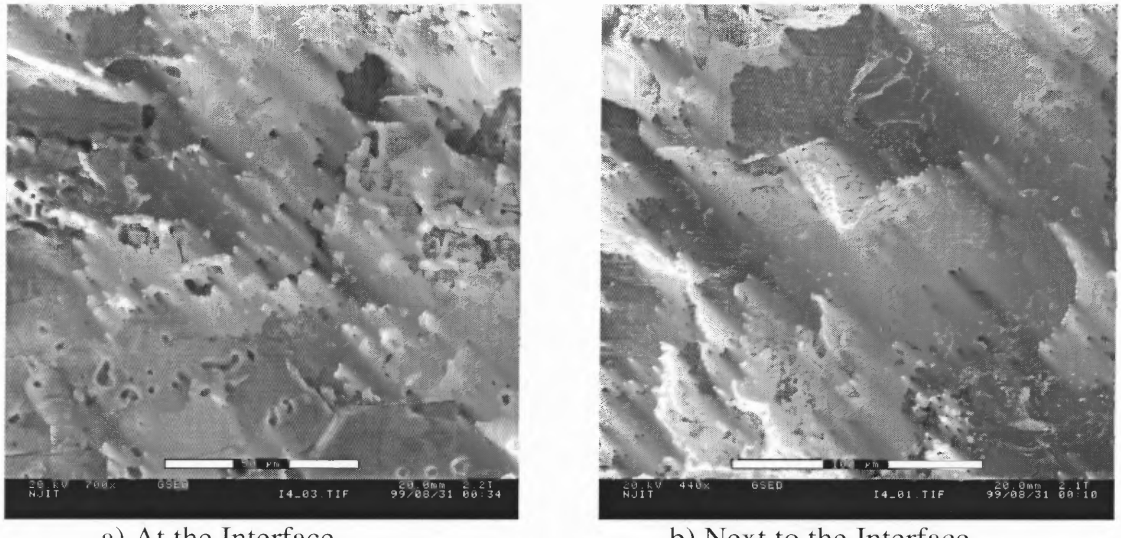

a) At the Interface b) Next to the Interface

Figure 7.6 Morphology of the Crucible/Sample Interface

7.1.2 Metal Separation inTGA, with Sand Addition

The addition of sand, an acid oxide to soils rich with CaO, a basic oxide, should bring the melting temperature down and ease the agglomeration of the metallic iron. The temperature was set at 1400°C for 3 hrs. The LSP soil was mixed with 20% carbon and 30% sand. Surprisingly, there was no MgO separation. The sample adhered strongly to the crucible. Figure 7.7 shows the metallic phase embedded within the oxide phase, with their compositions presented in Table 7.2.

Table 7.2 Compositions of Metal and Oxide Phases

Figures	Particles/Areas	Concentration (% wt)							
		Fe	Cr	Si	Mg	Al	Ti	Ca	O
Fig 7.7	a) Metal	47.8	25.1	27.2					
	b) Oxide	4.0	3.1	22.4	8.0	5.9	5.3	2.4	48.9
Fig 7.8	a) Sphere	15.5	5.6	22.5	2.7	3.1	1.0	0.6	49.0
	b) Sphere	21.1	6.1	23.3	2.4	2.4	1.0	0.7	43.0
	b) Oxide	2.0	1.0	18.6	10.4	9.4	2.8	2.9	52.8

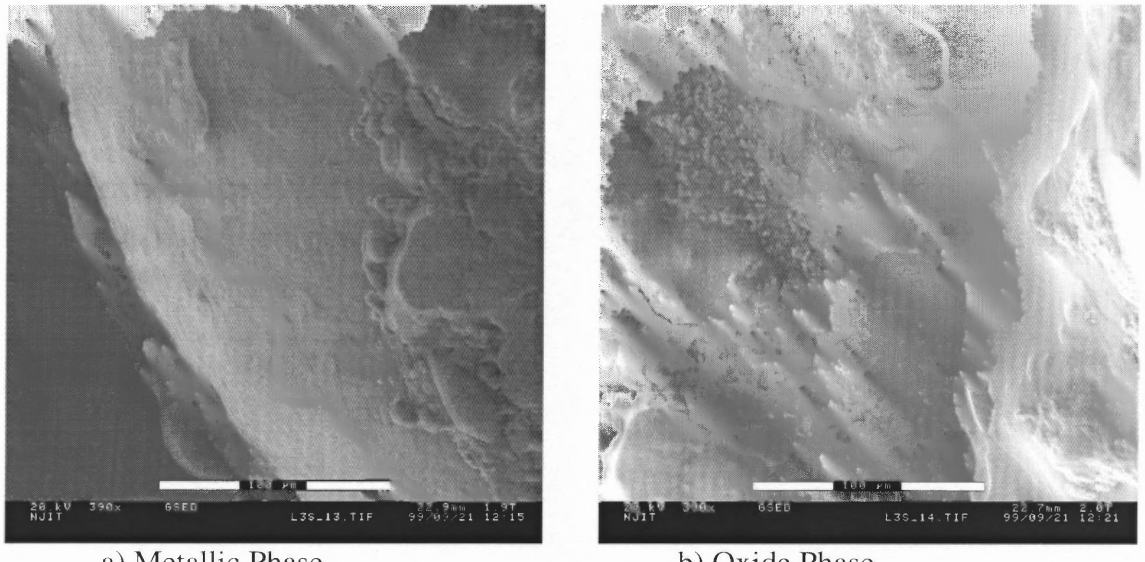

a) Metallic Phase b) Oxide Phase

Figure 7.7 Morphology of Metal Phase Surrounded by Oxide Phase

There were plenty of tiny hemi-spherical particles, which were identified as oxide instead of metal. Figure 7.8 shows different images of hemi-spherical particles with their compositions presented in Table 7.2. The oxide phase next to the hemi-spherical particle was also analyzed and the compositions are given in the same table.

Consistently, chromium was concentrated with iron in the metal droplet. The hemi-spherical particles contained rather high concentrations of both iron and silica. There was a chance that the hemi-spherical particle contained an oxide of iron and silica as fayalite – $2FeO.SiO_2$. The fayalite has a low melting temperature, as low as 1200°C.

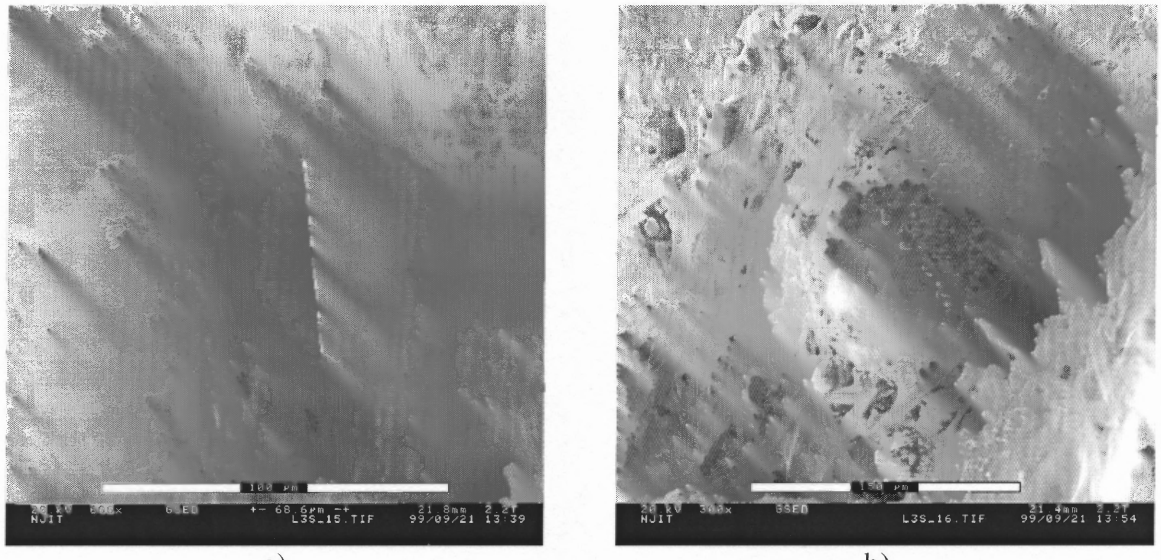

a) b)

Figure 7.8 Morphology of Hemi-Spherical Particles

7.1.3 Metal Separation inTGA using Graphite Crucible, with Sand Addition

Since alumina from crucibles affected the reaction and separation, graphite crucibles were used for the following tests. The LSP soil was mixed with 15% carbon and different percents of sand: 10, 20, and 30%. The test conditions were 2 hr flushing, 1 hr isothermal at 1400°C. All tested samples showed two distinct phases: glass and crystalline phases. The glass, from the 30% test, was light gray, the others were black.

Weight percentages of glass phase were approximately 54%, 67%, and 78% for the test with 10%, 20% and 30% sand additions. The compositions of glass phases, using EDX, are given in Table 7.3.

Table 7.3 Compositions of Glass Phase, using EDX.

Samples	Concentration (% wt)					Remarks
	Ca	Si	Al	Mg	O	
TL15%C10%S	25	22	7	5	42	Small black glasslike droplets
TL15%C20%S	7	21	8	10	54	Single black glasslike droplet
TL15%C30%S	4	21	5	7	62	Single light gray glasslike droplet

The fast cooling rate was resposible for the glass phase formation. The glass phase contained mostly of Ca, Si, Al, and Mg as identified by EDX. The intensities for Fe, Cr, Ti were not observable, indicating the separation of glass-forming elements from the deemed to be recycled metals. The results presented were the average numbers.

The diffractograms, Figure 7.9, show the reduction of iron oxide in soil to metallic phase. The iron tended to form as Fe_3Si at the expense of Fe as the sand content increased. Only from the 10% test that the diffractogram showed major oxide phases containing Mg, Al, and Si, while the others show only Si. The adding of more than 20% sand helped separating calcium and magnesium from the iron rich phase.

Figure 7.10 shows the attached crystalline droplets on the glass phases. The hemi-spherical droplets were initially believed to be metal. However, the analysis did not show the consistent identification of the hemi-sphere as a metallic phase. Table 7.4 contains the compositional analysis, given as average values, of the hemi-spherical droplets identified as metal and oxide from the 10% and 20% tests. The 10% test has a

pretty clean glasslike droplet and there was only a few hemi-sphere droplets which were identified as oxides. The 20% test contained both oxide and metallic phases.

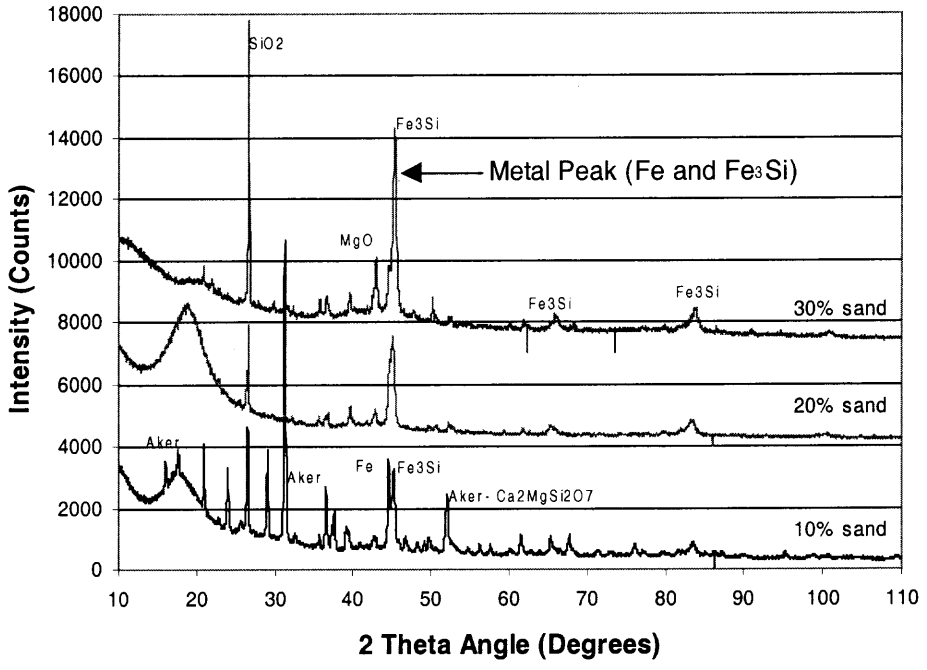

Aker : $CaO.2MgO.2SiO_2$ (Akermanite)
Scanning program: step size – 0.04° in 2θ, time/step – 2.5 seconds

Figure 7.9 Diffractograms of Crystalline Dust from LSP Soil Mixed with Different Amount of Sands

Table 7.4 Compositions of Hemi-Spherical Droplets, using EDX

Phases	Concentration (% wt)							
	Fe	Cr	Ti	Si	Al	Ca	Mg	O
10%S-Oxide (Fig.7.10 a)	31.7	5.5	19.9	12.3	1.7	3.2	2.3	20.1
20%S-Metal (Fig.7.10 b. sp1)	50.0	18.3	24.9	9.5	-	-	-	-
20%S-Oxide (Fig.7.10 b. sp2)	30.0	5.6	18.7	10.1	3.0	2.7	4.0	23.7

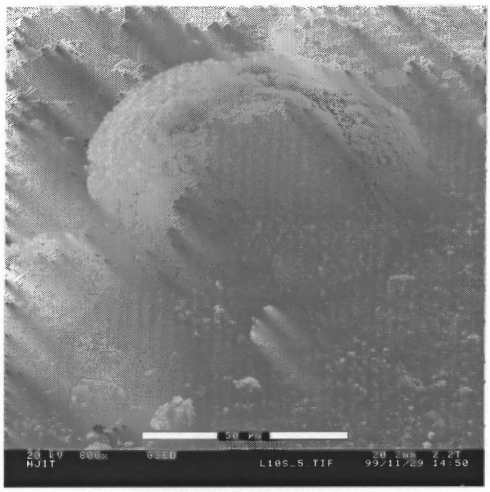

a) 10 % sand

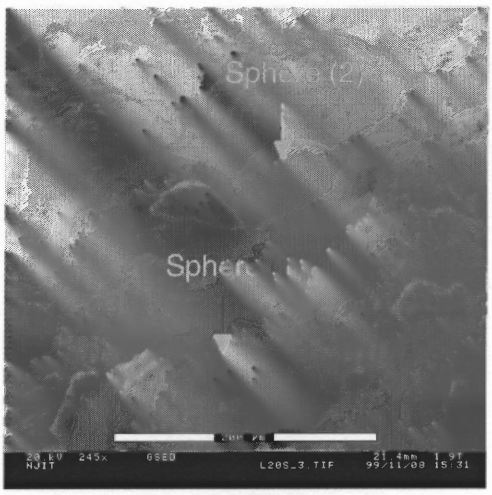

b) 20 % sand

Figure 7.10 Images of Hemi-Spherical Droplets on Top of Glass Phases

The preliminary test results showed the possibility to separate metal at higher temperature and with sand additions. The addition of 20% sand seemed to promote the separation of metal and other oxides.

7.2 Separation of Metal from Soils

This section includes the results on the metal separation conducted in the high temperature furnace and the prediction of the slag behavior and metal separation with different sand fractions. Soils from LSP, CD, GAR, and TPR are selected for the study.

7.2.1 Phase Diagrams and Metal Separation

The factors governing the metal separation include but are not limited to the melting temperature and the slag viscosity which depend on slag compositions. The behavior of slag or oxide system can be partly described through phase diagrams. The slag components of interest are CaO, MgO, SiO_2, and Al_2O_3.

At high temperature, intermediate compounds with low melting temperatures may form through the solid state diffusion at points of contact between different oxides. For example, the melting temperature of $MgO.SiO_2$ is 1557°C when compared to pure MgO and SiO_2, which have melting temperature of 2800°C and 1700°C, respectively. Upon the melting of the intermediate compound the other oxides can dissolve into the liquid mass and change the viscosity or fluidity accordingly. Various melting spaces propagate and meet to form a larger liquid pool. Phase diagrams provide information on thermodynamically stable states, i.e. as liquid or liquid in equilibrium with solids, depending on sample compositions.

7.2.1.1 Liquidus and Solidus Surfaces. Liquidus temperature is the first temperature where the crystallization takes place and liquid phase is in equilibrium with solid. At the temperatures higher than liquidus temperature the liquid phase is the only stable phase and vice versa for the solidus temperature. Between the liquidus and solidus temperatures, there are two phases, liquid and solid, in equilibrium at different proportions and compositions at different temperatures. In binary phase diagram, liquidus and solidus lines connect liquidus and solidus temperatures of solid solution at different compositions. For the ternary system or higher order, the presentation of a complete phase diagram in 2-dimentional space is not possible. The 2-dimentional presentation is presented as a projection of the 3-dimentional phase diagram. The appearance of the liquidus lines in the projected plane is similar to the contour lines in a topological map. Each line represents different compositions of solid solutions that have the same liquidus temperatures, the liquidus isotherm. Observing Figure 7.11, the

compositions of solid solution bounded by the 1500°C liquidus isotherm have liquidus temperatures lower than 1500°C. These solid solutions, therefore, will totally melt down when heated to 1500°C. The temperatures used in this experiment were 1480°C and 1530°C. Figures 7.11 to 7.14 show the liquidus isotherms of a quaternary system, CaO-MgO-SiO_2-Al_2O_3, represented by several ternary systems, each with a constant concentration of Al_2O_3. The shaded areas are bounded by the liquidus isotherm at 1500°C. The locations of mixtures of soils with different percentages of sand from Table 7.7 are marked on different phase diagrams. Within shaded areas, there are large composition ranges of soils that could melt and possibly allow the metal separation.

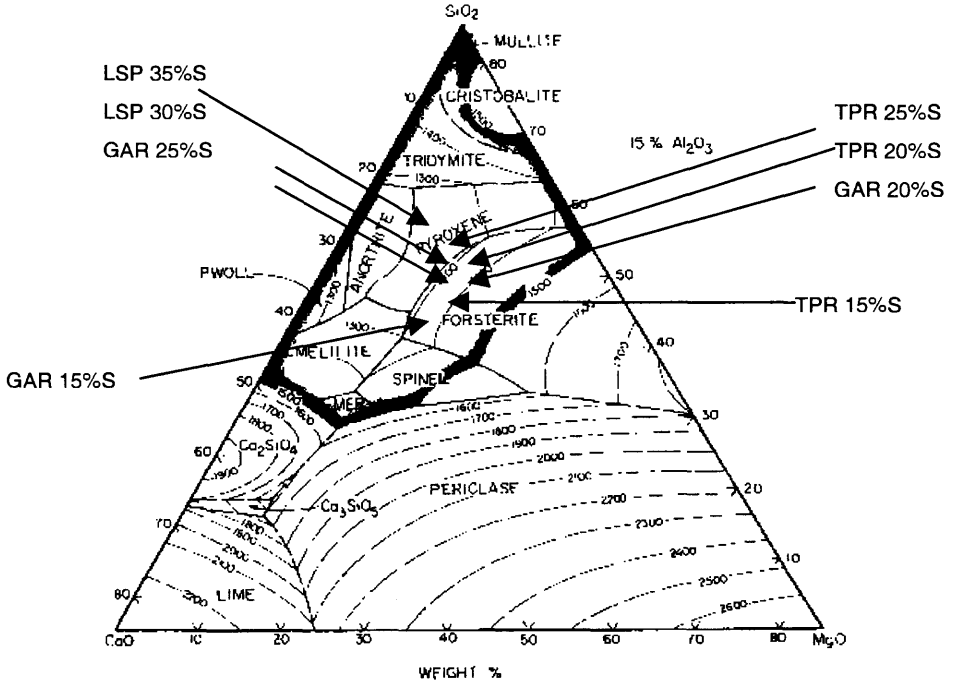

Figure 7.11 Liquidus Temperatures of a CaO-SiO_2-MgO-Al_2O_3 System in a Constant Concentration Plane at 15% Al_2O_3 (Muan and Osborn, 1985)

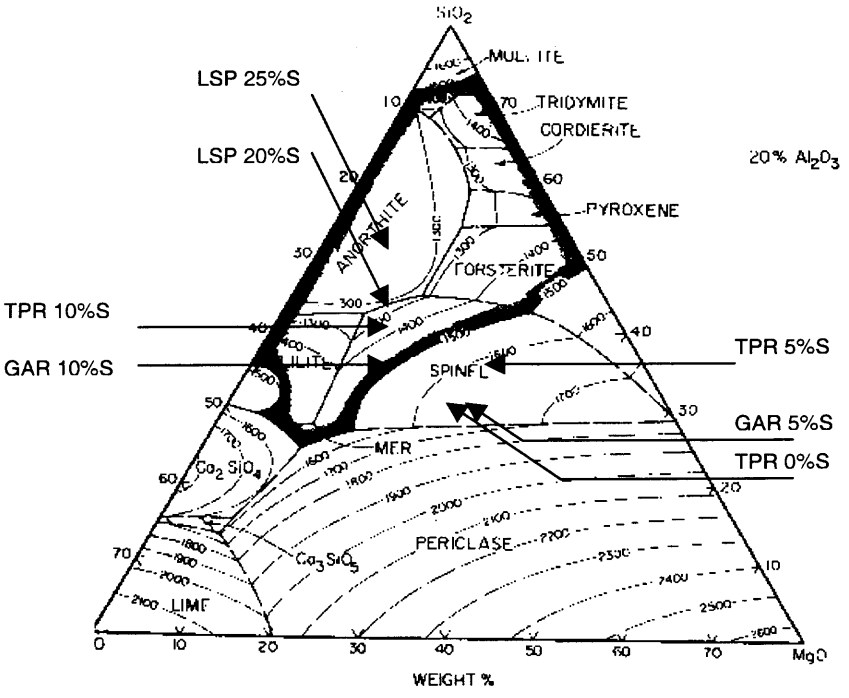

Figure 7.12 Liquidus Temperatures of a CaO-SiO_2-MgO-Al_2O_3 System in a Constant Concentration Plane at 20% Al_2O_3 (Muan and Osborn, 1985)

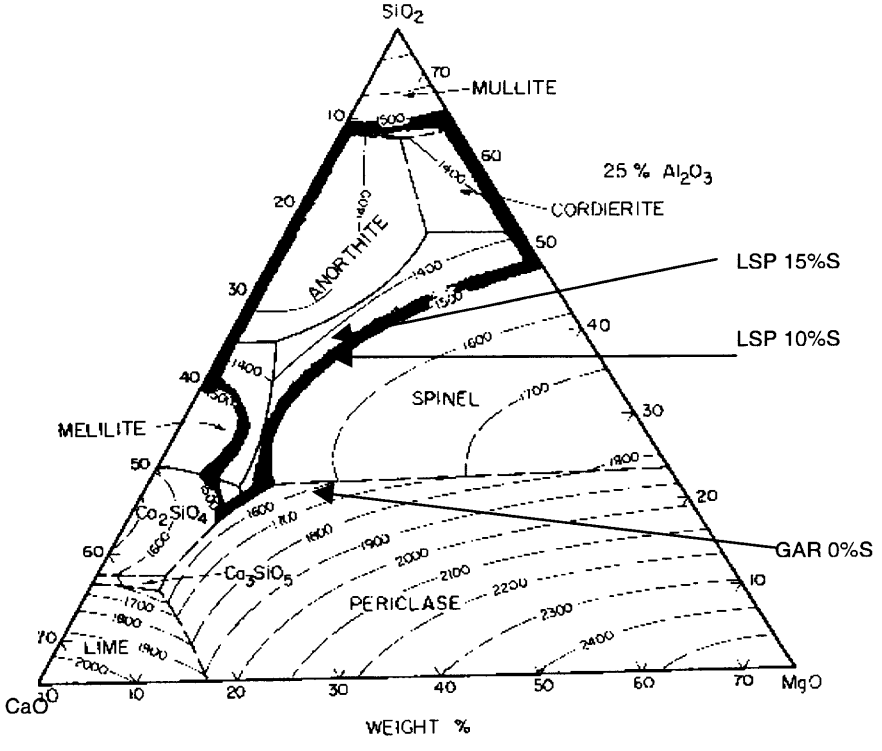

Figure 7.13 Liquidus Temperatures of a CaO-SiO_2-MgO-Al_2O_3 System in a Constant Concentration Plane at 25% Al_2O_3 (Muan and Osborn, 1985)

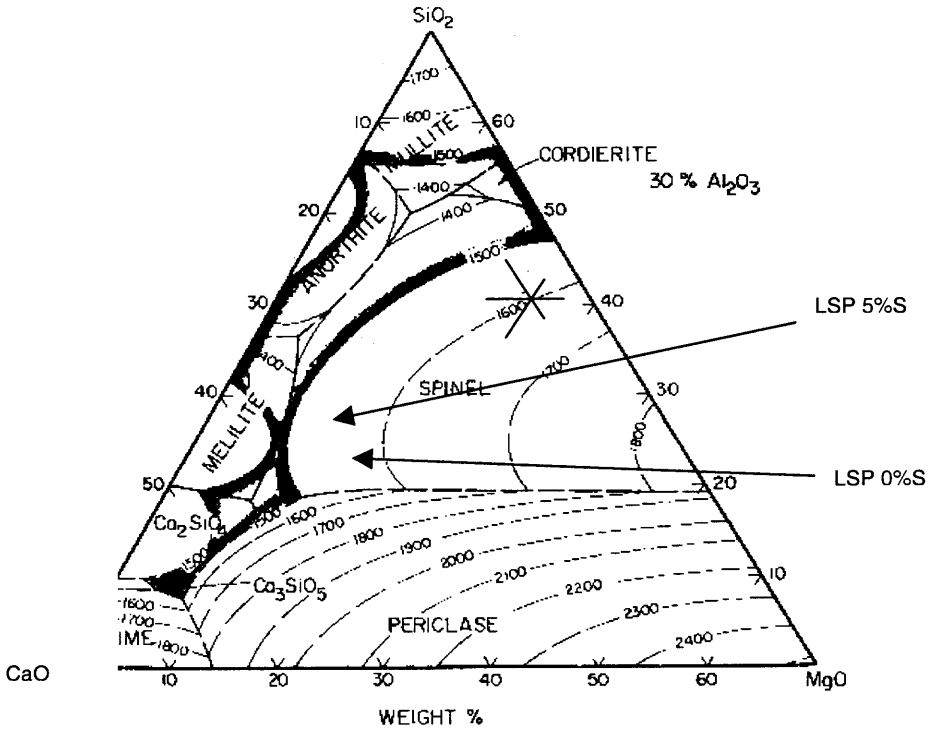

Figure 7.14 Liquidus Temperatures of a CaO-SiO_2-MgO-Al_2O_3 System in a Constant Concentration Plane at 30% Al_2O_3 (Muan and Osborn, 1985)

The liquid state is maintained until the temperature drops to the liquidus surface, where the compound of primary phase starts crystallizing. The primary phase field is the phase area to which the initial slag compositions are bounded. For example, the primary phase field of the solid solution, 30% of Al_2O_3, 10% of CaO, 20% of MgO, and 40% of SiO_2 (Figure 7.14), is spinel. As the temperature continually decreases, the primary phase compound crystallizes out and the composition of the liquid changes along the crystallization path. The liquid completely changes into solid when the temperature falls below the solidus temperature. The example of solidus surface for quaternary system CaO-MgO-SiO_2-Al_2O_3 is given in Figure 7.15. The solidus surface identifies final phases of the slag according to the initial slag composition. Table 7.5 gives an example of the phases and melting temperature for some areas.

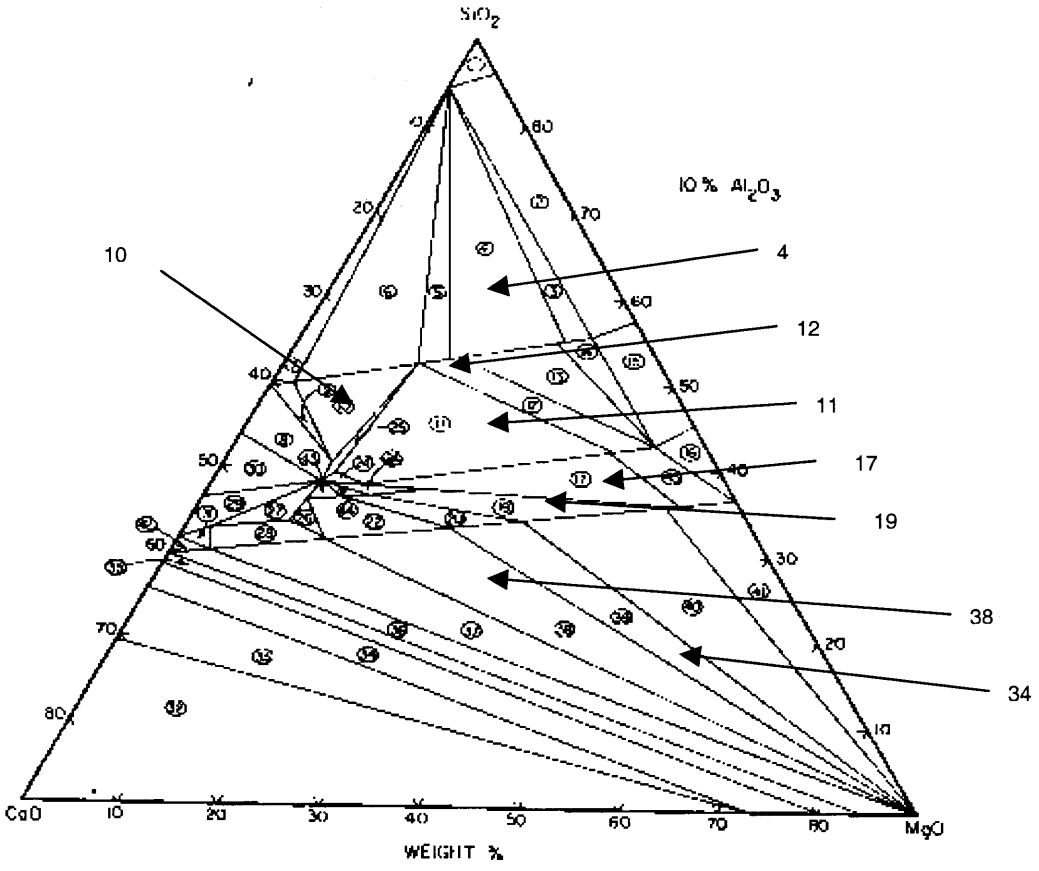

Figure 7.15 Solidus Surface of the $CaO-SiO_2-MgO-Al_2O_3$ System (Muan and Osborn, 1985)

Table 7.5 Crystalline Phases at the Solidus Surface (Maun and Osborn, 1985)

Area	Solidus Temp (°C)	Phases
10	1210	Anorthite +Diopside+Melilite+Wallastonite(93)
11	1225	Anorthite+Diopside+Forsterite(83)+Melilite(70)
12	1200-1270	Anorthite+Diopside(78-100)+Forsterite(83-100)
17	1285	Anorthite+Forsterite(80)+Melilte(70)+Spinel
19	1380	Forsterite(75)+Millite(63)+Monticelite(75)+Spinel
38	1400	Merwinite+Monticelite+Periclase+Spinel
39	1400	Monticelite(74-100)+Periclase+Spinel
4	1170	Anorthite+Diopside(78)+Enstatite(82)+Silica

Anorthite: $CaO.Al_2O_3.2SiO_2$ Diopside: $CaO.MgO.2SiO_2$
Merwinite: $3CaO.MgO.2SiO_2$ Periclase: MgO
Monticelite: $CaO.MgO.SiO_2$ Spinel: $MgO.Al_2O_3$
Wallastonite: $CaO.SiO_2$ Enstatite: $MgO.SiO_2$ Merwinite :
Parenthesis indicates the formation of solid solution. Diopside formed solid solution with enstatite, forsterite with Monticellite. The number in the parenthesis is the weight percentage of that phase in the solid solution.

Phase diagrams are great tools in understanding the behavior and property of slag at equilibrium at different temperatures. It is noteworthy to realize that the temperature change must be sufficiently small to maintain the state of equilibrium along the crystallization path. It is often that the change in temperature is too fast and results in the remaining of freeze-in metastable phases.

7.2.1.2 Viscosity. From Figures 7.16 to 7.19, at a constant concentration of SiO_2 the iso-viscosity lines are parallel to the concentration line of Al_2O_3, especially at the low concentration of Al_2O_3. The viscosity increases with the Al_2O_3 concentration. At low Al_2O_3 concentration, the viscosity does not change much with the changing content of CaO and MgO provided their combined content remains the same. The models for the prediction of slag viscosity are available with pretty high accuracy for the binary mixture, i.e. the Weymann equation (Urbain, 1981), Hole Theory (Reddy and Hebbar, 1991), and other structural related models (Zhange and Jahanshahi, 1998). The prediction on the multi-component system is not as good as the one or two component systems. The parameters in every model were calculated by fitting the model with available viscosity diagrams. The accurate model is the one that predicts viscosity to a similar value from the diagram. In this research, the viscosity will be read directly from diagrams (Figures 7.16 to 7.19).

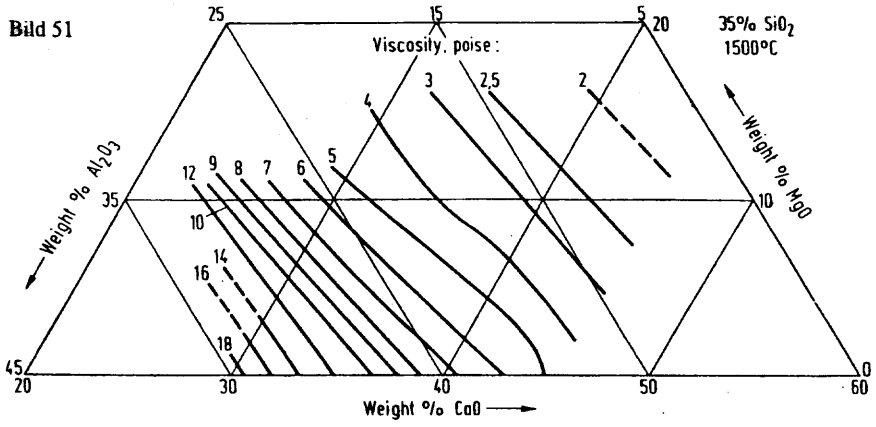

Figure 7.16 Isoviscosity Lines of the CaO-MgO-SiO_2-Al_2O_3 System at a Constant Concentration of 35 % SiO_2 (Dusseldorf, 1981)

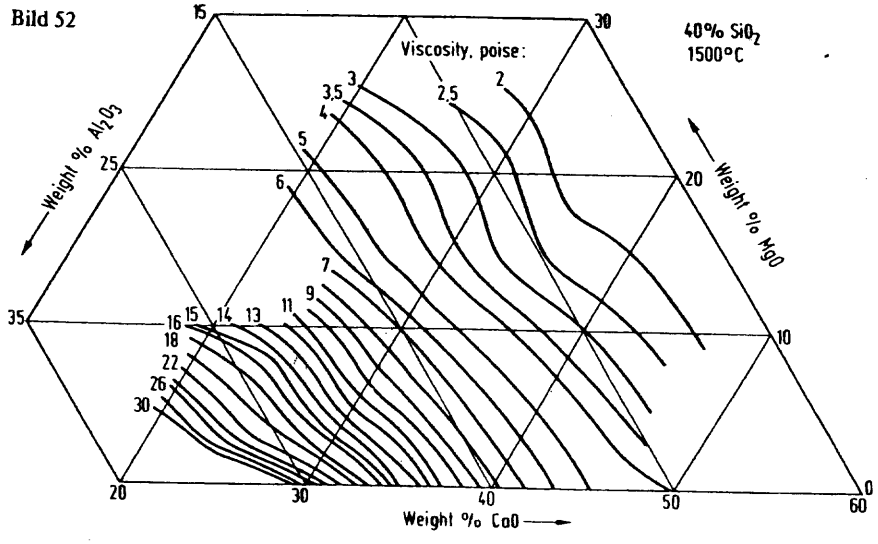

Figure 7.17 Isoviscosity Lines of the CaO-MgO-SiO_2-Al_2O_3 System at a Constant Concentration of 40% SiO_2 (Dusseldorf, 1981)

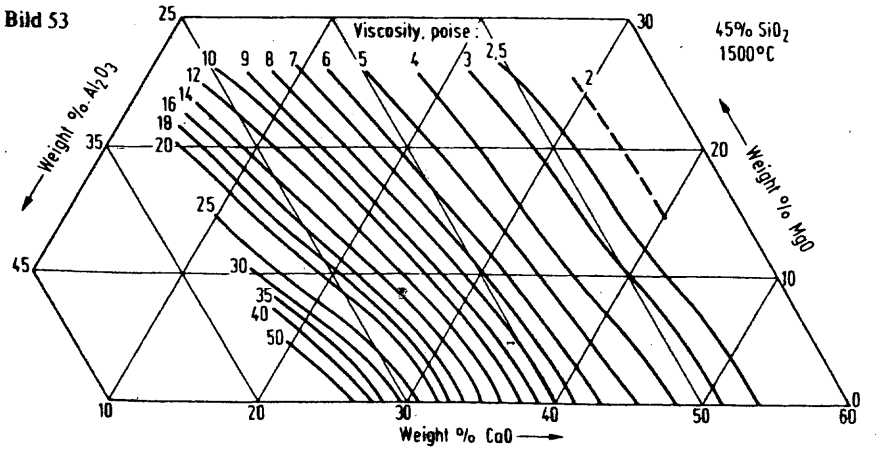

Figure 7.18 Isoviscosity Lines of the CaO-MgO-SiO_2-Al_2O_3 System at a Constant Concentration of 45% SiO_2 (Dusseldorf, 1981)

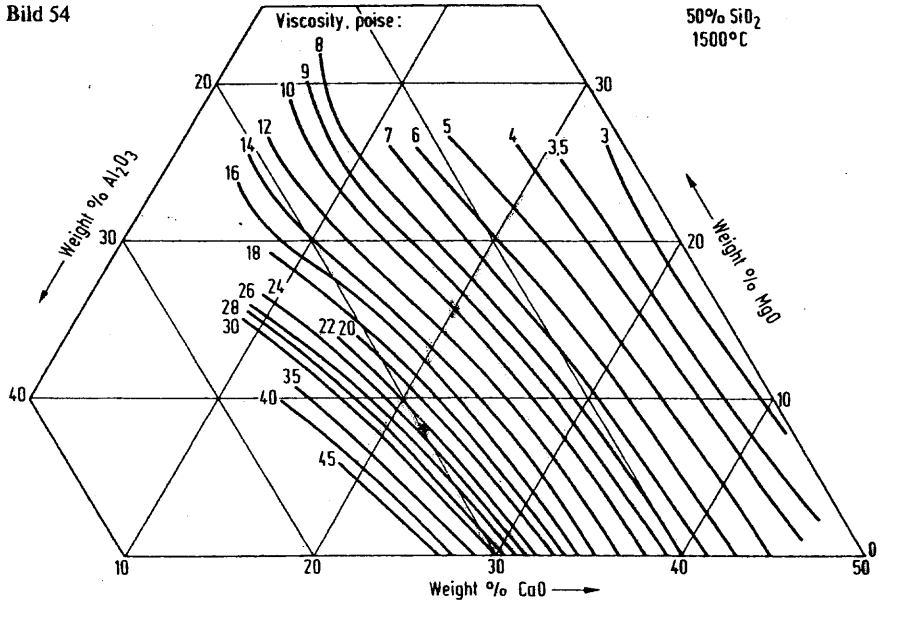

Figure 7.19 Isoviscosity Lines of the CaO-MgO-SiO_2-Al_2O_3 System at a Constant Concentration of 50% SiO_2 (Dusseldorf, 1981)

7.2.1.3 Mixtures of soils and sand. The slag compositions made of mixtures of soil and sand after the reduction process can be estimated, assuming the reduction of iron oxide to metal is rapid and only major and stable oxides remain and govern the slag behavior. Tables 7.6 and 7.7 show the sample calculation and the estimated compositions of soils from GAR, TPR, and LSP.

Table 7.6 Sample Calculation of Soil Composition Added with Sand

Samples	Concentration (% wt)				Sum
	CaO	MgO	SiO_2	Al_2O_3	(%)
Original, GAR	16.0	8.2	10.0	10.8	45
After 20% sand, [ ]/1.2	13.3	6.8	25.0	9.0	54.1
Adjusted to 100%, [ ]/0.54	24.6	12.6	46.2	16.6	100

Table 7.7 Estimated Soil Compositions

Mixtures	Concentration (% wt)				Sum
	CaO	MgO	SiO_2	Al_2O_3	(%)
GAR					
0% sand	35.6	18.1	22.2	24.0	100.0
5% sand	31.7	16.1	30.7	21.4	100.0
15% sand	26.1	13.3	43.1	17.6	100.0
20% sand	23.9	12.2	47.8	16.1	100.0
25% sand	22.1	11.2	51.7	14.9	100.0
TPR					
0% sand	29.4	17.4	29.4	23.7	100.0
5% sand	26.4	15.7	36.6	21.3	100.0
15% sand	21.9	13.0	47.4	17.7	100.0
25% sand	18.8	11.1	55.0	15.1	100.0
LSP					
0% sand	36.4	15.1	17.3	31.1	100.0
5% sand	32.3	13.4	26.6	27.7	100.0
15% sand	26.4	11.0	40.0	22.6	100.0
20% sand	24.2	10.1	45.0	20.7	100.0
25% sand	22.3	9.3	49.3	19.1	100.0
30% sand	20.7	8.6	52.9	17.7	100.0
35% sand	19.4	8.0	56.0	16.6	100.0

Figures 7.11 to 7.14 show positions of each soil composition as points on phase diagrams. The graphical illustration of the complete quaternary system on the two-dimensional space is not possible. Some parameters have to be fixed for the simplified presentation, i.e. fixing the concentration of components. The given phase diagrams have alumina concentrations fixed as constants for each diagram. The soil mixtures were marked on phase diagrams with the closest alumina content. From Figures 7.12 and 7.13, LSP, GAR, and TPR soils mixed with less than 10% sand located outside the shaded areas. The sample may partially melt and establish the equilibrium between the liquid phase and the solid phase, the primary phase field. For example, mixtures of LSP with 0% and 5% sand fall into the primary phase field of spinel at temperature slightly higher than 1550°C. The system at 1530°C would be a mixture of liquid, of different composition, in equilibrium with spinel. The final phases at lower temperature are read from the solidus surface diagram. In fact, the partially melting behavior of sample is complex especially for heterogeneous system. The local composition varies and liquid phase of different compositions may be formed in equilibrium with different solid phases.

The larger the difference between the furnace temperature and the liquidus temperature, the larger the chance that metal will separate. According to the diagrams, Figures 7.11 and 7.12, metal separation should occur for the LSP, GAP, and TPR at and above the sand addition of 15%. The liquidus temperature of the mixtures is around 1300°C to 1400°C.

7.2.2 Metal separation of Iron from Soils

7.2.2.1 GAR and TPR Soils. The GAR and TPR soils were initially tested to verify the applicability of the process. However, both of them yielded astounding results in term of the metal separation. The temperature for the study was 1530°C. Tables 7.8 and 7.9 describe the physical appearances of both soils. The separation of metal was a very difficult task due to the fineness of the metal balls for the 0 and 5% tests. They partly incorporated within the solid phase, which caused the identification of metal phase in the diffractogram.

The results from both TPR and GAR were presented together since they yielded very similar outcomes both in terms of metal separation and final phases. Figures 7.20 and 7.22 illustrate changes of phases for GAR and TPR in products with the changing percentages of sand. With no sand addition, there was no metal separation, however, there were tiny shiny specks concentrating at the lower portion of the slag matrix. The metal pool formed at 15% sand addition and above. The slag adhered strongly to the graphite, or wetted the graphite crucible, when there was a metal pool. According to the phase diagrams the 15%, 20%, and 25% have compositions where liquidus temperatures are below 1400°C with forsterite and pyroxene as primary phase fields. Figure 7.21 shows a picture, though not of a good quality, of metal separated and ground slag from the 25% test, GAR soil.

Table 7.8 Physical Description of Tested GAR Soil

Sand (%)	Wt Loss (%)	Phases	Weight** (%)	Metal Phase	Magnetic	Shiny Specks	Remarks
0%	38.5	3: Slag –gray	<72.6	Yes	Yes	Yes	-Embedded with tiny metal balls, partly liberated upon grinding
		Dust –gray	24.4	Yes	Yes	Yes	-Deposited on top of sample
		Metal	>>2.7*				
5%	37.4	2: Slag – gray	<95.7	Yes	Yes	Yes	-Embedded with tiny metal balls, partly liberated upon grinding
		Metal	>>4.3*				
15%	34.0	2: Slag – gray	70.8	No	No	No	-Slightly embedded with tiny metal dust, mostly separated by magnet.
		Metal	29.2				-Metal pool, 25.4% by weight of original soil
20%	34.9	2: Slag – gray	63.0	No	No	No	-Clear separation between slag and metal. The slag wetted and stuck to the graphite crucible.
		Metal	37.0				-Metal pool, 32.7% by weight of original soil
25%	34.1	2: Slag – gray	67.0	No	No	No	-Clear separation between slag and metal. The slag wetted and stuck to the graphite crucible.
		Metal	33.0				-Metal pool, 30.8% by weight of original soil

*: The actual weight of metal should be larger than the weight of clean separated metal due to the metal dissemination in the solid matrix.

**: The weight percentages are the weight proportion of each phase (slag, metal, and dust) physically separated after the experiment.

Table 7.9 Physical Description of Tested TPR Soil

Sand (%)	Wt Loss (%)	Phases	Weight** %	Metal Phase	Magnetic	Shiny Specks	Remarks
0%	35.3	1: Slag –gray	100	Yes	Yes	Yes	-Embedded with tiny metal specks
5%	34.0	2: Slag – gray Metal	<84.9 >15.1*	Yes	Yes	Yes	-Embedded with tiny metal balls, partly liberated upon grinding
15%	41.4	2: Slag – gray Metal	66.7 33.3	No	No	No	-Clear separation between slag and metal. The slag wetted and stuck to the graphite crucible. -Metal pool, 25.4% by weight of original soil
25%	32.2	2: Slag – gray Metal	66.7 33.3	No	No	No	-Clear separation between slag and metal. The slag wetted and stuck to the graphite crucible. -Metal pool, 30.8% by weight of original soil

*: The actual weight of metal should be larger than the weight of clean separated metal due to the metal dissemination in the solid matrix.

**: The weight percentages are the weight proportion of each phase (slag, metal, and dust) physically separated after the experiment.

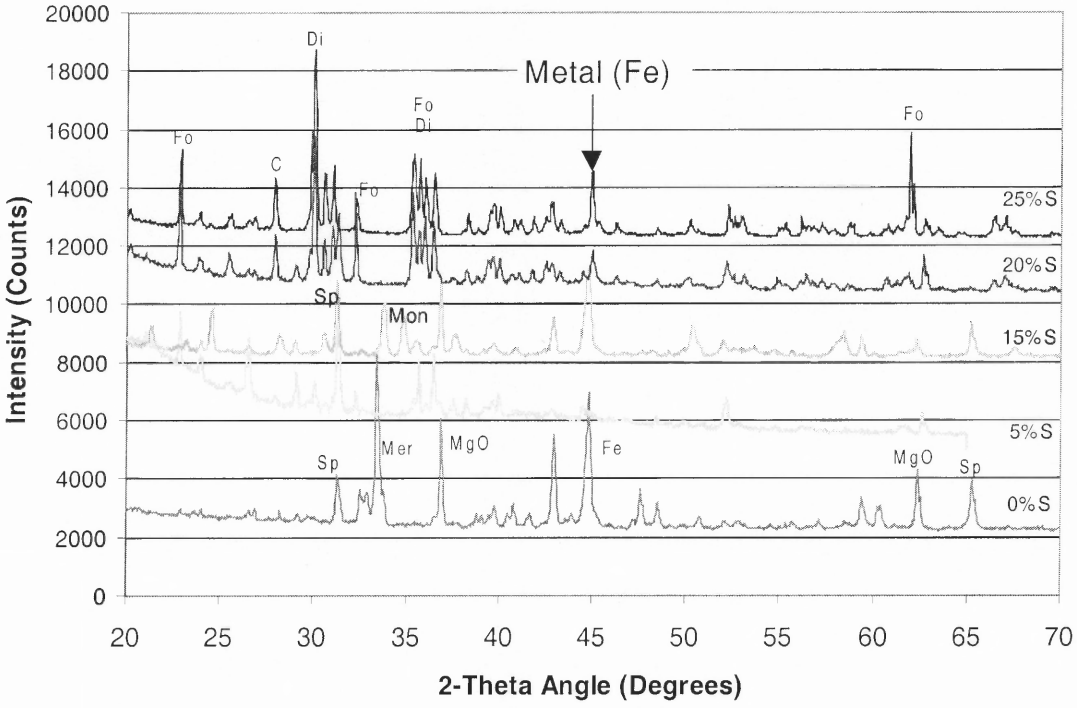

Me : $3CaO.MgO.2SiO_2$ (merwinite)
Sp : Spinel
Fo : $2MgO.SiO_2$ (forsterite)
Di : $Ca(Mg, Al)(Si, Al)_2O_6$ (Diopside)
C : Carbon
Scanning program: step size – 0.04° in 2θ, time/step – 2.5 seconds

Figure 7.20 Diffractograms of GAR Samples at Different Sand Additions

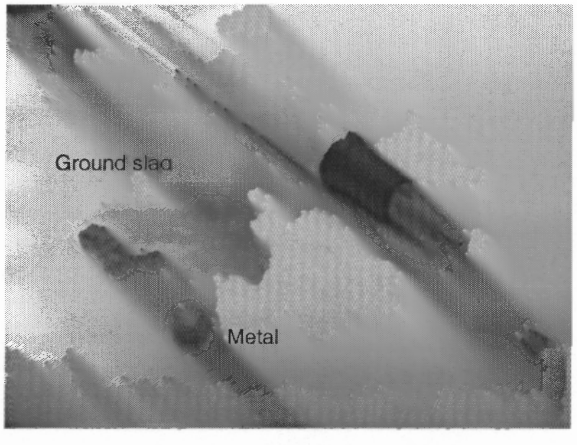

Figure 7.21 Picture of Separated Metal and Ground Slag from a Mixture of GAR and 20% Sand

With no sand addition, there was a formation of dust with MgO as a major phase on top of the GAR soil. The 0% test yielded metal, MgO (periclase), and $MgAl_2O_4$ (spinel), and $3CaO.MgO.2SiO_2$ (merwinite), as its major phases. The result agreed well with the prediction from phase diagram where the 0% fell at the boundary of the spinel and periclase primary phase fields. It is worth mentioning again that the spinel has a formula of $MgAl_2O_4$. However, in the past chapter the word "spinel" was used as a name for a group of compound with a formula $AO.B_2O_3$. To avoid confusion, the chemical formula will be used instead of the mineral names. The major phases changed to MgO and $CaO.MgO.SiO_2$ (monticelite) at 5% sand addition, to $2MgO.SiO_2$ (forsterite) and $2CaO.MgO.2SiO_2$ (akermanite) at 15% sand addition, and to $2MgO.SiO_2$(forsterite) and $Ca(Mg, Al)(Si, Al)_2O_6$ (Diopside) at 20 and 25% sand addition. The final phase identification agrees fairly well with the phase diagram.

The phases of TPR mixtures at different temperatures, Figure 7.22, are similar to those from GAR mixtures. They both have a similar composition and are plotted close to each other on the phase diagrams. In Chapter 6, the reduction from TPR soils was not complete. The addition of sand appeared to be beneficial to the reduction of iron oxide and also the metal separation for soils containing hard to reduce spinel. Lekatou and Walker (1997) found that silica addition, at 1400°C, promoted the reduction of the difficult to reduce $MgO.Cr_2O_3$ by forming stable oxides of MgO and SiO_2. The addition of silica at 1300°C had no influence on the reduction since the solid state of silica inhibited its reaction with MgO.

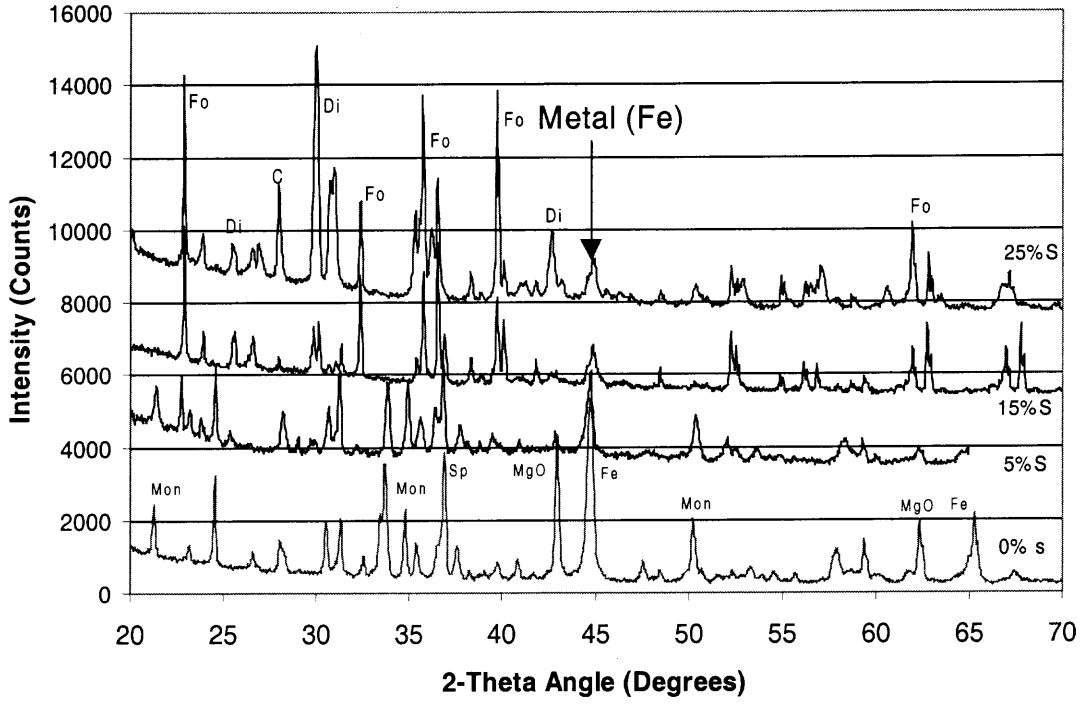

Mon : $CaO.MgO.2SiO_2$
Sp : $MgAl_2O_4$
Fo : $2MgO.SiO_2$ (forsterite)
Di : $Ca(Mg, Al)(Si, Al)_2O_6$ (Diopside)
Scanning program: step size – 0.04° in 2θ, time/step – 2.5 seconds

Figure 7.22 Diffractograms of TPR Samples at Different Sand Additions

According to the viscosity diagrams, the viscosity of the mixtures of 20% and 25% sand are approximately 6 and 10 poise. The 20% mixture is better in term of the flowability of the slag. The metal separation results also showed the 20% mixture, GAR soil, gave the largest quantity of separated metal. The XRF results though qualitative also showed the least metal concentration in slag at this composition (Table 7.10). Nonetheless, the slag viscosity of 10 poise allowed the metal formation and was also good for the metal separation. The XRF analysis was not used to verify the estimated composition due to the poor quality of the result because of the small sample size. The result showed very low concentrations of SiO_2 even with the 25% sand addition.

Nonetheless, it consistently showed low iron and chromium content in slag at 20 and 25% sand tests.

Table 7.10 Compositions of Slag, Semi-Quantitative XRF

Samples	Concentration (% wt)					
	MgO	Al_2O_3	SiO_2	CaO	Cr_2O_3	Fe_2O_3
GAR 5%S	28.3	14.5	11.1	13.8	12.1	19.7
GAR 15%S	28.2	21.0	20.0	22.2	4.2	4.1
GAR 20%S	31.1	21.2	24.2	21.9	0.4	0.5
GAR 25%S	28.8	20.7	26.4	19.9	1.7	2.0
LSP 25%S	25.1	22.7	26.5	22.0	0.9	2.1
TPR 25%S	29.0	22.7	29.5	15.5	1.1	1.0

Though the phase identification from both soils was the same, the final composition of each tested soil can be different, depending upon the initial composition of soil. The tested soils from GAR seemed to have larger ratio of the intensity of diopside/forsterite than that from TPR.

The slag composition of $2MgO.SiO_2$ was also similar to the prediction of the good slag composition given by Yazawa and Hino (1993) using regular solution model. There were convexities of the iso-activity lines at the intermediate compound of formula $2BO.SiO_2$, where B is basic oxide (Figure 7.23). The intermediate compound of this formula should allow the least dissolution or reoxidation of wustite (FeO) into the slag matrix.

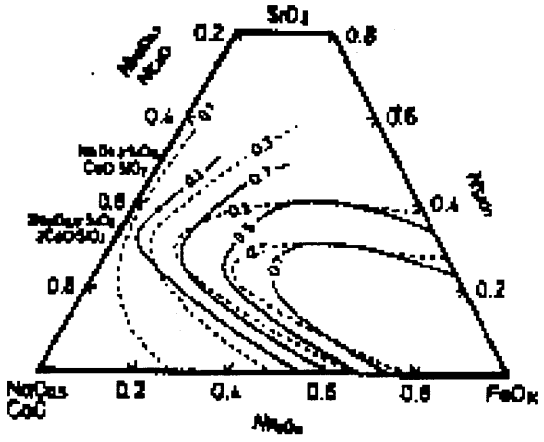

Figure 7.23 Isoactivity Lines of the Ternary Phases, Metal Oxide-Basic Oxide-Acid Oxide (Yazawa and Hino 1993)

Table 7.11 Physical Description of CD Samples

Sand addition (%)	Wt Loss (%)	Phases	Metal Phase	Magnetic	Metal separation
0%	25.1	2; black glasslike droplets black dust	No Yes	No Yes	-
10%	23.7	2; black glasslike droplets and black dust	No Yes	No Yes	-
15%	23.6	2; black glasslike droplets and black dust	No Yes	No Yes	-
20%	22.7	2; black glasslike droplets and black dust	No Yes	No Yes	-
25%	21.7	2; black glasslike droplets and black dust	No Yes	No Yes	-
30%	20.8	2; black glasslike droplets and black dust	No Yes	No Yes	-

7.2.2.2 CD Soil. The results of CD soils are summarized in Table 7.11. All mixtures yielded two phases: glasslike droplet and dust. The glass phase comprised of diopside and glass. The formation of glass implied the high viscosity of the melt. There was neither the metal separation nor the presence of tiny shiny specks like the other soils. The metal separation was not achievable with CD soil.

7.2.2.3 LSP Soil. LSP soils was tested at both 1480°C and 1530°C. It was the first soil to be tested in the high temperature furnace and the temperature was first set at 1480°C. The 1530°C test was conducted to see the temperature effect on the metal separation. The description of tested LSP soils are given in Tables 7.12 and 7.13.

For the tests with 20 and 25% sand, there were three distinct phases: the solid gray droplet, the dark black dust, and the small metal of different sizes separated from and embedded in mass of dark black dust. There was a larger quantity of gray phase with the larger quantity of sand addition. It started appearing with 10% sand. The separation of metal balls was observable with 20 and 25% sand. The inside wall of the graphite crucible with 0 – 15% sand showed the white dust deposition, no deposition with 20 and 25% sand but there was observable metal separation.

Figures 7.24 and 7.25 show the diffractogram of the gray phase at 1480°C and at 1530°C. The phases of the slag are quite similar to the ones from GAR and TPR mixtures, as they were marked next to each other in the phase diagram. The final phase for the 1480°C at 25% sand were identified as to $2MgO.SiO_2$(forsterite) and Ca(Mg, Al)(Si, $Al)_2O_6$ (Diopside). However, for the 1530°C test the final phases were $2MgO.SiO_2$(forsterite), and Ca(Mg, Al)(Si, $Al)_2O_6$ (Diopside) or $MgO.SiO_2$ (enstatite).

The dust was identified as a combination of carbon and Fe or Fe_3Si, Figure 7.26. The dissemination of the tiny metal in the black dust did not allow the clean metal separation. Both dust and metal specks were attracted by magnet. Table 7.13 shows results from the 1530°C test.

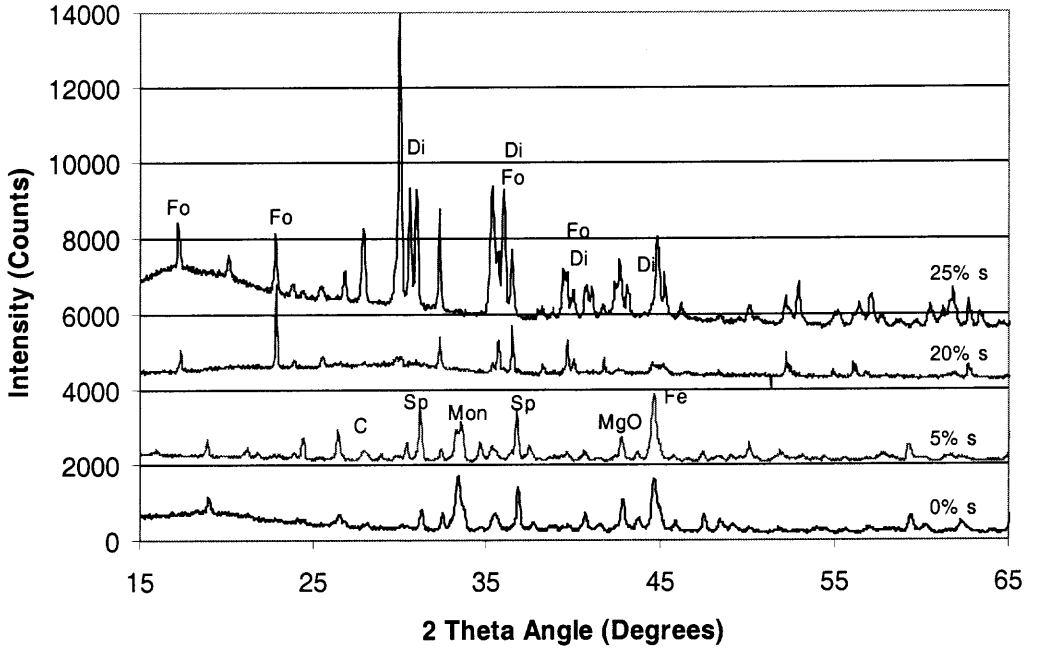

Mon : $CaO.MgO.2SiO_2$, Sp : $MgAl_2O_4$
Fo : $2MgO.SiO_2$ (forsterite), Di : $Ca(Mg, Al)(Si, Al)_2O_6$ (Diopside)
Scanning program: step size – 0.04° in 2θ, time/step – 2.5 seconds

Figure 7.24 Diffractograms of LSP Soil at Different Sand Additions at 1480°C

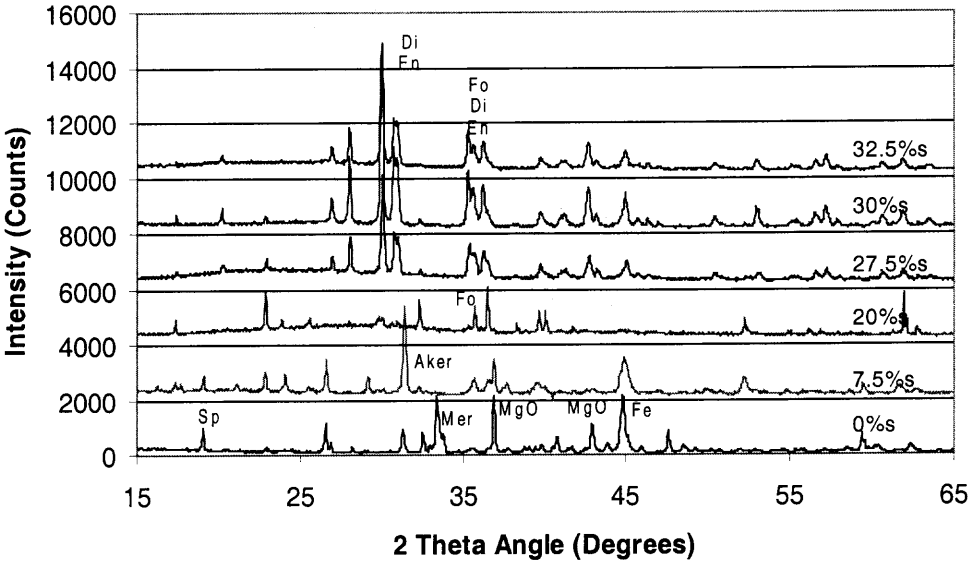

Mer : $3CaO.MgO.2SiO_2$
Sp : $MgAl_2O_4$
Fo : $2MgO.SiO_2$ (forsterite)
Di : $Ca(Mg, Al)(Si, Al)_2O_6$ (Diopside)
En : $MgOSiO_2$ (Enstatite)

Figure 7.25 Diffractograms of LSP Soil at Different Sand Additions at 1530°C

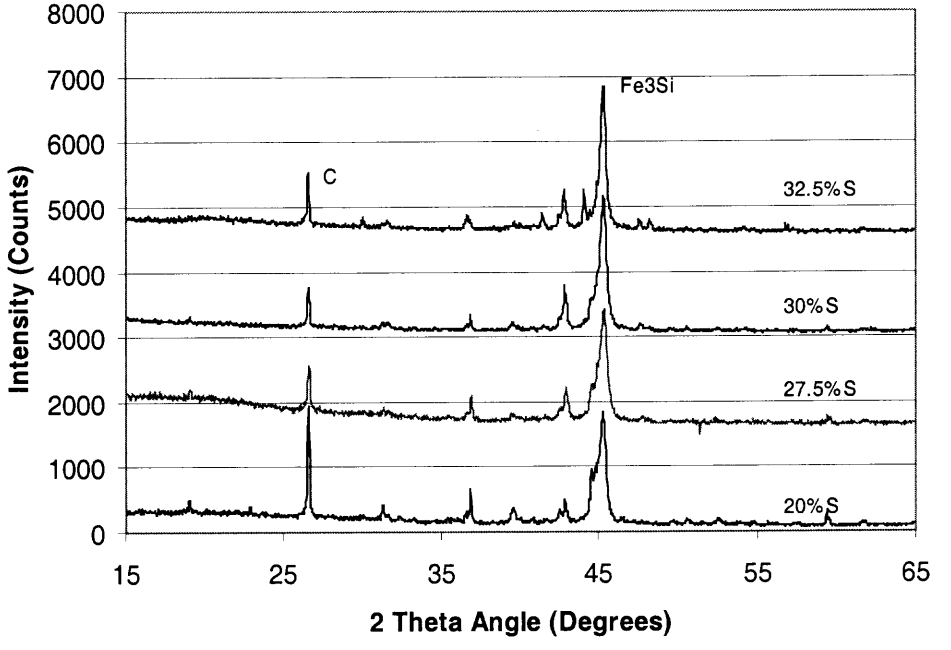

Figure 7.26 Diffractograms of LSP Soil at Different Sand Additions at 1530°C, Metal Dust

Table 7.12 Physical Descriptions of LSP Samples at 1480°C

Sand addition (%)	Wt Loss (%)	Phases	Weight** (%)	Metal Phase	Magnetic	Shiny specks	Metal separation
0%	33.9	1: dark gray		Yes	Yes	No	-White dust deposited on the inner wall of crucible
5%	32.9	1: dark gray		Yes	Yes	No	-White dust deposited on the inner wall of crucible
10%	33.3	1: dark gray		Yes	Yes	No	-White dust deposited on the inner wall of crucible
20%	32.6	3: dark gray, Metal& dust, Metal	- - 19.0*	No Yes	No Yes	No Yes	-Partly attached to metal&dust -Mostly tiny metal balls -19% of initial soil weight
25%	32.3	3: solid - gray Metal&dust Metal	42.8 54.2 >>3*	No Yes	No Yes	No Yes	Partly attached to metal&dust at the bottom of the solid mass. Mostly tiny metal balls

*: The actual weight of metal should be larger than the weight of clean separated metal due to the metal dissemination in the solid matrix.

**: The weight percentages are the weight proportion of each phase (slag, metal, and dust) physically separated after the experiment.

Table 7.13 Physical Descriptions of LSP Samples at 1530°C

Sand (%)	Wt Loss (%)	Phases	Wt** (%)	Metal Phase	Magnetic	Shiny specks	Metal separation
0	34.8	2: Solid dark gray Brown crystal		Yes	Yes	No	- -Deposited on top of the sample and inside the crucible
7.5	27.6	1: Solid dark gray		Yes	Yes	No	-White dust deposited on the inner wall of crucible
20	33.2	1: Solid dark gray Metal&dust Metal	69.0 27.0 >4*	No Yes	No Yes	No Yes	-Attached to metal&dust, separated upon grinding. -Mostly metal specks
25	33.1	1: Solid dark gray Metal&dust Metal	55.9 32.4 >11.7*	No Yes	No Yes	No Yes	-Attached to metal&dust, separated upon grinding -Mostly metal specks
27.5	35.7	1: Solid dark gray Metal&dust Metal	70.9 4.9 >24.0*	No Yes	No Yes	No Yes	-Attached to metal&dust, separated upon grinding -Mostly metal specks ->18.2% of initial soil weight
30	31.7	1: Solid dark gray Metal&dust Metal	66.0 20.4 >13.5*	No Yes	No Yes	No Yes	-Attached to metal&dust, separated upon grinding -Mostly metal specks ->11.0% of initial soil weight
32.5	35.6	1: Solid dark gray Metal&dust Metal	70.2 19.7 >10.0*	No Yes	No Yes	No Yes	-Attached to metal&dust, separated upon grinding -Mostly metal specks ->8.5% of initial soil weight

*: The actual weight of metal should be larger than the weight of clean separated metal due to the metal dissemination in the solid matrix.

**: The weight percentages are the weight proportion of each phase (slag, metal, and dust) physically separated after the experiment.

Increasing the temperature did not really help the separation of metal from LSP soil. The slag from the LSP mixture had never wetted the graphite crucible unlike the slag from the GAR and TPR mixtures. They hardly formed a single gray droplet, but several small droplets. Though mixtures of GAR, LSP, and TPR, were located on phase diagrams close to each other, the viscosity can be different. The viscosity of the LSP mixtures was found slightly higher than the values from GAR and LSP mixtures. Carbon was also abundant in the LSP metal dust and it might interfere with the agglomeration of both metal and slag. The melting temperature of carbon is over 3000°C. The result agreed with phase diagrams with respect to the metal separation. The metal agglomeration might be affected by the viscous nature of the melt or the carbon particles.

7.2.2.4 Metal. The quality of metal is not in the scope of this research due to the lack of knowledge in metallurgy. Nonetheless a metal chunk from GAR at 25% sand addition was observed by the ESEM and analyzed for the composition using EDX. Figure 7.27 shows the image of the same piece of metal but at different location. The compositions varied from one location to another, Table 7.14. The composition ranged from very high iron content to very high titanium content. During the actual operation, metal is periodically tapped or drained from the furnace. The quality of metal can be well controlled by adjusting the slag composition. The separation of metal after the solidification, similar to this research, does not allow controlling slag properties as much as when tapping metal in liquid state.

Table 7.14 Compositions of Metal Chunk at Different Locations

Areas	Concentration (% wt)						
	Fe	Cr	Ti	Si	Ca	Al	Mg
Area a)	87.8	7.4	1.9	2.9	-	-	-
Area b)	27.9	7.2	44.3	7.7	6.7	3.4	2.8
Area c)	41.0	26.6	21.9	4.6	1.9	4.1	-
Area d)	90.9	2.5	1.9	4.7	-	-	-

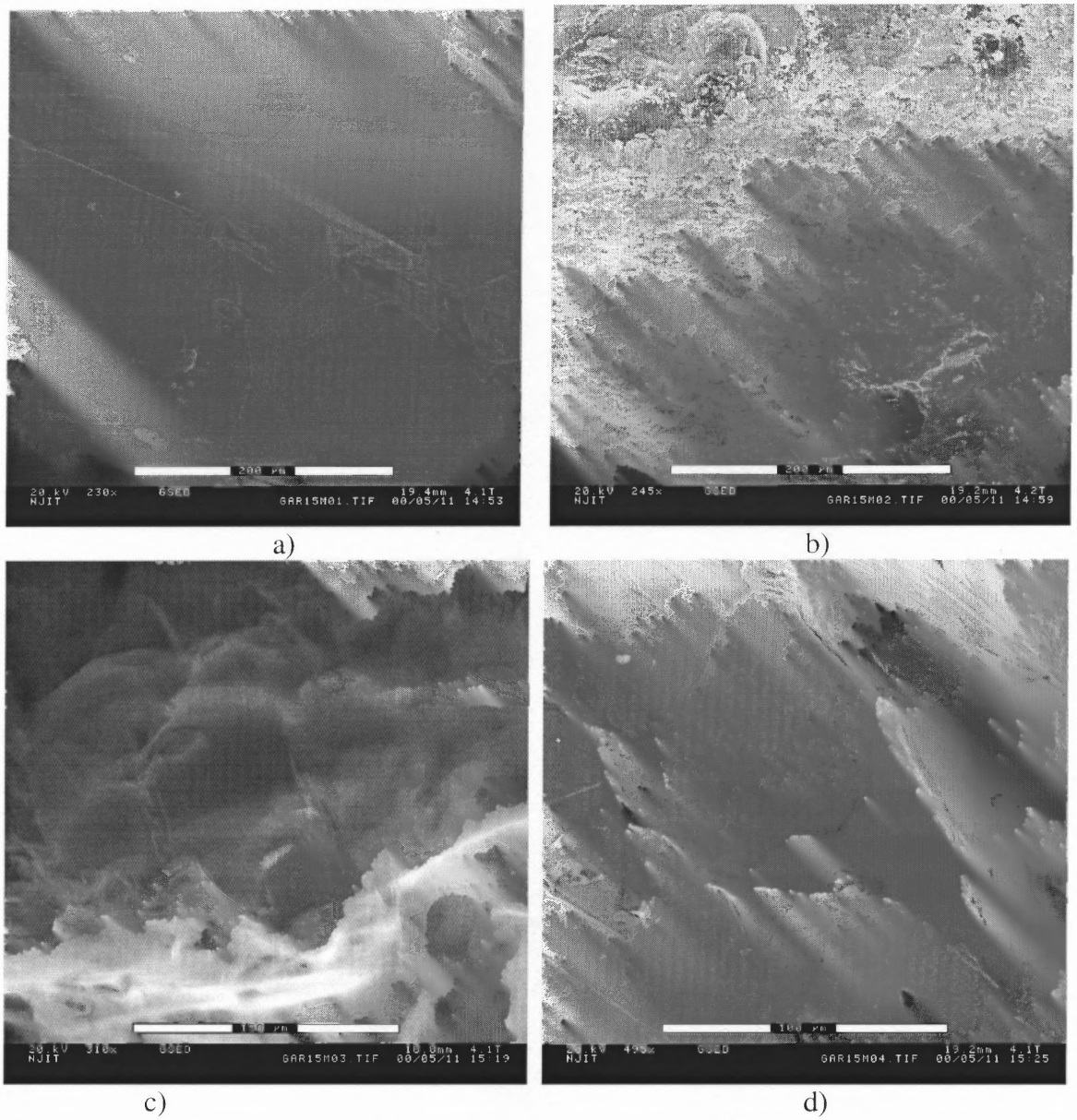

Figure 7.27 Morphology of a Metal Chunk from GAR at Different Locations

7.3 Summary

As concluded in Chapter 6 that the metal separation did not occur due to the difficulty in solid state agglomeration of metal. Therefore the criteria in determining the melting point of the sample should be applicable to the prediction of metal separation. Phase diagrams provide the information on liquidus temperatures of different compositions of oxides. Referring sample compositions to phase diagrams might allow us to predict the liquefaction of the sample and subsequently metal separation. Adding sand, acidic oxide, to soil rich in basic oxide, CaO, brings the melting temperature of the mixture down and possibly allows a better metal separation. The preliminary tests using TGA reviewed the metal separation as tiny metal droplets when raising temperatures or adding silica. The sand addition at 20% seemed to promote the separation between metal and other oxides.

GAR, TPR, LSP, and CD soils were mixed with different sand additions and 15% carbon. There was no metal agglomeration from all soils when no sand added. Mixtures of soil from GAR and TPR yielded metal pool with 15-25% sand at 1530°C. At 5% sand, there was metal separated in a form of tiny metal droplets embedded in the slag matrix. The addition of sand promoted the reduction of TPR soils, which did not attain complete reduction during the reduction study. Sand is beneficial is two possible ways: lowering the melting temperature of the mass, and combining with MgO from the hard to reduce spinel. There was metal separation as metal droplets, though not as metal pool, from LSP mixtures with 20% sand and above, at 1480°C. Parts of metal droplets were embedded within the slag matrix. Increasing sand content to 32.5% and temperature to 1530°C did not improve the metal separation. The slag from LSP did not agglomerate but form several slag droplets separated by metal and dust, unlike the formation of a

single piece of slag from GAR and TPR. It is more likely that LSP mixtures have higher viscosity than the GAR and TPR mixtures. The slag from GAR, TPR, and LSP shared similar major phases as forsterite and diopside. There was no metal separation from CD soils, a representative of soils having low iron concentrations and being non-magnetic. The metal separation of soil can be predicted fairly well, especially for GAR and TPR mixtures, using phase diagrams of pure oxides in a quaternary system, CaO-MgO-SiO_2-Al_2O_3.

GAR and TPR soils produced 30 % metal, by weight of the initial soil, at the 20% sand addition where there were the least concentrations of Fe and Cr in slag. The metal phase showed local variations. The major phase contained high concentration of Fe, around 90%. Nonetheless, the content of Cr, Fe, Ti, combined in all phases was around 90%. The iron and steel scrap contains Fe no less than 90%. The separated metal therefore might be suitable for recycling to steel industry.

Further research is required to verify the application of extracted metal in the industry and to characterize the metal phase in detail. There are additives, which are known to decrease the viscosity of silicate melt, i.e. CaF_2. The effect of these additives in metal separation is also a promising subject for the future research.

CHAPTER 8

SUMMARY AND CONCLUSIONS

The feasibility to extract chromium and iron from chromium contaminated soils was explored. The study began with the characterization of contaminated soils in terms of compositions, phases, and morphology, from nine locations in Hudson County, New Jersey, using non-destructive instruments: XRF, XRD, and ESEM. After the characterization of soils, the feasibility to concentrate and extract iron and chromium in oxide and metallic form was investigated. The results from the concentrating experiment of iron and chromium oxides will be used to determined the possibility of using concentrated soils as a substitute for iron ore. The concentrating techniques included magnetic and gravitational separations. These two techniques were selected because of the different magnetic properties and specific gravity of minerals constituting soils. The extraction of iron and chromium in metallic form was also studied. It included the iron oxide reduction and the separation of metal. The reduction and metals separation occurred at high temperature. At this high temperature, >1000°C, hexavalent chromium was reported to reduce to non-toxic trivalent chromium. The previous study on treating chromium contaminated soils through cold top ex-situ vitrification concluded the great efficiency of the process and the reusable vitrified products. The process of reduction and metal separation of contaminated soils is in fact a combination of treating soils through vitrification process and extracting iron and chromium as in ironmaking process. The products are non-toxic metal and slag. The extracted metal promises to be a valuable material that could possibly be recycled in the steel industries. The separation of metal

from slag reduces the specific gravity of slag and eliminates the long term and other detrimental effects from metals. The entire experimental results could be summarized as following;

- On average chromium contaminated soils contain of 23 % iron oxide, 24% calcium carbonate, 6% magnesium oxide, 13% aluminum oxide, 23% silica, and 5.6% chromium. Chromium in soil was found to coexist with iron. From the study of nine chromium contaminated sites, these soils can be classified into two groups. One has high iron concentration, over 20%, these soils have iron and chromium in a form of magnetic spinel, $(Mg, Fe)(Fe, Cr, Al)_2O_4$. The others have low iron concentrations and high silica or calcium. Their iron and chromium oxides do not have magnetic properties.
- The magnetic separation is able to concentrate iron and chromium oxides from 25.5-37.9% and 4.5-7.8% to 34.9-40.9% and 6.3-8.6%. The recovery rate of iron and chromium oxides, weight percentages of iron and chromium oxides concentrated in magnetic portion, are 84.9-99.2% and 86.6-99.8%. The magnetic separation concentrated oxides of iron, chromium, magnesium, and calcium in the magnetic portion and silica in the non-magnetic portion. The magnetic soil mostly consisted of chromite ore subjected to different degrees of oxidation during the chromate extraction process. The magnetic separation gave a better separation efficiency than the gravitational separation for this experimental setup.
- The attempt to recycle the concentrate as a substitute for iron ore was not successful due to the concentration of iron, which was not as high as the concentration in high grade or processed ore. That does not mean it can not be

reused, but rather it may not prove comparable to the iron and steelmaking processes in which high-grade or processed ore containing 60-70% Fe is used.

- The reduction of iron oxide was rapid at high temperature and readily finished before reaching 1400°C. The reduction by the solid carbon, direct reduction, started above 900°C. Afterwards, indirect reduction was the main reaction path for the reduction of iron oxide in soils. The reduction of iron and chromium oxide in LSP soil seemed to constitute of two steps: from 900 –1200°C for the reduction of easily reduced spinel, and above 1200°C for the spinel of types containing MgO, and Cr_2O_3. The gasification was the limiting process for the reduction of iron oxide by solid carbon with activation energy between 45-55.6 kcal/mol, based on the selection of kinetic models. The reduction pattern of LSP soil was similar to the combined pattern of Fe_2O_3 and $MgO.Fe_2O_3$. TPR and GAR soils followed closely to the reduction pattern of $MgO.Fe_2O_3$.
- The metal agglomeration and separation occurred when sand was added to soils. The GAR and TPR soils yielded substantial amount of metal, 25-33% of their initial weights, when mixed with 15-25% sand and 15% carbon by weight. The 20% sand addition seemed to produce the most of separated metal and the least iron and chromium contents in slag. The LSP soil mixtures yielded metal separation with sand addition above 20%. The metal from LSP was embedded with dust portion unlike the metal separation in TPR and GAR. They formed metal pool under the covering of slag, which was easy to separate. The metal yield from LSP was 3-18% of its initial weight. The number was low, as it was hard to separate metal from the agglomeration of dust and metal. Slag from all soils was identified

as $2MgO.SiO_2$ (Forsterite) and $Ca(Mg, Al)(Si, Al)_2O_6$ (Diopside). There was no metal separation from CD soil, a representative of a soil group having low iron concentration.

- There is local variation in composition of the extracted metal: a principal phase with high Fe content (~90%) and the minor phase with high Ti and Cr. The concentration of Fe, Cr, and Ti combined in any area is close to or larger than 90% by weight.
- The prediction of the metals separation using the quaternary phase diagram and the viscosity diagram agreed quite well with the experimental results. The minor and trace elements in soils do not affect the experimental results. The pure phase diagram can be applied to study the behavior of melted of chromium contaminated soils.
- It is possible to extract metal from soils in this research. The application of the concept to the larger scale still needs verification. The pilot scale demonstration of vitrification process of LSP soil yielded metal separation of 3.3% of initial weight. The process conditions were not controlled in such a way to promote metal separation. Nonetheless, the result suggested the possibility of application the metal separation to the process. By adding carbon in sufficient amount to the mixture of soil, more metal should be reduced and separated. Purging the system with an inert gas might not be required as the reduction of iron oxide under thick layer of slag with top-blowing of oxygen was reported (Katayama, 1992).
- The recycling of metal is a general practice in iron and steel industry. Steel slag containing 15-25 % Fe (Tables 2.5 and 2.6) is crushed and put through magnetic

separation to recycle Fe back to the steelmaking process. The LSP, GAR, TPR, CPR, RM soils contain 14-22%Fe which are in the same or higher concentration range as of the steel slag. The concept of recycling iron from chromium contaminated soils, therefore, is viable.

- Iron and steel scrap is sold at 108 $/metric ton (Table 2.14). The iron and steel scrap contains not less than 90% Fe and the compositions vary with types of scrap. The principal phase of extracted metal contains about 90% Fe and might be sold as steel scrap. With the potential revenue from the extracted metal, the application of the research concept to the vitrification process might bring the operating cost down. The treatment cost of chromium contaminated soils, including pretreatment and additives, by vitrification is $80/metric ton, when the vitrified product is used as aggregate. If three hundred kilograms of metal can be extracted from one metric ton of initial soil, 30% by weight according to GAR soil with 20-25% sand addition, a revenue of 30$ was created for every metric ton of soil. The cost of vitrification process might be reduced to $50/ton.

Conducting research is a never-ending mission. The future research can be classified into 2 groups: the further fundamental study on the reduction process and the metal separation, and the integration of the proposed concept into the steelmaking line. Appendix A includes a future research plan to determine the activity of iron oxide, the quantitative dependency of the reduction process on the amount of carbon, carbon and CO_2 oxidation kinetics, and iron oxide and CO reduction kinetics. An attempt to create a model to describe the reduction behavior was also initiated and briefly explained in

Appendix A. This future study will provide insight into the reduction process of iron oxide in more detail. In term of metal separation, the LSP soil experienced difficulty in metal separation possibly due to its high viscosity; the future study shall include the effect on decreasing viscosity by additives, i.e. CaF_2, in metal separation.

To fully recycle the extracted metal in the steel industry is a very important aspect. This research lacks of information on the quality of the extracted metal and other details of the real steelmaking process, i.e. its limitation on the quality of the feed, and the effect of slag composition on the refractory material. The research is at a step where it needs a further support both financially and technically to fully utilize the ideas and develop a real world practical process. The cooperation from the steel industry or personnel with expertise in the field of metallurgy would be advantages. The future of the research now depends on the verification of quality of the extracted metal.

The research provides information on the separation, reduction, and metal separation of chromium contaminated soils. It also includes the thorough investigation of the contaminated soils. The information is possibly useful not only for the thermal treatment process, but also the other processes and different kinds of contaminated soils.

APPENDIX A

PROPOSED FUTURE RESEARCH ON COMPUTATIONAL MODEL

In this Appendix, the attempt to address the future research on the reduction process and to incorporate all parameters into a model to predict and explain the process is briefly described. The research in this part of dissertation is very limited and at the inception. It will provide a guideline for future study. Brief description of experimental design and principal will also be given.

The reduction of iron oxide by carbon involves two major processes: the carbon gasification by CO_2 and the reduction of iron oxide by CO. The parameters effecting the reduction process include but not limited to the reactivity of carbon, the carbon concentration, the reductions kinetics of both carbon gasification and iron oxide reduction, activity and equilibrium constant, and the diffusion of CO and CO_2. The change in one parameter influences the other. For example, the partial pressure of CO and CO_2 change when the reduction of iron oxide occurs. The change in CO/CO_2 ratio then affects the rates of reduction and gasification. The reduction ceases when the CO/CO_2 ratio falls below the equilibrium ratio. The iron oxide activity varies with the composition of solid solution of iron oxide. The equilibrium ratio of CO/CO_2 increases as the activity of iron oxide decreases. The behavior can not be described by a continuous mathematical function. The numerical approach is rather a better approach. The behavior of a complex system can be represented by a set of simple and well-understood processes. The reduction of iron oxide by solid carbon may be studied through its subprocesses: gasification of carbon by CO_2 and reduction of iron oxide by

CO. The other parameters effecting the process are the dependency of reduction on the carbon contact sites, the activity of iron oxide and iron in metal. Upon these subprocesses are well described and incorporated into a model, the behavior of the reduction process could be predicted. The verification of the predicted results against the experimental data validates the model. All these aspects are mentioned in brief.

A.1 Gasification of Carbon by CO_2

The reaction kinetics can be determined from a series of tests at different temperatures and different partial pressures of CO_2. Different sources of carbon, graphite, coal, coke, have different reactivity. Their kinetic parameters need to be calculated. Literature (Table 3.1) suggested relations to describe the oxidation kinetics of carbon, which followed either first order kinetics or shrinking core models. The phase boundary reaction is proposed as a rate limiting process.

A.2 Reduction of Iron Oxide by CO

The experimental design in this part is similar to the gasification by CO_2. The reduction kinetics is also given in Table 3.1. The research results suggested the phase boundary reaction as a rate limiting process. The use of a mixture of CO and CO_2 is preferred. Pure CO does not allow the calculation of a valid equilibrium temperature. Bogdandy and Engell (1971) describe the extrapolation of a reduction rate from a mixture of CO/CO2 to pure CO. The dependency of the reduction on the CO/CO_2 should be addressed as well.

A.3 Dependency of Gasification on the Amount of Carbon

The research results suggested the dependency of the reduction on the amount of carbon, which relates to the contact sites. A fixed weight of sample with different additions of carbon shall be tested. Using fixed sample weight disallows the effect of larger contact areas of iron oxide, which might accelerate the reduction. The reduction rate should increase with the increasing of carbon addition to a concentration where the contact sites are excessive and the reduction rate remains constant. Increasing the carbon addition might as well relate to the change in the partial pressure of CO_2. The result from this section and the first sections should be compared and their relations, if any, should be determined.

A.4 Activity of Oxide and Metal

The oxides of interest are iron, chromium, and magnesium oxides. The alloy is limited to iron-chromium alloy. Gurevich et al. (1973) suggested the reduction of iron oxide proceeded and finished before the reduction of chromium oxide occurred. According also to results from Chapter 6, FeO phase was present at 1000°C and FeO_xMgO_{1-x} at 1100°C. The reduction therefore occurs in a stepwise manner.

A.4.1 Pure iron oxide. At this first state of reduction, the activity of iron oxide can be taken to be unity, since it is in its standard state. The activity of metal phase is also unity; there is no reduction of chromium at this moment.

A.4.2 Solution of Iron Oxide with Other Oxides besides Chromium. The activity of iron oxide deviates from unity. The activity of iron oxide in soil can be determined from the temperature where the reduction to metal of MgO_xFeO_{1-x} occurs. The experimental procedure could be as following: obtain MgO_xFeO_{1-x} phase by running an experiment at 1100C; determine the approximate mole ratio of MgO and FeO by EDTA titration method; heat the sample under fixed CO/CO_2 ratio and record the temperature where the reduction starts; do the same experiment for FeO; relate the reduction temperature from pure FeO and MgO_xFeO_{1-x} to obtain activity from Equations A.3.

$$\Delta G^o_{FeO} = -RT_{FeO.MgO} \ln\left(\frac{a_{FeO}}{p_{O_2}^{1/2}}\right), \text{ for } MgO_x.FeO_{1-x} \quad (A.1)$$

$$\Delta G^o_{FeO} = -RT_{FeO} \ln\left(\frac{1}{p_{O_2}^{1/2}}\right), \text{ for FeO} \quad (A.2)$$

$$\frac{T_{FeO}}{T_{FeO.MgO}} = \ln(a_{FeO}) \quad (A.3)$$

There are several proposed models to estimate the activity of FeO in a solution of MgO-FeO for example the ionic regular solutions theory (Lykasov and Tarvid, 1978) and sublattice model (Fabrichnaya, 1998). They might be applicable with the solution of MgO and FeO in soils. Fabrichnaya (1998) summarized works on the Fe-Mg-O systems by many researchers using different approaches. The activity of metal phase, pure Fe, remains at unity.

A.4.3 Solution of Metal. Since all iron oxides are reduced prior to the oxide of chromium, the chromium oxide activity can be taken to be unity as well. The activity of Fe and Cr in alloy should be available as well in literature.

It is not an easy task when dealing with the solid solution and alloy of iron and chromium which have many oxidation states: Fe^{3+}, Fe^{2+}, Fe^{0}, Cr^{3+}, Cr^{2+}, and Cr^{0}. The percentages of each oxidation states can be determined by performing EDTA titration method. The concentrations of each species in each phase then can be used in the calculation of the iron oxide activity by different activity models.

A.5 Computational model

A.5.1 Initial Condition

Initial concentration is simply calculated from weight and molecular weight. A simple flow chart is shown in Figure A.1.

A.5.2 Iterative Calculation

The reacting time is divided into a series of infinitesimal time slices. Euler's Method is a simple tool used for numerical prediction. It predicts the next event when knowing the initial condition and the differential function: $C_{(t)} = C_{(t-\Delta t)} + \Delta t\ (dC/dt)$, where $C_{(t)}$ is parameters at time t, $C_{(t-\Delta t)}$ is parameter at time $t-\Delta t$, and Δt is the infinitesimal time slice. At each period the following parameters are calculated.

A.5.2.1 Concentrations. At the end of each period, the concentration of all components, oxides, gas, and metal, is calculated based on the reduction kinetics of reduction of iron oxide and gasification.

A.5.2.2 Activity. Similar to the concentration the activity of both iron oxide and metallic iron is also recalculated according to the extent of reduction.

A.5.2.3 Equilibrium Constant (CO/CO_2). The activity then is used in determining equilibrium constants and the CO/CO_2 ratio, which both set the required ratio for the calculation in the next period.

The other important aspect is to select the reactor model, plug flow or completely mixed reactor, which can best describe the reduction behavior in the process. The production of CO and CO_2 increase gas volume, or increasing atoms of gas, which later leave the sample. As they pass through sample, the reaction occurs. However, after they leave the sample mass they have no further influence on the reduction process. It might be possible to assume the constant reacting volume, which also means the constant moles of gas actively involving in the reduction. The excess gas has a brief resident time in the reacting volume depending on the production rate and the reacting volume.

A.5.3 Checking Conditions

The iterative calculation stops or pauses when the following occurs:

- The reduction is complete

- The CO/CO_2 ratio falls below the equilibrium ratio (allowing calculation in the next time slice)

- The temporarily depletion of CO and CO_2 (allowing calculation in the next time slice)

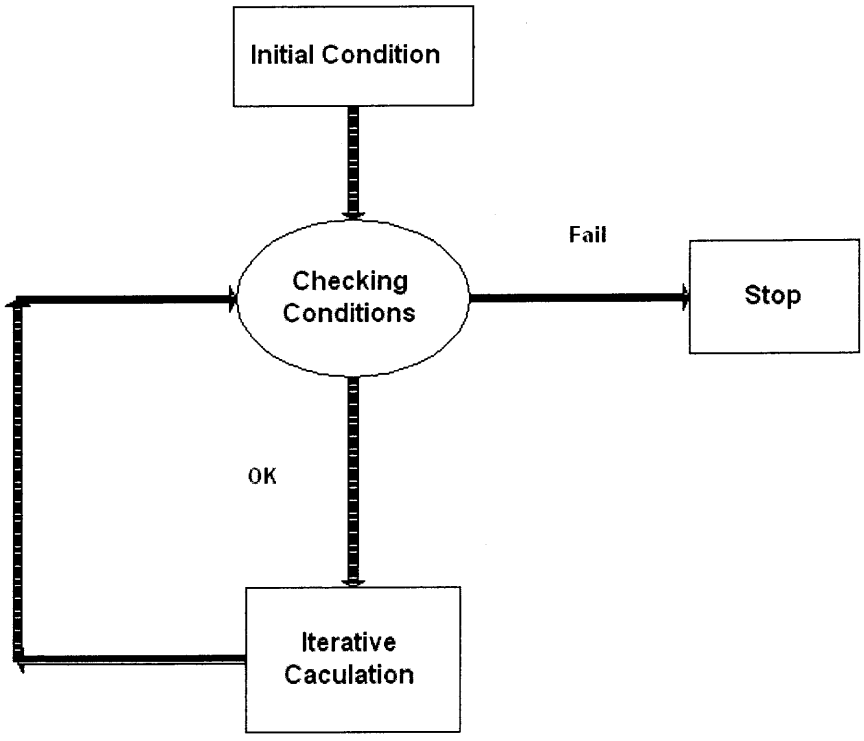

Figure A.1 Flow Chart for Computational Model229

APPENDIX B

ABBREVIATIONS

S.G.	Specific Gravity
wt.	Weight
T.Fe	Total Iron
$\Delta G°$	Standard free energy of a reaction at a reference state
$\Delta G°(T)$	Standard free energy of a reaction at a temperature T
$\Delta H°$	Standard enthalpy of a reaction at a reference state
$\Delta H°(T)$	Standard enthalpy of a reaction at temperature T
$\Delta S°$	Standard entropy change of a reaction in a reference state
$\Delta S°(T)$	Standard entropy change of a reaction at temperature T
$\Delta C°_p$	Heat capacity of a reaction (the heat capacity of products minus the heat capacity of reactants) at a reference state
$\Delta C°_p(T)$	Heat capacity of the reaction (the heat capacity of products minus the heat capacity of reactants) at temperature T
U	Internal energy
a_x	Activity of x components in a solution
p_x	Partial pressure of gas x
R	Gas constant
T	Temperature
K	Equilibrium constant
k	Rate constant
μ_x	Chemical potential of component x
n_x	Number of mole of component x
DOR	Degree of Reduction
Basicity	Mole ratio of CaO/SiO_2
ESEM	Environmental Scanning Electron Microscope
EDX	Energy Dispersive X-Ray Spectroscopy
XRD	X-Ray Diffraction Spectroscopy
XRF	X-Ray Fluorescence Spectroscopy
TGA	Thermo-Gravimetric Analyzer

REFERENCES

Abraham, M.C., and G.Ghosh, 1979, "Kinetics of Reduction of Iron Oxide by Carbon," Ironmaking Steelmaking, Vol. 6. No. 1, pp.14-23.

Ahmad, M., Masoud Kasiri Asgarani, 1999, "Producing Portland Cement from Iron and Steel Slags and Limestone," *Cement and Concrete Research*, Vol.29, pp.1373-1377.

Allen M. A., 1970, High Temperature Oxides. Part I; Magnesia, Lime, and Chrome Refractories. Refractory Materials, A series of Monographs, Academic Press, New York and London.

Amer, A. M., 1992, "Processing of Ras-Shait Chromite Deposits," *Hydrometallurgy*, Vol. 28, pp. 29-43.

Andrew, P. R. A., 1990, "Anionic Activation in the Flotation of Chromite from a Low-Grade Ore," *CIM Bulletin*, June, pp.67-69.

Annual Book of American Society for Testing and Materials, 1998, Concrete and Mineral Aggregates, Section 4, Vol. 04.02.

Baldwin, B.G., 1955, "Formation and Decomposition of Hercynite ($FeO.Al_2O_3$)," *J. Iron Steel Inst.*, London, Vol.179, No.30, pp. 142-146.

Basumallick, A., 1995, "Influence of CaO and Na_2CO_3 as Additive on the Reduction of Hematite-Lignite Mixed Pellets," *ISIJ International*, Vol.35, No.9, pp.1050-1053.

Belardi, G., N. Sheau, P. Plescia, and F. Veglio, 1995, "Recent Developments in Gravity Treatment of Chromite Fines," *Minerals and Metallurgical Processing,* August, pp.161-165.

Bertin, E.P., 1975, Principles and Practice of X-Ray Spectrometric Analysis, 2nd Edition, Plenum Press.

Bogdandy, L.V., and H.J. Engell, 1971, The Reduction of Iron Oxides. Springer. New York.

Chan, B. S. K., R. H. Mozley, and G. J. C. Childs, 1991, "Extended Trials with the High Tonnage Multi-Gravity Separator," *Minerals Engineering*, Vol.4, No.¾, pp.489-496.

Clark, R.P., et al., 1975, "Thermo-analytical Investigation of $CaCrO_4$," *Thermochem Acta.* Vol. 33, pp.141-445.

Conejo, A. N., G. P. Martins, 1997, "Conversion of Hematite to Iron Carbides by Gas Phase Carbidization," *ISIJ International,* Vol.37, No.10, pp.967-976.

Darken, L.S. and R. W. Gurry, 1953, Physical Chemistry of Metals, McGraw-Hill.

Davies, M.W., G.S. F. Hazeldean and P.N. Smith, 1973, Physical Chemistry of Process Metallurgy, the Richardson Conference.

Dehoff, R.T., 1993, Thermodynamics in Material Science, McGraw-Hill International Editions.

Dusseldorf, H., 1981, Slag Atlas, Verlag Stahleisen M.B.H. Dusseldorf.

El-Geassy, A.A., 1998, "Stepwise reduction of CaO and/or MgO Doped-Fe_2O_3 Compacts (Hematite-Wustite-Iron Transformation Steps)," *Scandinavian Journal of Metallurgy*, Vol. 27, pp.205-213.

El-Geassy, A.A., 1996, "Gaseous Reduction of MgO-Doped Fe_2O_3 Compacts with Carbon Monoxide at 1173-1473," *ISIJ International*, Vol.36, No.11, pp.1328-1337.

Emley, E.F., 1966, Principles of Magnesium Technology, Pergamon Press 1st edition.

Fabrichnaya, O, 1998, "The Assessment of Thermodynamic Parameters for Solid Phases in the Fe-Mg-O and Fe-Mg-Si-O Systems," *Calphad*, Vol.22, No.1, pp.85-125.

Fenton, M. D., 1998, "Iron and Steel," Mineral Yearbook, U.S. Geological Survey.

Fenton, M.D., 1998, "Iron and Steel Scrap" USGS Minerals Information: Statistical Compendium,
URL:
http://minerals.er.usgs.gov/minerals/pubs/commodity/iron_&_steel_scrap/stat/

Gaskell, D.R., 1995, Introduction to the Thermodynamics of Materials, 3rd Edition, Taylor&Francis.

Ghosh, A., 1994, "Kinetics of Reduction of FeO in Slag by Carbon," Proceeding of the Workshop on Production of Liquid Iron Using Coal. New Delhi, India, pp.139-142.

Gurevich, Y.G., I.D. Radomyselskii, L.F. Barshchevskaya, N.R. Frage, and Y.I. Pazhidaev, 1973, "Thermodynamic Analysis of the Reduction of a Mixture of Iron and Chromium Oxides by Hydrogen," *Soviet Powder Metallurgy and Metal Ceramics*, Vol.14, No.1, pp.13-16.

Hayhurst, A.N., and M.S. Parmar, 1998, "Does Solid Carbon Burn in Oxygen to Give the Gaseous Intermediate CO or Produce CO_2 Directly? Some Experiments in a Hot Bed of Sand Fluidized by Air," *Chemical Engineering Science*, Vol.53, No.3, pp.427-438.

Hauffe, K., 1967, "Kinetics of Compound Formation in the Solid State," *Sintering and Related Phenomena.* Proceedings of the International Conference. University of Notre Dame. June, pp.139-167.

Hencl, V., and J. Svoboda, 1985, "The Possibility of Magnetic Flocculation of Weakly Magnetic Minerals," pp. 472-490.

Holt, J.B., 1967, "Role of Oxygen in Solid-Solid Reactions," *Sintering and Related Phenomena.* Proceedings of the International Conference. University of Notre Dame. June, pp.169-190.

Kalyoncu, R.S., 1998, "Slag-Iron and Steel" Mineral Yearbook. U.S. Geological Survey.

Kalyoncu, R.S., 1998, "Iron and Steel Slag." Mineral Commodity Summaries. U.S. Geological Survey.

Kamolpornwijit, W., 1996. "Remediation and Reuse of Chromium Contaminated Soils Through Cold Top Ex-situ Vitrification," Thesis submitted to the New Jersey Institute of Technology in partial fulfillment of the requirement for the degree of Master of Science.

Kasai, E., K. Mae, and F. Saito, 1995, "Effect of Mixed-Grinding on Reduction Process of Carbonaceous Material and Iron Oxide Composite," *ISIJ International*, Vol.35, No.12, pp.1444-1451.

Katayama, H., T. Ohno, M. Yamauchi, M. Matsuo, T. Kawamura, and T. Ibaraki, 1992, "Mechanism of Iron Oxide Reduction and Heat Transfer in the Smelting Reduction Process with the Thick Layer of Slag," *ISIJ International*, Vol.32, No., pp.195-101.

Kavanagh et al., 1998, Steel Industry Technology Roadmap. American Iron and Steel Institute.

Kirk, S.W., 1999, "Iron Ore." Mineral Commodity Summaries, U.S. Geological Survey

Kitsikopoulos, H., P. Tselepides, H.J. Ruff, and G. Ferrara, 1992, "Industrial operation of the First Two-Density Three-Stage Dense Medium Separator Processing Chromite Ores," Mines&Cariers; Les Techniques, December, pp.40-44.

Koch, K., U. Harter, and R. Bruckhaus, 1988, "Laboratory Studies on Smelting Reduction – a Contribution to Reaction Mechanism in the Production of Liquid Iron from Iron Oxide Melts," Process Metallurgy.

Kuck, P., 1998, "Iron Ore Statistic Compendium," USGS Minerals Information: Statistical Compendium, Sept.
URL: http://minerals.er.usgs.gov/minerals/pubs/commodity/iron_ore/stat/.

Lankford, W.T., N.L. Samways, R.F. Craven, and H.E. McGannon, 1985, "The Making, Shaping and Treating of Steel," Unites States Steel. 10th edition.

Lekatou, A., and R.D. Walker, 1997, "Effect of SiO_2 Addition on Solid State Reduction of Chromite Concentrate," *Ironmaking and Steelmaking*, Vol.24, No.2, pp.133-143.

Lykasov, A.A., and L.S. Travid, 1978, "Using of Theory of Ionic Regular Solutions to Describe Thermodynamic Properties of Magnesiowustite," *Steel in the USSR*, Vol.10, pp.9-12.

Lupis, C.H.P., 1983, Chemical Thermodynamics of Materials, North-Holland.

Mazanek, E., and S. Jasienska, 1964, "Effect of Al_2O_3 on Mineral Constitution of Self-Fluxing Sinters," *J. Iron Steel Inst.*, 202, pp.319-324.

Meegoda, J. N., W. Kamolpornwijit, D. Vaccari, A. Ezeldin, B.A. Noval, R.T. Mueller, and S. Santora, 1999, "Remediation of Chromium Contaminated Soils - A Bench Scale Investigation" *ASCE Practice Periodical of Hazardous, Toxic, and Radioactive Waste Management,* Vol. 3, No.3, pp. 124-131, July.

Meegoda, J. N., K. Partymiller, M.K. Richards, W. Kamolpornwijit, W. Librizzi, W, T. Tate, B.A. Noval, R.T. Mueller, and S. Santora, 2000, "Remediation of Chromium Contaminated Soils -A Pilot Scale Investigation" *ASCE Practice Periodical of Hazardous, Toxic, and Radioactive Waste Management*, Vol. 4, No.1, January.

Monshi A., M.K. Asgarani, 1999, "Producing Portland Cement from Iron and Steel Slags and Limestone," *Cement and Concrete Research*, Vol. 29, pp. 1373-1377.

Morales R.D., H. Rodriguez-Hernandez, P. Garnica-Gonzalez, and J.A. Romero-Serrano, 1987, "A Mathematical Model for the Reduction Kinetics of Iron Oxide in Electric Furnace Slag by Graphite Injection," *ISIJ International*, Vol. 37, No.11, pp.1072-1088.

Mroz, J., 1994, "Reduction of iron Oxides from Liquid Slags with Solid Carbon," *The Scandinavian Journal of Metallurgy*, Vol.23, pp.171-183.

Muan, A., Osborn, E. F., 1965, Phase Equilibria among Oxides in Steelmaking, Addison-Wesley, Reading Massachusetts.

Murthy, G.G.K., A. Hasham, and U.B. Pal, 1994, "Removal of FeO During Foaming of $CaO-Al_2O_3-SiO_2$-FeO Slag by Low Carbon-Iron Melts," *ISIJ*, Vol. 34, No. 5, pp. 408-413.

Nasr, M. I., A.A. Omar, M.H. Khadr, and A.A. El-Geassy, 1994, "Analysis of Solid-State Reduction of Iron Ore from a Couple of Experimental Measurements," *Scandinavian Journal of Metallurgy*, Vol. 23, pp.119-125.

New Jersey Department of Environmental Protection, 1998, "Summary of the Basic and Background of the Soil Cleanup Criteria for Trivalent and Hexavalent Chromium," New Jersey Department of Transportation (NJDOT), Trenton, New Jersey.

New Jersey Department of Transportation, 1998, "Standard Specification for Road and Bridge Construction," Section 901-03-901.13, New Jersey Department of Transportation (NJDOT), Trenton, New Jersey.

New York State Air Guide-I, 1991, "Guideline for the Control of Toxic Ambient Air Contaminants," New York State Department of Environmental Conservation (NYSDEC), Division of Air Resources, Albany, NY.

O'Keeffe, M., 1967, "Diffusion in Oxides and Sulfides," *Sintering and Related Phenomena. Proceedings of the International Conference*. University of Notre Dame. June, pp.57-87.

Okumura, H., 1993, "Recycling of Iron and Steelmaking Slags in Japan," Proceedings of the 1st International Conference on Processing Material for Properties. Mineral, Metals&Materials Society. pp. 803-806

Otsuka, K., and D.Kunii, 1969, "Reduction of Ferric Oxide Mixed with Graphite Particles,"*J.Chem Eng Jpn.*, Vol.2, No.1, pp. 46-50.

Ozturk, B. and R.J. Fruehan, 1992, "Dissolution of Fe_2O_3 and FeO Pellets in Bath Smelting Slags," *ISIS International*, Vol.32, No.4, pp.538-544.

Papp, J. F., 1998, "Chromium," Mineral Yearbook. U.S. Geological Survey.

Papp, J.F., 1999, "Chromium," Mineral Commodity Summaries. U.S. Geological Survey.

Parker, M. R., 1993, "Processing of Mineral Ores by Modern Magnetic Separation techniques,"

Paramguru, R.K., H.S. Ray, P. Basu, and A.K. Jouhari, 1996, "Kinetic and Mechanism of Reduction of FeO in Molten Slag. Part 1: Soild Carbon as Reductant," *Ironmaking and Steelmaking*, Vol.23, No.5, pp.411-415.

Paramguru, R.K., H.S. Ray, R. Basu, and A.K. Jouhari, 1996. "Kinetics of Reduction of FeO in CaO-SiO_2-FeO Slags: Part2 Reduction by Solid Carbon," *Iron and Steelmaking*, Vol.23, No.5, pp.411-414.

Paul, A., R.W. Douglas, 1966, "Mutual Interaction of Different Redox Pairs in Glass," Physics and Chemistry of Glasses, Vol.7, pp.1-13.

Pei, W., and O. Wjik, 1993, "A Kinetic Study on Chromite Ore Smelting Reduction," *Scandinavian Journal of Metallurgy*, Vol.22, pp.38-44.

Pei, W., and O. Wjik, 1993, "Mechanism of Reduction of Chromium Oxide Dissolved in the CaO-SiO_2-MgO-Al_2O_3 Slag by Solid Carbon," *Scandinavian Journal of Metallurgy,* Vol.22, pp.30-37.

Pei, W., and O. Wjik., 1993, "Chromite Ore Smelting Reduction by a Carbon Saturated Iron Melt," *Scandinavian Journal of Metallurgy*, Vol.23, pp.216-223.

Pugh, R.J., Y. Wang, E. Forresberg, 1994, "The Influence of Magnetic and Surface Forces on the Coagulation of Hematite and Chromite," *Minerals and Metallurgical Processing*, August, Vol.1, No.3, pp.133-140.

Raju, G.B., S. Prabhakar, and C. Sankaran, 1993. "Beneficiation of Iron Ores by Column Floatation," *Transactions of the Institution of Mining & Metallurgy, Section C: Mineral Processing and Extractive Metallurgy,* Vol.102, May-Aug, pp.132-135.

Ray, A.K., K.K. Prasad, P.K. Sen, 1992, "A Model for the Isothermal Reduction of Iron Ore with Coal Char," *Solid State Ionics*, Vol.50, pp.217-226.

Reddy, R.G., K. Hebbar, "Viscosity of FeO-SiO_2 Slags," pp.1-11.

Ricketts, J.A. Ispat Inland, Inc., How A Blast Furnace Works,
URL: http://www.steel.org/learning/howmade/blast_furnace.htm,

Sasaki, Y., and T. Soma, 1978, "Kinetics of the Reduction of FeO in CaO-SiO_2 Slag with Solid Carbon," *Tetsu To Hogane*, Vol.64, No.3, pp.376-384.

Sivamohan, R., 1990, "The Problem of Recovering Very Fine Particles in Mineral Processing – A Review," *International Journal of Mineral Processing,* Vol.28, pp.247-288.

Smith, J.M., H.C. Van Ness, and M.M. Abbott, 1996, Introduction to Chemical Engineering Thermodynamics, 5th edition, McGraw-Hill International Editions.

Srinivasan, N.S., and A.K. Lahiri, 1977, "Studies on the Reduction of Hematite by Carbon," *Metal. Trans. B.*, Vol.8B, pp.175.

Sugata, M., T. Sugiyama and S. Kondo, 1974, "Reduction of Iron Oxide Contained in Molten Slags with Solid Carbon," Trans. Iron Steel Inst Jpn. Vol.14. pp.88-95.

Szendrei, T., and P. Van Berge, 1988, *Thermochim. Acta*, 44 , 11

Taggart, A.F., 1947, Handbook of Mineral Dressing.

Udy, M.J., 1956, Chromium, Vol.1, Reinhold, New York.

Ulmer, C.G., 1970, "Chromite Spinels," High Temperature Oxides part I. Magnesia, Lime, and Chrome Refractories. Academic Press.

Urbain, G., 1981, "Viscosity of Silicate Melts," *Journal of British Ceramic Society*. Vol. 80, pp.139-141.

U.S. Environmental Protection Agency (USEPA), 1989, "Stabilization/Solidification of CERCLA and RCLA Wastes, Physical Tests, Chemical Testing Procedures, Technology Screening, and Field Activities," EPA/625/6-89/022, Washington DC.

U.S. Environmental Protection Agency (USEPA), 1992, "Vitrification Technologies for Treatment of Hazardous and Radioactive Waste," Handbook, EPA/625/R-92/022, Washington DC.

Valia, H.S. Ispat Inland Inc, Coke Production for Blast Furnace Ironmaking, URL: http://www.steel.org/learning/howmade/coal.htm,

Wang, Y., and E. Forresberg, 1994, "The Recovery of Hematite and Chromite Fines and Ultrafines by Wet Magnetic Methods," Minerals and Metallurgical Processing. May, pp. 87-95.

Weeda, M., P.J.J. Tromp, and J.A. Moulijin, 1990, "The Potential of Coal Gasification in a Novel Iron Oxide Reduction Process," *Chemical Engineering Science*, Vol. 45, No. 8, pp.1721-2728.

Yazawa, A., and M. Hino, 1993, "Thermodynamics of Phase Separation between Molten Metal and Slag, Flux and Their Process Implications," *ISIJ.* Vol. 33, No. 1. pp.79-87.

Yun, T. S., 1961, "Direct Reduction of Ferric Oxide by Solid Carbon in Vacuum," *Trans Amer. Soc. Metals* , Vol. 54, No. 2, pp. 129-142.

Zhang, L., S. Jahanshahi, 1998, "Review and Modeling of Viscosity of Silicate Melts; PartII. Viscosity of Melts Containing Iron Oxide in the CaO-MgO-MnO-FeO-Fe_2O_3-SiO_2," *Metallurgy and Material Transaction B.* Vol. 29B, pp. 187-194.